



Aalborg Universitet

AALBORG UNIVERSITY
DENMARK

Flexible Control for Local Heating and Transportation Units in Low Voltage Distribution System

Sinha, Rakesh

Publication date:
2019

Document Version
Publisher's PDF, also known as Version of record

[Link to publication from Aalborg University](#)

Citation for published version (APA):
Sinha, R. (2019). *Flexible Control for Local Heating and Transportation Units in Low Voltage Distribution System*. Aalborg Universitetsforlag.

General rights

Copyright and moral rights for the publications made accessible in the public portal are retained by the authors and/or other copyright owners and it is a condition of accessing publications that users recognise and abide by the legal requirements associated with these rights.

- Users may download and print one copy of any publication from the public portal for the purpose of private study or research.
- You may not further distribute the material or use it for any profit-making activity or commercial gain
- You may freely distribute the URL identifying the publication in the public portal -

Take down policy

If you believe that this document breaches copyright please contact us at vbn@aub.aau.dk providing details, and we will remove access to the work immediately and investigate your claim.

**FLEXIBLE CONTROL FOR LOCAL
HEATING AND TRANSPORTATION
UNITS IN LOW VOLTAGE
DISTRIBUTION SYSTEM**

**BY
RAKESH SINHA**

DISSERTATION SUBMITTED 2019



AALBORG UNIVERSITY
DENMARK

Flexible Control for Local Heating and Transportation Units in Low Voltage Distribution System

Ph.D. Dissertation
Rakesh Sinha

Dissertation submitted September 04, 2019

Dissertation submitted: September 04, 2019

PhD supervisor: Prof. Birgitte Bak-Jensen
Aalborg University

Assistant PhD supervisor: Assoc. Prof. Jayakrishnan Radhakrishna Pillai
Aalborg University

PhD committee: Associate professor Erik Schaltz (chairman)
Aalborg University

Associate professor Damian Flynn
University College Dublin

Professor Geert Deconinck
KU Leuven university

PhD Series: Faculty of Engineering and Science, Aalborg University

Department: Department of Energy Technology

ISSN (online): 2446-1636
ISBN (online): 978-87-7210-498-0

Published by:
Aalborg University Press
Langagervej 2
DK – 9220 Aalborg Ø
Phone: +45 99407140
aauf@forlag.aau.dk
forlag.aau.dk

© Copyright: Rakesh Sinha

Printed in Denmark by Rosendahls, 2019

Preface

The work carried out in this thesis is part of DiCyPS project that investigates the harmonised link of heating, transportation and electricity systems. The project is funded by “Innovationsfonden Denmark” (Innovation Fund Denmark). The programme is supported by Aalborg University in collaboration with Danish and international companies, other research institutions and public authorities, to create a foundation to support IT-Infrastructures for Control and Supervision in multi-carrier Energy Systems of the future. I would like to take this opportunity to deeply acknowledge the DiCyPs project and the Department of Energy Technology, Aalborg University, for the financial and technical support to carry out this work effectively. Working in Danish culture and society has always been so much fascinating.

The research work is performed under the supervision of Prof. Birgitte Bak-Jensen (main supervisor) and Assoc. Prof. Jayakrishnan Radhakrishna Pillai (co-supervisor) from Aalborg University. I would like to express my sincere and immense gratitude to my supervisors for their persistent support, cooperation, patience, guidance and generosity during my PhD. I would also like to thank Prof. Hamidreza (Hamid) Zareipour, from the University of Calgary, Canada, for his collaborative supervision and invaluable support during my study abroad period. I would like to thank industrial partner Bertil Møller Jensen from Aalborg Forsyning. His guidance to understand district heating technology in Denmark and data of thermal consumptions played a crucial role in the performance of this work. I would like to express my gratitude to Assoc. Prof. Carsten Bojesen and Assoc. Prof. Thomas Condra for their technical guidance in thermodynamics.

I am very much thankful to some of my colleague, Assoc. Prof. Sanjay Chaudhary, Bijay Neupane, Pavani Ponnaganti and Viktor Stepaniuk. I appreciate the technical discussions with them very much.

I would like to be grateful to all my beloved ones, Dr. Prem chandra Prasad (dad), Smt. Basanti Devi (mom), Dr. Ritesh Sinha, Ritu Sinha, Dr. Sabita Singh, Arnav Vir Sinha, Gopal krishan mehta, Smt. leelawati devi and in-laws, who motivated and supported me by all means through my

Preface

emotional journey of PhD away from homeland. I would like to honour my father in law late Prof. Raghunandan Singh, who passed away during my PhD with the dream to see me as a successful PhD scholar. And of course, ultimately, how can I forget to show courtesy to my awesome wife Kumari Neeta Singh and lovely son Rakshith Sinha for being with me unconditionally cheerful during ups and downs of PhD.

Rakesh Sinha
Aalborg University, September 4, 2019

Curriculum Vitae

Rakesh Sinha



Received B.E. Electrical and Electronics Engineering from Kathmandu University, Nepal (2005). M.Sc. in Energy Engineering, Aalborg University, Denmark (2013). Currently involved in PhD at Department of Energy Technology, Aalborg University, Denmark. The research focus is in the area of integrated energy systems, sustainable energy technologies, and power system.

Curriculum Vitae

Abstract

Global concern to reduce carbon footprints has led pursuit towards fossil fuel independent energy systems in every energy sectors. Various energy sectors such as electricity, heating/cooling, gas and transportation are operated independently. Integrated operation of thermal and electricity or transportation and electricity systems are popular among the researchers. To exploit long term benefit from renewables, the integrated operation of the multi-energy system is essential. Each energy system is capable of operating in harmony with mutual benefits from each other for its stable operation. To achieve security and efficiency in the integrated energy system, the flexible operation of the various energy system is necessary. Electricity being the most vulnerable system with fluctuating generation from renewables, flexibility is achieved from an integrated energy system. As electricity cannot be stored directly without high costs, it can take advantage of thermal, gas and transportation systems to store surplus generation from renewables. On the other hand, electricity conversion from these storages can serve as reserve capacity during deficit in electricity generation from renewables. The Danish energy model has supported technical innovation and development to enhance sustainable integration of renewables in multi-energy sectors.

Danish electricity and thermal energy infrastructure have evolved from centralised to decentralised systems in recent years. The decentralised system has improved security, efficiency and reliability in energy transmission and consumption. Thus, the concept of decentralised and integrated electrified thermal and transportation system in low voltage (LV) distribution networks is explored in this research work. The coupling of thermal, electrical and transportation system, in LV residential networks, generates unprecedented challenges in modelling, planning, operation and control of these systems. An appropriate and feasible methodology is investigated to identify and address these challenges. As a consequence, the compromise between numerical complexities and physical phenomena exhibited by the models of energy networks components are examined. A numerical model of an existing Danish LV residential network is considered

as a test platform for steady-state simulation of the integrated operation of electrified thermal and transportation units. Actual data from the energy distributors and survey are diagnosed to understand and improve the flexibility of the integrated system.

Relevant modelling of the active controllable loads and storages are crucial for optimal operation and flexible control. Thermal loads (electric boiler and heat pumps) and electric vehicles are considered as active loads. The general and specific capabilities of the average and stratified models of the thermal storage tank are presented. The influence of these models in the representation of technical parameters and scope of work is discussed in brief.

The consumption patterns of electricity, thermal and transportation needs are based on users comfort. Thus, data analytics is applied to estimate flexibility from these energy sectors to activate demand response. The complexity of social and external environment components, influencing thermal consumptions, are aggregated to estimate thermal demands using the neural net and similar day method. These methods are applicable and simple to generate appropriate estimated values, which are compared with values from time-series estimations techniques. The advantages of data analysis and thermal storage tank usage for optimal scheduling of an electric boiler based on the spot price of electricity is demonstrated.

From a spatial perspective, the individual thermal units in residences are examined for its relevance to flexibility and impact in integrated LV residential network. Then the heating sector is aggregated to provide services to the local area, represented by the LV grid. The outcome of these analyses is investigated to identify possible integration options concerning technical/social complexities, hosting capability and immediate need for electric grid reinforcement.

Finally, coordinated operation of thermal and transportation sector at each residence in the LV network are further analysed with demand response to enable efficient monitoring and flexible operation. The demand response control units are local and autonomous. A rule-based method for charging of electric vehicles is discussed to avoid communication infrastructure necessary for extensive data handling and optimisation process. Comprehensive models of control architecture deal with priority based on energy requirements and location of loads in the radial feeder of LV grid. This technique helps to support the flexible operation of thermal and transportation loads within the operational limits of the electricity network while securing end-users need simultaneously.

Resumé

Global bekymring om at reducere CO₂ udledning har ledt blikket mod energisystemer der er uafhængige af fossile brændstoffer i alle energisektorer. Forskellige energisektorer såsom elektricitet, opvarmning / køling, gas og transport drives i dag uafhængigt af hinanden. Mens integreret drift af det termiske og elektriske område eller transport- og elsystemet er populært blandt forskerne. For at udnytte den langsigtede fordel ved vedvarende energi er den integrerede drift af multienergisystemet afgørende. Hvert energisystem skal være i stand til at fungere i harmoni med gensidige fordele fra hinanden under stabil drift. For at opnå sikkerhed og effektivitet i det integrerede energisystem er den fleksible drift af de forskellige energisystemer nødvendig. På elområdet, der er det mest sårbare system med svingende produktion fra vedvarende energi, opnås fleksibilitet fra integrerede energisystemer. Da elektricitet ikke kan opbevares direkte uden høje omkostninger, kan der drages fordel af termiske, gas- og transportsystemer til at lagre overskudsproduktion fra vedvarende energi. På den anden side kan konvertering af elektricitet fra disse lagre tjene som reservekapacitet ved underskud i elproduktionen fra vedvarende energi. Den danske energimodel har støttet teknisk innovation og udvikling for at styrke en bæredygtig integration af vedvarende energikilder som en multi-energiesektor.

Dansk infrastruktur for el og varme har udviklet sig fra centraliserede til decentrale systemer i de senere år. Det decentraliserede system har forbedret sikkerhed, effektivitet og pålidelighed i energitransmission og -forbrug. Således undersøges begrebet decentraliserede og integrerede elektrificerede varme og transportsystemer i lavspændings (LV) distributionsnettet i dette forskningsarbejde. Koblingen af varme, el og transport systemerne i lavspændingsnettet i byområder skaber hidtil usete udfordringer inden for modellering, planlægning, drift og styring af disse systemer. En passende og gennemførlig metode undersøges for at identificere og tackle disse udfordringer. Som en konsekvens undersøges et kompromis mellem numeriske kompleksiteter og fysiske fænomener ved modellerne af energikomponenterne. En numerisk model for et eksisterende

dansk LV-net for et byområde betragtes som en testplatform til tilstand-simulering af den integrerede drift af elektrificerede varme og transportenheder. Faktiske data fra energidistributørerne analyseres og diagnosticeres for at forstå og forbedre det integrerede systems fleksibilitet.

Relevant modellering af de aktive styrbare laster og energilagere er afgørende for optimal drift og fleksibel kontrol. De termiske belastninger (el-kedel og varmepumper) og elektriske køretøjer betragtes som aktive belastninger. De generelle og specifikke muligheder ved en gennemsnitsmodel sammenlignet med en lagdelt model af den termiske lagringstank er præsenteret. Indflydelsen af disse modeller på de tekniske parametre og arbejdsomfang diskuteres kort.

Forbrugsmønstrene for el, varme og transportbehov er baseret på brugernes komfort. Dataanalyse anvendes således til at estimere fleksibilitet fra disse energisektorer for at aktivere fleksibelt elforbrug. Komplexiteten af sociale og eksterne miljøkomponenter, der påvirker den termiske forbrug, aggregeres for at estimere det termiske forbrug ved hjælp af neurale net og lignende dags metode. Disse metoder er anvendelige og enkle at anvende til at generere passende estimerede værdier, der sammenlignes med værdier fra tidsserieestimeringsteknikker. Fordelene ved dataanalyse og anvendelse af termisk lagertank til optimal planlægning af en elektrisk kedel baseret på spotprisen på elektricitet er vist.

Fra et rumligt perspektiv undersøges de individuelle termiske enheder i boliger for deres relevans for fleksibilitet og påvirkninger i det integrerede lavspændings i byområdet. Derefter aggregeres varmesektorens behov med henblik på at levere tjenester til det lokale område, repræsenteret ved lavspændingsnettet. Resultatet af disse analyser undersøges for at identificere mulige integrationsmuligheder vedrørende tekniske / sociale kompleksiteter, overførings kapacitet for nettet og behov for forstærkning af det elektriske net i nær fremtid.

Endelig analyseres koordineret drift af varme og transportsektoren ved hver bolig i lavspændingsnettet yderligere med henblik på fleksibel forbrug for at muliggøre effektiv overvågning og fleksibel drift. Enhederne til styring af det fleksible forbrug er lokale og autonome. En regelbaseret metode til opladning af elektriske køretøjer diskuteres for at undgå yderligere kommunikationsinfrastruktur, der ellers ville være nødvendig til omfattende datahåndterings- og optimeringsprocesser. Omfattende modeller af styringsopsætningen beskæftiger sig med prioritering baseret på energibehov og placeringen af belastningerne på lavspændingsradialen. Denne teknik hjælper med at understøtte den fleksible drift af varme- og transportbelastningerne inden for elnettets driftsgrænser samtidig med at man sikrer.

Contents

Preface	iii
Curriculum Vitae	v
Abstract	vii
Resumé	ix
I Report	1
Chapter 1	3
1 Introduction	3
1.1 Background	4
1.2 State of The Art	6
1.3 Hypothesis	8
1.4 Project Objective	8
1.5 Methodology	9
1.6 Limitations	11
1.7 Thesis Outline and Publications	13
Chapter 2	17
2 Modelling of Active Loads and Thermal Storage Tanks	17
2.1 Basic Terminologies	18
2.2 Electric Boiler (EB)	22
2.3 Heat Pump (HP)	23
2.4 Thermal Storage Tank	24
2.5 Comparison of Thermal Storage Tank Models	36
2.6 Modelling of EV	40
2.7 Low Voltage Residential Grid Network	41
2.8 Conclusion	42

Contents

Chapter 3	43
3 Data Analytics of Energy Consumption	43
3.1 Analysis of Thermal Data in Residential Area	43
3.2 Supply and Return Temperature Analysis of District Hot Water	47
3.3 Estimation of Thermal Demand	49
3.4 Residential and Thermal Load Profile	54
3.5 Analysis of Driving Distance of Passenger Car	56
3.6 Conclusion	59
Chapter 4	61
4 Optimal Schedule for Flexible Operation of The Electric Boiler	61
4.1 Optimisation of EB Operation	61
Chapter 5	69
5 Impact Assessment of Flexible Thermal Loads in Low Voltage Distribution Network	69
5.1 Characteristic of LV Residential Distribution Network .	69
5.2 Flexibility and Impact Assessment of The EBs and HPs in LV Residential Distribution Network	70
5.3 Accommodation of EBs in LV Grid	77
5.4 Grid Impact With EB as A Central Thermal Unit	79
5.5 Conclusion	83
Chapter 6	85
6 Integrated and Autonomous Operation of the Flexible Loads .	85
6.1 Operational Flexibility of Electrified Transport and Thermal Units in The Distribution Grid	86
6.2 EV Charging Management	88
6.3 Control of EV and HP	91
6.4 Results and Discussion	97
6.5 Conclusion	98
Chapter 7	99
7 Conclusion	99
7.1 Significant Outcome	100
7.2 Future Work	102
References	103
II Papers	111
A Modelling of hot water storage tank for electric grid integration and demand response control	113

Contents

B	Unleashing Flexibility from Electric Boilers and Heat Pumps in Danish Residential Distribution Network	121
C	Impact Assessment of Electric Boilers in Low Voltage Distribution Network	135
D	Autonomous Controller For Flexible Operation Of Heat Pumps In Low Voltage Distribution Network	143
E	Flexibility From Electric Boiler and Thermal Storage For Multi Energy System Interaction	165
F	Operational flexibility of electrified transport and thermal units in distribution grid	181

Contents

Part I

Report

Chapter 1

1 Introduction

With 42% of Denmark's electricity consumption produced by wind in 2015 along with surplus production for almost 16% of the time in a year [1], electric power sectors in Denmark have entered a new era. There are many unprecedented options in the electricity market to manage flexible consumption. Flexibility helps to utilise the surplus power produced with the help of flexible loads, e.g., electric boilers (EBs), heats pumps (HPs), electric vehicles (EVs) or any other forms of energy consumption units and storage systems. Still, there is a necessity to address some issues and challenges on the low voltage (LV) electricity networks, on how to integrate and coordinate these thermal and transportation systems and identify synergy between them [2].

Western Denmark and eastern Denmark had negative prices of electricity for 65 hours and 36 hours respectively in 2015 [3]. As a result, wind turbine owners are subjected to turn off their generation for hours during which the supply of electricity exceeds the demand. Meanwhile, 63% of the private Danish houses' thermal energy demands, for space heating and domestic hot water usages, are supplied through district heating (DH) in 2015 [4]. Various heat production technologies, such as combined heat and power (CHP), solar heating, waste to energy, gas boilers, biomass boilers and heating pumps and electric cartridges, are adopted in Denmark [C3]. With the incentive to become carbon neutral in the heating sector by 2030, renewables need to contribute 100% of heating demands. This incentive arises potential integration of the thermal and electric networks to support grid ancillaries as the flexible thermal load. Further, in February 2008, a new climate and energy agreement was established to promote a demonstration program for EVs [5]. These initiatives give strong motivation for the growth of EVs and distributed thermal units into a very sizeable niche in the future market. Thus, it is required to investigate the impact of the thermal and EV loads in the LV network. This investigation is useful to develop a control

system to manage and flexibly operate the integrated thermal and EV loads in the existing low voltage distribution system with or without any reinforcement.

1.1 Background

A flexible electricity system helps to support the variations in renewable generation to effectively balance the supply and demand. This balance is possible through the use of energy storage system [6]. The estimated reserve requirement increases with 1.5% - 4% for every 10% increment in wind penetration [7]. The researchers are dealing with the challenges to store the massive scale of electricity produced from renewables economically. On the other hand, active power management of flexible consumer loads is an alternative option. The examples of the flexible consumer loads are plugged-in electric vehicles (PEVs) [8], district heating or cooling [9] system, residential energy loads such as washing machine, heating and cooling systems [10] [11]. These loads can be scheduled and operated flexibly to support the electric grid. The concept of the integrated energy system, involving the integration of various energy storages and loads as a future perspective in Denmark, is shown in Fig. 1. Energy production, storage, distribution and consumption within an integrated energy system are linked in an intelligent way to flexibly operate and support for good synergy between each energy network [12].

Power to heat (P2H) and power to cooling (P2C): The thermal unit (EB or HP) is coupled to the electricity system either by CHP (produces electricity as well as generates heat), or by power-to-heat plants such as electric boilers and heat pumps (which produces both heating and cooling at the same time, based on its operating cycle). The storage capacity of thermal network can be utilised as a buffer between the thermal sources and loads, to increase the operational flexibility of combined electric and thermal systems [13]. The concept of 4th generation district heating, including the relations to district cooling and the concepts of smart energy and smart thermal grids, has been presented in [14]. It identifies the future challenges of non-fossil heat supply supported by renewable energy. The characteristic and problems of district cooling systems when integrated with different sustainable energy technologies are discussed along with optimisation operation and control in [15]. In [16] optimisation process based on, energy generation, energy distribution, heat substations, and terminal users are discussed.

Power to transport (P2T): Transportation accounts around 25% of all energy consumption in the world [17]. Electricity, biofuels, green gases, batteries, etc., are considered as a significant alternative to replacing fossil fuel for the transportation sector. The ability of PEVs to balance electric

1. Introduction

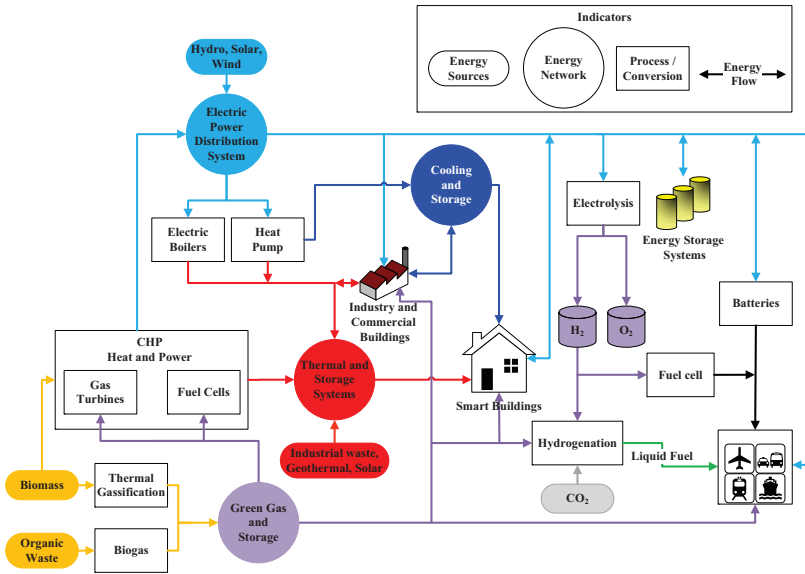


Fig. 1: Integrated energy system [12].

power demand has been studied in [18] with the concept of energy transportation. Integration of the electricity, heating, and transport sectors, in combination with various storage options, has been discussed in [19]. The application of vehicle to grid (V2G) concept launches alternatives to support grid as well as storage of power into batteries of EV [20] [21]. These potential applications of EVs give motivation for integration of transportation units in the multi-energy system.

Power to gas (P2G): There are several proven technologies for conversion of electricity into gas (such as hydrogen, oxygen, ammonia etc.,) which can be stored and utilised as a source of fuel. Denmark’s gas grid is on its way to being entirely supported by green gas in 2035 [22]. The gas grid has capabilities to support the electric grid with high share of renewables [23].

Application of the integrated energy system helps to manage the interaction between the integration of power systems incorporating higher shares of renewable energy. With the potential flexibility from heating and mobility infrastructures, there is no need for immediate grid extensions [24]. The proper interaction not only helps in eliminating power losses due to the human factor but also enhances the human decision-making process by providing adequate information about energy consumption frequently. The effective interaction can be done through smart metering, automation and

flexible demand-based control process. Demand response is termed as flexibility in electricity usage of the customer from their regular consumption pattern in response to change in electricity price or system reliability. It is foremost essential to enhance the power quality and maintain grid parameters such as voltage and frequency within the limit. Hence, control based on demand response is one of the possible solutions to overcome the challenges resulting from grid integration of plugged-in electric vehicles (PEV) and thermal systems without the need of immediate reinforcement in new infrastructure.

To utilise renewable energy sources as efficiently as possible and to make important planning and the operational decision based on demand response, load forecasting plays a vital role. Smart meter data and IT infrastructure (data related with district heating, cooling, EV, electric demand and generation) would be immensely useful for better forecasting to enable efficient coordination and use of smart energy systems. A forecast is the most crucial factor in resource planning and estimation of flexibility.

1.2 State of The Art

The average model of the thermal storage tank is widely used to evaluate performance from the integration of thermal and electricity grid [25,26]. To enhance the flexible operation of the thermal system the information of energy content in the thermal storage tank, in term of measurable physical parameters such as temperature and level of hot water, is vital. This information is possible with the use of stratified thermal storage tank models [27–29].

Diversity in thermal loads are investigated in several research [30–33]. However, the identification of daily average residential thermal load profile, considering seasonal, and everyday users' behaviour, is generally missing in the literature. Also, the analysis of temperature profiles of the district hot water circulating through the district heating provides better knowledge of energy carrier status in the district heating system. Proper understanding of thermal demand pattern provides essential details for investigation of reliable tools to estimate flexibility from power to heat system. On the other hand, the knowledge of EVs' state of charge (SOC) is crucial for flexibility study on their grid integration. The SOC of EVs based on the distance travelled by the passenger cars are widely applied by researchers in [8, 30, 34, 35]. However, there is one of the key factors affecting the SOC of EVs is the driving nature of the individual [36]. Incorporating this factor, in the generation of SOC, for EVs provides a more reliable value for charging requirements.

To utilize renewable energy sources as efficiently as possible and to make important planning and the operational decision based on demand response, load forecasting plays a vital role. Smart meter data and IT

1. Introduction

infrastructure are immensely useful for better prediction to enable efficient coordination and use of integrated energy systems. Establishment of these infrastructures is costly. The privacy policy is required to handle individual public data. Forecasting, of thermal demand in district heating, using time series neural network are investigated in [25, 37–39] and Box-Jenkins method in [40]. Here, the forecast is performed by the frequent update of the previous measurement of forecasting variables, which requires proper communication for continuous computation and measurement of the required parameters. Also, the results of estimated thermal demand are not compared with the average thermal demand to verify the users' consumptions behaviour patterns. The selection of environment variables for thermal demand estimation is presented in [41], without considering social components.

Few researchers have worked in the area focusing on the integrated operation of thermal, transportation and electrical energy network in low voltage residential grid. Feasibility study on integrated electrical and thermal units are cited and presented in [42–45]. Influence and flexibility benefits from integrated heat pumps and EVs to the power system is presented in [46–53]. However, the detail impact assessment due to the integrated operation of distributed flexible loads in the power system is missing. These details include the local characteristic of grid voltages at the point of coupling, cables and transformer loading, the electrical grid hosting capacity.

Demand response is widely used for the active participation of consumers. Consumers participate to flexibly operate energy consumptions devices, for shaping the load profile while balancing energy demand and supply in the integrated energy system [54]. Low priority loads can be subjected to a load shifting process so that it is operated when electricity demand is not in peak. A hierarchical structure for controlling the demand response of HP and PEV in a low voltage grid has been presented in [48, 55]. The hierarchical arrangement of the distribution system supervision helps to identify, evaluate, and tackle the technical constraints in the LV network, where a voltage drop is a crucial factor [48]. Control design methods based on model predictive control is discussed in [56]. These methods require expensive communication infrastructure. Optimal scheduling of thermal units has been studied in [57–62] without considering impact and violation of grid voltage and loadings. The concept of the local adaptive controller for flexible loads operation in LV grid is well-explored in [51, 54]. Here, the settings of the reference parameter for the grid voltage is specific at each node. This parameter requires regular update based on the change in loads and causes practical complexities.

The hypothesis and objectives determined in this research work to address the research gap, are as follows.

1.3 Hypothesis

Thermal heating and transportation systems integrated into the low voltage electric network can serve as the flexible loads. The flexible load has direct/indirect storage potential to increase the dynamic stability of the grid in terms of power production from renewable sources and consumption. It leads to the research question, is it feasible to integrate heating and transportation system into the existing low voltage grid as the active-controllable loads? If yes, how will this huge amount of loads affect the existing network grid? Is there enough capacity? How can the active load management system support the network grid, while considering grid issues such as voltage dip, line loadings, grid congestion, utilisation of maximum capacity, and enhance optimal usage of storage flexibility? If not, what new alternatives are required to operate and control medium and low voltage networks considering technical and economic aspects? This project has tried to find this solution. The following hypothesis are based on these research questions.

- It is possible to integrate and use the thermal and transportation sectors as flexible loads in the existing low voltage electricity distribution network, with or without minimal reinforcement.
- It is possible to use a proper methodology for demand response control of thermal and transportation system integration into the grid. Using the appropriate model of demand response, for shaping the load profile and balancing energy demand/supply, helps to increase operational efficiency and hosting capabilities of the LV network.
- It is possible to use a large amount of thermal data generated by metering for training a forecasting tool, in association with dependent environment variables, to estimate the behaviour of the end-user consumption profiles, without hampering the privacy of individual consumers.
- The estimated thermal data is useful in the optimised operation of thermal unit with storage system, to store energy during surplus electricity generation from renewables, and fulfil customer demand simultaneously despite some error in estimation.

1.4 Project Objective

The project objectives are developed based on the hypotheses presented earlier.

- Develop parametric models of individual components of the energy network (thermal heating and storages, plugged-in electric vehicles),

1. Introduction

for steady-state analysis and flexibility estimation when integrated into the electrical low voltage network.

- Analyse the data from the meter reading, of the electrical and the thermal network, and identify the consumption profiles of the thermal and the electricity demand respectively.
- Investigate the surveyed data, on travel distance of passenger cars in Denmark, and identify the distribution of the energy consumptions when replaced with EVs.
- Develop a method to train the forecasting tools, to estimate the thermal demands, and use with demand response for active load management.
- Investigate on grid issues and optimal location of EBs and HPs when connected to LV grid. Investigations are done in electricity grid for voltage dip, grid congestion, utilisation of maximum capacity, utilisation of storage flexibility from active load management and overloading of transformer and cables.
- Combine the models of the electrical, thermal and plugged-in electric vehicles(PEVs) systems for load flow calculation and impact assessment of the combined system on electrical grid congestion. Investigate and set up the control method for demand response to support the integration of multi-energy systems (heating and transportation sector) in existing low voltage distribution network. The control method, on the other hand, makes sure to fulfil customer needs and priorities in general.

1.5 Methodology

The work starts with a simple idea, where the thermal demand in the individual houses is supplied using a heat pump or an electric boiler and thermal storage tank. Then the heating system is extended to involve a whole radial or area of the LV distribution network through a central heating system and the thermal distribution network, where different storages and heating possibilities are discussed. Finally, the transportation sector is taken into account where EVs are considered as the battery energy storages system. The storage possibilities from both the heating and transportation systems are considered simultaneously.

Mathematical modelling of thermal units (EB and HP), thermal storages system and EV is performed to suitably integrate into electrical grid network. Different mathematical models of the thermal storage tank, considering numerical complexities and dominant physical properties observed in practice such as stratification are developed, analysed and

compared with theoretical validation. The EV is modelled as the battery size of appropriate capacity. The depth of discharge of battery at the end of the day is considered for charging management.

The metering data, regarding consumption profiles of the electricity and heating networks, are studied to determine the consumer pattern and respective network limits. Thermal consumptions data, from Aalborg varmforsyning, are considered to investigate the thermal consumption profile of a residential area in Denmark. Hour by hour variation of the total load is used to illustrate the short term variation of consumption of thermal demand during different times of the year. Information on location, data acquisition and, analysis of the scenarios gave ideas on practical use case scenario (on metering of energy consumptions with the temperature of inlet and outlet of hot water into the residential building) under analysis.

An investigation of the EV users' driving pattern is used to develop the proper charging management strategy. Since there are very few EVs on the road in the present context, it is acceptable to assume that EV users will have the same behaviour as that of passenger cars. The statistics of passenger car use in Denmark are discussed to obtain the possible future use of electric vehicles (EVs). This study is useful to analyse the battery energy storage system to identify energy dissipation from EVs and energy requirement for charging.

These analyses of energy profiles from various energy networks help determine the integrated energy network limits and maintain network efficiency and reliability. Evaluation of thermal energy demand based on historical data is used for load forecasting. Simple yet effective load forecasting based on curve fitting techniques (neural net and similar day method) is used to estimate thermal demand based on environmental factors and consumption patterns. Historical records of energy meters of particular sites are used to train and verify the estimation model. Estimated values from the forecasting model are used to determine optimal active load management. The control signals, based on the optimal active load management, operates thermal generation unit. The optimisation procedure manages thermal energy storage in several time scales, considering spot electricity market pricing and peak electricity demands.

Active load modelling (using dynamic mathematical model) and control systems are implemented and validated. Different levels of control are investigated to study the impact on the electricity network such as grid voltage, line and transformer loadings, utilisation of capacity, and hosting capacity due to the integration of thermal loads in the LV grid network. Different case studies are simulated and analysed. Possible integration of locally centralise and decentralised heat generation unit and storage system, distributed throughout the residential area in Denmark, are analysed. Discussion on the significance of locally centralised and individual units, in

1. Introduction

terms of operational control, flexibility and network capacities are done.

The impact assessment of electric grid network integrated with thermal and transportation loads are performed. Based on this assessment, suitable grid reinforcement is suggested. The pattern of energy required by electricity, thermal and EVs are investigated to specify flexibility in demand response based on priorities and distributed control. Based on the knowledge of load profiles from individual energy networks, and electric grid limits, suitable control system for demand response is developed. System integration for flexibility estimation and demand response control, based on distributed control systems, are developed considering various issues. These issues are based on electricity grid constraints, heating and storage constraints, data handling and transfer, and communication constraints. The control system is based on ON/OFF operations of EBs, HPs and charging of EVs. The measurement voltage at the point of coupling of the thermal unit along with temperature and level of hot water inside the storage tank is used as essential information for flexible control of the thermal unit. The concept of ON/OFF delays in the operation of thermal and transportation loads is developed to prioritise operation of these loads at the far end of the radial feeder in the electrical network. The ON/OFF delays are based on terminal voltage measurement at the point of coupling and type of loads, such as thermal or transportation. A rule-based method is implemented to manage the charging of EVs. This method avoids the requirement of extensive data handling, complex optimisation problem and requirement of costly communication infrastructure.

The simulation model, for the integration of thermal and transportation units, is implemented in a typical Danish energy grid model. The outcome of the project serves as the basis for validation of the model and are useful to further determine the several test and case study scenarios for flexible consumer strategies. The simulation models are developed in various simulation environments such as MATLAB and DigSILENT power factory.

1.6 Limitations

The following limitations are considered on the modelling of the integrated systems under considerations.

- All the loads integrated to the electrical network are considered as 3-phase. This consideration simplifies the network analysis as a balanced system instead of unbalanced single-phase problems. As all the residences in Denmark are provided with 3-phase supply, the outcome of the project is quite significant with a practical scenario. However, unbalance problems associated with single-network were not investigated.

- Modelling of the hot water storage tank is simplified with a first-order linear differential equation. The modelling is based on energy balance. Hence, the information on physical phenomena such as temperature and level of hot water in the stratified layers are sufficient and reliable for flexible operation under operating limits of the system under study.
- The average load profiles, in terms of periodic measurements, of thermal and electrical measurements are considered. Appropriate noise, in the average electricity consumptions of individual houses, are integrated to emulate the real scenario. However, similar thermal load profiles with different magnitudes, based on analysis of historical data, are considered for thermal demand of individual houses. The use of a storage tank decouples the thermal demand and generation. Thus, the effect of an average load profile is still appropriate for impact assessment in the electricity grid and flexible operation of thermal units.
- The study of the thermal loads from individual residences are from a different area than the presented LV network and its associated electricity consumptions. The distribution of thermal loads is proportional to electricity consumptions, which may not stay true in reality.
- EVs driving profile is based on historical data of passenger car. This analysis, along with the aggressiveness factor of drivers, is used to determine the state of charge of EVs. EVs with different battery sizes and SOC levels are randomly distributed in individual houses, considering one EV in each house.
- The choice of EVs and the capacities of the thermal units, along with their energy requirements, are the personal choices of individual users. However, the randomness in energy consumptions with different sizes of EVs and thermal units are still good enough to investing hosting capacity of the electrical network, access significance of developing demand response controls, and access possible flexibility from thermal and mobility infrastructure.
- The spot price of electricity is related to the excess generation of electricity from renewables. It is assumed that when electricity prices are lower, there are more generations from renewable sources. This assumption is made without considering the complexities of electricity trading in the electricity market and penetration of renewable sources in the electricity grid. This assumption stays true as electricity is traded even with negative prices when there are surplus generations from renewables. The spot price of electricity in Nord pool is

1. Introduction

determined 24 hours prior, with one-hour trading duration, the electricity is sold in the market. Thus, the spot price of electricity provides initiative for optimal scheduling of thermal units to store and utilise thermal energy production from renewables.

- The power quality issues, due to connection and disconnection of loads by active control, are not considered.
- Only steady-state analysis is performed to investigate grid issues, based on operating limits of node voltages and loading of electrical network components, due to the integration of thermal and transportation units.

1.7 Thesis Outline and Publications

The thesis consists of two parts. Part I-Report and Part II-Publications.

Part I-Report

The report part consists of seven chapters. It consists of a summary of all the publications presented in part II, in an organised way. It also includes some extra relevant work done.

Chapter 1: It consists of a brief introduction and motivation related to design of concept and work performed. A short background of the integrated energy system and its significance in future Danish energy infrastructure is discussed. As a part of an integrated energy system, the objective of work is defined for thermal and mobility integration in Danish low voltage distribution network. Methodology and technical limitations are discussed in brief, along with the significance of work done. Finally, this chapter is concluded with the organisation of work done.

Chapter 2: It starts with the fundamental terminologies in thermodynamics to understand the modelling process of the thermal system and their significance as a flexible load. Modelling of thermal units, electrical grid and EV system are discussed in brief with appropriate and applicable equations. The thermal unit consists of an electric boiler/ heat pump and thermal storage tanks. The comparisons of different models of thermal storage tanks are discussed with their possible practical applications in control and flexible operations.

Chapter 3: It begins with an analysis of thermal demand in a residential area. Thermal energy consumptions along with the temperature of supply and return water in different feeders of district heating network supplying several residential buildings are analysed. Thermal demand estimation models, based on curve fitting tools, are developed and verified. It estimates the hourly average thermal consumptions of a particular residential area. Daily average energy consumption profile of electricity and thermal demand

are determined based on real measurement of data. The amount of thermal and electricity demand of individual houses are presented for further analysis. Also, the study of actual data on driving distance of passenger car is utilised to generate energy consumption by EVs at the end of the day.

Chapter 4: An application of thermal demand estimation, based on the spot price of electricity, is presented with optimisation of electric boiler operation. The EB and storage system is supplying thermal demand to several buildings in the residential area as a single central unit. The significant capability of the thermal storage tank to compensate for errors in thermal demand estimation and operational flexibility with proper control is demonstrated with several case studies. The case studies are based on different spot prices of electricity and errors in thermal demand estimations.

Chapter 5: Impact assessment of EBs and HPs, separately, in individual houses in LV distribution network are presented in this chapter. Various possible control parameters to control the operation of each EBs and HPs are identified for flexible service of thermal units within the operating limit of the electricity grid. The advantages of using central thermal units, providing thermal loads covering the area, within the LV residential network is discussed. Benefits in terms of user initiative for flexible control, user privacy and electricity grid limits regarding voltage and loading are detailed.

Chapter 6: The impact assessment and demand response control for the integration of HPs and EVs in all the houses connected in the LV distribution grid are presented. An adaptive and autonomous control architecture is discussed to flexibly operate and coordinate within the network utilising measurement of terminal voltage at the point of coupling of devices in operation.

Chapter 7: The summary of the thesis with its significant outcome and possible future work is presented.

Part II-Publications

This part of the report consists of peer-reviewed conferences and journal articles. The publications are the outcome of the researcher work as a part of PhD.

Conference Publications

- **C1:** R. Sinha, B. B. Jensen, J. R. Pillai, C. Bojesen, and B. Moller-Jensen, "Modelling of hot water storage tank for electric grid integration and demand response control," in *2017 52nd International Universities Power Engineering Conference (UIPEC), Greece, Aug 2017*, pp. 1–6.

1. Introduction

- **C2:** R. Sinha, B. B. Jensen, J. R. Pillai, and B. Moller-Jensen, "Unleashing flexibility from electric boilers and heat pumps in danish residential distribution network," in *CIGRE 2018, Paris*, 2018.
- **C3:** R. Sinha, B. Bak-Jensen, and J. Pillai, "Impact assessment of electric boilers in low voltage distribution network," in *Proceedings of the 2018 IEEE Power & Energy Society General Meeting (PESGM), United States: IEEE*, Aug. 2018, pp. 1–5.

Journal Publications

- **J1:** R. Sinha, B. Bak-Jensen, and J. Radhakrishna Pillai, "Autonomous controller for flexible operation of heat pumps in low-voltage distribution network," *Energies*, vol. 12, no. 8, 2019.
- **J2:** R. Sinha, B. Bak-Jensen, J. Radhakrishna Pillai and H. Zareipour, "Flexibility from electric boiler and thermal storage for multi energy system interaction," *Submitted for peer review in Sustainable Energy, Grids and Networks*, 2019.
- **J3:** R. Sinha, B. Bak-Jensen, and J. Radhakrishna Pillai, "Operational flexibility of electrified transport and thermal units in the distribution grid," *Submitted for peer review in International Journal of Electrical Power & Energy Systems*, 2019.

The major contents of chapters related to publications are compiled in table 1.

Table 1: Compilation of publications in respective chapters

Chapters	C1	C2	C3	J1	J2	J3
Chapter 1						
Chapter 2	X	X		X	X	X
Chapter 3			X		X	X
Chapter 4					X	
Chapter 5		X	X			
Chapter 6				X		X
Chapter 7						

Chapter 2

2 Modelling of Active Loads and Thermal Storage Tanks

In this chapter, some relevant definitions of thermodynamics are presented for a clear understanding of the modelling concept to define the thermal storage tank. Mathematical modelling of various active loads representing thermal heating and storage, and electric vehicles are introduced. Low voltage distribution grid, further used for impact and flexibility studies due to the integration of thermal and electrified transport, is discussed in brief. Thermal heating elements, such as heat pump (HP) and electric boiler (EB), are suitably modelled as a 3-phase load for electrical grid integration. Flexibility from the thermal system is attained using the thermal storage system. Three different mathematical models of a thermal storage tank: single-mass model, two-mass model, and multi-layered stratified model are discussed with its significant capabilities to analyse flexibility in energy transfer through demand response. Different measurable parameters, to reflect the energy stored in the thermal storage tank, such as temperature and level of hot water along with its significance to represent practical scenarios are discussed. Theoretical validations of these models are performed. All these models are compared based on average temperature, losses, and energy stored inside the storage tank. These comparisons help to understand how these models are capable of providing detailed information on the physical phenomena inside the tank. This information supports achieving flexibility in demand response within the operating limits of the system under study. The modelling and validation of the single-mass and the two-mass model of the storage tank is based on the work presented in [C1]. The modelling and validation of multi-layered stratified thermal storage tank have been performed in [J2]. The modelling of EB is presented in [C1] and HP in [C2],[J1]. The modelling of electric vehicles is performed in [J3].

2.1 Basic Terminologies

This section of the report provides some of the fundamental thermodynamics terminologies that helps understand the modelling process of the thermal storage systems.

Conservation of Energy: Regardless of energy sources, the amount of heat energy required to raise the temperature of the particular substance of mass (m) from temperature T_1 to T_2 is always the same. It is given by eq.(1) [63].

$$Q = Cm\Delta t \quad [J] \quad (1)$$

Where,

- Q = heat energy [J]
- m = mass of the object [kg]
- C = specific heat capacity [J/kgK]
- Δt = change in temperature ($T_2 - T_1$) [K]

Specific heat capacity: It is the amount of heat energy required to raise the temperature by one unit of the unit mass of material. Specific heat capacity of water (C_w) is given by eq.(2) [63].

$$C_w = \frac{Q}{m\Delta T} \quad \left[\frac{J}{kg.K}\right] \quad (2)$$

Here, Q is the amount of heat transfer (J), m is the mass of water (kg) and Δt is the rise in temperature (K). Water being approximated as an incompressible substance, its specific heat capacity at constant volume is considered to be equal as with constant pressure unless the pressure is extremely high [63].

Thermal capacitance: It is the capacity of a material to store heat energy. It is defined as the amount of heat flow required to raise the temperature of the substance by one unit per second. The thermal capacitance is calculated as shown in eq.(3) [63].

$$C_{th} = mC \quad \left[\frac{J}{K}\right] \quad (3)$$

Where,

- C_{th} = thermal capacitance [$\frac{J}{K}$]
- V = volume [m^3]
- C = specific heat capacity [$\frac{J}{kgK}$]
- m = mass of the object [kg]

Heat transfer due to conduction: The heat transfer due to conduction is calculated using eq.(4) [63].

$$\dot{Q}_{cond} = \frac{kA(T_h - T_c)}{x} \quad \left[\frac{J}{s}\right] \quad (4)$$

Where,

2. Modelling of Active Loads and Thermal Storage Tanks

\dot{Q}_{cond} = heat conduction rate through the layer of storage [$\frac{J}{s}$]
 k = thermal conductivity of barrier [$W/m.K$]
 A = Area [m^2]
 T_h = temperature of hot surface [K]
 T_c = temperature of cold surface [K]
 x = thickness of barrier [m]

Heat transfer due to convection: The heat transfer due to convection is calculated using eq.(5) [63].

$$\dot{Q}_{conv} = hA(T_h - T_c) \quad \left[\frac{J}{s}\right] \quad (5)$$

Where,

\dot{Q}_{conv} = rate of heat conduction through a layer of storage [$\frac{J}{s}$]
 h = convective heat transfer coefficient [W/m^2K]
 A = Area [m^2]
 T_h = temperature of hot surface [K]
 T_c = temperature of cold surface [K]

Overall heat transfer coefficient: Let the wall of the storage tank or boiler be of uniform and homogeneous material having constant thermal conductivity (k). The storage tank wall is exposed to hot water at temperature (T_b) and cold air at temperature (T_a) on either side of the wall as shown in Fig. 2. Following assumptions are considered.

- Same amount of heat (\dot{Q}_{loss}) passes through each section during steady state.
- Heat transfer is by convection across the hot and cold thin film layer near the surface of the wall and by conduction through the wall.
- Fluid temperatures sufficiently far from the wall, (T_b) and (T_a) are known.
- Surface temperatures (T_1) and (T_2) are unknown.
- Heat transfer area (A) is the same for all sections.

Let us consider the convective heat transfer coefficient of (h_h) and (h_c), wall thermal conductivity (k), and wall thickness (x). Then, the overall heat transfer coefficient (U), for the combined conductive-convective heat transfer \dot{Q}_{loss} between the tank and the ambient environment, is calculated as follows. Thermal losses through the hot film, tank wall, and cold film are calculated using eq.(6), eq.(7) and eq.(8) respectively.

$$\dot{Q}_{loss} = h_h A (T_b - T_1) \quad \left[\frac{J}{s}\right] \quad (6)$$

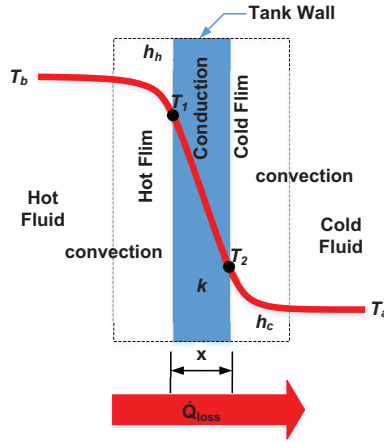


Fig. 2: Heat loss between hot water inside tank and ambient temperature.

$$\dot{Q}_{loss} = kA(T_1 - T_2) \quad \left[\frac{J}{s}\right] \quad (7)$$

$$\dot{Q}_{loss} = h_c A(T_2 - T_a) \quad \left[\frac{J}{s}\right] \quad (8)$$

solving eq.(6), (7) and (8).

$$\dot{Q}_{loss} = \frac{A(T_b - T_a)}{\left(\frac{1}{h_h} + \frac{x}{k} + \frac{1}{h_c}\right)} \quad \left[\frac{J}{s}\right] \quad (9)$$

Thus,

$$U = \frac{1}{\left(\frac{1}{h_h} + \frac{x}{k} + \frac{1}{h_c}\right)} \quad \left[\frac{W}{m^2 \cdot K}\right] \quad (10)$$

Mixing of liquid at two different temperatures:

Let,

the mass of hot liquid = m_h [kg]

the temperature of hot liquid = T_h [K]

the specific heat capacity of hot liquid = C_h [J/kgK]

the mass of cold liquid = m_c [kg]

the temperature of cold liquid = T_c [K]

the specific heat capacity of cold liquid = C_c [J/kgK]

the temperature of mixing of hot and cold liquid = T_x [K]

Then,

Heat lost by hot liquid = $m_h C_h (T_h - T_x)$ [J]

Heat gained by cold liquid = $m_c C_c (T_x - T_c)$ [J]

2. Modelling of Active Loads and Thermal Storage Tanks

Since, heat lost = heat gain

$$m_h C_h (T_h - T_x) = m_c C_c (T_x - T_c) \quad [J] \quad (11)$$

Rearranging eq.(11), we get eq.(12) which gives the final temperature of the mixture.

$$T_x = \frac{m_h C_h T_h + m_c C_c T_c}{m_h C_h + m_c C_c} \quad [K] \quad (12)$$

Considering $C_h = C_c$, eq.(12) can be written as eq.(13)

$$T_x = \frac{m_h T_h + m_c T_c}{m_h + m_c} \quad [K] \quad (13)$$

Let us consider the stratified layered storage tank as shown in Fig. 3. The mass of hot water inside the tank can be calculated as per eq.(14).

$$m_h = m_b - m_c \quad [kg] \quad (14)$$

m_h = total mass of hot water inside storage tank [kg]
 m_c = total mass of cold water inside storage tank [kg]
 m_b = total mass of storage tank ($m_b = m_h + m_c$) [kg]

Let us consider the thermal storage tank, where the ratio of hot water inside tank with respect to the total mass of water inside tank is given by eq.(15).

$$X_h = \frac{m_h}{m_b} \quad (15)$$

Thus,

$$m_h = X_h m_b \quad (16)$$

Similarly, the ratio of cold water inside tank with respect to the total mass of water inside tank is given by eq.(17)

$$X_c = \frac{m_c}{m_b} = 1 - X_h \quad (17)$$

Thus,

$$m_c = (1 - X_h) m_b \quad (18)$$

Hence, using eq.(16) and eq.(18) in eq.(13) and simplifying gives eq.(19) for average temperature (T_x) of mixing hot and cold water inside the storage tank.

$$T_x = X_h T_h + (1 - X_h) T_c \quad [K] \quad (19)$$

where, X_h is defined by eq.(15) as the ratio of hot water inside the storage tank.

Stratification: Difference between the density of hot and cold water causes buoyancy effect. As a consequence, there exists a layer of hot and cold water inside a storage tank. As cold water is denser than hot water, it remains at the bottom of the tank. This formation of different layers of water with different temperature is known as thermal water stratification [64]. The region between the layers with the steepest gradient of change in temperature is known as the thermocline. Thermocline prevents mixing of fluid within adjacent stratified layers. Fig. 3 illustrates the stratification of thermal layers in the storage tank with rapid change in temperature due to the reach of the thermocline. The thickness of a thermocline is determined by the parameter called effective diffusion factor (ϵ). The perfect stratification is caused by the laminar flow represented as $\epsilon = 1$ [65].

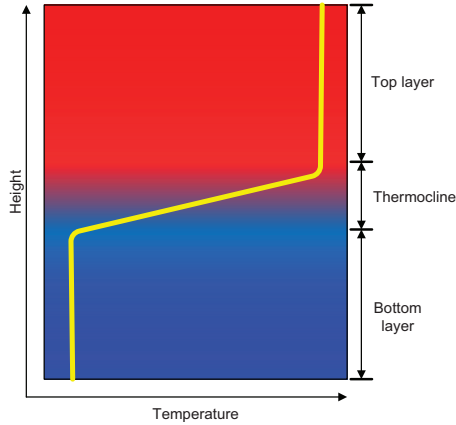


Fig. 3: Rapid change in temperature due to the reach of the thermocline and stratification of thermal layers.

2.2 Electric Boiler (EB)

With the resistive heating element, the electric boiler is assumed to be a constant impedance load [C1] [66]. Then, the heat delivered by EB is given by eq.(20) [C1].

$$\dot{Q}_{heat} = \frac{\eta}{100} \left(\frac{V_{poc}}{V_{r,b}} \right)^2 P_{r,b} \quad [W] \quad (20)$$

Where, η =efficiency of boiler [%], $P_{r,b}$ = rated power of boiler [W], $V_{r,b}$ = rated voltage of boiler [V] and V_{poc} = voltage at the point of coupling of the boiler into the grid [V].

The dependency of the heating load and the grid terminal voltage at the point of coupling discussed in [C1] [66], is seen from eq.(20). Eq.(20) plays

a vital role during the investigation of the interaction between thermal load and the electrical grid. The investigations are done for demand response management and flexibility in terms of operation of the thermal load while supporting grid voltage and thermal demand simultaneously.

2.3 Heat Pump (HP)

The heat pump transfers heat energy from source to sink with the help of a refrigerant. The basic operation principle of HP is well explained in [67]. The major components of the heat pump are evaporator, compressor and condenser. The energy from the low temperature and pressure source is extracted by the liquid refrigerant, through the heat pump's evaporator coil, and changes its state from liquid to gas. The gaseous fluid is then pressurised in a compressor, increasing its temperature. The heated refrigerant releases its energy in the form of heat and condenses back into liquid form in the condenser. The condenser is in the form of a coil or a pump heat exchanger which feeds a separate water storage tank. After condensation the refrigerant is passed through an expansion valve to release its pressure and the cycle is repeated again [67],[1]. Thus HPs, when activated, does not produce and deliver hot water instantly. A simple heat pump, for water heating system, is shown in Fig. 4.

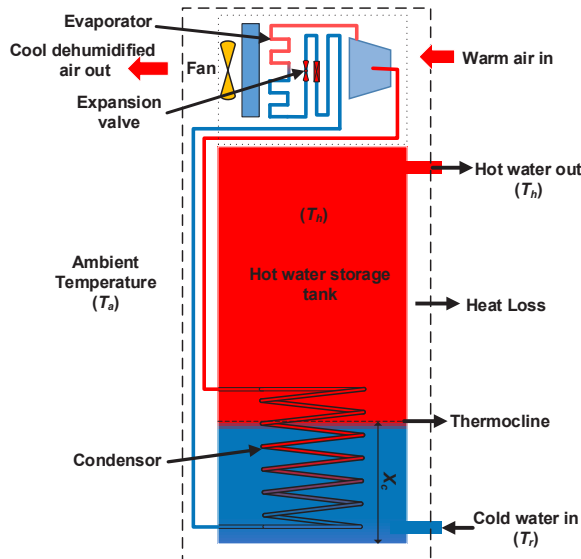


Fig. 4: A simple heat pump base water heating system [1]

The production and delivery of hot water from the HP is simplified as a step response presented in Fig. 5. When the HP is turned ON at time T_1 , hot

water is delivered after T_2 .

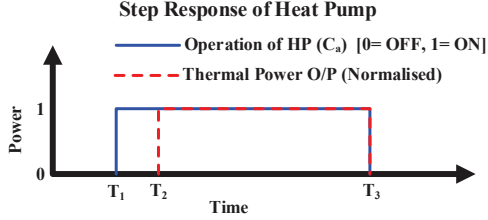


Fig. 5: Step response of HP during its ON and OFF operation [J1]

The detailed modelling of HP is discussed in [J1], [C2]. Eq.(21) represents the thermal power delivered by the HP. Here, P_{HP} is the electrical power rating of the HP (W), \dot{Q}_{Heat} is the heat delivered by HP (W), and COP is the coefficient of performance of HP. The COP of HP depends upon the temperature difference between the source and the sink. Seasonal fluctuation of source temperature affects the COP. The expression of COP as a function of ambient temperature, for a particular manufacturer, using polynomial interpolation is shown in eq.(22) [48]. Eq.(22) shows that, for analysis involving a particular day where temperature fluctuation is minimal, COP can be considered to be constant. The reactive power delivered or consumed by the HP is given by eq.(23), where θ is the phase angle.

$$\dot{Q}_{Heat} = COP \times P_{HP} \quad [W] \quad (21)$$

$$COP = -1.6e^{-5}T_a^3 + 0.00052T_a^2 + 0.073T_a + 3.4 \quad (22)$$

$$Q_{HP} = \mp P_{HP} \times \tan\theta \quad [VAR] \quad (23)$$

2.4 Thermal Storage Tank

The thermal storage tank plays an important role in providing flexibility in energy system networks and to optimise their functioning by decoupling demand and production. The size of the storage tank determines the extent of flexibility that can be exploited from the system. Larger the storage tank, higher is the flexibility. So, more amount of thermal energy can be stored and utilised for a long time without the frequent need for energy replenishment in the storage tank.

The thermal behaviour of the water inside the storage tank can be studied through numerical simulations which provides good agreement with the experimental results [68]. There are several ways to determine the mathematical modelling of the thermal storage tank. These modellings are based on energy equation, differential energy conservation equation in one

2. Modelling of Active Loads and Thermal Storage Tanks

direction, or all differential equations that govern the problem [68]. Most of the existing models are either one dimensional (where mass momentum is in the axial direction only), or two dimensional (where the mass momentum is in both radial and axial direction). The two-dimensional models are highly accurate and are capable of providing much detailed information regarding physical phenomena inside the tank. However, it requires enormous computational power and longer simulation time for a short real-time period. On the other hand, overly simplified models lack to reproduce some dominant physical phenomenon, whose effects are observed in practice, such as stratification in the storage tank. The necessary trade-off between numerical complexity in the model is required based on the scope of work [27,68].

Three different mathematical models of the thermal storage tank are modelled and verified theoretically in this thesis.

- Single-mass model (with a uniform temperature inside the storage tank)
- Two-mass model (with variable stratification height)
- Multi-layered stratification model (n-stratified layers)

The detailed derivations of, the single-mass and the two-mass, models are presented in [C1] along with theoretical validation of the work.

Single-mass model of the thermal storage tank

Consider the typical thermal storage tank, as shown in Fig. 6, with the heating element at the bottom of the tank. The hot water is drained from the top of the tank getting replaced with cold water from the bottom with the same flow rate.

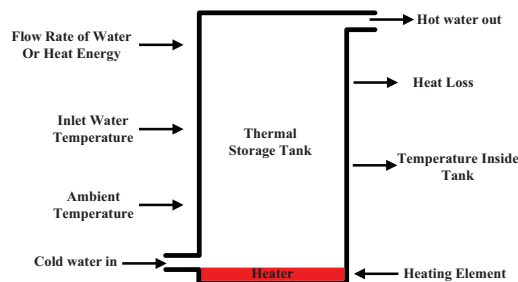


Fig. 6: Variable flow diagram in the thermal storage tank [C1]

In a single-mass model, it is considered that the entire tank, as shown in Fig. 6, has a uniform average temperature ($T_{avg,1}$). The temperature inside the tank changes with change in time due to energy losses to the ambient and net energy addition or withdrawal during the flow of water.

According to the law of energy conservation,

$$\dot{Q}_{boiler} = \dot{Q}_{heat} - \dot{Q}_{loss} - \dot{Q}_{demand} \quad (24)$$

Where,

- \dot{Q}_{boiler} = rate of net heat entering and leaving the boiler [J/s]
- \dot{Q}_{heat} = heat flow rate of heating element [J/s]
- \dot{Q}_{loss} = heat loss rate between tank and ambient environment due to conduction and convection [J/s]
- \dot{Q}_{demand} = Heat transfer due to water flow rate [J/s]

Thus, the average temperature gradient in the thermal storage tank is calculated using eq.(25) [C1].

$$\frac{dT_{avg,1}}{dt} = \frac{1}{C_b} [\dot{Q}_{heat} - \dot{Q}_{demand} - UA(T_{avg,1} - T_a)] \quad (25)$$

Where,

- C_b = Thermal capacitance of boiler [J/K]
- U = overall heat transfer coefficient [$W/m^2.K$]
- A = surface area of the tank [m^2]
- T_a = temperature of ambient environment [K]

Two-mass model (with variable stratification height)

The following assumptions are considered to model the storage tank, with stratified thermal layers [C1].

- The effective diffusivity factor (ϵ) equals to 1 indicating laminar flow and perfect stratification [65].
- The temperature of inlet cold water is constant.
- Two stratified layers of hot and cold water, with uniform temperatures, are present inside the storage tank.
- The thermocline is independent of radial distance and is horizontal as the effect of buoyancy is dominant compared to the radial distribution of stratification [27].

2. Modelling of Active Loads and Thermal Storage Tanks

- The heat transfer between the hot and cold zone within the tank, responsible for the widening of the thermocline, is neglected. This causes thickness of the thermocline to be very thin i.e, $\Delta x \rightarrow 0$ [69].
- The heating element is attached at the bottom of the storage tank allowing the presence of thermocline as long as stratified layers are undisturbed. The presence of thermocline is only possible when the boiler is turned OFF. The turbulence due to direct heat transfer from the bottom of the tank, during operation of heating element, eventually destroys the thermal stratification [28] resulting in the mixing of the hot and cold fluid.

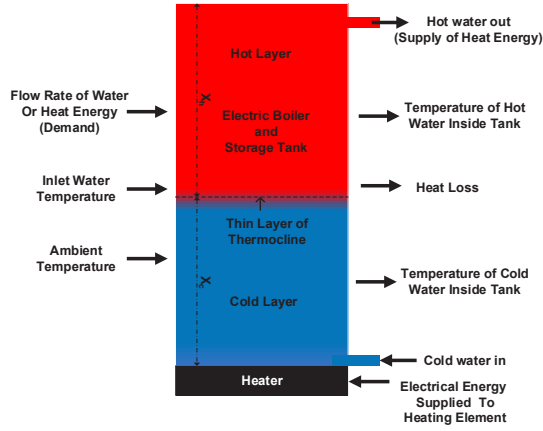


Fig. 7: Two-mass model of hot water storage tank [C1]

With one inlet and one outlet, the two-mass model shown in Fig. 7 accounts for perfect stratification with uniform temperatures (T_h) and (T_c) for the hot and cold layers respectively. The horizontal position of the thermocline changes depending upon the flow of hot water outside the tank, which is eventually replaced by cold water with the same amount. The temperature inside the layers varies with time due to energy losses to the ambient, and net energy addition or withdrawal during the flow of water.

During the presence of thermocline (i.e, the heater is turned OFF), the temperature gradient of hot and cold water is calculated as in eq.(26) and eq.(27) respectively [C1].

$$\frac{dT_h}{dt} = \frac{-1}{C_b X_h} [UA_s X_h (T_h - T_a) + UA_t (T_h - T_a)] \quad (26)$$

$$\frac{dT_c}{dt} = \frac{-1}{C_b X_c} [UA_s X_c (T_c - T_a) + C_w \dot{m}_2 (T_c - T_{iw})] \quad (27)$$

Where,

A_s and A_t = surface area of sidewall and top roof of the tank respectively [m^2] and $A = A_s + A_t$

C_b = thermal capacitance of boiler [J/K]

C_s = status of stratification

\dot{Q}_{demand} = heat demand transfer rate due to flow of water (Thermal Demand) [J/s]

\dot{Q}_{heat} = heat flow rate of heating element [J/s]

T_h , T_c , T_{out} , and T_a = temperature of the hot water, cold water, outlet and ambient respectively [K]

U = overall heat transfer coefficient [$W/m^2.K$]

X_h and X_c = normalised height of hot and cold water respectively in the tank

The average temperature inside the tank ($T_{avg,2}$) is determined using eq.(28) [C1].

$$\frac{dT_{avg,2}}{dt} = \frac{1}{C_b} [-\dot{Q}_{demand} - UA_s X_h (T_h - T_a) \bar{C}_a - UA_t (T_h - T_a) \bar{C}_a - UA_s X_c (T_c - T_a) \bar{C}_a + \dot{Q}_{heat} C_a - UA (T_{avg,2} - T_a) C_a] \quad (28)$$

where, C_a represents signal for operation of actuator for heating. The average temperature of hot water inside the tank ($T_{avg,2}$) is monitored thorough the period. The temperature of hot water delivered from the storage ($T_{out} = T_h$) tank is calculated using eq.(26) while $C_a = 0$ (ie, heater is OFF) and $T_{out} = T_{avg,2}$ using eq.(28) while $C_a = 1$ (ie, heater is ON and stratification is destroyed causing uniform temperature through out the storage tank).

Theoretical validation of the single-mass model and the two-mass model

Both storage models were implemented in DigSILENT PowerFactory (simulating tool for power system analysis). \dot{Q}_{demand} is manually determined to verify and validate the dynamics of storage models. The results from simulation investigating the dynamics of both storage tanks concerning the temperature of hot water, flow rate and losses are compared and illustrated in Fig. 8. The net flow of energy, to and from the tank, is the same for both models. All the necessary parameters of the storage tank, electric boiler and the control unit is present in table 2, table 3 and table 4 respectively [C1]. Simple hysteresis control of the heating element is implemented to maintain the temperature of hot water inside the tank above $65^\circ C$. The heating element is subjected to turn ON only when $T_{out} < 70^\circ C$ or $X_c \geq 0.2pu$ and is turned OFF when $T_{out} = 80^\circ C$.

2. Modelling of Active Loads and Thermal Storage Tanks

Table 2: Parameter of storage tank [C1]

Parameter	Value
Volume of storage tank (V) [m^3]	12.5
Overall heat transfer coefficient (U) [$W/m^2\text{°C}$]	2.5
Specific heat capacity of water (C_w) [$J/kg\text{°C}$]	4180
density of water (ρ) [kg/m^3]	1000
Ambient temperature of storage room (T_{amb}) [°C]	15
Incoming cold water temperature (T_{iw}) [°C]	30
Ratio of height to diameter of tank (H/D) [pu]	2.5

Table 3: Parameter of electric boiler [C1]

Parameter	Value
Rated power of electric boiler ($P_{r,b}$) [kW]	200
Rated voltage of electric boiler ($V_{r,b}$) [pu]	1
Efficiency of electric boiler (η) [%]	100

Table 4: Parameter for control of electric boiler [C1]

Parameter	Value
Maximum temperature allowed inside tank (T_{max}) [°C]	80
Minimum temperature allowed inside tank (T_{min}) [°C]	70
Allowed height of cold water to accumulate (X_c) [pu]	0.2

Fig. 8a shows the plot of \dot{Q}_{demand} varying from 0-50kW. Fig 8b shows the ON/OFF status of the heater (C_a) along with the level of X_h and X_c inside the storage tank. When the heating element is turned ON ($C_a = 1$), the thermocline inside the tank gets destroyed causing mixing of hot and cold water, indicated by $X_c = 0$ and $X_h = 1$. When $C_a = 0$, changes in the level of X_h and X_c occurs due to stratification.

The delivered temperature of hot water from the storage tank for the two-mass model (T_{out}), and single mass model ($T_{avg,1}$) is illustrated in Fig. 8c. When $T_{out} < T_{min}$ at $t = 03:30\text{hrs}$ or $X_{cold} \geq 0.2$ at $t=10:00$ and $20:00$ hrs, heater turns ON ($C_a = 1$) delivering hot water. Initially, at these points, the temperature of hot water in the two-mass model decreases abruptly, due to rupture of thermal stratification and mixing of hot and cold water inside the

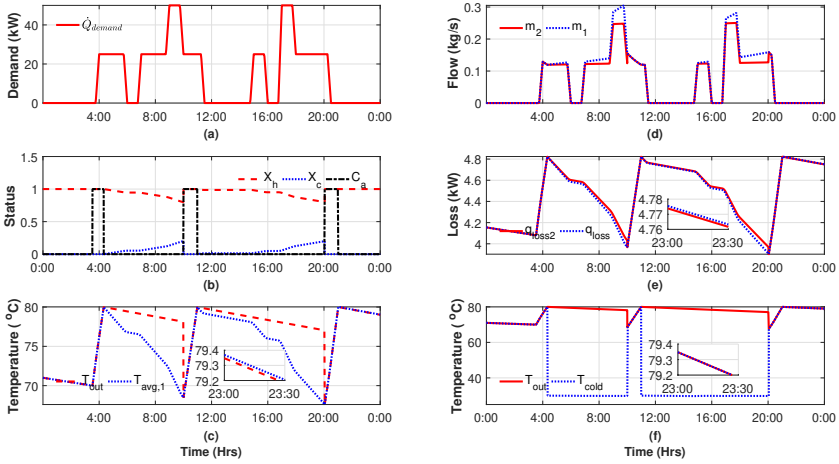


Fig. 8: Simulation results for single mass and two mass model of hot water storage tank [C1] (a) thermal Demand, (b) status of heater and level of water in the tank, (c) temperature of outlet water for both models, (d) flow rate of water for both models to fulfil thermal demand, (e) total losses from the wall of tank for both models, (f) temperature of cold water and outlet water in tank for the two mass model

tank. Then, the temperature of the water inside the tank rises until it reaches the maximum allowable temperature ($T_{max} = 80^{\circ}\text{C}$) as per eq.(28).

Once the heater is turned OFF, there is again the presence of stratified hot and cold layers due to the outflow of hot water and inflow of cold water in the storage tank. As a consequence, the temperature of hot water decreases only due to loss from the surface of the tank eq.(26). On the other hand, the temperature of hot water in the single-mass model ($T_{avg,1}$) decreases significantly due to the effect of loss and thermal demand. Between 23:00 to 23:30 hrs, when $C_a = 0$ and $\dot{Q}_{demand} = 0$ it is observed that temperature of hot water for the single-mass model is more than that for the two-mass model. This difference in temperature is due to more thermal losses from the surface area of the storage tank (especially from the top of the storage tank during the presence of stratified layer when $T_h > T_{avg,1}$) than in the single-mass model, as seen in Fig. 8e. Thus, the energy content in the two-mass model is less than the total energy contained in the single-mass model, despite the energy input and energy demand are the same in both models.

Fig. 8d illustrates the flow rate of hot water from the storage tank for the single-mass model (m_1) and the two-mass model (m_2). During the presence of thermocline $m_1 > m_2$ for the same energy demand. The difference in flow rate is due to the lower temperature difference between outgoing and incoming water from the storage tank for the two-mass model compared with the single mass model. Thus, for economic analysis based on the flow rate of

2. Modelling of Active Loads and Thermal Storage Tanks

hot water for district heating, the two-mass model is reliable (as it emulates practical condition) compared to the single-mass model.

The temperature of the cold water layer in the tank is shown in Fig. 8f. During the presence of the thermocline, the temperature of the cold layer is around 30°C.

Hence, to manage the demand response control of the hot water tank, the value of (T_{out}) and height of cold water in the tank (X_c) gives reliable information. These pieces of information can be measured practically using instrumentation and measurement. Whereas, the average temperature ($T_{avg,1}$) for the single-mass model cannot be measured practically using instrumentation and measurement, and need theoretical calculations. Thus, the single mass model is useful for studies related to gathering insight based on energy flow. At the same time, the two-mass model is more appropriate for studies related to demand response where various signals for control and measurement can be realised practically.

Multi-layered stratification model (n-stratified layers)

The supply of hot water from the top of the storage tank develops stratified temperature profile, when mass momentum is considered to be only in the axial direction [27]. Modelling of the hot water storage tank with stratified layers has been well-defined in [70]. The following derivation is based on the principle of conservation of energy in a control volume and surface, adapted to utilise the flexibility of storage tank in synergy operation with electricity network [J2].

Let, us consider a cylindrical storage tank with volume $V(m^3)$ and the inner height to diameter ratio $H/D = x$. Then, the relation between diameter and volume of the tank is given by eq.(29).

$$V = \frac{\pi D^2 H}{4} = \frac{\pi D^3 x}{4} \quad [m^3] \quad (29)$$

$$D = \left(\frac{4V}{\pi x} \right)^{\frac{1}{3}} \quad [m] \quad (30)$$

Let there be n number of stratified layers divided into equal height as shown in Fig. 9. Then the thickness of each stratified layer (z) is calculated as eq.(31).

$$z = \frac{1}{n} \left(\frac{4Vx^2}{\pi} \right)^{\frac{1}{3}} \quad [m] \quad (31)$$

The surface area of the sidewalls of each stratified layer is equal and is calculated as eq.(32), neglecting its thickness.

$$\begin{aligned} A_{sn} &= \frac{1}{n} \pi x \left(\frac{4V}{\pi x} \right)^{\frac{2}{3}} = \frac{1}{n} (16\pi x V^2)^{\frac{1}{3}} \quad [m^2] \\ &= \frac{A_s}{n} \end{aligned} \quad (32)$$

where, A_s is the total surface are of the sidewall of the storage tank. The horizontal area of each layer (A_q) is given by eq.(33).

$$A_q = \frac{\pi D^2}{4} = \frac{\pi}{4} \left(\frac{4V}{\pi x} \right)^{\frac{2}{3}} = \left(\frac{\pi V^2}{4x^2} \right)^{\frac{1}{3}} \quad [m^2] \quad (33)$$

The mass of water in each stratified layer is equal and given by eq.(34).

$$m = \frac{V\rho}{n} \quad [kg] \quad (34)$$

ρ is density of water.

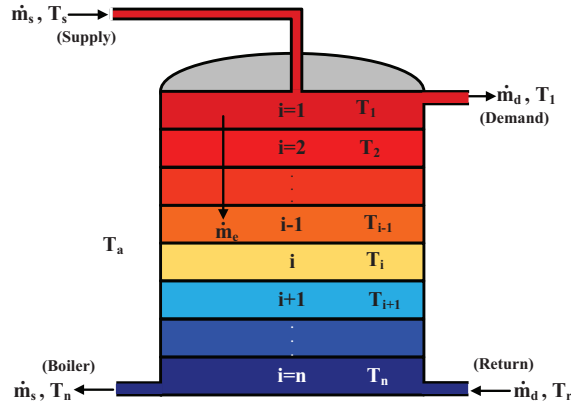


Fig. 9: Stratified storage tank with n layers [J2]

Fourier's law of heat conduction: Fourier's law of heat conduction (35) states that, "heat transfer by molecular interaction at any point in a solid or fluid is proportional in magnitude and coincident with the direction of the negative gradient of temperature." [71].

$$\dot{q}'' = -k\nabla T \quad \left[\frac{W}{m^2K} \right] \quad (35)$$

Where, \dot{q}'' is defined as the heat transfer rate per unit area (W/m^2K). k is the thermal conductivity of conducting media (W/mK).

Thermal conductivity: Thermal conductivity of a material is defined as the amount of heat that is transmitted through a unit thickness of a material with a unit surface area, induced by a unit temperature difference between the two body surfaces in contact.

Convection heat transfer conductance: In simple convective heat transfer, the convenient way to define convection heat transfer conductance

2. Modelling of Active Loads and Thermal Storage Tanks

or coefficient is (36), where the heat flux at the surface is the product of the conductance and temperature potential difference [71].

$$\dot{q}_s'' = h\Delta T \quad \left[\frac{W}{m^2} \right] \quad (36)$$

Here, \dot{q}_s'' is the heat flux, heat-transfer rate per unit area (W/m^2). h is defined as the heat transfer coefficient, or convection conductance, (W/m^2K).

Heat transfer in each stratified layer of the storage tank: The amount of heat exchanged (\dot{Q}_{exc}) by the layer i with the adjacent layers ($i - 1$) and ($i + 1$) due to natural convection and thermal conduction in the vertical direction of the storage tank is calculated using eq.(37) [70].

$$\begin{aligned} \dot{Q}_{exc,i} &= \dot{Q}_{exc,i-1 \rightarrow i} - \dot{Q}_{exc,i \rightarrow i+1} \\ &= \frac{A_q \lambda_w}{z} (T_{i-1} - T_i) - \frac{A_q \lambda_w}{z} (T_i - T_{i+1}) \\ &= \frac{A_q \lambda_w}{z} (T_{i-1} + T_{i+1} - 2T_i) \end{aligned} \quad (37)$$

Where,

λ_w = effective vertical heat conductivity of water (1–1.5 W/mK) [70]
 \dot{Q}_{exc} = is heat exchange due to natural convection and thermal conduction [W]

The effective mass flow of water between the stratified layer (\dot{m}_e) is given by eq.(38) as difference between inlet mass flow of water from the heating source (\dot{m}_s) and mass flow of water out from the storage tank due to demand (\dot{m}_d).

$$\dot{m}_e = \dot{m}_s - \dot{m}_d \quad [kg/s] \quad (38)$$

Let, the direction of flow of water inside the storage tank from top to bottom and bottom to top be indicated by symbol δ^+ and δ^- respectively. Thus, $\delta^+ = 1$ represents the heat transfer due to water mixing from top to bottom (downwards) and $\delta^- = 1$ from bottom to top (upward). $\delta^+ = 0$ for top layer (i.e, $i = 1$) and $\delta^- = 0$ for bottom layer (i.e, $i = n$). The relation of δ^+ and δ^- with \dot{m}_e is given by eq.(39) and eq.(40) respectively [J2].

$$\begin{aligned} \delta^+ &= 1 & \text{if } \dot{m}_e > 0 \\ &= 0 & \text{if } \dot{m}_e \leq 0 \end{aligned} \quad (39)$$

$$\begin{aligned} \delta^- &= 1 & \text{if } \dot{m}_e < 0 \\ &= 0 & \text{if } \dot{m}_e \geq 0 \end{aligned} \quad (40)$$

Balancing the flow of energy in each layer due to heat transfer between surrounding layers, losses from the sidewall of the tank due to conduction, and flow of water to and from the storage tank as shown in Fig. 10, following equations (eq. 41 to eq. 44) can be written for n stratified layers. $i = 1$ for the top layer and $i = n$ for the bottom layer.

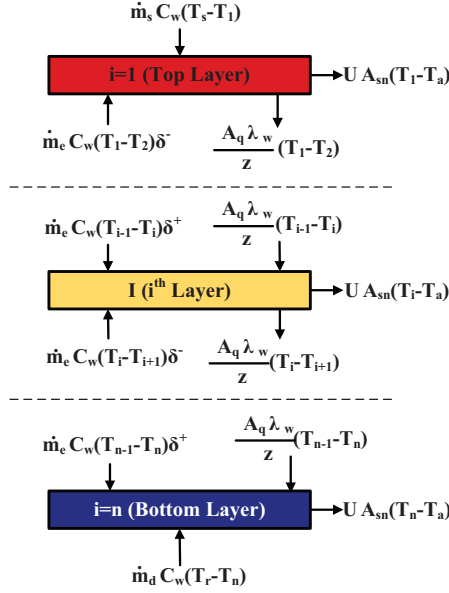


Fig. 10: Energy flow diagram [J2]

$$m C_w \frac{dT_1}{dt} = \dot{m}_s C_w (T_s - T_1) + \dot{m}_e C_w (T_1 - T_2) \delta^- - U A_{sn} (T_1 - T_a) - \frac{A_q \lambda_w}{z} (T_1 - T_2) \quad (41)$$

$$m C_w \frac{dT_2}{dt} = \dot{m}_e C_w (T_1 - T_2) \delta^+ + \dot{m}_e C_w (T_2 - T_3) \delta^- - U A_{sn} (T_2 - T_a) + \frac{A_q \lambda_w}{z} (T_1 + T_3 - 2T_2) \quad (42)$$

$$m C_w \frac{dT_i}{dt} = \dot{m}_e C_w (T_{i-1} - T_i) \delta^+ + \dot{m}_e C_w (T_i - T_{i+1}) \delta^- - U A_{sn} (T_i - T_a) + \frac{A_q \lambda_w}{z} (T_{i-1} + T_{i+1} - 2T_i) \quad (43)$$

$$m C_w \frac{dT_n}{dt} = \dot{m}_e C_w (T_{n-1} - T_n) \delta^+ + \dot{m}_d C_w (T_r - T_n) - U A_{sn} (T_n - T_a) + \frac{A_q \lambda_w}{z} (T_{n-1} - T_n) \quad (44)$$

2. Modelling of Active Loads and Thermal Storage Tanks

Where,

- T_r = temperature of return water in the tank [K]
- T_a = temperature of ambient environment [K]
- T_i = temperature of stratified layers where, (i=1,2,...n) [K]
- U = overall heat transfer coefficient [$W/m^2.K$]
- C_w = specific heat capacity of water [$J/kg.K$]

Let $\delta_{(X)} = 1$ for all the condition defined by term X is true, else $\delta_{(X)} = 0$ as represented by eq.(45) [J2].

$$\begin{aligned} \delta_{(X)} &= 1 \quad \text{if } X = \text{True} \\ &= 0 \quad \text{if } X = \text{False} \end{aligned} \quad (45)$$

Finally, Eq.(41) to eq.(44) can be written as one single equation as shown in eq.(46) [J2] for determining temperature of each stratified layers in the storage tank.

$$\begin{aligned} mC_w \frac{dT_i}{dt} &= \dot{m}_s C_w (T_s - T_1) \delta_{(i=1)} + \dot{m}_d C_w (T_r - T_n) \delta_{(i=n)} \\ &+ \dot{m}_e C_w (T_{i-1} - T_i) \delta^+ \delta_{(i \neq 1)} + \dot{m}_e C_w (T_i - T_{i+1}) \delta^- \delta_{(i \neq n)} \\ &- UA_{sn} (T_i - T_a) + \frac{A_q \lambda_w}{z} [(T_{i-1} - T_i) \delta_{(i \neq 1)} - (T_i - T_{i+1}) \delta_{(i \neq n)}] \end{aligned} \quad (46)$$

Analysis of model

The temperature distribution for a 500-litre hot water storage tank for various cases are shown in Fig. 11 The overall heat transfer coefficient of the storage walls (U) is $0.9 \text{ W/m}^2\text{K}$, and the effective heat conductivity of water (λ_w) is 0.644 W/mK . The store diameter to height ratio (x) is 2.24, and the ambient temperature (T_a) is considered to be 10°C .

Case I: Charging of storage tank: The storage tank is fully discharged and is filled with cold water with an initial temperature of all layers ($T_{i,ini}$) be 10°C . The tank is being charged with hot water ($T_s = 80^\circ\text{C}$) at a constant rate of 100 l/hr keeping load demand to be zero. Other relevant parameters are presented in Table 5. The temperature gradients of each layer are shown in Fig. 11(a).

Case II: Discharging of storage tank: The storage tank is fully charged and is filled with hot water with an initial temperature of all layers ($T_{i,ini}$) be 80°C . The tank is only being discharged at a constant rate of 100 l/hr with return temperature of cold water ($T_r = 10^\circ\text{C}$). Other relevant parameters are presented in Table 5. The temperature gradients of each layer are shown in Fig. 11(b).

Case III: Charging and Discharging of storage tank: The storage tank is fully discharged and is filled with cold water with an initial temperature of all layers ($T_{i,ini}$) be $10\text{ }^{\circ}\text{C}$. The tank is being charged with hot water ($T_s = 80\text{ }^{\circ}\text{C}$) at a constant rate of 100 l/hr . At the same time, the flow of water from the tank towards load is 50 l/hr . Other relevant parameters are presented in Table 5. The temperature gradients of each layer are shown in Fig. 11(c). The temperature gradient of the top layer remains the same as in the case I as the net flow of energy in the top layer remains the same for both cases (I and III). Temperatures of other bottom layers are flattened compared to the case I as the effective flow of hot water in these layers are different than in case I.

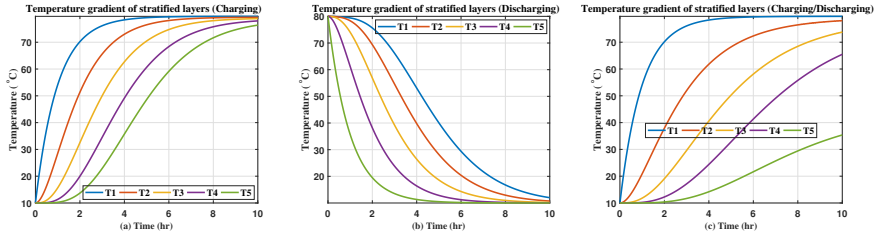


Fig. 11: Temperature gradient of stratified layers (a) during charging of storage tank, (b) during discharging of storage tank, and (c) during charging and discharging of storage tank.

Table 5: Case I, II and III Parameters

Parameter	Case I	Case II	Case III
	Charging	Discharging	Charging and Discharging
\dot{m}_s	100 l/hr	0	100 l/hr
T_s	$80\text{ }^{\circ}\text{C}$	-	$80\text{ }^{\circ}\text{C}$
\dot{m}_d	0	100 l/hr	50 l/hr
T_r	-	$10\text{ }^{\circ}\text{C}$	$10\text{ }^{\circ}\text{C}$
$T_i(ini)$	$10\text{ }^{\circ}\text{C}$	$80\text{ }^{\circ}\text{C}$	$10\text{ }^{\circ}\text{C}$

2.5 Comparison of Thermal Storage Tank Models

Comparison of storage tank models based on the temperature of hot water and thermal losses only from the sidewall of the storage tank (to maintain same thermal losses for all storage tank models) is presented in this section. This comparison provides significant information about how these models can reflect various physical properties, such as temperature and losses, of the hot water storage tank and their significance within the scope of studies. The necessary parameters are shown in table 6.

2. Modelling of Active Loads and Thermal Storage Tanks

Table 6: Parameter of Storage tank for comparison of different models

Parameter	Value
Volume of storage tank (V) [m^3]	25
Overall heat transfer coefficient (U) [$W/m^2\text{°C}$]	0.12
Specific heat capacity of water (C_w) [$J/kg\text{°C}$]	4190
density of water (ρ) [kg/m^3]	1000
Ambient temperature of storage room (T_{amb}) [°C]	10
Incoming cold water temperature (T_{iw}) [°C]	40
Ratio of height to diameter of tank (H/D) [pu]	2.24
Heat conductivity of water (λ) [$w/m\text{°C}$]	0.644

Average Temperature

The average temperature for the single-mass model is calculated using eq. (47). The heat loss is considered only from the sidewall of the hot water storage tank. The same amount of energy flow, in and out of the storage tank, is considered.

$$m_b C_w \frac{dT_{x,1}}{dt} = \dot{Q}_{heat} - \dot{Q}_{loss,1} - \dot{Q}_{demand} \quad (47)$$

Where $T_{x,1}$ is the average temperature inside the storage tank for single mass model.

The average temperature in the two-mass model, by mixing hot and cold liquid, is calculated using eq. (48) as derived in eq. (19).

$$T_{x,2} = X_h T_h + (1 - X_h) T_c \quad [K] \quad (48)$$

In the multi layered stratification model, all the layers are equally divided into n-numbers. Thus, the average temperature due to mixing of liquids can be calculated as in eq. (49).

$$T_{x,n} = \frac{\sum_{i=1}^n T_i}{n} \quad (49)$$

Considering \dot{Q}_{heat} and \dot{Q}_{demand} of the thermal storage tank as shown in Fig. 12a, the temperatures of the n-stratified layered and the two-mass model of storage tank are shown in Fig. 12b&c respectively. The comparison of $T_{x,1}$, $T_{x,2}$ and $T_{x,n}$ is shown in Fig. 12d. It is observed that $T_{x,1} = T_{x,2} = T_{x,n}$.

Losses

The total heat loss due to conduction and convection from the sidewall of the storage tank in the single-mass model, two-mass model and n-stratified layer storage tank model is calculated using eq.(50), eq.(51) and eq.(52) respectively.

$$\dot{Q}_{loss,1} = UA_s(T_{x,1} - T_a) \quad (50)$$

$$\begin{aligned} \dot{Q}_{loss,2} &= UA_s X_h (T_h - T_a) + UA_s X_c (T_c - T_a) \\ &= UA_s X_h (T_h - T_a) + UA_s (1 - X_h) (T_c - T_a) \\ &= UA_s [X_h T_h + (1 - X_h) T_c - T_a] \\ &= UA_s (T_{x,2} - T_a) = \dot{Q}_{loss1} \end{aligned} \quad (51)$$

$$\begin{aligned} \dot{Q}_{loss,n} &= \sum_{i=1}^n UA_{sn} (T_i - T_a) \\ &= UA_{sn} \left[\sum_{i=1}^n T_i - \sum_{i=1}^n T_a \right] \\ &= U \frac{A_s}{n} \left[\sum_{i=1}^n T_i - \sum_{i=1}^n T_a \right] \\ &= UA_s \left[\frac{\sum_{i=1}^n T_i}{n} - \frac{\sum_{i=1}^n T_a}{n} \right] \\ &= UA_s (T_{x,n} - T_a) \end{aligned} \quad (52)$$

Thus, thermal losses are the same in all storage tank model as seen from Fig. 12e. Also eq.(50), eq.(51) and eq.(52) are equal when $T_{x,1} = T_{x,2} = T_{x,n}$. However, if the losses from top of the storage tank is also considered then, $T_{x,1} \leq T_h$ ($T_{x,1} = T_h$ during absence of thermocline and $T_{x,1} < T_h$ during presence of thermocline). As a consequence $UA_t(T_{x,1} - T_a) \leq UA_t(T_h - T_a)$. This shows that the losses from the two-mass model are greater than the single mass model if the top of the storage tank is considered for thermal losses. Hence, the average temperature in the storage tank with two mass model as calculated using eq.(28) is lower than the average temperature of single mass model storage tank calculated using eq.(25). ie, ($T_{x,2} \leq T_{x,1}$).

Fig. 12f illustrates the flow rate of hot water from the different models of the storage tank. It is observed that for the single mass model, the flow rate of hot water ($\dot{m}_{d,1}$) is greater than the other two models. However, for two mass model, the flow rate is almost constant while heating is turned OFF, and is equal to that of the average temperature model while heating is turned ON.

State of energy (SOE)

SOE of the thermal storage tank is defined as the total amount of usable energy stored in it normalised with respect to maximum amount of usable

2. Modelling of Active Loads and Thermal Storage Tanks

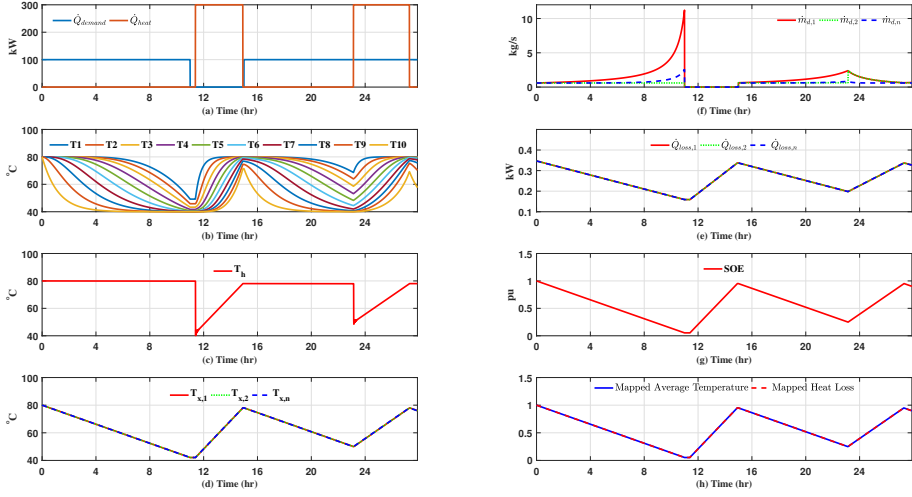


Fig. 12: (a) Thermal demand and thermal input to storage tank, (b) temperature of stratified layers in multi stratified layered storage tank with 10 layers, (c) temperature of hot water in mass model storage tank, (d) average temperature in single mass model, two mass model and n-layered stratified tank model, (e) heat loss from sidewall of storage tank in single mass, two mass and n-layered stratified storage tank model, (f) flow rate of hot water from storage tank for single mass, two mass and n-layered stratified model, (g) SOE in storage tank, (h) mapped average temperature and heat loss in storage tank.

energy that can be stored in the tank. SOE is considered to be 1pu when it is filled with hot water with maximum allowable temperature (T_{max}) and is considered to be 0pu when filled with cold water of return temperature (T_r). SOE of storage tank is calculated using eq.(53). Fig. 12g illustrates the SOE inside the thermal storage tank

$$\frac{dSOE}{dt} = \frac{\dot{Q}_{heat} - \dot{Q}_{loss} - \dot{Q}_{demand}}{m_b C_p (T_s - T_r)} \quad (53)$$

Liner mapping of average temperature and thermal losses

Linear mapping of average temperature and heat losses from the sidewall of the storage tank is represented in Fig. 12h. Maximum allowable temperature ($T_{max} = 80^\circ\text{C}$) is Mapped as 1 and return temperature $T_r = 40^\circ\text{C}$ is mapped as 0 (see Fig. 13a). Maximum and minimum heat loss from the storage tank occurs when the average temperature of hot water in the storage tank is 80°C and 40°C respectively. Maximum and minimum heat loss from the storage tank is mapped as 1 and 0 respectively. Linear mapping of heat loss is illustrated in Fig. 13b. Fig. 12h shows that the mapped temperature and losses are proportionally equal to the normalized value of SOE of the storage tank. Thus, with the knowledge of SOE in the storage tank, thermal loss and

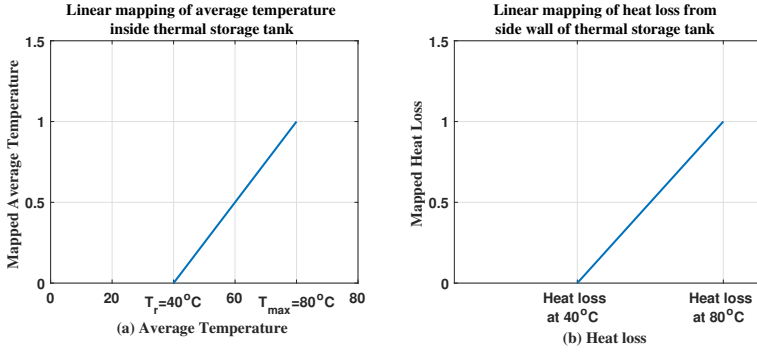


Fig. 13: Linear mapping of (a) average temperature inside the storage tank, (b) Heat loss from sidewall of the storage tank with average temperature.

average temperature of hot water inside the storage tank can be determined. These parameters can be determined using linear mapping, for the system modelled with energy flow equation governing the storage system.

The selection of the thermal storage tank model depends on the type of study and the level of accuracy of parameters that can be measured physically. The energy status inside the tank along with temperature and level of hot water from the stratified layered storage tank is appropriate for demand response control.

2.6 Modelling of EV

The EV is modelled as a battery of suitable capacity to represent electrical energy flow during charging and discharging. The dynamics of energy discharged from the battery during a travel period are collectively represented as the total amount of energy used and is represented as the depth of discharge of the battery (DOD). The state of charge (SOC) of the battery is defined as in eq.(54). The SOC of battery is determined from eq.(55) or eq.(56) during charging [3].

$$SOC = \frac{\text{Remaining Capacity [Ah]}}{\text{Rated Capacity [Ah]}} \quad [\%] \quad (54)$$

$$SOC_t = SOC_{t_0} + \frac{100}{\text{Rated Capacity [Ah]}} \int_{t_0}^t i(\tau) d\tau \quad (55)$$

$$SOC_t = SOC_{t_0} + \frac{100}{\text{Rated Capacity [kWh]}} \int_{t_0}^t P_{cb}(\tau) d\tau \quad (56)$$

2. Modelling of Active Loads and Thermal Storage Tanks

Here, SOC_{t_0} is the initial SOC(%) at time t_0 when EV is connected for charging, and SOC_t is the SOC(%) at any time t . The integral period t_0 to t is in hours. i is the battery current(A). The current (i) is +ve during charging. P_{cb} is the charging power of the battery (kW).

The analysis of the driving pattern of passenger cars is performed in chapter 3 to generate the state of charge of EVs. The detailed discussion on the flexible operation of EVs is presented in chapter 6.

2.7 Low Voltage Residential Grid Network

To investigate the impact and flexibility obtained from thermal units and electrified transport in synergy with the electric grid network, a low voltage (LV) substation is considered. The LV network, consisting of 10/0.4 kV transformer and belonging grid, is situated in Northern Jutland Denmark, as shown in Fig. 14. This LV grid network is considered in some of the further case studies and simulation. The LV grid, in the present context,

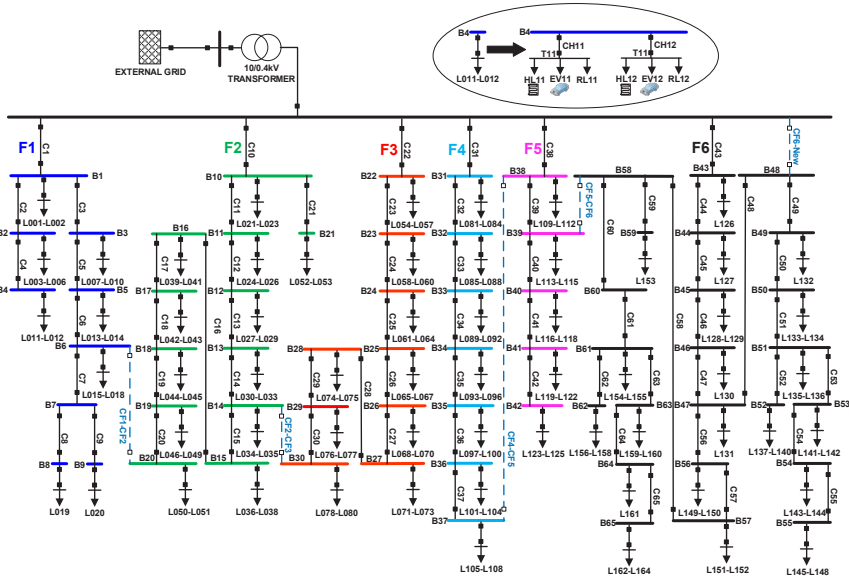


Fig. 14: Low voltage residential grid network [C2]

supplies customer load without electrical heating and plugged-in electric vehicles. The detailed design parameters of cable and lines in the network are obtained from [72]. All the relevant electric grid data were supplied by the distribution grid company that owns the network. Summary of grid specification is tabulated in table 7.

The analysis of residential base loads, thermal loads and EVs loads

Table 7: Grid Specifications [J1].

Transformer Specification	630 kVA, 10/0.4 kV Dyn5, Uk = 4.66% Copper Loss = 6.5 kW, Iron Loss =1.5 kW					
Number of feeders	6					
number of households	164					
Feeder representation and color	F1	F2	F3	F4	F5	F6
Total HH Load in respective feeder (kWh/day)	226	376	277	223	278	421
Number of houses in respective feeder	20	33	27	28	17	39

integrated into the LV grid are performed in chapter 3. The detailed analysis of the presented network is performed in chapter 5. The impact assessment in the electrical grid due to the integration of thermal and EV loads are performed in chapter 5 and 6.

2.8 Conclusion

Mathematical models representing thermal and EV loads, to be considered in further research in integration with LV distribution network, are presented. Theoretical validation of thermal storage tanks as single-mass, two-mass and n-layered stratified models are discussed with their significant advantages in studies related to energy management. Considering numerical complexities, thermal storage tanks modelled with energy flow equations (eq.24) and single-mass model are equally reliable for energy optimisation studies. However, there are certain advantages of using stratified layered storage tank model over the average temperature model. An average model is unable to project the actual supply temperature. This temperature is responsible for regulating the flow of hot from EB to storage tank while charging process, and monitor the status of the storage tank as realised in practice. The two-mass and n-layered stratified model of storage tanks have significant advantages, for studies related to economic analysis based on the flow rate of energy carrier and demand response, as information on the temperature of supply hot water and level of hot water inside the storage tank are reliable and physically measurable in practice. EVs are modelled as a battery of suitable capacity. Its depth of discharge represents the overall dynamics involved in the daily commute of EVs. The state of charge of batteries is monitored while recharging EVs. The LV distribution network, for the integration of thermal and transportation load, is presented in brief.

Chapter 3

3 Data Analytics of Energy Consumption

This chapter aims to study the analysis of residential thermal load, electrical load, and driving distance based on real measurements. Detailed thermal behaviour study based on hours, days, weeks, weekdays, weekends and seasons are performed. The application of data analysis is for developing estimation models. The estimating models are presented and compared with other existing literature. Thermal and electrical load profiles along with the state of charge in electric vehicles are generated with the knowledge of relevant data analysis performed. These load profiles are used further in the research work to analyse the impact on the electrical grid network and propose a suitable control system for flexibility in demand response. This chapter summarises the part of work done in [C3]: analysis and generation of residential base loads profile and thermal consumptions profile of individual houses, [J2]: analysis of thermal data in a residential area and its estimation, and [J3]: analysis driving pattern of passenger cars for a generation of the state of charge in EVs.

3.1 Analysis of Thermal Data in Residential Area

In this section, the hourly consumption of heat energy circulated through hot water by district heating (Q_{DHW}) has been analysed from different aspects to know the pattern of usage. The data, from the real measurements at thermal distribution feeders, has been provided by Aalborg Varme A/S for research propose. Thermal consumption data from terminals of five different thermal distribution feeders ($F_1 - F_5$) of district heating are analysed. These feeders are supplying several residential buildings, in a particular residential area in Aalborg, Denmark. Q_{DHW} consist of two components, i.e., Space heating (SH) and domestic hot water (Q_{dhw}). The combined effect of these components of Q_{DHW} is analysed further, as these demands are produced and transmitted by the same network of district heating. Q_{DHW} data is available for the period of 21st Dec 2015 to 4th Dec

2016. The brief overview of the analysis is presented in [J2].

Daylight Saving starts on March 27, 2016 and ends on October 30, 2016. On March 27, 2016 the are no data set between period 02:00-02:59. Missing data is not considered during this period (in Matlab, the data in this period is considered as 'NaN'-not a number). On Oct 30, 2016, there are two data set for the period 02:00-02:59. The average value of these data set is considered for this period.

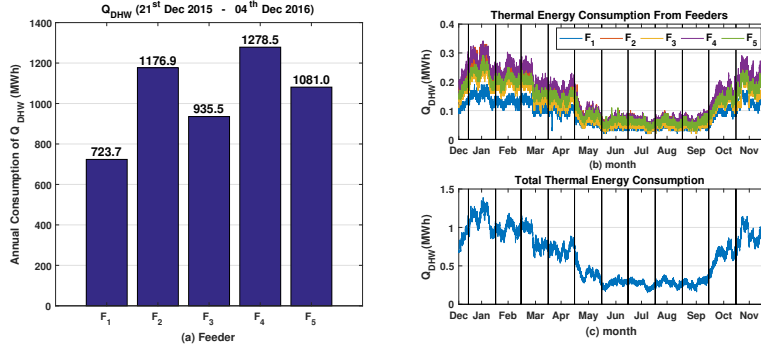


Fig. 15: (a) Bar diagram of yearly Q_{DHW} in different feeders, (b) Yearly Q_{DHW} pattern of all feeders, (c) total Q_{DHW} pattern of all feeders [J2]

Fig. 15a shows the annual Q_{DHW} (from the period 21st Dec 2015 to 4th Dec 2016) at the different feeders. The annual consumption varies from 723.7 MWh at F_1 to 1278.5 MWh at F_4 . The total annual consumption was 5195.7 MWh. Fig. 15b shows the hourly Q_{DHW} for feeder $F_1 - F_6$ and the total consumption in Fig. 15c. The graph clearly shows that there is seasonal variation. For simplicity, December to April is considered as winter season and May to September as summer Season. Between the two seasons, there is a transition period of 2 weeks, where Q_{DHW} falls or rises. Observation of data are made from two different aspects

- Hourly Q_{DHW} for summer and winter
- Q_{DHW} based on different days of the weeks, weekdays and weekends

Table 8: Data period used for analysis

Data period	21 st Dec 2015 to 4 th Dec 2016
Winter season analysis	21 st Dec 2015 to 1 st May 2016
	10 th Oct 2016 to 4 th Dec 2016
Summer season analysis	9 th May 2016 to 25 th Sept 2016

3. Data Analytics of Energy Consumption

Analysis of the Q_{DHW} consumption during winter

The average Q_{DHW} during winter is 0.881 MWh which is around 205% more than average consumption during summer (0.288MWh). Fig. 16 contains graphs of hourly average pattern of Q_{DHW} during winter for different days of weeks and their overall average. During Saturdays and Sundays, the consumption is more than weekdays, where the consumption is highest during Sundays. To simplify the graphs shown in Fig. 16, graphs with average consumption of thermal energy during the weekdays, weekends and the average consumption throughout the weeks during winter has been plotted in Fig. 17

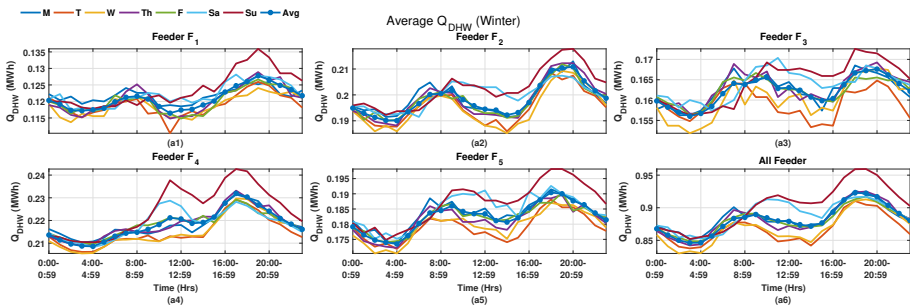


Fig. 16: Average winter Q_{DHW} in different feeders during different days of weeks

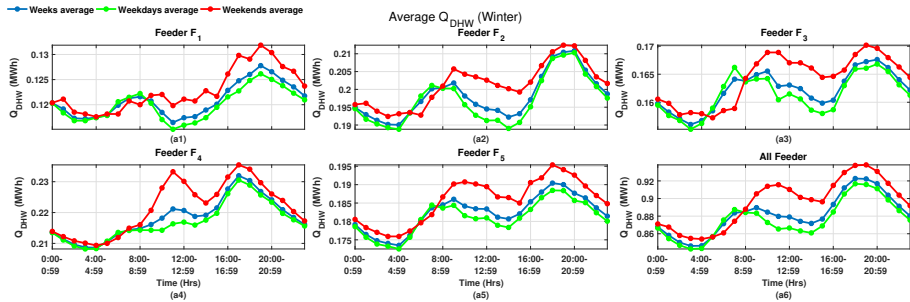


Fig. 17: Weeks, weekdays and weekends average Q_{DHW} during winter

From the graphs shown in Fig. 17, it is observed that there are similar patterns of average hourly usage of Q_{DHW} in all feeders. There are two peaks and two valleys. The period of lowest thermal consumption is from 03:00 to 04:59Hrs. Hereafter, there is a gradual rise in Q_{DHW} with morning peak between 07:00 to 07:59 Hrs during regular weekdays, when people get ready for their job. There is increment as well as the shift in this peak in weekdays, which is around 10:00-12:59 Hrs, as the majority of people are relaxed with their morning activities compared to weekdays. After the morning peak,

decrement in Q_{DHW} is observed until 2:00-3:59 Hrs, due to low consumption of domestic usage of hot water, as people are in offices in weekdays. There is also a fall in Q_{DHW} during this period in weekends, with the time shift of an hour. However, the minimum consumption is higher than that of during weekdays. The evening peak is observed around 18:00 to 20:59 with gradual decrement until 4:59 Hrs in the early morning.

Analysis of the Q_{DHW} consumption during summer

The average Q_{DHW} during summer is 0.288MWh which is around 32% of the average winter consumption. Fig. 18 presents the graph of an average hourly pattern of Q_{DHW} during summer for different days of the week and their overall average. Similar to winter, the consumption in weekdays are more than other days of the week. The consumption is highest during Sundays. The graphs with the average Q_{DHW} during weeks, weekdays, weekends in summer is presented in Fig. 19. From the figure shown in Fig. 17 and Fig. 19,

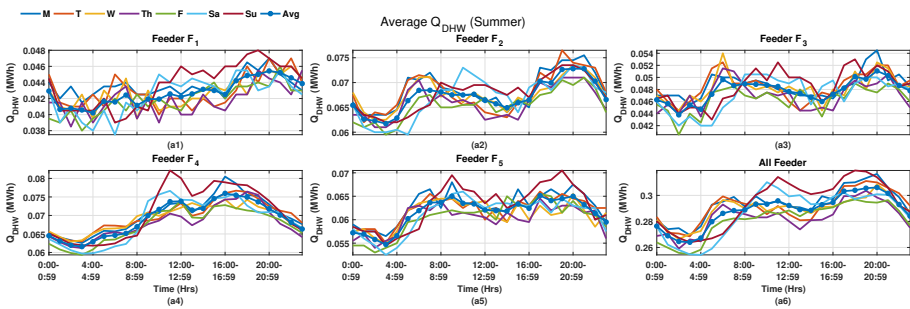


Fig. 18: Average summer Q_{DHW} in different feeders during different days of the week

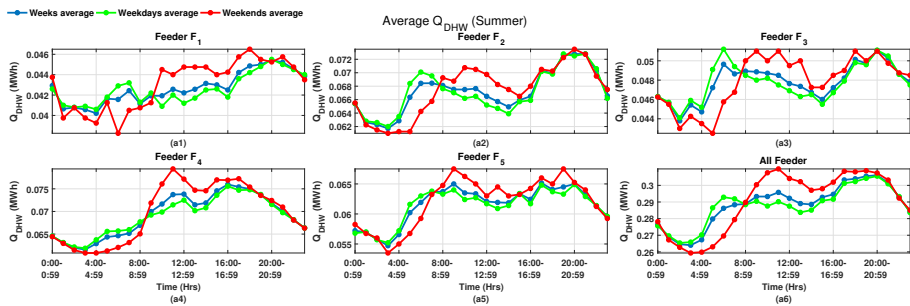


Fig. 19: Weeks, weekdays and weekends average Q_{DHW} during summer

similar patterns of hourly usage of Q_{DHW} in a residential area are observed with the change in magnitudes. The shift in the evening peak is observed by

3. Data Analytics of Energy Consumption

an hour during summer in comparison to winter as people enjoy long and sunny days.

Comparison of winter and summer Q_{DHW}

The average Q_{DHW} in various feeders during winter and summer are represented in Fig. 20a and the % of winter consumption in summer is represented in Fig. 20b. The relevant values of data points are presented in

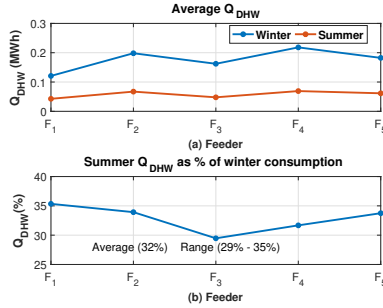


Fig. 20: (a) Average Q_{DHW} in various Feeders during winter and summer, (b) % of winter Q_{DHW} in summer.

table 9. Summer thermal consumptions are around 32% of winter thermal consumptions, which ranges between 29% to 35%. There is significant amount of Q_{DHW} in summer.

Table 9: Average Q_{DHW} during winter and in different feeders and increment

Feeder	Winter Average Q_{DHW} (MWh)	Summer Average Q_{DHW} (MWh)	Summer % of winter Q_{DHW} (%)
F_1	0.121	0.043	35
F_2	0.198	0.067	34
F_3	0.162	0.048	29
F_4	0.218	0.069	31
F_5	0.182	0.062	33
F_{all}	0.881	0.288	32

3.2 Supply and Return Temperature Analysis of District Hot Water

Along with thermal consumptions, it is also interesting to observe the seasonal variation of the temperatures of hot water and return cold water in

the district heating system network. These observations provide a better understanding of seasonal thermal losses during transmission as well as in simplifying the thermal model dynamics of the thermal storage tank concerning supply and return temperatures values. Fig. 21 shows the

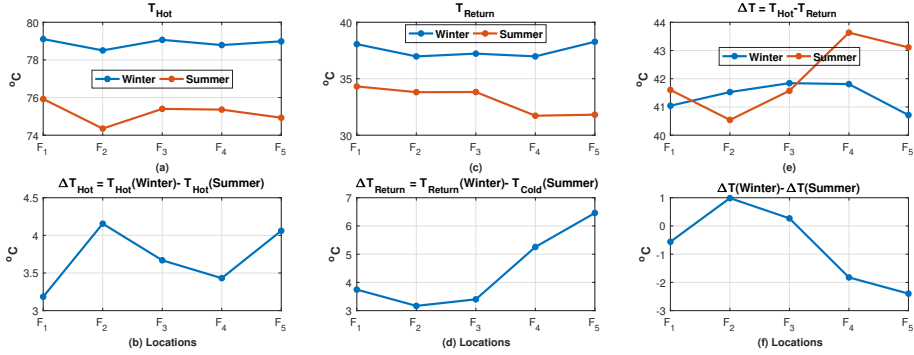


Fig. 21: (a) Supply temperature during summer and winter, (b) difference in supply temperature during summer and winter, (c) return temperature during summer and winter, (d) difference in return temperature during summer and winter, (e) difference between supply and return temperature in winter in summer, (f) difference between winter and summer ΔT .

analysis of the hourly supply and return temperatures of hot water at the feeder terminals. Fig. 21a shows that there are differences in the supply temperature of hot water during summer and winter, which is around 3-4°C (Fig. 21b). Supply temperature in winter and summer is around 79°C and 75°C respectively. Similarly, the return temperature in winter is 3-6°C higher than in summer as seen from Fig. 21c,d. The difference between supply and return temperature (ΔT) for summer and winter is between 40-44°C as seen in Fig. 21e. As seen in Fig. 21f, the difference of difference between supply and return temperature during summer and winter is around 3°C. The temperature analysis, as represented in Fig. 21 provides a clear understanding of supply and return temperatures during summer and winter. Although the temperature differences, between the supply and return water, is around 40-44°C all the time (Fig. 21e), the temperatures of supply and return water are higher during winter (Fig. 21a) than during summer (Fig. 21b). Thus, there are more transmission losses in winter than in summer. On the other hand, there are more energy content in the supply and return water during winter than in summer. For simplicity in model dynamics of the thermal storage tank, it is appropriate to consider the seasonal temperature of return cold water be constant.

3.3 Estimation of Thermal Demand

Estimation of thermal demand is essential to access optimal flexibility from the thermal system based on demand, supply, storage, capacity and energy prices. Thermal demand estimation in the residential area is quite challenging due to its dependency on users behaviour and buildings geometry, apart from the environmental variables. Real-time information on occupancy and user-level comforts for thermal demand estimation lead to challenges incorporated with privacy issues of the individuals. Thus, there is a significant compromise between errors in the estimated variable and dependent parameters. The information on the average hourly pattern of thermal demand from the residential area, during weekdays and weekends for summer and winter, provides valuable insight on aggregated users behaviour. The aggregated user pattern is thus helpful to estimate thermal demand without compromising the privacy issue of individuals. Based on these pieces of information estimating tools using curve fitting techniques, such as neural net and similar day method, are trained to integrate the perspective of users behaviour and comfort. Other depended environmental factors such as environment temperature, relative humidity, wind speed and water vapour pressure are also used for the training of estimating tools. The details and comparison of thermal demand estimation based on neural net and similar day method are well-presented in [J2].

Thermal data associated with aggregated demand of all the feeders ($F_1 - F_5$) as shown in Fig. 22, from the period of December 2016 to August 2017, are used for training and validation of estimated values. This period is selected as the associated environmental variables are available only for this period. The average Q_{DHW} pattern for the weeks, weekdays and weekends

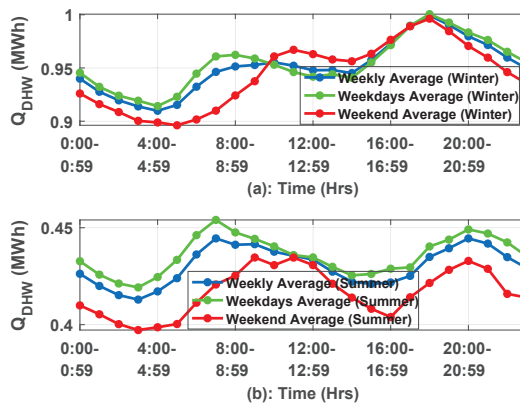


Fig. 22: Average hourly thermal consumption of weeks, weekdays and weekends from the period (Dec 2016- Aug 2017) (a) Winter (b) Summer [J2]

for the period of Dec 2016 to Aug 2017 for winter and summer respectively are illustrated in Fig. 22. Although the patterns remain similar corresponding to the peaks and valleys, the consumption during weekends are lower than weekdays, unlike in Fig. 17 and Fig. 19. This variation in magnitude of Q_{DHW} can be due to environmental factors. These Q_{DHW} patterns are used to train the estimation tool to compensate for the temperature-independent factors such as users behaviour and geometry of buildings. As residents prefer to wake up late during weekends, there is a shift in Q_{DHW} morning peak compared to weekdays. There is also a shift of evening peaks during summer, as residents prefer to enjoy daylight, compared to winter. Thus, the dependency of time, day and season regarding average Q_{DHW} is significant for estimation of thermal demand as seen in [37]

The significant influence of hourly Q_{DHW} against corresponding average external temperature is seen in Fig. 23a. Decrease in air temperature increases thermal demand and vice versa. Cold air with high relative humidity increases the heat loss from body due to conduction as compared to dry air with the same temperature. Hence, apparent temperature is considered to incorporate the combined effect of relative humidity, wind and air temperature. The apparent temperature is calculated using (57) and (58) [73]. The correlation coefficient of thermal demand with respect to external ambient temperature and apparent temperature, is -0.88 and -0.89 respectively. The effect of apparent temperature and Q_{DHW} is illustrated in Fig. 23b.

$$AT = T_a + 0.33e - 0.7v - 4.00 \quad (57)$$

$$e = \frac{RH}{100} 6.105 \exp\left(\frac{17.27T_a}{237.7 + T_a}\right) \quad (58)$$

Where, AT = Apparent Temperature [$^{\circ}C$].

T_a = Dry bulb temperature of external environment [$^{\circ}C$]

e = water vapour pressure [hpa]

v = wind speed [m/s]

RH = Relative humidity [%].

The distribution of thermal demand with respect to apparent temperature during summer and winter, as in Fig. 23c, clearly shows inverse proportionality between apparent temperature and thermal demand during winter. Whereas, during summer, proportionality is very small as thermal consumption is mostly for domestic purposes such as bathing, washing, space heating for toilet/bathroom, and transmission losses. Thus, it is logical to conclude that seasonal effect along with users profile needs to be considered as input variable in the model for estimation. Hence, data set for

3. Data Analytics of Energy Consumption

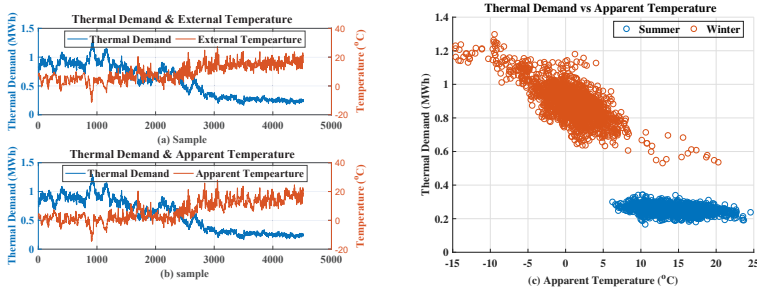


Fig. 23: (a) Thermal demand and external temperature, (b) thermal demand and apparent temperature, (c) thermal demand vs apparent temperature during winter and summer [J2]

training curve fitting tools to estimate Q_{DHW} is prepared as shown in Fig 24. Neural net fitting and similar day method are used as estimating tools [J2].

Data Set								
Hour	Summer				Winter			
	Weekdays		Weekend		Weekdays		Weekend	
1	[AT]	[QDHW]	[AT]	[QDHW]	[AT]	[QDHW]	[AT]	[QDHW]
2	[AT]	[QDHW]	[AT]	[QDHW]	[AT]	[QDHW]	[AT]	[QDHW]
3	[AT]	[QDHW]	[AT]	[QDHW]	[AT]	[QDHW]	[AT]	[QDHW]
-	-	-	-	-	-	-	-	-
-	-	-	-	-	-	-	-	-
-	-	-	-	-	-	-	-	-
-	-	-	-	-	-	-	-	-
-	-	-	-	-	-	-	-	-
24	[AT]	[QDHW]	[AT]	[QDHW]	[AT]	[QDHW]	[AT]	[QDHW]

Fig. 24: Data set [J2]

The estimation model, based on the neural net fitting tool, is developed using inbuilt tools and functions from MATLAB. 50% of the seasonal data set is used for developing the model, out of which 50% is used for training 25% for validating and 25% for testing the model. The datasets are randomly selected for training, testing, and validation of the model. After developing the model, 50% of the remaining seasonal data set are used in estimation and comparison with actual demand [J2].

For the similar day approach, 50% of the seasonal data set are used for training as the historical data to build a Euclidean distance (ED) for measure of similarity. The thermal demand is associated with apparent temperature (AT) for similar day and is assumed to produce similar thermal demand. The values of EDs, based on normalised AT (\tilde{AT}) at particular hour(h) of the day (d), are calculated for each and every historical similar days(d^i) using (59) [74]

$$ED(\tilde{AT}, d, d^i) = \sum_{h=1}^{24} (\tilde{AT}_h^{(d)} - \tilde{AT}_h^{(d^i)})^2 \quad (59)$$

Here, $ED(\tilde{AT}, d, d^i)$ is the ED between day d and historical days d^i with

respect to \tilde{AT} . The thermal demand corresponding to smallest value of EDs is selected, as days with similar pattern of AT generates very small values of ED.

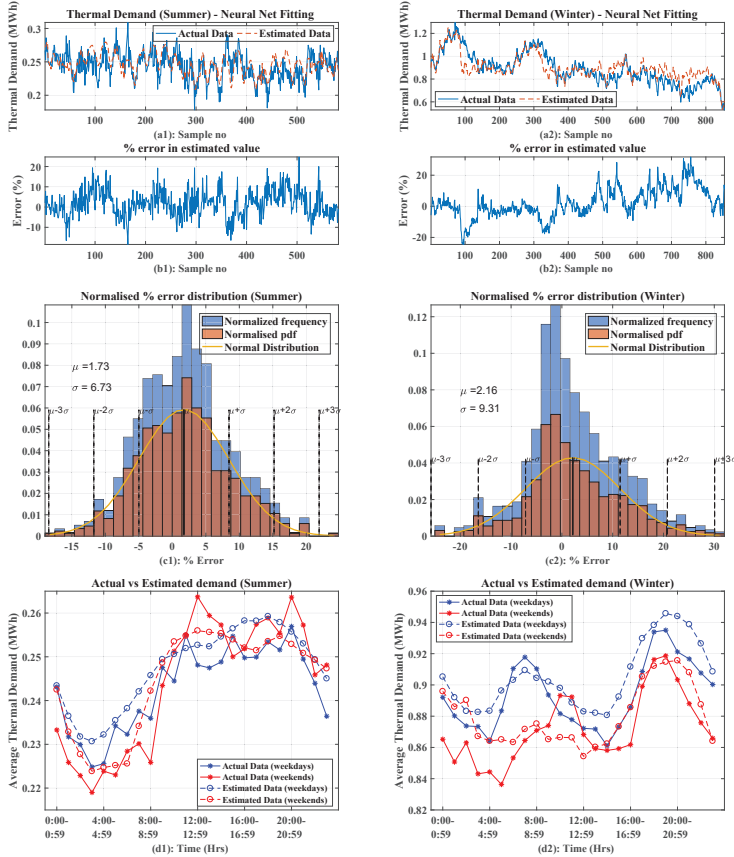


Fig. 25: Forecasting of thermal demand using neural net fitting tool for summer and winter [J2].
Row a: actual data and estimated data
Row b: % error associated with estimation of thermal demand
Row c: histogram of %error and its normal distribution
Row d: Analysis of average thermal demand (actual and estimated) in hourly basis for different weekdays and weekends

The results from the estimation of Q_{DHW} during summer and winter, using a neural net fitting tool, is summarised in Fig. 25. The estimated and actual demand is presented in Fig. 25a while Fig. 25b shows the associated %error in estimation. Normalized %error distribution is illustrated with the mean and standard deviation in Fig. 25c. Finally, the average value of estimated data and actual data are compared with respect to time of day, weekdays and weekend for summer and winter in Fig. 25d. The estimated

3. Data Analytics of Energy Consumption

data closely follow the trend and pattern associated with thermal demand. Similar observations are illustrated in Fig. 26 for estimation analysis using similar day method. The range of percentage error as seen from Fig. 26b is

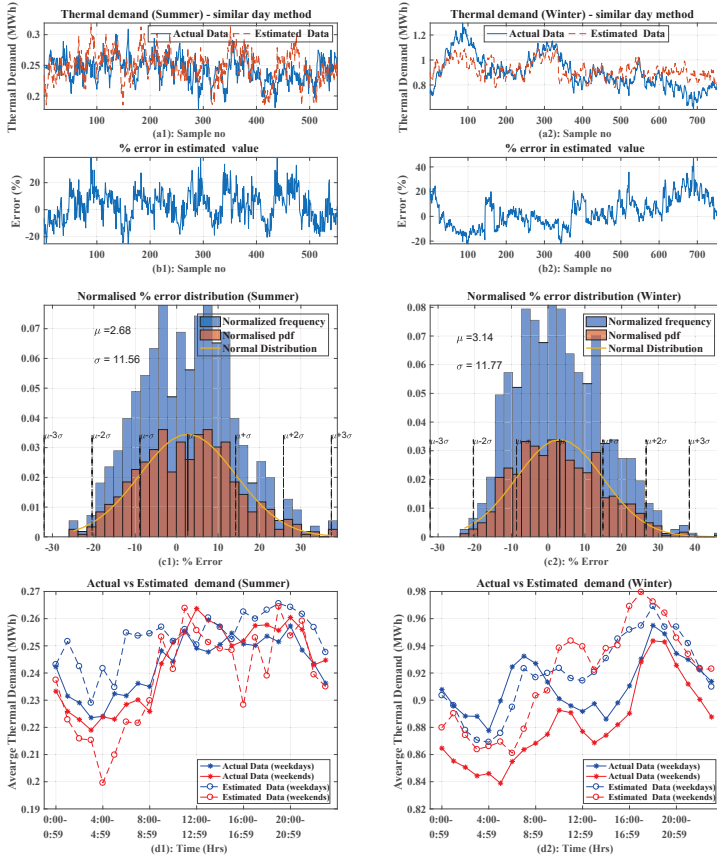


Fig. 26: Estimation of thermal demand using similar day method for summer and winter [J2].
Row a: actual data and estimated data
Row b: % error associated with prediction of thermal demand
Row c: histogram of %error and its normal distribution
Row d: Analysis of average thermal demand (actual and estimated) in hourly basis for different weekdays and weekends

higher than with the neural net fitting tool, see Fig. 25b. However, with less number of the dataset, similar day approach is equally reliable as a neural net fitting tool. Important facts and figures from the analysis are presented in table 10 for both methods of estimation. Difference between the estimated value by a model and the actual value observed is measured using root mean square error (RMSE). Mean absolute percentage error (MAPE) is used to estimate how close the estimated values are to actual values in

percentage.

Table 10: Errors from thermal demand estimations [J2]

	Neural Network		Similar Day	
	Summer	Winter	Summer	Winter
MAPE	5.459	7.30	9.57	9.72
RMSE	0.016	0.08	0.028	0.103
Mean (μ) %error	1.73	2.16	2.68	3.14
Std.Dev (σ)	6.73	9.31	11.56	11.77

Results from Fig. 25 and Fig. 26 support that the knowledge of apparent temperature and users pattern behaviour in aggregate is good enough for the estimation of thermal demand. The Q_{DHW} pattern with peaks and valleys are well preserved with estimated values as seen in Fig. 25(d1-d2) and Fig. 26(d1-d2). However, the error in the magnitude of estimated demand is expected from the thermal components that are not much dependent on the external temperature, eg., domestic hot water usage. Using a thermal storage tank, error in estimated demand can be compensated.

The results of curve fitting techniques are compared with the time series estimation, in existing literature, based on estimation errors. Here, the %Errors in the estimated value using the neural net fitting and similar day method for winter season ranges between -23% to 31% and -21% to 45% respectively. Whereas, in [38] it ranges from -33 to 15 with use of time series ANN. According to [40], the MAPE for 24hrs ahead forecast is 7.28% for winter which is similar to the results, as discussed here, with MAPE of 7.3% during winter using neural net fitting and 9.72 using similar day method. Further, in [39] the MAPE errors for different machine learning technique for different area varies between 5-27%. Hence, the curve fitting techniques discussed here is a well competent and simple estimation tool for thermal demand estimation using AT and hourly pattern concerning weekdays and seasons.

3.4 Residential and Thermal Load Profile

Residential load profile

Generation of residential load profile without heating is detailed in [C3]. The electricity consumption measured at the secondary of the transformer, during typical winter days, is distributed as a percentage of total daily load with an interval of 15min as shown in Fig. 27a. The daily average electricity consumption of residents, shown in the LV network of Fig. 14, are generated from their annual demands and is illustrated in Fig. 27b. These demands are multiplied with the profile, Fig. 27a, and generates in this way the load

3. Data Analytics of Energy Consumption

profile of 164 houses for 24 hours. Thus, the electricity demand of 164 houses has the same profile but different magnitudes. Random noise is further introduced to the individual house's profile in order to introduce unique load patterns with several peaks and to emulate daily activities resulting in transients of significant magnitudes [C3].

Noises, with exponential distribution rate of 1 and an interval of 3 minutes using a sample and hold function in DigSILENT power factory, are chosen to represent average peaks of 2-3kW. These peaks, in general, represent an electric kettle, an oven or some baseload operated 3-15 times per day for 2-5 minutes [75]. The load profile of four houses (H001, H002, H003 and H004 with daily demand as shown in Fig. 27a) with peaks of magnitudes at various time intervals are illustrated in Fig. 27c. The peaks range between 0.5-16kW for 164 houses with an average of 4.18kW and standard deviation of 2.47kW. Higher peaks represent the operation of several loads such as microwave, electric cooking stoves, induction heater, and other electric appliances that are turned ON simultaneously for a short period of time. The range of daily load factor is 6.7-19.5% with an average of 11.4% and standard deviation of 2.4% and is comparable to 6-43% with most being 8-15% [75].

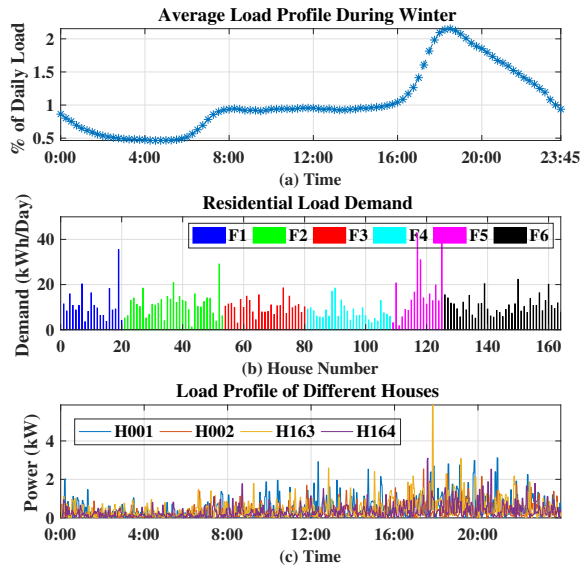


Fig. 27: (a) Residential load profile as a percentage of daily consumption with 15-minute interval, (b) Simulated residential load demand per day with noise, (c) Simulated daily residential load with noise [C3].

Thermal load profile

This section deals with the thermal consumption of the individual houses. The thermal demands of the individual houses are measured data from a residential area in Denmark, different from the grid shown in Fig. 14. The hourly load profile of thermal demand during peak winter is presented in Fig. 28a as a percentage of total consumption in 24 hours. The maximum thermal consumption of the different houses during a peak winter day is illustrated in Fig. 28b. The profile, as shown in Fig. 28a, is multiplied with the thermal demand per day for individual houses as shown in Fig. 28b to generate the daily heating load profiles of the individual houses. Thus, all houses have similar demand profile with different magnitudes. Considering the storage system in the thermal network, the transient behaviour of demand is not taken into consideration. Flexibility from the thermal storage systems, modelled based on the single-mass and the two-mass systems, are analysed in further studies. Thermal demands are distributed based on the electricity consumption of houses, as shown in Fig. 14 network. Higher electricity demand houses are associated with higher thermal demand and vice versa. This thermal profile is used in the further simulation model to evaluate the grid condition, impact assessment and flexibility due to the integration of the thermal system in the existing electricity network.

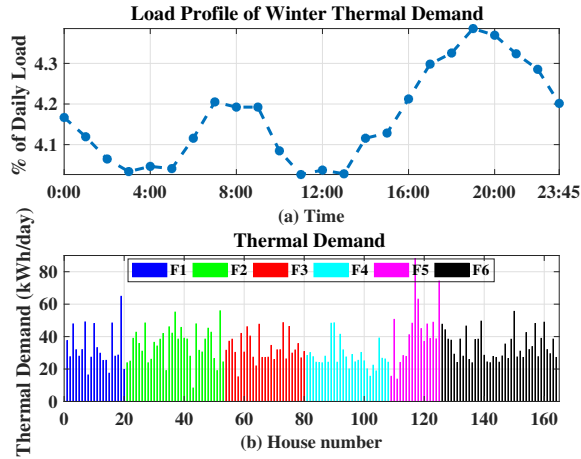


Fig. 28: (a) Thermal heat demand profile, (b) Thermal Demand of houses [C3].

3.5 Analysis of Driving Distance of Passenger Car

Analysis of Driving distance and state of charge (SOC), as discussed in [J3], gives insight on battery energy status to establish flexible charging management. Preference for car or public transport increases with the

3. Data Analytics of Energy Consumption

travelling distance exceeding more than 4km for walking and 8km for biking, due to benefit in terms of comfort and travel time. According to [76], trip distances (between source and destination) of 500-750m holds equal shares of people walking, biking and driving whereas, the choice of the car remains relatively stable between 60-70% for approximately 8 km and exceeding. The average and standard deviation of the trip distance for a passenger car is 15.89km and 28.81km respectively [76]. However, the average travel distance per day is 39.5km in 2014 as per [77] with three trips per day on average. Driving distance data for a single trip from the Danish national travel survey is analysed in [8] and a summary is tabulated in table 11.

Table 11: Individual driving distance distribution [8]

Distance (km)	Percentage (%)
0-10	60.5
10-20	17.5
20-30	8.3
30-40	4.2
40-50	2.7
50-60	1.5
60-70	1.1
>70	4.3

Driving Distance and SOC

The generation of SOC of individual EV's is presented in [J3]. It is assumed that all houses in Fig. 14 has one EV. Data presented in table 11 are used to generate driving distance. For trip greater than 70km, the maximum distance travelled is taken to be 80km as there are a negligible amount of cars travelling distance more than 80km. The random number is generated for each interval of distances, based on its percentage of occurrence as presented in table 11. This generated value gives the average distance travelled in a single trip to be 15km with a standard deviation of 18km. These values are comparable with analysis from [76] where average distance travelled by the car driver and car passenger is 12.7km, 15.89km with the standard deviation of 21.85, 28.81km respectively.

Looking towards the charging profile of EVs', around 70% of vehicles are charged once a day [78] where only 65% of them are fully charged. It is true when there are not enough infrastructures developed for charging EVs at parking places except than their residences, where start charging time varies. Though people are travelling alone for the shorter distance, sharing

is higher for the distance of more than 40 km travel [76]. Thus, there are different discharge from the battery for the same distance travelled, based on the number of passenger in the car. Several factors like the number of passenger in the car, driving habits, user comfort level, battery efficiency, weather conditions (hot/cold), and vehicles type and model affect the SOC of EV batteries. Thus, for the same distance travelled, SOC of different vehicles will be different. This difference in SOC can be taken into an advantage for allocating delay time to charge EV.

The energy consumed by EV for the generated driving distances is calculated by considering 1.4kWh of energy consumption per 10km distance [8]. Initially, the depth of discharge(DOD) is calculated for 24kWh battery size. Random increment of 0-46% in DOD is added, based on [J3], to emulate driving aggressiveness of users [36]. The DOD is then doubled to represent at least two trips per day (origin to destination and destination to origin). In case, the generated DOD is more than 80%, battery size of 60kWh is considered and DOD are calculated based on new battery size. The 3-phase charger of 7.4kW and 11kW are selected for EVs with 24kWh and 60kWh battery sizes respectively, to carry out balanced load flow studies in the electrical grid. Randomly distribution of EVs in 164 houses, for LV distribution grid shown in Fig. 14, and their SOC at the time of connection to charging point are shown in Fig 29. Majority of SOC are scattered between 90-100% with very few less than 50%.

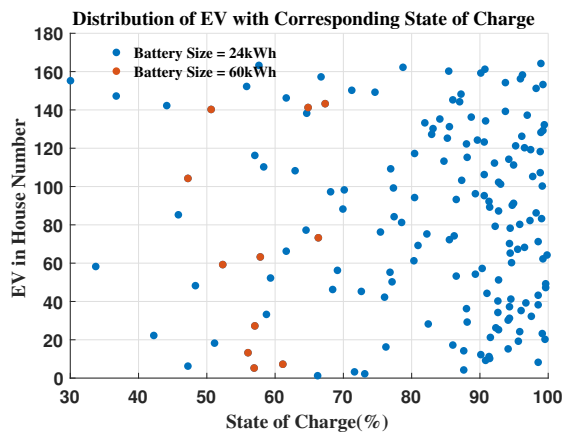


Fig. 29: State of charge in EVs battery when connected for charging in respected house [J3]

The most common time to start the first trip of the day is 7:00-8:00 hrs and last one between 15:00-16:00 hrs, considering only two trips (home-work-home) [30]. The availability of EV is higher than 94% from 16:45hrs [34]. For simplicity, the arrival time of EV is randomly distributed between the period of 15:30 to 16:45 with a time resolution of 15min. Hence, 100% of EV is

3. Data Analytics of Energy Consumption

available for charging after 16:45.

3.6 Conclusion

Daily thermal load patterns, based on aggregated users behaviour in the residential area, are observed with definite peaks and valleys during weekdays, weekends and seasonal variations. With knowledge of apparent temperatures curve fitting tools, Neural net and similar day method, are trained based on thermal load patterns (to compensate for data from individual users and geometry of buildings). The estimated thermal demands retain their user pattern with appropriate accuracy. Methods to generate thermal and electrical load profile based on their total daily consumption is presented. SOC for several EVs is generated based on analysis from driving distances.

Chapter 4

4 Optimal Schedule for Flexible Operation of The Electric Boiler

This section summarises the part of work presented in [J2] as an application of estimated thermal demand in energy management, to support the future smart grid system. The significance of the thermal storage system supporting the flexible operation of EB, based on its optimised operational schedule under dynamic tariff conditions, is presented. EB is capable of providing flexibility, with easy start-stop in short period, during balancing services of the electrical grid network.

4.1 Optimisation of EB Operation

An example of scheduling ON/OFF operation of an EB, with multiple stratified layers storage tank system as shown in Fig. 9, in district heating based on estimated Q_{DHW} under dynamic tariff condition is detailed in [J2]. Although there are possibilities to control the EB power in several stages, the problem here is simplified with just ON and OFF. The technical parameters of the EB and the storage are presented in table 12.

The optimization procedure given by eq.(60) and eq.(61) are followed to schedule optimal operating hours of the EB [J2]. The objective function minimizes the cost of electricity for production and storage of hot water demand. The constraints limits the maximum and minimum allowable hot water storage in the tank. The storage is never scheduled to discharge more than 60% of its maximum capacity (i.e, $SOE \geq 40\%$) in order to accommodate substantial error in the estimation of thermal demand. The energy extracted from the grid is constant during operation of the EB and is equal to the rated power of the EB heater (P_b). The energy extracted from the grid is able to charge the storage as well as fulfil the demand simultaneously. The operation of EB during peak hours in evening are restricted to minimise problems related to grid congestion and under

Table 12: Technical Parameters of EB and Storage [J2]

Parameters	Definition	Value	Units
V	storage volume	200	$[m^3]$
n	number of stratified layers in storage tank	10	-
λ_w	effective heat conductivity of water	0.644	$[W/mK]$
U	heat transfer coeff. of the storage walls	0.12	$[W/m^2K]$
x	diameter to height ratio of storage	2.24	-
T_a	ambient Temperature	10	$[^{\circ}C]$
T_s	supply Temperature	80	$[^{\circ}C]$
T_r	return Temperature	40	$[^{\circ}C]$
P_b	Rated Power of EB	2.4	$[MW]$
C_w	specific heat capacity of water	4190	$[J/kg.K]$

voltage in the Danish low voltage residential grid. The stored thermal energy in the tank at the end of the day is maximized to illustrate that storage tank is not only providing flexibility by supplying the thermal demand at the time of high electricity price and peak electricity demand, but also stores energy during the period of low electricity price during the 24 hour period of spot price in the electricity market.

$$\text{Minimize} \quad \sum_{t=1}^{24} C_t P_{g,t} \quad (60)$$

Constraints

$$\begin{aligned} S_{t+1} &= S_t - Q_{DHW,t} + P_{g,t} \\ S_{min} &\leq S_t \leq S_{max} \\ P_{g,t} &\in [0, P_b \Delta t] \\ P_{g,t} &= 0 \text{ for } 17 \leq t \leq 20 \\ (S_{max} - P_b \Delta t) &\leq S_t \leq S_{max} \text{ for } t = 24 \end{aligned} \quad (61)$$

Here,

C = energy price [EUR/MWh]

P_g = energy extracted from the grid [MWh]

S = energy that can be extracted from storage [MWh]

Q_{DHW} = thermal demand [MWh]

P_b = rated power of EB [2.4 MW]

subscripts: t = time [hr], min = minimum, max = maximum,

4. Optimal Schedule for Flexible Operation of The Electric Boiler

ini = initial value.

The maximum energy stored in hot water storage tank is given by (62)

$$S_{max} = M_b C_w (T_s - T_r) / (3600 \times 10^6) \quad [MWh] \quad (62)$$

$$S_{min} = 0.4 \times S_{max} \quad [MWh] \quad (63)$$

Here,

M_b = Mass of water in storage [2×10^5 kg]

T_s = temperature of supply hot water in the tank [80°C]

T_r = temperature of return water in the tank [40°C]

C_w = specific heat capacity of water [4190]/kg.K]

The large estimation error of thermal demand can lead the storage tank temperature of different layers to be away from the specified limit. $T_7 < 46^\circ\text{C}$ when the storage is discharge up to 70% of its capacity, (i.e, $SOE = 30\%$). The limit controllers, based on hysteresis control, realised with RS flip-flop, as shown in Fig. 30, are thus reinforced to provide security in demand and supply. During charging of storage tank, the EB is turned OFF when the

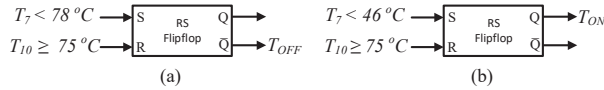


Fig. 30: Temperature limit controller schematic for ON/OFF operation of EB [J2]

temperature of the bottom layer $T_{10} \geq 75^\circ\text{C}$ (Fig. 30a), to limit the maximum flow of hot water from EB. It is turned OFF only for a short period until the temperature of the seventh layer (T_7) is less than 78°C , so that it can further follow the schedule. Control scheme shown in Fig. 30b ensures that if $T_7 < 46^\circ\text{C}$, EB is turned ON until it is fully charged (i.e., $T_{10} \geq 75^\circ\text{C}$). Apart from these two conditions, the EB is operated as per the determined schedule. The overall control strategy is shown in table 13, where C_a is the Control signal for turning ON and OFF of EB, and C_{a1} is the scheduled ON/OFF signal for EB.

Table 13: Control of EB [J2]

T_{OFF}	T_{ON}	C_a
1	x	0
x	1	1
0	0	C_{a1}

The complete methodology of the proposed system implemented for flexible operation of the EB is illustrated in Fig. 31. Tools developed in

MATLAB are used for estimating thermal demand and further applied in optimising the operational schedule for the EB. Then the flexibility in the operation of the EB based on actual thermal demand is investigated using DigSILENT power factory simulation tool.

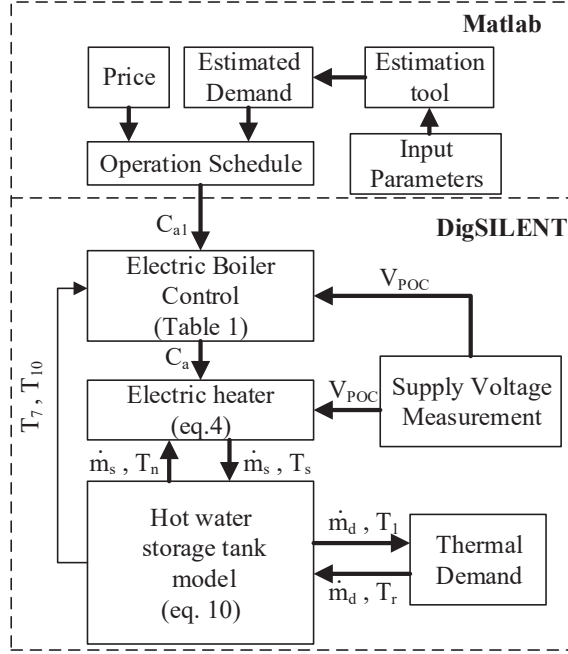


Fig. 31: System implementation for flexible operation of EB [J2]

EB is scheduled to turn ON during low electricity prices based on the optimised scheduler. The day-ahead hourly spot price of Denmark's northern region on 6th Jan 2017 and 24th Dec 2016, based on data taken from [79], are considered as case 1 and case 2 respectively as illustrated in Fig. 32a. In case 1, the hourly spot prices decrease gradually according to the time of the day. On the other hand, as in case 2, the hourly spot prices even go to negative. Negative prices are because of the high electricity generation from renewable sources such as wind or solar. These two case studies clarify the effectiveness of the optimal scheduler based on the optimisation problem as discussed in eq.(60) and (61), for the same estimated thermal demand. The estimated thermal demand, using the neural net tool, of 6th Jan 2017 and the corresponding actual thermal demand on the same day are illustrated in Fig. 32b. MAPE of estimated demand is significantly low with the value of 2.12%.

Observations from case 1: The optimal operation schedule (C_{a1} : 1= ON, 0= OFF) of EB and the corresponding energy status (PS_{status} : 1= fully

4. Optimal Schedule for Flexible Operation of The Electric Boiler

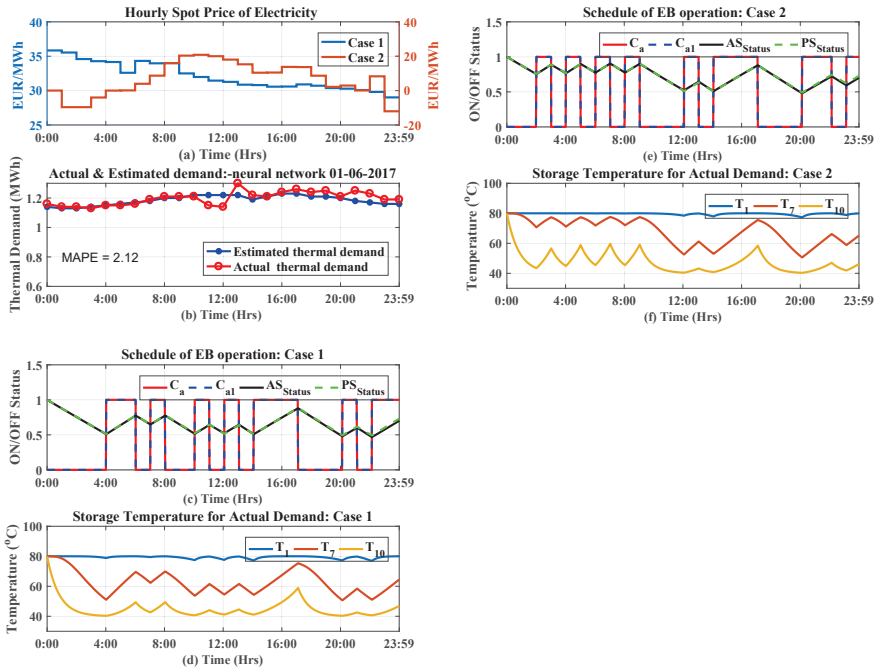


Fig. 32: Results of flexible operation of EB [J2] (a) Hourly spot prices of electricity in Denmark region DK1 case 1: 6th Jan 2017 and case 2: 24th Dec. 2016 (b) Actual and estimated thermal demand on 6th Jan 2017 (c) estimated EB schedule based on estimated demand (C_{a1}), estimated EB status (PS_{status}), and actual schedule of EB based on actual demand (C_a), and actual EB status (AS_{status}) (case 1). (d) Storage temperature of various layers for actual demand and schedule (case 1). (e) estimated EB schedule based on estimated demand (C_{a1}), estimated EB status (PS_{status}), and actual schedule of EB based on actual demand (C_a), and actual EB status (AS_{status})(case 2). (f) Storage temperature of various layers for actual demand and schedule (case 2)

charged, 0= fully discharged) of the storage tank based on estimated demand are presented in Fig. 32(c). At the same time, these values are compared with the actual operation status (C_a determined using controller shown in Fig. 30) of EB along with the corresponding energy status of the storage (AS_{status}) based on actual thermal demand. The comparison shows that the EB is operated as per the determined schedule. There is slight variation in the actual energy status of the storage due to estimation error in thermal demand. Temperatures of three different layers (top, seventh and bottom) in the storage tank are shown in Fig. 32(d). The temperature (T_1) of the first layer in the storage tank remains fairly consistent around 80°C. This consistency in the temperature means that the thermal demand has been fulfilled taking care of grid flexibility and end-user satisfaction.

Observations from case 2: Similar observations as in case 1 (Fig. 32c,d) are observed from Fig. 32e and Fig. 32f. The operation schedule is different from case 1, to optimise the energy price for charging storage.

Observations from case 3: In case 3, the effectiveness of thermal storage system to cope up with larger estimation error is visualised with the help of Fig. 33. On 23rd Mar 2017, the estimated thermal demand has larger MAPE

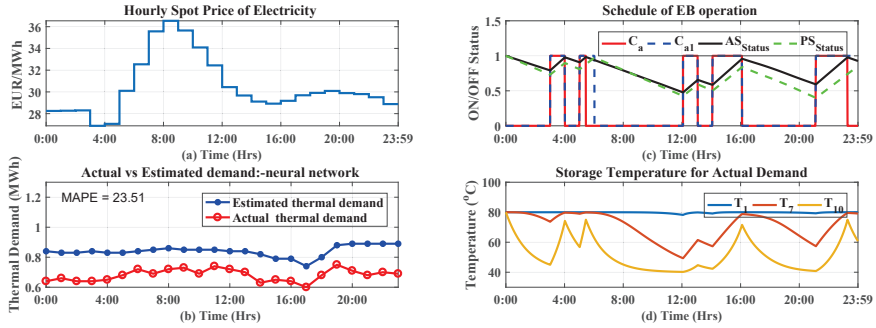


Fig. 33: Case 3: (a) Spot price of electricity in Denmark region DK1 on 23rd Mar. 2017, (b) Actual and estimated thermal demand on 23rd Mar., (c) estimated EB schedule based on estimated demand (C_{a1}), estimated EB status (PS_{status}), and actual schedule of EB based on actual demand (C_a), and actual EB status (AS_{status}), (d) Storage temperature of various layers for actual demand and schedule [J2].

(23.51%), see Fig. 33b. The hourly spot prices of electricity on the same day, taken from [79], is illustrated in Fig. 33a. While following the scheduled operation of EB (see Fig. 33c) the controller shown in Fig. 30 turns OFF EB twice, during 6th and 24th hour, as the storage tank is fully charged. There is a significant difference between the estimated and actual energy status of the storage due to the overestimation of thermal demand. The temperature of the top layer in the storage tank, as seen from Fig. 33d, indicates that the supply hot water has consistence temperature.

Conclusion

Optimum scheduling of EB with the storage tank in the multi-energy system is immensely supported by estimated thermal demand. The EB is scheduled when energy prices are lower during high generation from renewable sources such as solar and winds. The substantial error in the estimation of thermal demand is efficiently handled by the storage tank operating as a flexible load, and enhancing accommodation of renewable energy simultaneously. On the other hand, sufficient thermal energy is stored to fulfil the thermal demand and to avoid electricity consumption during evening peak simultaneously.

4. Optimal Schedule for Flexible Operation of The Electric Boiler

Operation of large EB during evening peak hours of electricity consumption can be responsible for grid congestion and under voltage in the distribution network [C3] under present condition.

Chapter 5

5 Impact Assessment of Flexible Thermal Loads in Low Voltage Distribution Network

In this chapter, the terminal voltage characteristic of the LV network presented in Fig. 14 is analysed at first. This analysis is used as the base case to compare the results from impact assessment of individual thermal units (EBs and HPs with associated thermal storage tank as the flexible thermal loads) when integrated into the LV network in each house. Finally, the significance of a central thermal station, supplying hot water to all the residences associated with LV network in Fig. 14, is compared with the use of single thermal units in all the residences. The central thermal station is based on a single EB and a thermal storage tank with a thermal distribution network. This chapter summarises the results from work presented in [C2] and [C3].

5.1 Characteristic of LV Residential Distribution Network

The knowledge of grid voltage profile, for the LV network as presented in Fig. 14, is helpful to define proper strategies and control parameters, under demand response. The proper demand response helps to accommodate and operate flexible devices such as thermal (EB and HP) and EV loads. It further supports to maintain the node voltages of the LV network within its operating limit of $\pm 10\%$, as recommended standard EN 50160. The electrical load profile and daily demands, as presented in section 3 Fig: 27, has detailed discussion in [C3]. The performance of the LV grid is investigated using Steady-state power system analysis in DigSILENT Power Factory. Fig. 34 summarises the result of observation based on minimum terminal voltages attained in each feeder (F1-F6). Feeders F3 and F4 are the strongest feeders of all, with minimum terminal voltages at T19 and T99 is 0.98pu, followed by F2-T47 (Feeder 2, terminal 47). On the other hand, feeders with terminals F1-T19, F5-T125, and F6-T162 attain the minimum

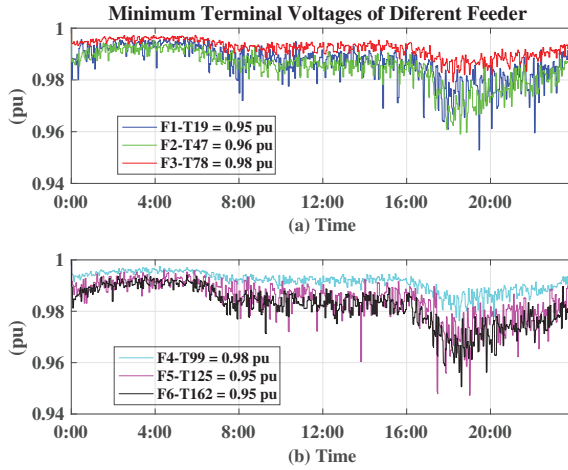


Fig. 34: Terminal voltages with the maximum voltage drop of different feeders [J1] (a) Terminals in feeder F1, F2, and F3 (b) Terminals in feeder F4, F5, and F6.

voltage of 0.95 pu during peak hour. F6 is the most heavily loaded feeder, with 421 kWh/day and 39 houses.

5.2 Flexibility and Impact Assessment of The EBs and HPs in LV Residential Distribution Network

Flexibility from thermal units is unleashed with the help of a proper control system. Various ON/OFF control schemes, of thermal system, based on measurement of local parameters from LV grid (terminal voltage at the point of coupling of the thermal unit) and thermal storage system (level and temperature of hot water in the storage tank) are presented in this section. The significances of control systems concerning grid impact, flexible operation of thermal units, and fulfilment of thermal demands are analysed in this section.

Control unit for ON/OFF operation of EBs and HPs

The temperature of hot water (T_h) and the level of cold water (X_c) in the storage tank, modelled based on the two-mass model in Fig. 7, is maintained with the help of hysteresis control. The hysteresis in control is logically represented as RS-flip-flop, as illustrated in Fig. 35. The signal T from the temperature controller in Fig. 35a remains high when $T_h < T_{min}$ and continues as long as $T_h < T_{max}$. In the same way, the signal H from the level controller in Fig. 35b remains high when $X_c < X_{max}$ and continues as long as $T_h < T_{max}$. The hysteresis in the voltage controller, as illustrated in

5. Impact Assessment of Flexible Thermal Loads in Low Voltage Distribution Network

Fig. 36, is implemented further to restrict the operation of the EBs and HPs during the under-voltage situation. If the terminal voltage at the point of common coupling of the EBs and HPs are below V_{min} , the signal V1 remains low until V_t recovers to recovery voltage of V_{rec} .

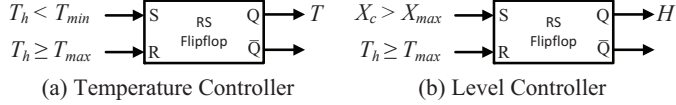


Fig. 35: Logic diagram representation of hysteresis control for (a) Temperature and (b) level of hot water in the storage tank.

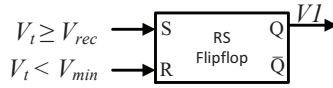


Fig. 36: Logic diagram representation of hysteresis control based on terminal voltage.

The flexibility from the EBs and HPs are accessed based on two control approaches illustrated in Fig. 37.

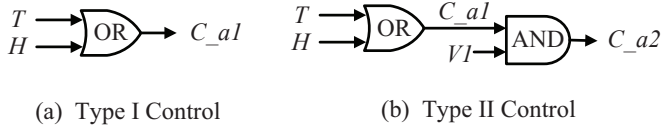


Fig. 37: Control signal for ON/OFF Operation of thermal actuator (a) Type I control, (b) Type II control.

Type I control, with temperature and level control as illustrated with logic diagram in Fig. 37a, helps to understand the impact of the EBs and HPs in the LV grid. Type II control is primarily based on grid voltage at the point of common coupling and secondarily on temperature and level control based on the logic diagram shows in Fig. 37b. The controller prevents the LV grid voltage from attaining the lower operational limit of -10% . C_{a1} and C_{a2} are the signal to turn ON/OFF the thermal actuator for type I and type II control respectively. Logic status high is ON, and low is OFF.

The parameters used in the control unit illustrated in Fig. 35 and Fig. 36 are presented in table 14, for EB and HP. The difference in T_{max} for EB and HP is due to the limit from manufactures. The upper bound for X_{max} is selected to maintain the temperature inside the storage tank to remain greater than T_{min} . The lower bound of $V_{min} = 0.92\text{pu}$ is selected to maintain grid terminal voltage at the point of coupling above 0.9pu . The recovery voltage is set to avoid the hunting effect due to the voltage controller.

Table 14: Parameter of Storage tank [C2]

	$T_{max}(^{\circ}C)$	$T_{min}(^{\circ}C)$	V_{min} (pu)	V_{rec} (pu)	$X_{max}(\%)$
EB	80	65	0.92	0.98	25
HP	70	55	0.92	0.98	25

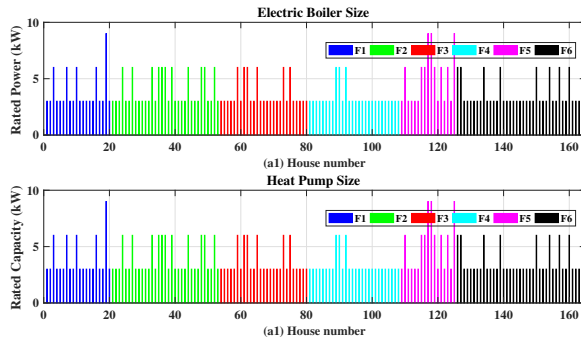
Case studies

Impact on the LV network in Fig. 14, due to the integration of EBs and HPs separately in all residences, is analysed with four case studies as presented in [C2]. Daily demands and load profiles of the residential and thermal loads discussed in section 3 Fig. 27 and Fig: 28 respectively are considered in the analysis. The heating units and storage sizes for the EBs and HPs are presented in table 15 and their distribution in the LV network is illustrated in Fig. 38. The sizes and power ratings are commercially available and

Table 15: EB and HP size allocation [C2]

Thermal Demand (kWh)	Storage Size (m^3)	EB Rated Power (kW)	HP Heat Capacity (kW)	No of units
< 40	0.5	3	3	122
40-60	0.75	6	6	38
60-90	1	9	9	4

selected based on the thermal demand of individual houses to ensure a continuous supply of hot water for 16hrs when fully charged.

**Fig. 38:** Size of thermal units associated with different houses [C2]: (a) EB, (b) HP

The case studies are carried out to analyse and compare the dynamic behaviour, of the proposed system and controllers, in time domain using

5. Impact Assessment of Flexible Thermal Loads in Low Voltage Distribution Network

DigSILENT power factory simulation tool. The simulations for case studies are carried out for the period of 24hrs.

- Case I: Residential Load.
- Case II: Residential Load with EBs and HPs separately in all residences based on type I control.
- Case III: Residential Load with EBs and HPs separately in all residences based on type II control.
- Case IV: Residential Load with EBs modelled as the single-mass model of the storage tank, and temperature control.

Case I is the base case. Grid conditions such as transformer and lines loadings and terminals voltages are observed. Case II studies the grid dynamics due to the connection of thermal units, first with only EBs and then with only HPs, in all residences and type I controller. The results of the case I and II are compared. Case III is the repetition of case II using type II controller to overcome the problem associated with under-voltage observed in case II. Finally, case IV provides a better understanding of using the stratified layered storage tank model compared to the average model.

Initial conditions

The amount and time of thermal energy consumptions depend upon users behaviour, their comfort level and geometry of buildings. Thus, the ON/OFF status of the EBs/HPs, and the status of T_h and X_c of the thermal storage tank, at any particular instant of time are inconsistent. Hence, the initial

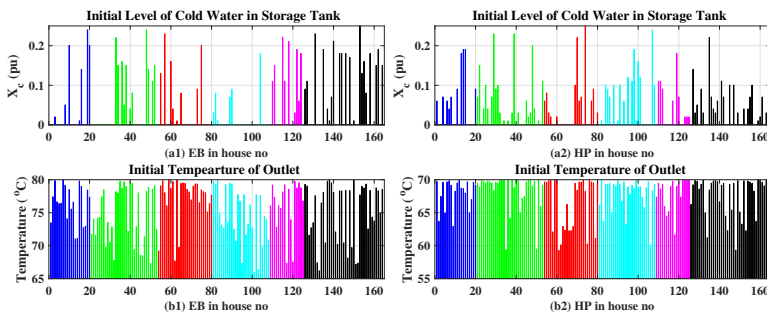


Fig. 39: (a1),(a2): Initial condition of cold water level in storage tank for EB and HP, (b1),(b2): Initial condition of temperature of outlet for EB and HP [C]

conditions are generated using case II. First off all $X_c = 0$, $T_h = T_{max}$ and $C_{a1} = 0$ are selected. Then the simulations as per case II were carried out for a simulation period indicating 72hrs, and the final values of X_c , T_h and

C_{a1} were selected as initial conditions for all relevant case studies. The initial conditions of X_c and T_h for the EBs and HPs are illustrated in Fig. 39. The initial condition for $C_{a1} = 1$ if $X_c = 0$, as there are no stratification in the storage tank during charging process.

Results and discussions

case I: Fig. 40 shows results from case I. The transformer is utilised only up to 28% of its rated capacity (Fig. 40a), while grid voltages at far end buses in feeders ranges between 0.95-0.99pu (Fig. 40b). The Maximum line loadings are always below 50% (Fig. 40c). Thus, there are opportunity to integrate thermal heating system such as EBs and HPs. The summary of results from all case studies are presented in table 16.

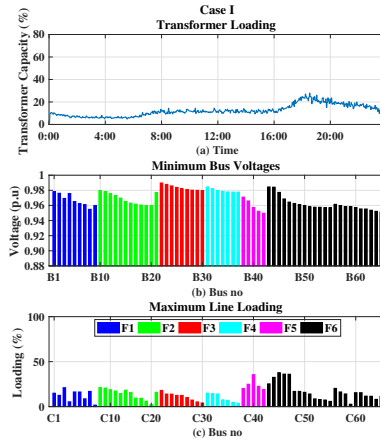


Fig. 40: Results of case I [C2], (a) Transformer loading, (b) minimum bus voltages, (c) Maximum line loadings.

case II: Results from case II are presented in Fig. 41. Integration of the EBs with type I control (temperature and level control) increases the transformer loadings up to 75% (Fig. 41a1). Bus voltages in feeder F2 and F3 drops below 0.88pu violating the grid regulation of $\pm 10\%$ (Fig. 41b1). The maximum line loadings reaches up to 96%(Fig. 41c1). These situations are quite critical for any fluctuation or growth of sizeable loads, although 25% of transformer capacity remains underutilised. However, the daily load factor of the network improves, with an average value of 30.49% , compared to the case I as seen from table 16. When EBs are replaced with HPs, able to supply same thermal demand, the grid conditions improves drastically. The transformer and line loadings, observed from Fig. 41a2 and Fig. 41c2, decreases to value of 45% and 61% respectively, while the minimum bus voltages attained is within the operating limit with ranges between 0.91-0.98pu (Fig. 41b2). This is possible

5. Impact Assessment of Flexible Thermal Loads in Low Voltage Distribution Network

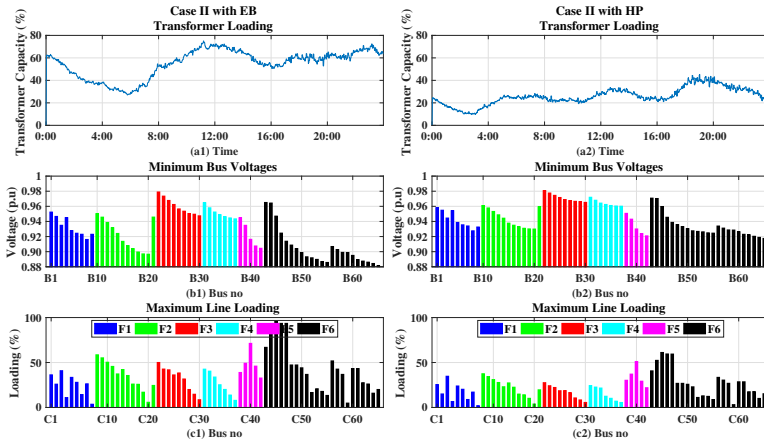


Fig. 41: Results of case II: column 1 for EB, column 2 for HP, (a) Transformer loading, (b) minimum bus voltages, (c) Maximum line loadings [C2].

due to the COP of HP, where less electricity is utilised to deliver the same amount of heat as in EBs. The use of HPs also increases the average daily load factor to 33.42% (table 16), indicating its effectively utilisation for peak shaping.

case III: The under-voltage problems associated with type I controller is tackled using type II controller in case III. Similar observations as in case II, are presented for case III in Fig. 42. Grid dynamics are improved and are

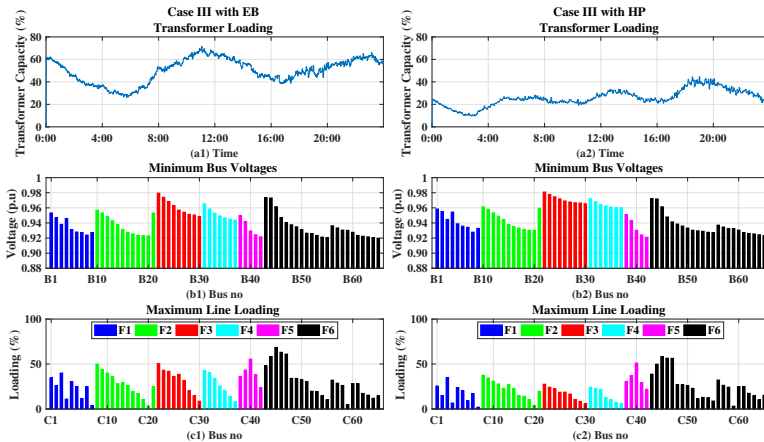


Fig. 42: Results of case III: column 1 for EB, column 2 for HP, (a) Transformer loading, (b) minimum bus voltages, (c) Maximum line loadings [C2].

within the allowable limit. However, some EBs, especially at the far end of

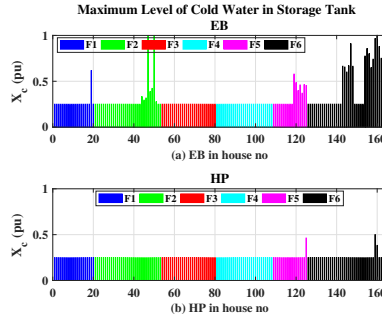


Fig. 43: Results of case III: Maximum level of cold water in the storage tank, (a) EB, (b) HP [C2].

the feeders, are not able to operate and fulfil the thermal demand (Fig. 43a) due to the poor voltage at POC (point of coupling). Under similar conditions, HPs provides better performance for the electrical grid as well as fulfilling the thermal demand (Fig. 43b) simultaneously. Compared to case II with HP, maximum line loadings are reduced, and minimum bus voltages are improved (table 16). However, the daily load factor decreases as the voltage controller limits the operation of HPs during under-voltage.

case IV: The initial condition of the temperature inside the storage tank is the average temperature, calculated using eq.(19) for the initial condition for EBs presented in Fig 39. The results from case IV are presented in Fig. 44. The

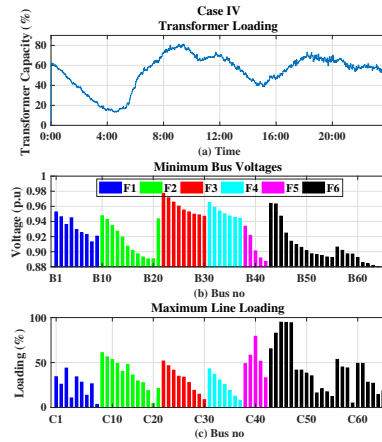


Fig. 44: Results of case IV [C2], (a) Transformer loading, (b) minimum bus voltages (c) Maximum line loadings.

use of the non-stratified tank in case II, shows deeper voltage drops ranging from 0.87-0.97pu as seen from table 16. This drop is due to the gradual fall of supply temperature in the average model storage tank, which needs the

5. Impact Assessment of Flexible Thermal Loads in Low Voltage Distribution Network

frequent operation of thermal units. Thus, the use of a better model of storage can accommodate higher grid integration of thermal loads. The stratified model provides reliable information based on the level and temperature of hot water in the storage tank. These informations are used for further smart control of EB and HP, showing potential for giving more flexibility than the average models are showing.

Table 16: Summary of case studies results [C2]

	Case I	Case II (temp. control)		Case III (voltage control)		Case IV Case IV
	Res. load	EBs	HPs	EBs	HPs	EB (Avg)
Transformer Loading (%)	4.5-28	27-75	9.6-45	26-72	9.6-45	13-81
Minimum Bus Voltages (pu)	0.95-0.99	0.88-0.98	0.91-0.98	0.92-0.98	0.92-0.98	0.87-0.97
Maximum Line Loading (%)	1.6-38	3.6-96	2-61	2.7-69	2-58	3.4-95
Daily load factor (%) of 164 houses						
Range (%)	6.8-19.5	18.2-44.5	17.6-45.3	10.5-42.6	7.6-45.3	15.3-43.6
Mean	11.43%	30.49%	33.42%	28.77%	30.16%	30%
Std.	2.42%	5.38%	5.53%	6.55%	8.71%	5.57%

Conclusion

A brief overview of EBs and HPs with storage operated as flexible thermal loads in Denmark's low voltage distribution network is presented. Stratified model of the thermal storage tank has significant advantages over average model storage tank. The advantages are in terms of showing the right flexibility in operation, storage and fulfil thermal demand with the possible practical measurement of temperature and level of hot water in the storage tank, and for demand response. A strategy based on temperature and voltage control associated with flexible control of the HPs is discussed, to mitigate the problems with low voltage in week feeders and satisfying the end-user need simultaneously.

5.3 Accommodation of EBs in LV Grid

As observed from case study III in section 5.2, the proposed system is not able to fulfil the thermal demand due to the idling caused by the voltage control. Thus, modification in EB controller is performed to flexibly operate the EB and storage units to fulfil the thermal demand as well as operate EBs within the grid voltage limits simultaneously. The type II controller presented in Fig. 37 is further facilitated with an overriding control as represented with

the logic diagram in Fig. 45. The overriding control sends a signal to operate

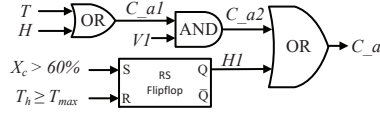


Fig. 45: ON/OFF control signal for operation of thermal actuator with priority.

EB, irrespective of terminal voltages when 60% of the storage tank is filled with cold water. The signal remains high until the temperature of hot water reaches the maximum allowable temperature of 80°C. This control assures that the user comfort is not compromised due to voltage control limits of the EB. This section summarises the part of work presented in [C3].

Result and discussion

The simulation results, as in case III of section 5.2 with modified control system for operation of EBs presented in Fig. 45, are illustrated in Fig. 46. Compared to the results from case III of section 5.2, The transformer is is

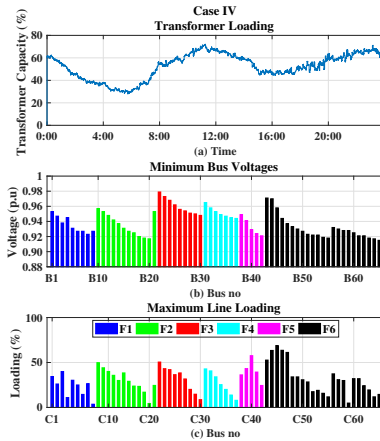


Fig. 46: Simulation results of EB with priority control in Fig. 45 [C3], (a) Transformer loading, (b) minimum bus voltages, (c) Maximum line loadings.

loaded between 25-70% (Fig. 45a), which is lower than 27-75% (Fig. 46a). The minimum bus voltage attained is 0.91pu (Fig. 46b). The maximum line loading is 68.9% (Fig. 46c). The accumulation of cold water, in some of the terminals in feeder F3 and F6, is more than 25%, due to the action of the voltage controller, as seen from Fig. 47a. The provision of the overriding control, discussed in Fig. 45, allows operation of EBs with $X_c > 60\%$. During the charging process mixing of liquids from stratified layers causes a sudden

5. Impact Assessment of Flexible Thermal Loads in Low Voltage Distribution Network

drop of hot water temperature causing the minimum temperature of hot water in the storage tank drops to around 42°C as seen from Fig. 47b. The temperature then rises gradually until the storage tank is fully charged. The daily load factor ranges between 17.29-42.64% with a mean and standard deviation of 29.68% and 5.56% respectively.

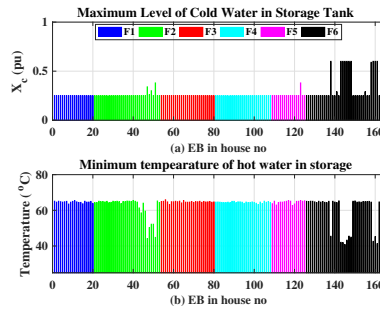


Fig. 47: Results of case III: (a) maximum level of cold water in the storage tank, (b) minimum temperature of hot water in the storage tank [C3].

Conclusion

The use of proper controller as demand response can fulfil thermal demand while operating the EBs within the operational limit of $\pm 10\%$. The grid reinforcement is necessary to handle further growth in electrical load as the bus voltages are in a critical state, as seen in Fig. 46. The use of HPs, on the other hand, is a better option due to its high coefficient of performance.

5.4 Grid Impact With EB as A Central Thermal Unit

The impact of the central thermal unit is evaluated to examine its significance over the use of small thermal units in individual houses. Fig. 48 shows the integration of an EB and a thermal storage system with a control unit in the LV grid network of Fig. 14. As the cable ratings of the LV network ranges from 98-281Amp, the existing network is not able to integrate large EB at any of its terminals. Thus, the EB is connected at the secondary of the distribution transformer.

As seen from section 5.2 and 5.3, the transformer is loaded between 4.5-30% with only residential load whereas with EB and voltage controller (case III with type II controller in section 5.2) the transformer is loaded between 25-70%. Thus, there is an increment in transformer loading by 20-40% (126-252kW) due to the integration of EBs. Also, The total Thermal demand is 5.57MW/day, i.e. in average 232kW of thermal demand is necessary per hour. Hence, considering the peak loading of the transformer

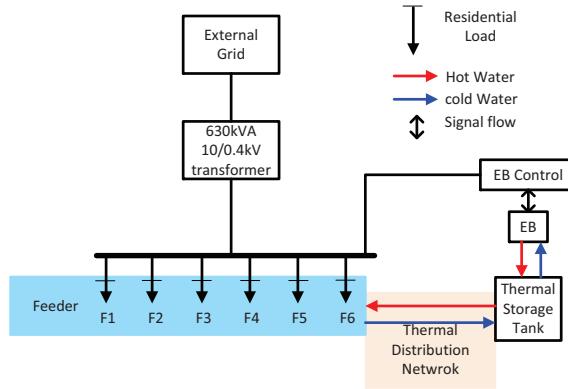


Fig. 48: Integration of an EB and a thermal storage system in LV grid network.

due to EBs (252kW) and an average thermal demand of 232kWh, the EB of size 250kW seems to be a good choice with thermal storage tank. However, to enhance operational flexibility from the EB by storing thermal energy during peak electricity consumption or high electricity generation from renewables, an EB of 400kW is selected. This rated size of the EB operated in low voltage electric grid is available in the market. The supply and return temperature is considered to be 80 and 30 °C, respectively. The size of the thermal storage tank is calculated to be 40m³, so that it can continuously supply average thermal demand for 8hrs. The appropriate size of storage tank helps to attain flexibility in the operation of thermal units by decoupling supply and demand. The size of the EB and its associated storage tank can be optimised based on the need of flexibility in terms of the total hour for the operation of the EB, storage of thermal energy, and the cost of equipment. However, the selected rating and size of the EB (400kW) and storage tank (40m³) are to show the effect of using the central thermal unit for the small residential area compared to those in individual houses.

Based on the optimisation problem discussed in chapter 4, given by given by eq.(60) and eq.(61), the optimal schedule of EB is determined for average thermal demand. The n-stratified layered thermal storage tank is modelled as per eq.(46) in section 2.4. The ON/OFF control system, relevant parameters and the system implementation for flexible operation of EB are based on chapter 4. The technical parameters of the EB and the storage are presented in table 17. The electrical load profiles and values without thermal heatings and EVs for 144 houses are presented in Fig. 27. The thermal load profile and value is the aggregate of thermal demand of the individual houses presented in Fig. 28. To simplify the problem, associated transmission losses for thermal demand is neglected. However, the losses are important for economic analysis. The results of the steady-state

5. Impact Assessment of Flexible Thermal Loads in Low Voltage Distribution Network

Table 17: Technical Parameters of EB and Storage

Parameters	Definition	Value	Units
V	storage volume	40	$[m^3]$
n	number of stratified layers in storage tank	10	-
λ_w	effective heat conductivity of water	0.644	$[W/mK]$
U	heat transfer coeff. of the storage walls	0.12	$[W/m^2K]$
x	diameter to height ratio of storage	2.24	-
T_a	ambient temperature	15	$[^\circ C]$
T_s	supply temperature	80	$[^\circ C]$
T_r	return temperature	40	$[^\circ C]$
P_b	rated power of EB	0.4	$[MW]$
C_w	specific heat capacity of water	4180	$[J/kg.K]$
Total Q_{DHW}		5.57	$[MW/day]$

simulation, in DigSILENT powerfactory, representing 24 hours period are shown in Fig. 49

Result and discussion

Fig. 49a shows the hourly spot price of electricity in Denmark region DK1 dated on 23rd Mar 2017 [79]. Fig. 49b shows the hourly profile of total thermal demand feeding 164 houses, and is equal to aggregated values of thermal demand presented in Fig. 28. Based on the hourly spot price of electricity and the total thermal demand, the EB is optimally scheduled to operate based on optimisation problem represented with eq.(60) and eq.(61). The optimal operational schedule of the EB is presented in Fig. 49c as C_{a1} . The signal C_a indicates the ON/OFF operation of EB, based on control system presented in Fig. 30 with control logic given in table 13. As C_a precisely follows the optimised value (C_{a1}), the optimisation problem with average hourly consumption of Q_{DHW} is reliable. The SOE in the storage tank (Fig. 49c) Indicates that the thermal energy is stored during the low electricity price to fulfil the thermal demand during peak electricity demand between 17:00-20:00hrs without the operation of the EB. Temperatures of top (T_1), bottom (T_{10}) and 7th layer (T_7) in the stratified layers of storage tank presented in Fig. 9 is illustrated in Fig. 49d. The temperature of hot water in the top layer (T_1) ranges between 74-80 $^\circ C$, indicating that the user demand

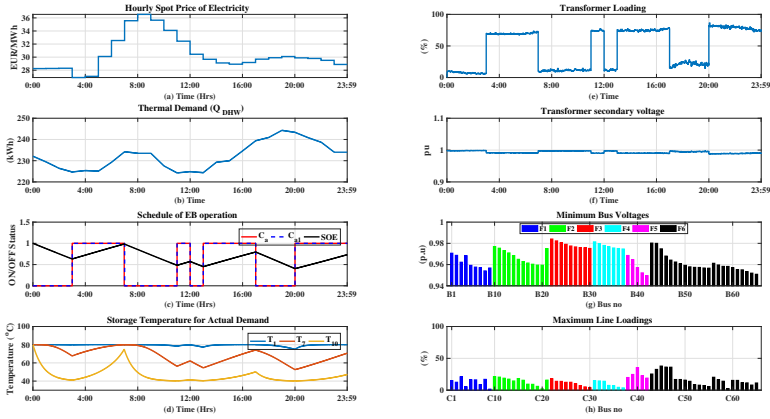


Fig. 49: (a) Spot price of electricity in Denmark region DK1 on 23rd Mar 2017, (b) Thermal demand, (c) SOE: state of energy in thermal storage tank, C_{a1} : scheduled ON/OFF operation of the EB, C_{a2} : actual ON/OFF operation of the EB., (d) temperatures of top (T_1), bottom (T_{10}) and 7th layer (T_7) of EB, (e) Transformer loading, (f) secondary terminal voltage of transformer, (g) minimum bus voltages in feeders of LV grid, (h) maximum line loadings in feeders of LV grid.

is fulfilled all the time.

The impact assessment of the LV network due to the operation of the EB is presented in Fig. 49e-h. The distribution transformer is loaded between 5.6-86.4% as seen from Fig. 49e. Whereas, with EBs in individual houses, the transformer loadings range between 26-75% [C2]. Thus, the use of a single EB creates more peaks and valleys. This problem can be solved by operating large EB in different discrete power levels or continuous power control using power electronic controller. Fig. 49f shows the voltage at the secondary of distribution transformer ranging between 0.99-1pu, which is well within its operating limit of $\pm 10\%$. Fig. 49g and Fig. 49h show the minimum bus voltages and the maximum line loadings respectively in the LV network. The bus voltages and line loadings range between 0.95-0.1pu and 1.6-38% respectively, which is similar to results from the case I in [C2] with only residential loads. The summary of results with a single EB, centrally representing a particular residential area to fulfil thermal demand, and individual EBs in the houses in the same residential area is presented in table 18.

Without considering the economic analysis for installation of EBs and storage tanks, either centrally located with a thermal distribution network for a small area or in individual houses, there are several advantages of using local central EB and thermal storage system. One of the significant benefits with the use of central EB and storage system is that there is no need for expensive existing grid reinforcement. Also, there is no need for intensive communication network infrastructure and complex handling of

5. Impact Assessment of Flexible Thermal Loads in Low Voltage Distribution Network

Table 18: Technical Parameters of EB and Storage

	Single large EB	One EB in individual houses
Transformer Loadings (%)	5.6-86.4	26-75 [C2]
Bus Voltages(pu)	0.95-1	0.88-0.98 [C2]
Line loadings (%)	1.6-38	2.7-96 [C2]
User initiative to control EB	NO	YES
Fulfil thermal demand	YES	Compromise between terminal voltage and thermal demand [C3]
Size of EB	400(kW)	630kW in total
Size of storage	40 (m^3)	93.5 (m^3) in total

big data for optimal and flexible operation of the EBs, compared to EBs in individual houses. On the other hand, the central unit has no control problem regarding user initiative. The total size of EB and storage in the central system is smaller than combine values from individual houses. This reduction in sizes solves the problem of under-voltage in LV terminal, and overloading of transformer and transmission lines when all EBs in single houses are operated at the same time [C2].

5.5 Conclusion

The impact of EBs and HPs in individual houses in LV distribution network is significant in terms of under voltages and line loadings, despite enough capacity in the transformer to accommodate an increase in thermal loads. The use of a proper control system and thermal units (HPs instead of EBs), problems associated with under-voltages and line loadings can be mitigated up to some extent. However, there is limited room for further growth in thermal and electricity demand with the use of EBs. The use of the central thermal station for a small residential area mitigates all these problems, while utilising transformer capacity, and enhances flexibility in operation and storage of thermal energy without user initiative.

Chapter 6

6 Integrated and Autonomous Operation of the Flexible Loads

This chapter summarises the results from work presented in [J1] and [J3]. Flexibility from distributed flexible loads, such as HPs with storage and EVs charging in individual houses, is unleashed with the use of the proposed autonomous controller. The proposed controller is attached with individual HP and EV charging system. The significance of the proposed ON/OFF control system is evaluated, for successful operation and control of integrated multi-carrier energy systems, in the low voltage distribution network. The controller, associated with individual thermal and EV charging units, manages to flexibly operate within the recommended lower operating limits of grid terminal voltages (-10%) at the point of coupling (POC). The flexibility from thermal and EV charging systems are shared flexibly within the specific network by sensing local control parameters like node voltages at POCs, state of charge of EVs battery, and temperature and level of hot water in the thermal storages. These control parameters complement the decision making the process for scheduling and re-scheduling the operation of individual thermal and EV charging units. Thus, sharing of flexibility with proper coordination, control, and management of thermal and EV charging systems in integrated multi-energy systems network are enhanced with mutual technical benefits. Also, the impact assessment in the LV distribution network, in terms of grid terminal voltages and the network's hosting capacity, is evaluated. The proposed demand response architecture effectively manages grid congestions and local voltages, satisfying the thermal energy requirements of the customers as well as charging needs of EVs.

6.1 Operational Flexibility of Electrified Transport and Thermal Units in The Distribution Grid

Flexibility imposes benefits to a cost-effective solution towards the need for LV grid reinforcement for the integration of heating and transport units. The potential ability of HPs and EVs, as a decentralized and controllable flexible load is well explored in [46] [52] [47] [80] [49] with the use of central control system based on well developed communication infrastructure. The use of a local adaptive controller, based on specific reference parameter of terminal voltage for the individual controller at each node, to adjust active and reactive power of thermal and photovoltaic in LV network is explored in [51]. This is only possible with a frequent update of reference parameters based on changes in LV grid loads. Use of individual power electronics devices for all loads in a building for voltage regulation is investigated in [81]. It increases the cost of implementation, and also the power quality suffers.

Variation in grid voltages over a period with high penetration of HPs in LV network supported by ON/OFF controllers are investigated in [J1]. The HP controller presented in [J1] is modified, concerning the position and parameters of ON/OFF delay, for improved coordination between integrated HPs and EVs as well as utilisation of electric grid. The rule-based decision-making approach for charging of EVs, based on analysis of available data from [8], is implemented to avoid proper communication infrastructure as in optimisation based techniques. The proposed controller is autonomous and adaptive for real-time grid support with the integration of EVs and HPs. It is autonomous since there is no proper communication infrastructure between any EVs, HPs and the grid. It is adaptive and flexible as it is capable of prioritising and shifting the operating time of the associated load (EV or HP) based on the measurement of control parameters. The reference parameters for the EV and HP controller is uniform throughout the network.

The overall architecture of the proposed system for operation and control of EVs and HPs integrated with LV grid, as a multi-energy-system, is illustrated in Fig. 50. Three different types of loads are connected to the LV residential grid: residential baseload, EV and HP. Flexibility from EVs and HPs is unleashed with the help of their respective controller. The EVs controllers monitor the state of charge (SOC) of EVs battery and categorise it into different groups and user priorities. Then the charging time slot of EVs, based on determined groups and priorities, are allocated. The charging time slots of different groups are distributed over a period in a rule-based method further described in this chapter. Then the charging time of an EV in the allocated slot is determined. Based on this charging time, user priority, and grid voltage at POC at the time of coupling, the delay in ON/OFF operation of an EV is determined. This delay in ON/OFF is the key to allow sharing of flexibility and prioritising the operation of EVs and

6. Integrated and Autonomous Operation of the Flexible Loads

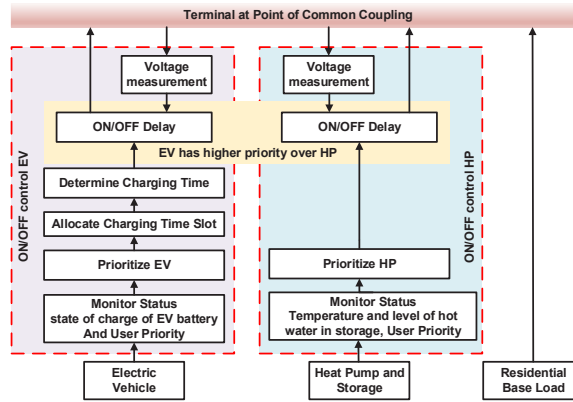


Fig. 50: System Architecture [J3]

HPs to support LV grid terminal voltage remain above the lower operating limit of -10% . The operation of HPs are prioritised based on T_h , X_c and user priority. The ON/OFF delays are then introduced based on V_t . Lower turn-ON and higher turn-OFF delays for lower V_t prioritise devices at the far end of a radial feeder to operate first. At the same time, for EVs and HPs connected at the same POC, higher turn-ON and lower turn OFF-delays of EVs over HPs priorities EVs charging over HPs operation.

EV and HP Integration Scenario in LV Network

As feeder F6 is the longest feeder, as shown in Fig. 14, the terminal voltages at the far end is 0.91pu [J1] when operated with HPs. Thus, the feeder F6 is modified by splitting it in two radial sections, as illustrated in Fig. 51, by adding a new cable (CF6-New) from the transformer secondary and disconnecting cable C48. This modification allows the integration of EVs in the existing grid.

The residential electricity and thermal demands, along with their profiles, are presented in section 3.4. The size of HP and storage, associated with each house, determined to attain flexibility from the thermal storage system to integrate EVs as detailed in [J1] is tabulated in table 19. Fig. 52 shows the distribution of HPs units in the individual house [J1]. The 3-phase charger of 7.4kW and 11kW are allocated for EVs with a battery capacity of 24kWh and 60kWh respectively. The distribution of EVs' SOC and charger capacities for each house is shown in Fig. 29 [J3].

Hosting capacity of LV grid and terminal voltages are investigated through steady-state power system simulation in DigSILENT power factory. As investigated in [J1], around $10\text{-}30\%$ of HPs are in operation at a time in long-run despite any initial conditions. So, the ON/OFF status of HP along

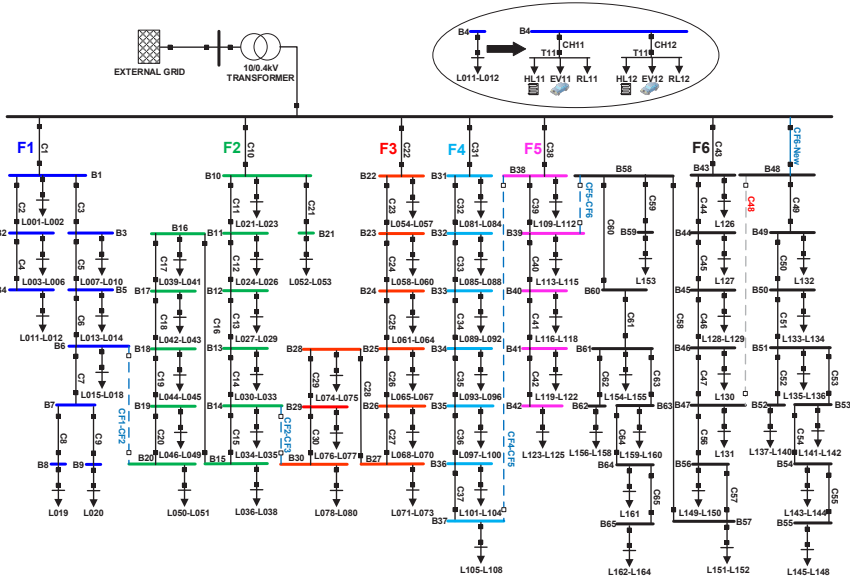


Fig. 51: LV residential grid network with reinforcement in feeder F6 [J3]

Table 19: HP and storage tank size allocation [J3].

Thermal Demand (kWh)	Storage Size (m ³)	Rated Electrical Power (kW)	No of HP
< 40	1	3	122
40-60	1.5	6	38
60-90	2	9	4

with temperature and level of hot water in the thermal storage tank, when 10% of HPs are in operation, is taken as an initial condition. The two-mass model of the thermal storage tank is considered. The EV is modelled as discussed in section 2.6

6.2 EV Charging Management

Rule-based charging distributes the charging time of EVs over the period, based on its initial SOC (SOC_{to}), to avoid grid congestion. The concept of EV charging management is illustrated in Fig. 53 and is detailed in [J3]. EVs are categorised into different groups ($P1 - P7$) based on SOC_{to} to distribute charging time within the allocated charging period (T_P). EVs in group $P1$ are defined by the users for immediate charging. Since EVs in $P2$ has $SOC_{to} < 50\%$ and are very few in numbers, they are also subjected to immediate charging to allow any further short distance commute. On the

6. Integrated and Autonomous Operation of the Flexible Loads

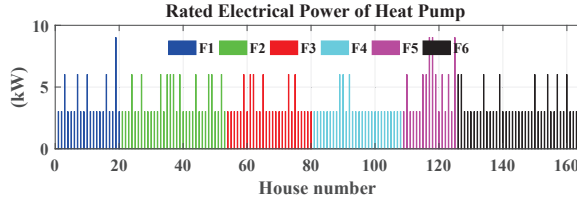


Fig. 52: Rated electrical power of HP in individual houses [J3].

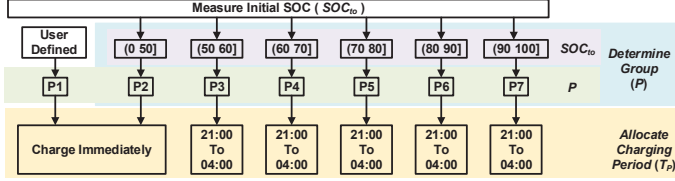


Fig. 53: EV charging management [J3]

other hand, EVs in $P3 - P7$ are scheduled to charged only between 21:00 hrs to 04:00 hrs next day. The charging period avoids evening peak, due to residential demand, and keeps buffer time to charge any fully uncharged EVs until 04:00hrs, due to events such as under voltage, later discussed in section 6.3. The charging time of EV (T_{ev}) is distributed through their respective charging period T_P . The EV starts charging only from or after T_{ev} based on terminal voltage at POC. The calculation of T_{ev} , for individual EV associated with group $P3 - P7$, are based on [J3] as following procedure and is summarized in table 20. EVs with lower SOC (SOC_l) are subjected to charge prior to EVs with higher SOC (SOC_u) in the same group (P).

In a group (P), the required duration to charge a battery with lower (SOC_l) and upper (SOC_u) limit of SOC_{to} is given by eq.(6.2) and eq.(65) respectively [J3].

$$d_u = \frac{B_s \times (100 - SOC_l)}{P_{cb} \times 100} \times 60 \quad [min] \quad (64)$$

$$d_l = \frac{B_s \times (100 - SOC_u)}{P_{cb} \times 100} \times 60 \quad [min] \quad (65)$$

Where, B_s and P_{cb} are the battery size in kWh and charging power in kW respectively.

$d_l > d_u$ as $SOC_l < SOC_u$. Thus, to allow EVs with SOC_l gets fully charged by 04:00hrs, the charging should start at time t_l eq.(66) [J3].

$$t_l = t_e - d_l \quad [hh : mm] \quad (66)$$

Where, $t_e = 04 : 00hrs$ is the end time.

d_t is the total duration required for charging of EV with SOC_l under group (P), and is given by eq.(67) [J3].

$$d_t = t_l - t_s \quad [min] \quad (67)$$

EVs with lower SOC_{to} is prioritised to charge before EVs with higher SOC_{to} . So, the delay is introduced for charging of EVs. d_t is evenly distributed into 10 equal parts for every 1% increment in SOC_{to} , using constant power charging. The delay to start charging ($D(P)_{SOC}$) is given by eq.(68) [J3].

$$D(P)_{SOC} = (SOC_{to} - SOC_l) \times \frac{d_t}{10} \quad [min] \quad (68)$$

Finally, $D(P)_{SOC}$ is added to allocated charging time $t_s = 21 : 00hrs$ to determine charging time of EV as per eq.(69) [J3].

$$T_{ev} = 21 : 00 + D(P)_{SOC} \quad [hh : mm] \quad (69)$$

Table 20: Scheduling of EV charging [J3]

with 7.4kW charger for 24kWh battery size				
Group	SOC_{to} (SOC_l SOC_u] (%)	Charging duration (d_u d_l] (min)	t_l ($t_e - d_l$] (hh:mm)	Total Duration (d_t) ($t_l - t_s$) (min)
Fig.53-b	Fig.53-b	eq.(6.2)	eq.(65)	eq.(66)
P3	(50 60]	(100 80]	02:40	340
P4	(60 70]	(80 60]	03:00	360
P5	(70 80]	(60 40]	03:20	380
P6	(80 90]	(40 20]	03:40	400
P7	(90 100]	(20 0]	04:00	420
with 11kW charger for 60kWh battery size				
P3	(50 60]	(165 132]	01:48	288
P4	(60 70]	(132 99]	02:21	321
P5	(70 80]	(99 66]	02:54	354
P6	(80 90]	(66 33]	03:27	387
P7	(90 100]	(33 0]	04:00	420

As and example, let us consider an EV with $SOC_{to} = 60$ and battery size 24kWh. Then, with reference to Fig. 53, $P = P3$ and $SOC_l = 50$. Using eq.(68), $D(P3)_{60} = (60 - 50) \times 340/10 = 340min$. Thus, EV starts charging at 21:00hrs + 340min = 02:40hrs, using eq.(68). EV is then fully charged by 04:00hrs. In similar way, for EV with $SOC_{to} = 51$ and

6. Integrated and Autonomous Operation of the Flexible Loads

$B_s = 24\text{kWh}$, $P = P3$ and $\text{SOC}_l = 50$. Using eq.(68), $D(P3)_{51} = 34\text{min}$. So, the EV with $\text{SOC}_{t_0} = 51$ starts charging at 21:34hrs and gets fully charged by 96min (22:36hrs) [J3].

The graphical illustration of the charging management of 50 EVs, with a battery size of 24kWh and SOC_{t_0} between 51-100% with an increment of 1%, is shown in Fig. 54. Fig. 54a-e illustrates the SOC level (top) and charging

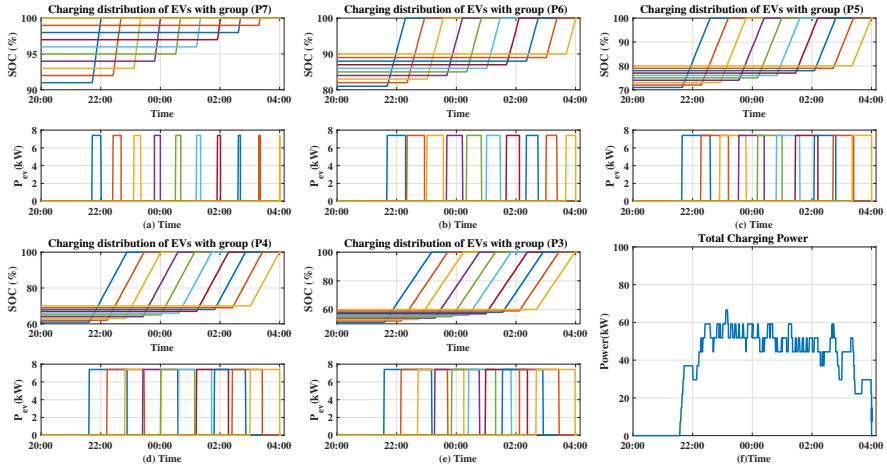


Fig. 54: Illustration of charging management of EVs and charging power [J3]. (a) group P7, (b) group P6, (c) group P5, (d) group P4, (e) group P3, (e) Total Charging power

power (bottom) for EVs in group P3-P7. The charging of EVs within each group is distributed evenly between 21:00hrs to 04:00hrs next day. EVs with lower SOC_{t_0} in each group is subjected to prior charging. The total charging power is shown in Fig. 54f.

6.3 Control of EV and HP

To prioritize the operation of EVs and HPs in at the far end of the feeder, where terminals voltages (V_t) are lower than V_t at the beginning of the feeder, the concept of ON/OFF delay based on V_t is introduced. Lower ON delay and higher OFF delay, for lower V_t , prioritise the operation of EVs and HPs at the lower end of the distribution feeder. Whereas, EVs have lower ON delay and higher OFF delay compared to HPs. This delay prioritises the charging of EVs against the operation of HP, for EVs and HPs connected at the same terminal or near its neighbourhood. The ON/OFF delay parameters for EVs and HPs based on V_t at POC is tabulated table 21 and is illustrated in Fig. 55

The minimum delay of 30s avoids the controllers to respond at short duration variations in V_t . The delay is increased or decreased by two

Table 21: ON delay and OFF delay Duration Based On V_t [J3]

$V_t \geq 0.94$	
ON delay EV	$(V_t - 0.94) \times m + 30$
ON delay HP	$(V_t - 0.94) \times m + 60$
$V_t < 0.92$	
OFF delay EV	$(0.92 - V_t) \times m + 60$
OFF delay HP	$(0.92 - V_t) \times m + 30$
$m = 3000$ for minimum delay of 30s	
if $V_t \leq 0.9$ for $t > 60s$	
ON delay EV	1200s
ON delay HP	1800s

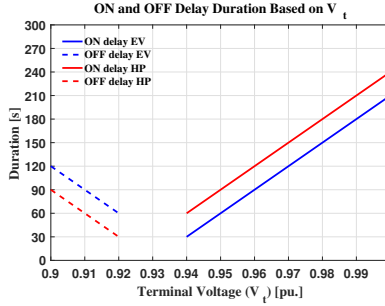


Fig. 55: ON delay and OFF delay duration based On V_t [J3]

simulation step size (30s) for every 0.01pu changes in V_t . EVs and HPs are only allowed to connect at POC while $V_t \geq 0.94$ pu, to maintain V_t within the operation range of -10%, and remains connected until $V_t \geq 0.92$ pu. EVs and HPs, at the POC where $V_t < 0.92$ pu, are disconnect based on the OFF delay duration illustrated in Fig. 55. When V_t drops below 0.9pu for more than 60s (to have four samplings to avoid transients), EVs and HPs at these terminals disconnect immediately. Then the new connections are possible only after 20min for EVs and 30min for HP. This condition avoids stressing grid frequently as well as to give EVs priority over HPs.

EV control

The logic diagram representation of EV control, based on [J3], is shown in Fig. 56 and reference parameters are presented table 22. Voltage limit violation is mostly a local problem and is a cascading effect in the radial network. Thus, switching OFF the loads in vicinity of low voltage region helps to improve local terminal voltages and is possible with the use of a voltage controller. The voltage controller, Fig. 56a, provides the signal $V1$

6. Integrated and Autonomous Operation of the Flexible Loads

and V . The hysteresis in control is logically represented by RS-flip-flop logic. When the signal $V1$ is high, new connections of EVs are possible at POC. Once $V < 0.92pu$, $V2$ is low, and V is low only after OFF-delay time, else it remains high. The EVs get disconnected once signal V is low. This feature allows EVs at lower V_t remains connected at POC, while EVs connected at higher V_t in the neighbourhood disconnects, during the event when $V_t < 0.92pu$. Hence, the consumer at the weaker point in the LV grid does not feel discriminated, and grid voltage is maintained above the lower operating limit. This coordination is a good example of sharing flexibility within the network without the use of extensive communication infrastructure. For the proper coordination, the minimum voltage (V_{min}) and the recovery voltage (V_{rec}) is either set by the regulation or the practical experience of the distribution system operator.

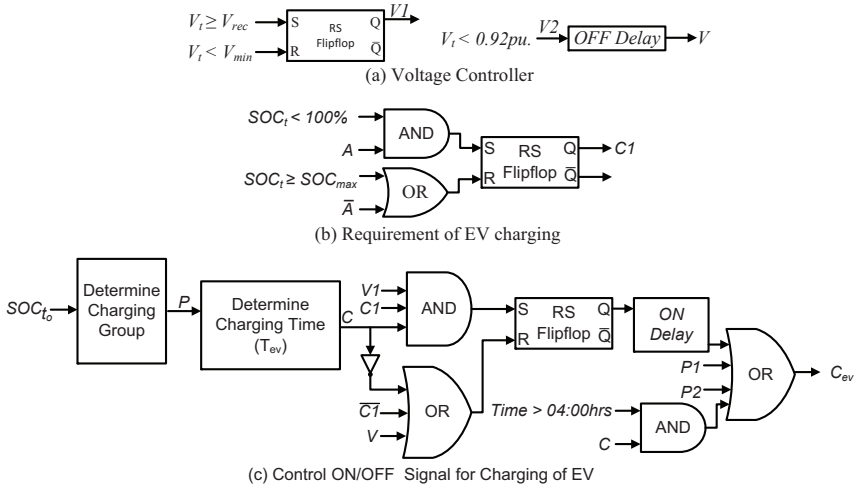


Fig. 56: Logic diagram representation of EV controls (a) voltage control, (b) SOC control, (c) complete control logic for charging of EV.

The charging of EV is monitored with the help of controller presented in Fig. 56b. The signal $C1$ represents the requirement for charging. $C1$ is high when $SOC_t < 100\%$ and EV is connected for charging ($A = 1$). $C1$ is low once the $SOC_t \geq SOC_{max}$ or EV is disconnected for charging. SOC_{max} is defined by the user and is useful while selecting priority charging, during high electricity price, to charge EV for certain distance commute.

The overall control logic for EV charging is presented in Fig. 56c. C_{ev} is high indicating connection of EV for charging at POC. First of all the EVs are distributed into different charging groups (P1-P7) based on its SOC_{to} (see Fig: 53) and the respective charging time of EVs (T_{ev}) as per eq.(69) is

determined. Then, under favourable voltage conditions and requirement of charging, EVs are connected for charging with ON-delay, see Fig. 55. This ON-delay prioritizes connection of EVs at lower voltage terminals for charging as discussed earlier. EVs, which are not fully charged by 04:00hrs due to poor voltage conditions, are connected for charging with priority despite any terminal voltages at POC.

Table 22: Reference parameters of EV charging control

$SOC_{max}(\%)$	V_{min} (pu)	V_{rec} (pu)
100	0.94	0.96

The verification of EV control logic presented in Fig. 56 is illustrated in Fig. 57. The terminal voltage, prepared manually to verify control dynamics,

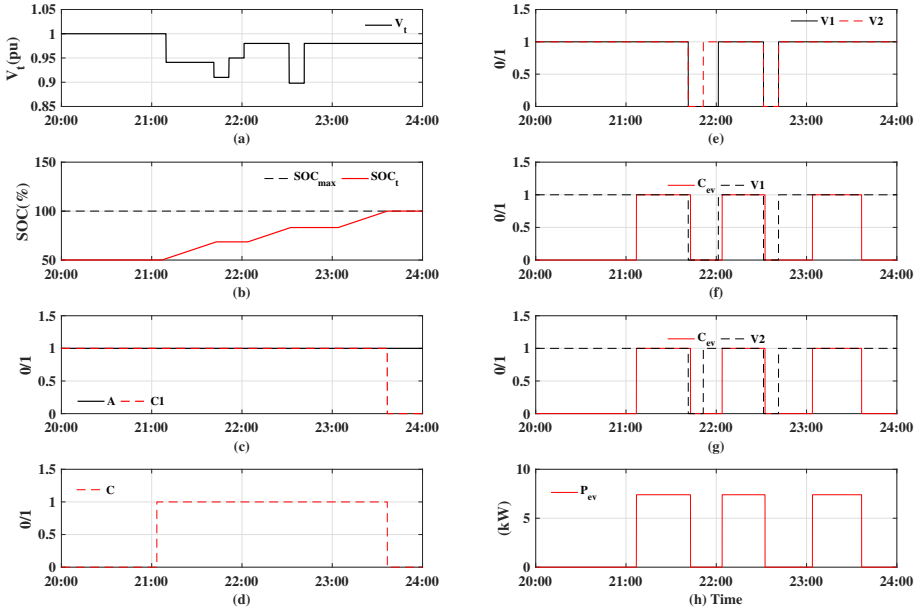


Fig. 57: EV control signals [J3] (a): terminal voltage (V_t), (b): SOC_t , (c): availability of EV A and status of control logic C1, (d): logic status C, (e): logic status V1 and V2 (f): C_{ev} and V1 to illustrate turn ON delay, (g): C_{ev} and V2 to illustrate turn OFF delay, (h): Power consumed by EV charger

is presented in Fig. 57a. SOC_{max} and SOC_t is illustrated in Fig. 57b. Signals for availability of EV (A) and requirement for charging C1 is shown in Fig. 57c. The logic signal C, Fig. 57d, is high when $Time \geq T_{ev}$ and remains high until $SOC_t = SOC_{max}$.

The status of logic signal V1 and V2 is presented in Fig. 57e. While the voltage is favourable ($V1=1$) for connection of EV at POC and EV ready to

6. Integrated and Autonomous Operation of the Flexible Loads

charge ($C1=1$), The EV is finally connected at POC for charging with ON-delay (Fig. 57f). Similarly, when $V2$ is low, EV gets disconnected from charging with OFF-delay (Fig. 57g). The charging power of EV is shown in Fig. 57h. EV gets charged with a constant power of 7.4kW.

HP control

The logic diagram representation of HP control, based on [J3], is shown in Fig. 58 and reference parameters are presented table 23. The voltage control shown in Fig. 58a is similar to Fig. 56a. The level and temperature controller, as shown in Fig. 58b&c , monitors and control the level of cold water and temperature of hot water in the storage tank respectively. The priority controller, as Fig. 58d&e, prioritize the operation of HP when the temperature of hot water in the storage tank T_h is less than $50^\circ C$ or the level of cold water X_c in the storage tank is more than 40%. The detailed function and validation of level and temperature controller is presented in [J1]. The complete logical diagram of HP control is shown in Fig. 58e. During favourable voltage condition ($V1=1$) and the signals T or H are high, the actuator signal to turn on the HP (C_{hp}) is high with On-delay. In case of priority (when $T1$, $H1$ or $P1$ is high) C_{hp} is high without any delay despite any voltage condition. The validation of HP control logic is illustrated in Fig. 59.

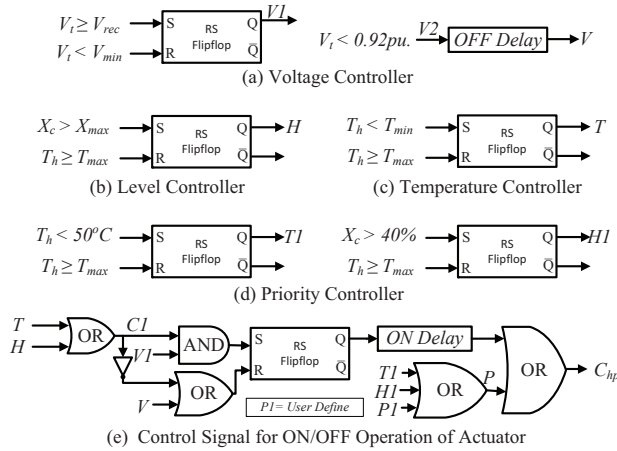


Fig. 58: Logic diagram representation of HP controls (a) voltage control, (b) level control, (c) temperature control, (d) priority control, (e) complete control logic for ON/OFF control of HP.

The terminal voltage, prepared manually to verify control dynamics, is presented in Fig. 59a. Temperature of hot water T_h in the storage tank with

Table 23: Parameter of Storage tank

$T_{max}(^{\circ}C)$	$T_{min}(^{\circ}C)$	V_{min} (pu)	V_{rec} (pu)	$X_{max}(\%)$
70	60	0.94	0.96	25

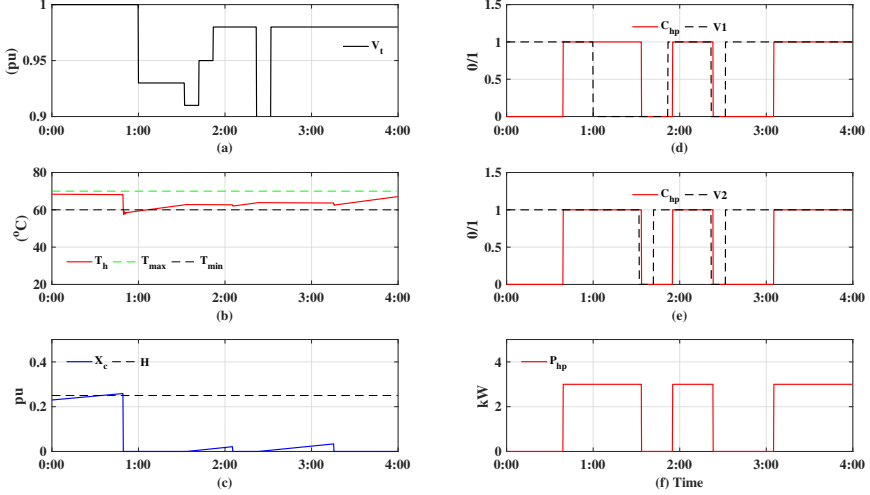


Fig. 59: HP control signals [J3] (a): terminal voltage (V_t), (b): T_h , (c): X_c , (d): C_{hp} and $V1$ to illustrate turn ON delay, (e): C_{hp} and $V2$ to illustrate turn OFF delay, (f): Power consumed by HP

maximum and minimum allowable temperature range is illustrated in Fig. 59b. The level of cold water in the storage tank and signal H is shown in Fig. 6.3c. Fig. 59d&e shows the ON/OFF operation of HP (C_{hp}), based on change in voltage at POC, with ON and OFF delays respectively. Fig. 59f shows the power consumed by HP during its operation.

Coordination between EV and HP Operation

The coordination between EVs and HPs operation is illustrated in Fig. 60 [J3]. The terminal voltages are selected manually, see Fig. 60a, to illustrate the priority in the operation of EVs and HPs as proposed. EV1 and HP1 are connected at terminal T1 and so on. When $V_t < 0.92pu$ in terminals T1, T2 and T3, EVs and HPs are disconnected consecutively with their respective OFF-delay. HP disconnects prior to EV in same terminal, see Fig. 60b&c. Similarly, when $V_t \geq 0.96pu$ the EVs and HPs are connected at POC with ON-delay. EV is connected prior to HP in same POC, see Fig. 60b&c. When $V_t < 0.92pu$ for 45s, only HP1 at T1 is turned OFF, while others remain connected. This condition illustrates that EVs and HPs at POC with lower terminal voltages has higher priorities for its operation while EVs have more

6. Integrated and Autonomous Operation of the Flexible Loads

priority over HPs in the same POC.

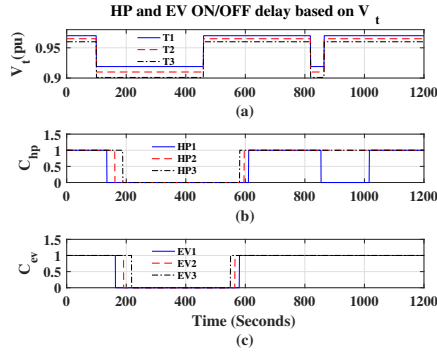


Fig. 60: HP and EV ON/OFF delay based on V_t [J3] (a): terminal voltage (V_t), (b): C_{hp} , (c): C_{ev}

6.4 Results and Discussion

Fig. 61 illustrates the results of steady state simulation with EVs and HPs integrated into LV distribution network shown in Fig.51. The summary of the simulation results is presented in table 24. Fig. 61a shows the percentage loading of the distribution transformer, along with the percentage of EVs and HPs connected at POCs. The % of EV charging after 04:30hrs suggest that all EVs are fully charged. The terminals voltages attaining minimum values in different feeders are illustrated in Fig. 61b&c. The maximum loading of the transformer and cables are 64% and 60% of its rated capacity. Thus, the hosting capability of the LV network can be improved with the proper demand response as there are enough capacity in the LV network to handle further increment in the loads. However, the minimum terminal voltages attained at the far end of the feeder is between 0.95pu and 0.91pu. These low voltages suggest the requirement of new feeder for the increment of new loads in the existing LV network.

Table 24: Summary of Result [J3]

Transformer loading (%)	EV charging (%)	HP operated (%)	Max.line loading (%)	Min. T_{hot} ($^{\circ}C$)	Max. X_c (%)
64	14	35	60	52	32

The maximum level of cold water in storage tank attained is 32% with a minimum temperature of hot water at $52^{\circ}C$ indicating that thermal demand is fulfilled at all time.

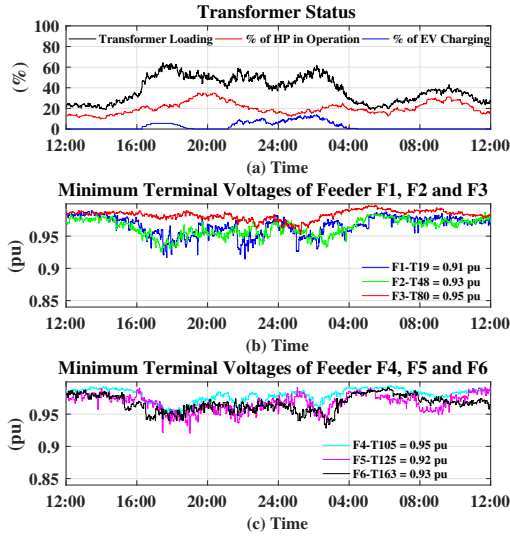


Fig. 61: Simulation results [J3] (a): transformer loading, percentage of HP in Operation, and percentage of EV being charged; (b): minimum voltage attained in terminals of feeder F1, F2 and F3; (c): minimum voltage attained in terminals of feeder F4, F5 and F6

The hosting capacity of the LV network, without any modification in feeder F6 of Fig. 51, integrated with EVs, is well-explored in [72]. During maximum and minimum demand hours, 6-17% of EVs can penetrate in the existing LV network [72]. The voltage drop in some feeders was more than -6% despite 44% of transformer capacity was remaining. With a minor reinforcement in the LV grid and a proper demand response for integrating HPs and EVs the hosting capacity of the LV grid has been improved. The autonomous ON/OFF control logic proposed here is effective in managing EVs and HPs flexibly while fulfilling customer demand and maintaining grid terminal voltage within its lower operating limit of -10%.

6.5 Conclusion

This chapter provides the insight in integrating EVs and HPs flexibly in LV distribution network as a concept of the multi-energy system. The synergy between thermal, electricity and transportation units based on proposed control strategy has been illustrated. The proposed control enhances flexibility in the operation of integrated EVs, and HPs satisfying end-users need and supporting grid voltages. As an autonomous and local control system, there is no need for costly communication infrastructure to handle big data and control.

Chapter 7

7 Conclusion

The significance and outcome of the thesis are as presented in brief. The following conclusions are drawn on the hypothesis defined in Chapter 1.

- Thermal and transportation loads bear potential capacity as flexible loads and can be integrated into the existing low voltage electricity grid with minimal modifications. However, due to the resistive nature of LV distribution grid, there exist the problem of under-voltage at the far end of the long radial feeders. Thus, it is necessary to reinforce or split very long feeder as discussed in chapter 6.
- With the use of appropriate demand response model, thermal and transportation loads can be flexibly integrated into the LV grid. The demand response can help in peak shaping of electrical load, balance energy demand and supply, and increase operational efficiency and hosting capacity of the LV network. These outcomes are possible by shifting the operation of the flexible loads (thermal and transportation loads) using the proper algorithm, based on appropriate measurements, to prioritise their operations. The results are demonstrated in chapter 6.
- The data generated from the meter measurement are analysed to determine the end-users consumption behaviour. The average consumption profile based on every hour of the day considering weekdays, weekends, and seasonal variations can reflect the end-users consumptions behaviour. This information, along with the knowledge of apparent temperatures, is used to train the forecasting tools. The results from the forecasting tools, based on curve fitting technique such as neural net and similar day method, can estimate the thermal demand incorporating users behaviour. This technique, without real-time measurement of thermal data, helps to protect user privacy. The results are demonstrated in chapter 3.

- The estimated thermal demand in association with spot electricity price can operate the thermal unit flexibly, to store energy during surplus electricity generation from renewable and balance demand and supply of thermal and electrical energy simultaneously, despite some error in estimation. The results are presented in chapter 4.

7.1 Significant Outcome

Concerning the project objectives, several outcomes of the research work are discussed further. The texts in the paragraphs are in bold to highlight the significant contributions and outcomes of the thesis.

Three different mathematical models of the thermal storage tank are analysed and compared with theoretical validation. The different models of thermal storage tanks are:

- Single-mass model: The average temperature of the water inside the tank is considered based on energy flow and a first-order linear differential equation.
- Two-mass model: Two stratified layers, one each with the uniform temperature of hot and cold water, separated with a variable height of thermocline responsible for stratification.
- multi-layered stratification model using the first-order differential equation in each layer to determine its temperature.

These models are suitably adapted for electric grid integration in association with EBs or HPs. **The two-mass and multi-layered stratification models of the storage tank closely reflected the practical solution towards flexibility in measurement and demand response control.** These modellings were performed using DigSILENT power factory simulation tool. This tool has the flexibility for scripting and developing models and control algorithms for energy system components, for further use in the analysis of the integrated power system with multi-energy integration.

The analysis of hot water usage profile in Danish residential locality provided useful information on seasonal and daily end-users consumption behaviour in aggregate. The end-users consumption profiles, along with the external environmental factors such as temperature, relative humidity and wind, are selected to train and verify the thermal demand estimation model. **The developed thermal demand estimation models, based on curve fitting techniques, can integrate end-users behaviour without effecting their privacy as in case of real-time monitoring of individual users consumptions.** This method also avoids expensive communication infrastructure, and extensive computation and data handling required for real-time management. **The thermal demand estimation is used for**

7. Conclusion

optimised scheduling of thermal unit considering spot market electricity prices and avoiding the period of peak electrical demand. Thermal units are integrated into the electrical grid, as flexible consumer load to store and fulfil thermal energy demand.

The survey data on average distance travelled by passenger cars in Denmark are analysed to investigate driving profile behaviour in Danish scenario. This profile, together with the factor affecting the energy consumption in EVs battery (such as how aggressive the driver is accelerating the vehicle), is implemented to determine the depth of discharge of EVs. **The depth of discharge of battery represented the overall performance of EVs, without considering the actual dynamic of EVs on the road, and closely reflected the present scenario of driving pattern of the passenger cars.** Based on this discharge values of EVs battery, the algorithm for charging management of EVs are determined for peak shaping of EV loads. **A simple method for rule-based scheduling of EVs is presented** for peak shaping of electricity consumption and avoid extensive data handling, computation and communication infrastructure for optimisation based problem.

Analysis of consumption pattern of electrical and thermal loads in residential buildings in Northern Jutland, Denmark, is used in the low voltage distribution network grid. Modelling of integrated energy systems (thermal and EVs and electrical load) in DigSILENT power factory is performed for steady-state analysis. The results are discussed with several case studies to investigate the technical challenges such as under-voltage, transformer capacity, line loading limits and operational flexibility. **Electric boilers and storage integrated with the electricity grid in individual houses had a significant impact on the LV grid.** Under-voltage and line loadings were significant, although enough capacity in the transformer is still available. **The use of HPs instead of EBs or a central thermal station plant, with storage and transmission networks to fulfil the thermal demands of these houses, mitigates all these problems.** This concept of the locally central thermal station for a small residential area utilises transformer capacity and enhances control flexibility in the operation of the thermal system without consumer initiatives. Thus, economic benefit can be easily share among the users, which can create LV grid congestion problem if distributed in individual house. On the other hand, the total size of EB and storage required in the central system is smaller than combine values from individual houses.

A strategy with local autonomous control of the thermal and EV units are discussed to mitigate the identified problems in the LV grid due to the integration of individual thermal and EV loads. The consumers located at the weakest point of the network does not feel discriminated and participates in flexible operation with the concept of operational delays in connection and

disconnection of thermal and EV loads. **Adaptive and autonomous control for flexible and coordinated operation of EVs and HPs are possible based on the priorities, local measurements such as terminal voltage, temperature and level of water in the storage tank.** These controllers do not require any communication infrastructure for its coordinated operations within the network.

As a part of the DiCyPS project, the outcome of this project enhances the state-of-the-art in the area of power to heat and power to transport. It is useful for the researcher for further research and design of a platform used for control based on the embedded software. The use of a large amount of data for assessment in this project will contribute significantly to the DiCyPS project members. It helps to quantify the various aspect of the power system network (including generation, heating, transportation and consumer load) to be interacted, monitored and controlled by software. These aspects are helpful to demonstrate close interdisciplinary collaboration with the end-users in the future smart communities with IT infrastructure for better service. DSO, district heating companies, smart city municipalities and system balance authorities, can benefit from the results.

7.2 Future Work

This research work provides significant contributions towards integration of thermal and transportation loads in the low voltage distribution network. However, future trend and concept in the development of energy systems and components are always important.

- The effects from the limitations mentioned earlier in the introduction chapter can be evaluated in future work.
- The use of continuous control for thermal and EV charging units with variable power consumptions can be evaluated with demand response when integrated into the LV network.
- The dynamic stability of the LV network can be studied.
- Economic analysis of the system based on central and individual thermal systems can be performed.
- Integration of photovoltaic systems, thermal units, thermal storages and EVs in the individual houses and the impact in the LV grid network can be evaluated.

References

- [1] Danish Wind Industry Association. Accessed on 12-Aug-2016. [Online]. Available: http://www.windpower.org/en/knowledge/statistics/the_danish_market.html
- [2] Danish Ministry of Climate, Energy and Building, "Smart grid strategy- the intelligent energy system of the future," techreport, 2013.
- [3] Energinet.dk. Accessed on 12-Aug-2016. [Online]. Available: <http://energinet.dk/EN/EI/Nyheder/Sider/Dansk-vindstroem-slaar-igen-rekord-42-procent.aspx>
- [4] Danish Energy Agency, "Regulation and planning of district heating in denmark," techreport, 2015.
- [5] Denmark-On the Road and Deployments. Accessed on 27-Sept-2016. [Online]. Available: <http://www.ieahev.org/by-country/demark-on-the-road-and-deployments/>
- [6] V. Knap, R. Sinha, M. Swierczynski, D. Stroe, and S. Chaudhary, "Grid inertial response with lithium-ion battery energy storage systems," in *2014 IEEE 23rd International Symposium on Industrial Electronics (ISIE)*, June 2014, pp. 1817–1822.
- [7] H. Holttinen, "Impact of hourly wind power variations on the system operation in the nordic countries," *Wind Energy*, vol. 8, no. 2, pp. 197–218, 2005.
- [8] R. Sinha, E. R. Moldes, A. Zaidi, P. Mahat, J. R. Pillai, and P. Hansen, "An electric vehicle charging management and its impact on losses," in *IEEE PES ISGT Europe 2013*, Oct 2013, pp. 1–5.
- [9] K. Skytte and O. Olsen, "Regulatory barriers for flexible coupling of the nordic power and district heating markets," in *13th European Energy Market Conference, EEM 2016*. IEEE, 2016.
- [10] M. Tasdighi, H. Ghasemi, and A. Rahimi-Kian, "Residential microgrid scheduling based on smart meters data and temperature dependent thermal load modeling," *IEEE Transactions on Smart Grid*, vol. 5, no. 1, pp. 349–357, Jan 2014.
- [11] M. Tasdighi, P. Jambor Salamati, A. Rahimikian, and H. Ghasemi, "Energy management in a smart residential building," in *2012 11th International Conference on Environment and Electrical Engineering*, May 2012, pp. 128–133.

References

- [12] B. R. Pokhrel, N. Karthikeyan, R. Sinha, B. Bak-Jensen, and J. Radhakrishna Pillai, "Architecture of integrated energy systems," *Submitted for peer review in Reliable and Sustainable Electric Power and Energy Systems Management, Springer*, 2019.
- [13] Z. Li, W. Wu, J. Wang, B. Zhang, and T. Zheng, "Transmission-constrained unit commitment considering combined electricity and district heating networks," *IEEE Transactions on Sustainable Energy*, vol. 7, no. 2, pp. 480–492, April 2016.
- [14] H. Lund, S. Werner, R. Wiltshire, S. Svendsen, J. E. Thorsen, F. Hvelplund, and B. V. Mathiesen, "4th generation district heating (4gdh): Integrating smart thermal grids into future sustainable energy systems," *Energy*, vol. 68, pp. 1 – 11, 2014.
- [15] W. Gang, S. Wang, F. Xiao, and D. ce Gao, "District cooling systems: Technology integration, system optimization, challenges and opportunities for applications," *Renewable and Sustainable Energy Reviews*, vol. 53, pp. 253 – 264, 2016.
- [16] Y. Li, Y. Rezgui, and H. Zhu, "District heating and cooling optimization and enhancement – towards integration of renewables, storage and smart grid," *Renewable and Sustainable Energy Reviews*, vol. 72, pp. 281 – 294, 2017.
- [17] eia, "International energy outlook 2016-executive summary - energy information administration," Tech. Rep., 2017, accessed on 01-Aug-2019. [Online]. Available: https://www.eia.gov/outlooks/ieo/pdf/exec_summ.pdf
- [18] R. Yu, W. Zhong, S. Xie, C. Yuen, S. Gjessing, and Y. Zhang, "Balancing power demand through ev mobility in vehicle-to-grid mobile energy networks," *IEEE Transactions on Industrial Informatics*, vol. 12, no. 1, pp. 79–90, Feb 2016.
- [19] B. Mathiesen, H. Lund, D. Connolly, H. Wenzel, P. Østergaard, B. Möller, S. Nielsen, I. Ridjan, P. Karnøe, K. Sperling, and F. Hvelplund, "Smart energy systems for coherent 100% renewable energy and transport solutions," *Applied Energy*, vol. 145, pp. 139 – 154, 2015.
- [20] W. Choi, W. Lee, and B. Sarlioglu, "Reactive power compensation of grid-connected inverter in vehicle-to-grid application to mitigate balanced grid voltage sag," in *2016 IEEE Power and Energy Society General Meeting (PESGM)*, July 2016, pp. 1–5.

References

- [21] Y. Tang, J. Zhong, and M. Bollen, "Aggregated optimal charging and vehicle-to-grid control for electric vehicles under large electric vehicle population," *IET Generation, Transmission Distribution*, vol. 10, no. 8, pp. 2012–2018, 2016.
- [22] Grøn Gas Denmark. Accessed on 01-Aug-2019. [Online]. Available: <https://grongasdanmark.dk/nyheder/gron-gas-danmark-danish-gas-system-asset-green-transition-danish-energy-system>
- [23] M. Bailera, P. Lisbona, L. M. Romeo, and S. Espatolero, "Power to gas projects review: Lab, pilot and demo plants for storing renewable energy and co₂," *Renewable and Sustainable Energy Reviews*, vol. 69, pp. 292 – 312, 2017.
- [24] W. Kusch, I. Stadler, and R. Bhandari, "Heat pumps in low voltage distribution grids by energy storage," in *2015 International Energy and Sustainability Conference (IESC)*, Nov 2015, pp. 1–6.
- [25] H. Harb, T. Schutz, R. Streblow, and D. Muller, "Adaptive model for thermal demand forecast in residential buildings," *Proceedings of WSB*, 2014.
- [26] S. Wischhusen, "An enhanced discretisation method for storage tank models within energy systems," in *Proc. of the 5-th International Modelica Conference*, Sept. 2006.
- [27] N. Beeker, P. Malisani, and N. Petit, "Dynamical modeling for electric hot water tanks," *IFAC-PapersOnLine*, vol. 48, no. 11, pp. 78 – 85, 2015, 1st IFAC Conference on Modelling, Identification and Control of Nonlinear Systems MICNON 2015.
- [28] Y. Han, R. Wang, and Y. Dai, "Thermal stratification within the water tank," *Renewable and Sustainable Energy Reviews*, vol. 13, no. 5, pp. 1014 – 1026, 2009.
- [29] A. A. Farooq, A. Afram, N. Schulz, and F. Janabi-Sharifi, "Grey-box modeling of a low pressure electric boiler for domestic hot water system," *Applied Thermal Engineering*, vol. 84, pp. 257 – 267, 2015.
- [30] I. D. d. C. Mendaza, A. Pigazo, B. Bak-Jensen, and Z. Chen, "Generation of domestic hot water, space heating and driving pattern profiles for integration analysis of active loads in low voltage grids," in *IEEE PES ISGT Europe 2013*, Oct 2013, pp. 1–5.
- [31] C. Weissmann, T. Hong, and C.-A. Graubner, "Analysis of heating load diversity in german residential districts and implications for the application in district heating systems," *Energy and Buildings*, vol. 139, pp. 302 – 313, 2017.

References

- [32] U. Jordan and K. Vajen, "Dhwcalc: program to generate domestic hot water profiles with statistical means for user defined conditions," in *in: Proceedings ISES Solar World Congress, Orlando, 2005*, pp. 8.–12.8.
- [33] S. Clegg and P. Mancarella, "Integrated electricity-heat-gas modelling and assessment, with applications to the great britain system. part i: High-resolution spatial and temporal heat demand modelling," *Energy*, 2018.
- [34] Q. Wu, A. H. Nielsen, J. Ostergaard, S. T. Cha, F. Marra, Y. Chen, and C. Træholt, "Driving pattern analysis for electric vehicle (ev) grid integration study," in *2010 IEEE PES Innovative Smart Grid Technologies Conference Europe (ISGT Europe)*, Oct 2010, pp. 1–6.
- [35] Z. Liu and Q. Wu, "Ev charging analysis based on the national travel surveys of the nordic area," in *2014 IEEE PES General Meeting | Conference Exposition, July 2014*, pp. 1–6.
- [36] C. Bingham, C. Walsh, and S. Carroll, "Impact of driving characteristics on electric vehicle energy consumption and range," *IET Intelligent Transport Systems*, vol. 6, no. 1, pp. 29–35, March 2012.
- [37] K. Wojdyga, "Predicting heat demand for a district heating systems," *International Journal of Energy and Power Engineering*, vol. 3, no. 5, pp. 237–244, 2014.
- [38] R. Petrichenko, K. Baltputnis, A. Sauhats, and D. Sobolevsky, "District heating demand short-term forecasting," in *2017 IEEE International Conference on Environment and Electrical Engineering and 2017 IEEE Industrial and Commercial Power Systems Europe (EEEIC / I CPS Europe)*, June 2017, pp. 1–5.
- [39] S. Idowu, S. Saguna, C. Åhlund, and O. Schelén, "Forecasting heat load for smart district heating systems: A machine learning approach," in *2014 IEEE International Conference on Smart Grid Communications (SmartGridComm)*, Nov 2014, pp. 554–559.
- [40] B. Chramcov, "Heat demand forecasting for concrete district heating system," *International Journal Mathematical Models and Methods in Applied Sciences*, vol. 4, no. 4, p. 231–239, 2010.
- [41] D. Kapetanakis, E. Mangina, E. H. Ridouane, K. Kouramas, and D. Finn, "Selection of input variables for a thermal load prediction model," *Energy Procedia*, vol. 78, pp. 3001 – 3006, 2015, 6th International Building Physics Conference, IBPC 2015.

References

- [42] Zhaoxi Liu, Qiuwei Wu, A. H. Nielsen, J. Østergaard, and Yi Ding, "Electricity demand profile with high penetration of heat pumps in nordic area," in *2013 IEEE Power Energy Society General Meeting*, July 2013, pp. 1–5.
- [43] A. Shabanpour-Haghighi and A. R. Seifi, "An integrated steady-state operation assessment of electrical, natural gas, and district heating networks," *IEEE Transactions on Power Systems*, vol. 31, no. 5, pp. 3636–3647, Sep. 2016.
- [44] X. Liu, J. Wu, N. Jenkins, and A. Bagdanavicius, "Combined analysis of electricity and heat networks," *Applied Energy*, vol. 162, pp. 1238 – 1250, 2016.
- [45] B. Awad, M. Chaudry, J. Wu, and N. Jenkins, "Integrated optimal power flow for electric power and heat in a microgrid," in *CIREN 2009 - 20th International Conference and Exhibition on Electricity Distribution - Part 1*, June 2009, pp. 1–4.
- [46] D. Papadaskalopoulos, G. Strbac, P. Mancarella, M. Aunedi, and V. Stanojevic, "Decentralized participation of flexible demand in electricity markets—part ii: Application with electric vehicles and heat pump systems," *IEEE Transactions on Power Systems*, vol. 28, no. 4, pp. 3667–3674, Nov 2013.
- [47] S. Vachirasricirikul and I. Ngamroo, "Robust controller design of heat pump and plug-in hybrid electric vehicle for frequency control in a smart microgrid based on specified-structure mixed H_2/H_∞ control technique," *Applied Energy*, vol. 88, no. 11, pp. 3860 – 3868, 2011.
- [48] I. D. de Cerio Mendaza, I. G. Szczesny, J. R. Pillai, and B. Bak-Jensen, "Flexible demand control to enhance the dynamic operation of low voltage networks," *IEEE Transactions on Smart Grid*, vol. 6, no. 2, pp. 705–715, March 2015.
- [49] P. T. Bjerregaard, I. G. Szczesny, I. D. de Cerio Mendaza, and J. R. Pillai, "Intelligent control of flexible loads for improving low voltage grids utilization," in *IEEE PES ISGT Europe 2013*, Oct 2013, pp. 1–5.
- [50] I. D. de Cerio Mendaza, B. Bak-Jensen, Z. Chen, and A. Jensen, "Stochastic impact assessment of the heating and transportation systems electrification on lv grids," in *IEEE PES Innovative Smart Grid Technologies, Europe*, Oct 2014, pp. 1–6.
- [51] B. Bhattarai, I. Mendaza, B. Bak-Jensen, and J. Pillai, "Local adaptive control of solar photovoltaics and electric water heaters for real-time grid

References

- support," in *Proceedings of the Cigré Session 2016*. CIGRE (International Council on Large Electric Systems), 8 2016.
- [52] T. Masuta and A. Yokoyama, "Supplementary load frequency control by use of a number of both electric vehicles and heat pump water heaters," *IEEE Transactions on Smart Grid*, vol. 3, no. 3, pp. 1253–1262, Sep. 2012.
- [53] J. Kiviluoma and P. Meibom, "Influence of wind power, plug-in electric vehicles, and heat storages on power system investments," *Energy*, vol. 35, no. 3, pp. 1244 – 1255, 2010.
- [54] B. P. Bhattarai, K. Kouzelis, I. D. D. C. Mendaza, B. Bak-Jensen, J. R. Pillai, and K. S. Myers, "Smart grid constraint violation management for balancing and regulating purposes," *IEEE Transactions on Industrial Informatics*, vol. 13, no. 6, pp. 2864–2875, Dec 2017.
- [55] B. P. Bhattarai, B. Bak-Jensen, P. Mahat, J. R. Pillai, and M. Maier, "Hierarchical control architecture for demand response in smart grids," in *2013 IEEE PES Asia-Pacific Power and Energy Engineering Conference (APPEEC)*, Dec 2013, pp. 1–6.
- [56] A. Schirrer, O. König, S. Ghaemi, F. Kupzog, and M. Kozek, "Hierarchical application of model-predictive control for efficient integration of active buildings into low voltage grids," in *2013 Workshop on Modeling and Simulation of Cyber-Physical Energy Systems (MSCPES)*, May 2013, pp. 1–6.
- [57] C. Molitor, M. Marin, L. Hernández, and A. Monti, "Decentralized coordination of the operation of residential heating units," in *IEEE PES ISGT Europe 2013*, Oct 2013, pp. 1–5.
- [58] D. Pudjianto, P. Djapic, M. Aunedi, C. K. Gan, G. Strbac, S. Huang, and D. Infield, "Smart control for minimizing distribution network reinforcement cost due to electrification," *Energy Policy*, vol. 52, pp. 76 – 84, 2013, special Section: Transition Pathways to a Low Carbon Economy.
- [59] T. Esterl, L. Leimgruber, T. Ferhatbegovic, A. Zottl, M. Krottenthaler, and B. Weiss, "Aggregating the flexibility of heat pumps and thermal storage systems in austria," in *2016 5th International Conference on Smart Cities and Green ICT Systems (SMARTGREENS)*, April 2016, pp. 1–6.
- [60] J. Hong, N. J. Kelly, I. Richardson, and M. Thomson, "Assessing heat pumps as flexible load," *Proceedings of the Institution of Mechanical Engineers, Part A: Journal of Power and Energy*, vol. 227, no. 1, pp. 30–42, 2013.

References

- [61] T. S. Pedersen, K. M. Nielsen, and P. Andersen, "Maximizing storage flexibility in an aggregated heat pump portfolio," in *2014 IEEE Conference on Control Applications (CCA)*, Oct 2014, pp. 286–291.
- [62] L. Zhang, N. Chapman, N. Good, and P. Mancarella, "Exploiting electric heat pump flexibility for renewable generation matching," in *2017 IEEE Manchester PowerTech*, June 2017, pp. 1–6.
- [63] Y. A. Cengel and M. A. Boles, "Thermodynamics an engineering approach," *Energy*, vol. 1, p. 51, 2002.
- [64] P. González-Altozano, M. Gasque, F. Ibáñez, and R. P. Gutiérrez-Colomer, "New methodology for the characterisation of thermal performance in a hot water storage tank during charging," *Applied Thermal Engineering*, vol. 84, pp. 196 – 205, 2015.
- [65] Y. Zurigat, A. Ghajar, and P. Moretti, "Stratified thermal storage tank inlet mixing characterization," *Applied Energy*, vol. 30, no. 2, pp. 99 – 111, jan 1988.
- [66] I. Diaz de Cerio Mendaza, *An Interactive Energy System with Grid, Heating and Transportation Systems*. Department of Energy Technology, Aalborg University, 10 2014.
- [67] J. Perko, V. Dugec, D. Topic, D. Sljivac, and Z. Kovac, "Calculation and design of the heat pumps," in *Proceedings of the 2011 3rd International Youth Conference on Energetics (IYCE)*, July 2011, pp. 1–7.
- [68] R. D. C. Oliveski, A. Krenzinger, and H. A. Vielmo, "Comparison between models for the simulation of hot water storage tanks," *Solar Energy*, vol. 75, no. 2, pp. 121 – 134, 2003.
- [69] F. Opper, A. Ghajar, and P. Moretti, "Computer simulation of stratified heat storage," *Applied Energy*, vol. 23, no. 3, pp. 205 – 224, 1986.
- [70] U. Eicker, *Solar Technologies for Buildings*. John Wiley & Sons, 2006.
- [71] W. M. Kays, M. E. Crawford, and B. Weigand, *Convective Heat and Mass Transfer*, 4th ed. McGraw-Hill, New York, 2005.
- [72] J. R. Pillai, P. Thøgersen, J. Møller, and B. Bak-Jensen, "Integration of electric vehicles in low voltage danish distribution grids," in *2012 IEEE Power and Energy Society General Meeting*, July 2012, pp. 1–8.
- [73] Australian Government Bureau of Meteorology. Accessed on 15-Feb-2018. [Online]. Available: http://www.bom.gov.au/info/thermal_stress/

References

- [74] Y. Zhang, M. Beaudin, R. Taheri, H. Zareipour, and D. Wood, "Day-ahead power output forecasting for small-scale solar photovoltaic electricity generators," *IEEE Transactions on Smart Grid*, vol. 6, no. 5, pp. 2253–2262, Sept 2015.
- [75] M. Newborough and P. Augood, "Demand-side management opportunities for the uk domestic sector," *IEE Proceedings - Generation, Transmission and Distribution*, vol. 146, no. 3, pp. 283–293, May 1999.
- [76] M. K. Larsen, "Analysis of the danish travel survey data on private and public transportation," in *Annual Transport Conference at Aalborg University 2010*, 2010.
- [77] B. Z. S. Hjalmar Christiansen, "Documentation of the dansish national travel survey," DTU Transport Department of Transport, Tech. Rep., 2015.
- [78] J. Quirós-Tortós, L. F. Ochoa, and B. Lees, "A statistical analysis of ev charging behavior in the uk," in *2015 IEEE PES Innovative Smart Grid Technologies Latin America (ISGT LATAM)*, Oct 2015, pp. 445–449.
- [79] NordPool. Accessed on 06-Jun-2017. [Online]. Available: <https://www.nordpoolgroup.com/Market-data1/Dayahead/Area-Prices/DK/Hourly/?view=table>
- [80] S. Huang and Q. Wu, "Real-time congestion management in distribution networks by flexible demand swap," *IEEE Transactions on Smart Grid*, vol. 9, no. 5, pp. 4346–4355, Sep. 2018.
- [81] G. Connor, C. E. Jones, and S. J. Finney, "End user voltage regulation to ease urban low-voltage distribution congestion," *IET Generation, Transmission Distribution*, vol. 8, no. 8, pp. 1453–1465, 2014.

Part II

Papers

Conference C1

Modelling of hot water storage tank for electric grid
integration and demand response control

R. Sinha, B. B. Jensen, J. R. Pillai, C. Bojesen and B.
Moller-Jensen

The paper has been published in the
2017 52nd International Universities Power Engineering Conference (UIPEC),
Heraklion, 2017, pp. 1–6.

© 2017 IEEE

The layout has been revised.

Modelling of Hot Water Storage Tank for Electric Grid Integration and Demand Response Control

Rakesh Sinha⁽¹⁾, Birgitte Bak Jensen⁽¹⁾, Jayakrishnan Radhakrishna Pillai⁽¹⁾, Carsten Bojesen⁽¹⁾
Bertil Moller-Jensen⁽²⁾

⁽¹⁾Department of Energy Technology, Aalborg Univeristy, Denmark

⁽²⁾ Aalborg Energi Holding A/S, Aalborg, Denmark

Email: ras@et.aau.dk⁽¹⁾, bertil.moeller-jensen@aalborg.dk⁽²⁾

Abstract—District heating (DH), based on electric boilers, when integrated into electric network has potential of flexible load with direct/indirect storage to increase the dynamic stability of the grid in terms of power production and consumption with wind and solar. The two different models of electric boilers for grid integration are investigated: single mass model (with uniform temperature inside tank) and two mass model (with ideal single stratified layers). In order to investigate the influence of demand response and grid voltage quality with the measurable parameter of electrical boiler in practice, selection of a proper model is equally important. The results obtained from comparison of two models (when input to the model is thermal energy demand) are present with their significance and advantages for grid integration and demand response. Models mathematics are shown in detail with the validation of result.

Index Terms- District heating, Electric Boiler, Flexible load, Grid Integration, Hot water storage, Stratification in tank

I. INTRODUCTION

In order to maintain the balance between demand and supply, there are issues and challenges possessed on the medium and low voltage networks regarding how to integrate and coordinate the electricity sector with district heating (DH) and to identify synergy between them [1].

Electric boiler and storage system (EB) can serve as a flexible consumer load to store surplus electrical energy in the form of hot water. For efficient utilization of EB integrated in electrical grid, proper demand response is necessary [2]. [3] discusses the control strategy based on parameters determined from a single mass model of the tank. To enhance the decision making capability of demand response, accuracy of measured variable plays an important role. Thus an appropriate model of the system is very important.

In a single mass system, uniformly distributed average temperature inside the storage system decreases gradually and significantly due to continuous mixing of liquid at different temperature created by flow. In practice, it is not possible to measure the average temperature. Therefore, there is a necessity to come up with an appropriate model where temperature of the hot water can be determined more precisely. In [4], three different types of modeling approaches of the hot water tank: actual stratified, ideal stratified and fully mixed model has been discussed. Several layers of stratification with fixed volume and heat transfer between each consecutive layer has been

presented in [5] with experimental and simulation result. In [6] a model of stratification in the tank, with and without the external flow of water are compared and the paper finds a good compromise between accuracy and computational time. As per [7], the energy storage efficiency of a fully stratified water tank may be increased up to 6% in comparison to a fully mixed water tank.

A good hypothesis could be that, with a proper approximation, a theoretical model of two mass system would serve as a tool, where the height of the cold water as well as temperature of inlet and outlet can be measured and realised in practice. These measurements serves flexibility in demand control for practical use.

This paper consists of six sections. Section I discussed the state of art and problem statement. Section II gives the insight on the model of the hot water storage tank. Section III presents derivation of equations for: size of the storage tank, equations governing single mass model, equations for defining temperature and height of hot and cold layers for the two mass model during charging and/or discharging process. Discussions on suitable approximations for formation of the thermocline in the tank and control strategy of EB is done in section III. In section IV and V, discussion on simulation platform and results on performance of both the models considering energy flow (in MWh) are done respectively. Finally, the conclusion is made in section VI.

II. MODEL OF TANK

The storage tank of electric boiler under consideration, as shown in fig. 1, is different from the regular hot water tanks. The heating element and the storage system is inside the single unit. The heating element is situated at the bottom of the tank so that the water inside the tank can store more heat energy with lower temperature inside the tank. If the heating element is placed at a certain height of the tank, due to effect of stratification, only the volume of water above the heating element will get heated, whereas the lower portion remains cold. Hence, the temperature of water above the heating element rises and reduces the total heat storing capacity of the tank, considering the temperature limit of hot water inside the tank. Multiple positions of heaters could be used to maintain the temperature at the top of the tank (outlet). However, in

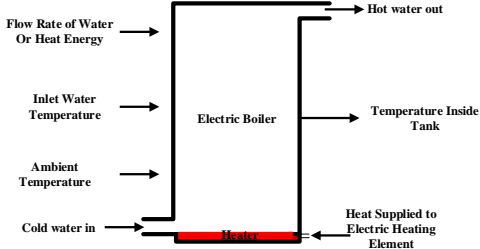


Fig. 1. Variable Flow Diagram in Electric Boiler

this paper only one heating element at the bottom of the tank is considered.

EB involve mass inflow and outflow of water. Thus, it is analysed as control volumes (open system) instead of a control masses (closed system) [8]. In order to achieve stratification and maintain constant temperature of hot water from the outlet, water outlet is set at the top of the tank and water inlet at the bottom of the tank [4]. Since hot water leaves the tank and is replaced by cold water, it is not convenient to model it as a fixed mass system. However, the volume formed by the interior surface of the tank can be considered as a fixed quantity as well as the control surface for this case [8]. Mass is crossing the control surface at two locations, bottom inlet and upper outlet. Hot and cold streams is modeled as mass leaving and entering the control volume respectively.

III. MODELLING OF HOT WATER STORAGE TANK

Let the shape of the tank be cylindrical with, volume $V(m^3)$ and the inner height to diameter ratio of the tank be $H/D = x$. Then the volume of the tank is given by equation (1)

$$V = \frac{\pi D^2 H}{4} = \frac{\pi D^3 x}{4} [m^3] \therefore \frac{H}{D} = x \quad (1)$$

$$\therefore D = \left(\frac{4V}{\pi x}\right)^{\frac{1}{3}} \quad (2)$$

Assuming that the tank thickness can be neglected, the surface area of the side wall of the tank A_s is given by

$$A_s = \pi DH = \pi D^2 x [m^2] \therefore \frac{H}{D} = x \quad (3)$$

Now, using equation (2) and (3), surface area of the side wall of the tank (which is mostly responsible for heat loss) can be calculated as per equation (4).

$$A_s = \pi x \left(\frac{4V}{\pi x}\right)^{\frac{2}{3}} = (16\pi x V^2)^{\frac{1}{3}} [m^2] \quad (4)$$

The surface area of the top portion of the tank (A_t) is given by equation (5)

$$A_t = \frac{\pi D^2}{4} = \frac{\pi}{4} \left(\frac{4V}{\pi x}\right)^{\frac{2}{3}} = \left(\frac{\pi V^2}{4x^2}\right)^{\frac{1}{3}} [m^2] \quad (5)$$

The total surface area of the tank (A) from where the heat loss due to conduction takes place is given by equation (6).

$$A = A_s + A_t [m^2] \quad (6)$$

A. Single mass model

It is a simple and most widely used model for general purpose simulations. In this model the average temperature ($T_{(b)avg}$) inside the tank is considered to be uniformly distributed. The temperature inside the tank changes with change

in time due to energy losses to the ambient and net energy addition or withdrawal during the flow of water. It is convenient to model the hot water storage tank by considering net flow of energy rather than with mass flow of water to meet the thermal demand (\dot{Q}_{demand}). The mass of hot water flowing out the tank is instantaneously replaced by same amount of cold water from the bottom inlet (as per equation 10) assuming that, the density of water remains the same for all temperature and is equal to 1 g/cc. The specific heat capacity of water (C_w) at constant volume is considered to be equal to specific heat capacity of water at constant pressure. This statement is valid when water is approximated as an incompressible substance and the pressure exerted on it is not extremely high [8]. Now, according to the law of energy conservation, rate of net heat entering and leaving the boiler (\dot{Q}_{boiler}) is given by equation (7).

$$\dot{Q}_{boiler} = \dot{Q}_{heat} - \dot{Q}_{demand} - \dot{Q}_{loss} \quad (7)$$

$$\dot{Q}_{boiler} = C_w m_b \frac{dT_{(b)avg}}{dt} [J/s] \quad (8)$$

$$\dot{Q}_{demand} = C_w m_1 (T_{(b)avg} - T_{iw}) [J/s] \quad (9)$$

$$\Rightarrow m_1 = \frac{\dot{Q}_{demand}}{C_w (T_{(b)avg} - T_{iw})} [kg/s] \quad (10)$$

$$\dot{Q}_{loss} = UA(T_{(b)avg} - T_a) [J/s] \quad (11)$$

Where,

\dot{Q}_{boiler} = rate of net heat entering and leaving the boiler [J/s]

\dot{Q}_{heat} = heat flow rate of heating element [J/s]

\dot{Q}_{demand} = heat demand transfer rate due to flow of water (Thermal Demand) [J/s]

\dot{Q}_{loss} = heat loss rate between tank and ambient environment, through the wall of tank due to conduction [J/s]

C_w = specific heat capacity of water [J/kg.K]

m_b = mass of water in boiler [kg]

$T_{(b)avg}$ = average temperature inside boiler [K]

U = overall heat transfer coefficient [W/m².K]

A = surface area of the tank [m²]

T_a = temperature of ambient environment [K]

\dot{m}_1 = mass flow rate of water [kg/s]

T_{iw} = temperature of inlet water [K]

Substituting equation (8), (9) and (11) in equation (7), we get equation (13) which gives the average temperature gradient inside the tank.

$$C_w m_b \frac{dT_{(b)avg}}{dt} = \dot{Q}_{heat} - \dot{Q}_{demand} - UA(T_{(b)avg} - T_a) \quad (12)$$

$$\frac{dT_{(b)avg}}{dt} = \frac{1}{C_b} [\dot{Q}_{heat} - \dot{Q}_{demand} - UA(T_{(b)avg} - T_a)] \quad (13)$$

Where, $C_b = C_w m_b$ = Thermal capacitance of boiler [J/K]

The flow rate of water to meet the thermal demand (\dot{Q}_{demand}) is calculated from the equation (10). \dot{Q}_{heat} can be expressed in terms of power extracted from grid as efficiency of boiler as per equation (14).

$$\dot{Q}_{heat} = \frac{\eta}{100} P_{grid} \left[\frac{J}{s} \text{ or } W\right] \quad (14)$$

Where, η =efficiency of boiler [%]. The electric boiler is assumed to be a constant impedance load [9]. Then,

$$P_{r,b} = \frac{V_{r,b}^2}{R_b} [W] \quad (15)$$

Where, $P_{r,b}$ = rated power of boiler [W].

$V_{r,b}$ = rated voltage of boiler [V]

R_b = impedance of boiler [Ω]

The power supplied from the grid to boiler can be written as,

$$P_{grid} = \frac{V_{poc}^2}{R_b} \quad [W] \quad (16)$$

Where, P_{grid} = power supplied from the grid [W].

V_{poc} = voltage at point of coupling of boiler into the grid [V]

R_b = impedance of boiler [Ω]

from equation (15) and equation (16),

$$P_{grid} = \left(\frac{V_{poc}^2}{V_{r,b}^2} \right) P_{r,b} = \left(\frac{V_{poc}}{V_{r,b}} \right)^2 P_{r,b} \quad [W] \quad (17)$$

from equation (14) and equation (17),

$$\dot{Q}_{heat} = \frac{\eta}{100} P_{grid} = \frac{\eta}{100} \left(\frac{V_{poc}}{V_{r,b}} \right)^2 P_{r,b} \quad [W] \quad (18)$$

Equation (18) shows the dependency of EB and the grid terminal voltage at the point of coupling. This property has also been discussed in [9]. This relation is useful to investigate interaction between thermal load (based on EB) and electrical grid, as well as for demand response management and control of EBs in future. Finally, the single mass model of tank is modelled using equation (6), (13) and (18).

B. Two mass model (with variable stratification height)

The two mass model is a theoretical, where two-layer of hot and cold water in the system is separated by the thermocline during favourable condition as stated below and will continue to be separated when hot water is discharge from the top and add cold water at the bottom of the tank.

Due to the gravity and buoyant effect, water with different temperature gets deposited at different heights based on the density difference. Difference between the density of hot and cold water at different temperatures, creates the layer of hot and cold water inside a storage tank. Cold water being denser than hot water, it remains at the bottom of the tank. This formation of the layer of water with different temperature is known as thermal stratification [10]. The region with the steepest gradient of change in temperature between layers is known as thermocline, which prevents mixing between the layers of water above and beneath it. The thickness of the thermocline is based on effective diffusivity factor (ε_{eff}) [11]. $\varepsilon_{eff} = 1$ for laminar flow at the inlet causes perfect stratification. $\varepsilon_{eff} \gg 1$ represents turbulent flow at the inlet, which causes mixing of the liquid creating wider thermocline [11]. To model a storage tank with stratified layer

- Assume two thermal layers, a high and a low temperature layer. The number of layers would depend on the number of supply temperatures to the storage. However, since the temperature of the inlet cold water to the storage tank is considered to be at constant value, only two layers (upper hot and lower cold) are considered.
- Assume the thermocline to be horizontal and independent of radial distance.
- Assume uniform temperatures for the two layers. There are heat loss from the hot and cold layers to the ambient through the surface of the tank wall. There is no transfer

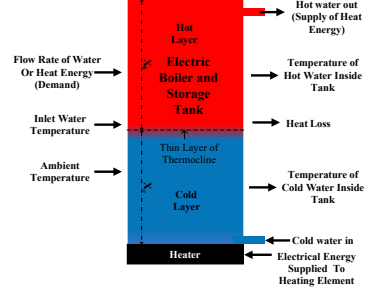


Fig. 2. Two mass model of hot water storage tank

of heat between hot and cold layer, or through the surface wall of the tank. This assumption confirms that the thermocline is dominated by conduction and convection in the fluid rather than conduction through the wall of tank [12].

- Thermocline inside tank remains for the certain time (t) known as dead time. If the layer remains undisturbed, this dead time can be assumed to be infinite. This is only possible when the boiler is turned off. When the heater is turned on, due to direct heat transfer from the bottom of the tank, thermal stratification gets easily destroyed by water turbulence [7] and there is mixing of hot and cold liquid.

With the above mentioned assumptions, the storage tank is assumed to have layers of hot and cold water separated by a thin layer of thermocline as shown in fig. 2. It is given the term two mass model as there are two masses of hot and cold water separated by the thermocline. This two mass model accounts for perfect stratification in two zones with two uniform temperatures, (T_h) and (T_c) for the hot and cold layers respectively. The position of the thermocline changes depending upon the flow of hot water out from the tank which is replaced by cold water. Only the temperature of hot water inside the layer changes with change in time due to energy losses to the ambient. Average temperature inside the tank has the effect of net energy addition or withdrawal during the flow of water as well. Let,

the volume of the tank be V [m^3]
total mass of water inside boiler be m_b [kg]
mass flow rate of water be \dot{m}_2 [kg/s]

1) *Case I when heater is turned off and there is formation of thermocline:* It is assumed that the tank is initially filled with hot water and heater is turned off. When there is thermal demand of hot water \dot{Q}_{demand} , the hot water inside the tank is replaced with cold water with same amount (with mass flow rate of \dot{m}_2 [kg/s] calculated from equation 26) if we consider density of water to remain constant as in the case of a single mass model. Assuming that the flow meets all the criteria mentioned above for the formation of stratified later, the mass of hot water inside the tank at any time (t) can be

calculated as per equation (19) and (20)

$$m_h = m_b - m_c \quad [kg] \quad (19)$$

$$m_c = \int_{t_1}^{t_2} \dot{m}_2 dt \quad ; \quad 0 \leq m_c < m_b \quad [kg] \quad (20)$$

Where,

m_h = total mass of hot water inside tank at time t [kg]

m_c = total mass of cold water inside tank accumulated during time interval($t_2 - t_1$) at time t [kg]

The boundary condition for m_c is to make sure that the accumulation of cold water is always less than the total volume of the tank.

The ratio of hot water inside tank with respect to the total mass of water inside tank is given by

$$X_h = \frac{m_h}{m_b} = \frac{m_b - m_c}{m_b} \quad ; \quad 0 \leq X_h \leq 1 \quad (21)$$

and the ratio of cold water inside tank with respect to the total mass of water inside tank is given by

$$X_c = \frac{m_c}{m_b} = 1 - X_h \quad ; \quad 0 \leq X_c \leq 1 \quad (22)$$

The boundary condition for X_h and X_c is between 0 and 1 representing that, the tank is either full with hot water if ($X_h = 1$) or cold water if ($X_c = 1$) and hence, no layer of thermocline.

Let, the surface of the side wall of tank be in contact with mass m_b be A_s [m^2] as given by equation (4). Then using unitary method, the surface area of the tank in contact with mass of hot water (m_h) is equal to

$$A_s \frac{m_h}{m_b} = A_s X_h \quad [m^2] \quad (23)$$

Considering the temperature of the outlet to be equal to the temperature of hot water ($T_{out} = T_h$), the total heat loss from the surface of the hot and cold region of the tank to the ambient is given by the equation (24) and heat loss from the tank due to flow of hot water is given by equation (25). A_t is the area of top roof of the tank which is in contact with hot water and is defined by equation (5).

$$\dot{Q}_{loss2} = [U A_s X_h (T_h - T_a) + U A_t (T_h - T_a) + U A_s X_c (T_c - T_a)] \quad [W] \quad (24)$$

$$\dot{Q}_{demand} = C_w \dot{m}_2 (T_h - T_{iw}) \quad [W] \quad (25)$$

$$\Rightarrow \dot{m}_2 = \frac{\dot{Q}_{demand}}{C_w (T_h - T_{iw})} \quad [kg/s] \quad (26)$$

Where, T_{iw} = temperature of inlet water [K]

The temperature of hot water inside the tank changes only due to loss of energy from the surface of the tank containing hot water. The temperature of the cold water inside the tank changes due to loss of energy from the surface of the tank in contact with cold layer and mixing of cold water incoming to replace the flow of hot water from the upper layer of tank. Thus the temperature of hot and cold layer during stratification is calculated using equation (27) and (28) respectively

$$\frac{dT_h}{dt} = \frac{-1}{C_b X_h} [U A_s X_h (T_h - T_a) + U A_t (T_h - T_a)] \quad (27)$$

$$\frac{dT_c}{dt} = \frac{-1}{C_b X_c} [U A_s X_c (T_c - T_a) + C_w \dot{m}_2 (T_c - T_{iw})] \quad (28)$$

Where, $C_b X_h$ and $C_b X_c$ and is thermal capacitance of hot layer and cold layer respectively in [J/K]. The thermal

capacitance of the hot and cold layers changes according to time as X_h and X_c depends on m_c which varies according to time.

During the presence of thermocline, the average temperature in the tank can be calculated similar to equations (13) by balancing the net heat content in the tank and this is presented as equations (29). Since, $\dot{Q}_{heat} = 0$

$$\frac{dT_{avg2}}{dt} = \frac{1}{C_b} [-\dot{Q}_{demand} - \dot{Q}_{loss2}] \quad (29)$$

From equation (24) and (29)

$$\frac{dT_{avg2}}{dt} = \frac{1}{C_b} [-\dot{Q}_{demand} - U A_s X_h (T_h - T_a) - U A_t (T_h - T_a) - U A_s X_c (T_c - T_a)] \quad (30)$$

Thus, when the heater is turned off, stratification comes into existence. The temperature of the outlet water ($T_{out} = T_h$) is calculated by equation (27) where decrease in temperature is only from heat loss due to conduction from the surface wall of the storage in contact with hot water. The total loss of the system due to conduction loss and flow of hot water is calculated as per equations (24) and (25) respectively. At the same time the average temperature inside the tank (T_{avg2}) can be calculated using equation (30)

2) *Case II when heater is turned on and thermocline is destroyed:* When the heater is turned on, due to direct heat transfer from the bottom of the tank, thermal stratification gets easily destroyed by water turbulence [7]. The formation of a stratified layer is disturbed and now the tank acts as single mass model. The temperature of outlet water (T_{out}) equals to the average temperature of the tank (T_{avg2}) as given by equation (30) due to mixing of hot and cold water that were separated by the thermocline. Now, T_{avg2} is calculated using equation (31) based on equations (13) used for the single mass model.

$$\frac{dT_{avg2}}{dt} = \frac{1}{C_b} [\dot{Q}_{heat} - \dot{Q}_{demand} - U A (T_{avg2} - T_a)] \quad (31)$$

Thus, when the heater is turned on, the temperature of the boiler is calculated using equation (31) and $T_{out} = T_{avg2}$, until the heater is turned off to allow favorable condition for stratification. This shows that the temperature of the outlet water (T_{out}) is equal to T_h during presence of stratification and T_{avg2} during absence of stratification.

3) *Determining T_{avg2} and T_{out} during charging and discharging:* By combining equation (30) and equation (31), the average temperature of the storage tank T_{avg2} at any time (t) for two mass model can be known through equation (32). This will ease the process to calculate the average temperature of mixing of liquid with variable volume due to flow.

$$\frac{dT_{avg2}}{dt} = \frac{1}{C_b} [\dot{Q}_{heat} \cdot \bar{C}_s - \dot{Q}_{demand} - U A (T_{out} - T_a) \bar{C}_s - U A_s X_h (T_{out} - T_a) C_s - U A_t (T_{out} - T_a) C_s - U A_s X_c (T_c - T_a) C_s] \quad (32)$$

Where, C_s represents the status of stratification. $C_s = 1$ represents that the tank has favorable condition for stratification. Further, there will be presence of the thermocline only if there is flow of cold water from the inlet to the tank and

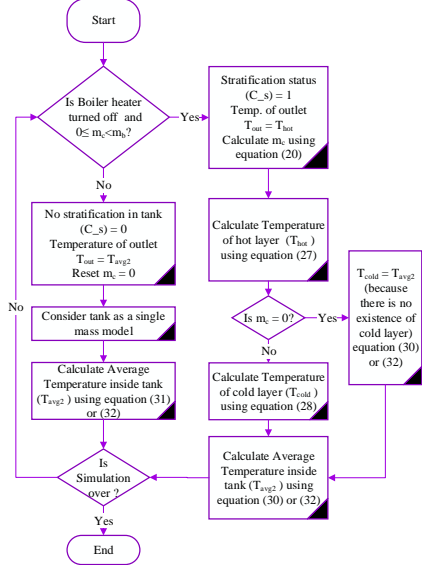


Fig. 3. Flowchart to calculate the temperature of water inside the tank for two mass model

accumulation of cold water is less than the volume of tank, else there is uniform temperature through out the tank.

During absence of the thermocline, $C_s = 0$, $\bar{C}_s = 1$, $m_c = 0$, and $T_{out} = T_{avg2}$. Equation (32) then becomes equal to equation (31).

During presence of the thermocline, $C_s = 1$, $\bar{C}_s = 0$, $0 < m_c < m_b$ and $T_{out} = T_h$. Equation (32) then becomes equal to equation (30).

Temperature from the outlet T_{out} during charging and discharging can be determine by following flowchart illustrated in fig. 3.

C. Control of EB heater

Hysteresis control of the heating element has been selected based on temperature of water from the outlet or accumulation of cold water. The control signal of the heater is denoted by ' C_a '. When $C_a = 1$, the heater is turned on, else turned off. The condition for turn on and turn off of heater is determined by equation (33) and (34) respectively.

$$C_a = 1, \quad \text{if } T_{out} < T_{min}, \quad \text{or}, \quad X_c > X_{cold} \quad (33)$$

$$C_a = 0, \quad \text{if } T_{out} > T_{max} \quad (34)$$

Where, T_{max} and T_{min} are defined maximum and minimum allowable temperature inside tank and X_{cold} is the defined allowable level of cold water inside the storage tank.

IV. SIMULATION ENVIRONMENT

Both storage models were programmed and implemented in DigSILENT PowerFactory (simulating tool for power system analysis) as DSL (DIGSILENT Simulation Language). Data of \dot{Q}_{demand} has been prepared manually to investigate the

TABLE I
PARAMETER OF STORAGE TANK, ELECTRIC BOILER AND CONTROL UNIT

Parameter of storage tank		Value
Volume of storage tank (V) [m^3]		12.5
Overall heat transfer coefficient (U) [$W/m^2 \circ C$]		2.5
Specific heat capacity of water (C_w) [$J/kg \circ C$]		4180
density of water (ρ) [kg/m^3]		1000
Ambient temperature of storage room (T_a) [$\circ C$]		15
Incoming cold water temperature (T_{iw}) [$\circ C$]		30
Ratio of height to diameter of tank (H/D) [μ]		2.5
Parameter of electric boiler		Value
Rated power of electric boiler ($P_{r,b}$) [kW]		200
Rated voltage of electric boiler ($V_{r,b}$) [μ]		1
Efficiency of electric boiler (η) [%]		100
Parameter of control unit		Value
Maximum temperature allowed inside tank (T_{max}) [$\circ C$]		80
Minimum temperature allowed inside tank (T_{min}) [$\circ C$]		70
Allowed height of cold water to accumulate (X_{cold}) [μ]		0.2

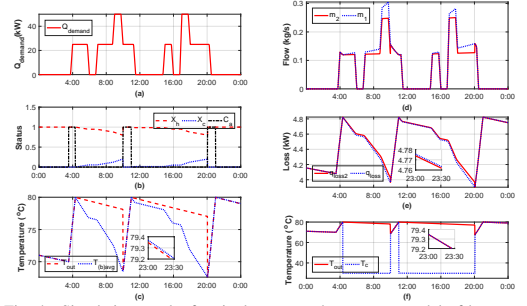


Fig. 4. Simulation results for single mass and two mass model of hot water storage tank

- (a) thermal Demand
- (b) status of heater and level of water in the tank
- (c) temperature of outlet water for both models
- (d) flow rate of water for both models to fulfil thermal demand
- (e) total losses from the wall of the tank for both models
- (f) temperature of cold water and outlet water in tank for the two mass model

behavior of the storage model during different situations and verify the models. The results from simulation of both the model has been compared and investigated.

The various parameters of the storage tank, electric boiler and the control unit has been presente in table I

V. RESULT AND DISCUSSIONS

Results of the simulation for the single mass and the two mass models are compared and presented in graphs shown in fig. 4. Fig. 4(a) shows the plot of (\dot{Q}_{demand}) with total thermal demand of 325kWh/day and is the input to the system.

Fig. 4(b) shows the status of the heater (C_a) if turned on or off. Graph of X_h and X_c are also plotted to visualise the level of hot and cold water level in the tank respectively. The value of X_h and X_c gets reset to their original value 1 and 0 respectively when the heater is turned on.

Temperature of hot water from the outlet (T_{out}) for the two mass model and ($T_{(b)avg}$) for single mass model has been shown in fig. 4(c). At time $t = 03:30$, the temperature of the hot water from the outlet (T_{out}) drops below the minimum

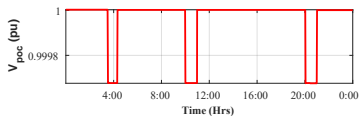


Fig. 5. Voltage at point of coupling of electric boiler

set value ($T_{min} = 70^{\circ}C$) and heater is turned on as seen from the status of (C_a) in fig. 4(b). The temperature of water inside the tank rises until it reaches the maximum allowable temperature ($T_{max} = 80^{\circ}C$). Then the temperature of hot water for the two mass model decreases only due to loss from the wall of the tank and decreases with constant rate, while the temperature of hot water in the single mass model ($T_{(b)avg}$) decreases significantly due to effect of loss as well as mixing of water at different temperature due to flow. At 10:00 and 20:00 Hrs, the heater is turned on because the accumulation of cold water inside the storage tank is more than the set limit of $X_{cold} = 0.2$. When the heater is turned on, the temperature of outlet water for the two mass model (T_{out}) drops abruptly to around $69^{\circ}C$ as given by equation (30) for T_{avg2} . This drop is due to loss of thermocline and mixture of hot and cold water in the tank, and then gradually rises as per equation (31). Hence, to manage the demand response control of hot water tank, the value of (T_{out}) and height of cold water in the tank (X_c) gives more reliable and applicable information than the average temperature ($T_{(b)avg}$) measured for single mass model.

Due to the presence of the thermocline, there is more losses from the two mass model than in single mass model as seen from fig. 4(e). Thus, energy content in the two mass model is less than the total energy content in the single mass model at any instance of time. The total energy loss for the two mass model is 0.3% more than that in single mass model.

Graphs in fig. 4(d), is for the flow rate of hot water for the single mass model (m_1) and the two mass model (m_2). It shows that $m_1 > m_2$ during presence of the thermocline, as the temperature difference of outgoing and incoming hot water for the single mass model is lower than for the two mass model. The maximum flow rate observed for the single mass model is 0.3 kg/s where as for the two mass model, it is 0.25 kg/s. The value of m_1 and m_2 would influence the price of consumption if metering is done based on flow rather than energy. Flow rate along with the temperature of outlet hot water (T_{out}) would give a good idea about the size of the tank and the heater.

Fig. 4(f) shows the graph of the temperature of the cold water layer in the tank. During presence of the thermocline, the temperature of the cold layer is around $30^{\circ}C$ and varies due to mixing of cold water from the inlet and loss from the surface wall of the tank.

Fig. 5 shows the voltage profile at the point of coupling of the electrical boiler. Since the chosen grid is strong, there is not much drop in voltage(pu). However, it can make a significant difference where the grid strength is medium or low.

VI. CONCLUSION

Since the difference in the losses between the two models is 0.3%, it can be concluded that the size/capacity (kW/MW) of the electric boiler has barely any influence on the selection of specific model if the thermal energy is taken as input and output parameter. When looking into the temperature, height of accumulation of cold water in the tank, and flow rate, the two mass model is superior to the single mass model. These parameters can be utilised for the demand response which can be easily implemented. Results can vary if the the system is modelled to take flow of hot water as input.

Voltage quality depends upon the type of grid as well as size of the boiler. Selection of boiler model does not have direct impact on the grid voltage. However, the status of amount of hot water present in the tank along with grid status during peak hour may significantly influence selection of boiler model. Thus, the two mass model discussed here is better than the single mass model for the purpose of flexible load and demand response to be implement in real system.

ACKNOWLEDGMENT

The authors would like to thank DiCyPS project funded by the Danish Innovation fund for funding this research project.

REFERENCES

- [1] "Smart grid strategy-the intelligent energy system of the future," Danish Ministry of Climate, Energy and Building, Tech. Rep., 2013.
- [2] I. D. De Cerio Mendaza, I. G. Szczesny, J. R. Pillai, and B. Bak-Jensen, "Flexible demand control to enhance the dynamic operation of low voltage networks," *IEEE Transactions on Smart Grid*, vol. 6, no. 2, pp. 705–715, 2015.
- [3] P. T. Bjerregaard, I. G. Szczesny, I. D. de Cerio Mendaza, and J. R. Pillai, "Intelligent control of flexible loads for improving low voltage grids utilization," in *IEEE PES ISGT Europe 2013*, Oct 2013, pp. 1–5.
- [4] A. C. Celador, M. Odriozola, and J. Sala, "Implications of the modelling of stratified hot water storage tanks in the simulation of {CHP} plants," *Energy Conversion and Management*, vol. 52, no. 8–9, pp. 3018 – 3026, 2011.
- [5] A. A. Farooq, A. Afram, N. Schulz, and F. Janabi-Sharifi, "Grey-box modeling of a low pressure electric boiler for domestic hot water system," *Applied Thermal Engineering*, vol. 84, pp. 257 – 267, 2015.
- [6] R. D. C. Oliveski, A. Krenzinger, and H. A. Viello, "Comparison between models for the simulation of hot water storage tanks," *Solar Energy*, vol. 75, no. 2, pp. 121 – 134, 2003.
- [7] Y. Han, R. Wang, and Y. Dai, "Thermal stratification within the water tank," *Renewable and Sustainable Energy Reviews*, vol. 13, no. 5, pp. 1014 – 1026, jun 2009.
- [8] Y. A. Bengel and M. A. Boles, "Thermodynamics an engineering approach," *Energy*, vol. 1, p. 51, 2002.
- [9] I. D. D. Cerio, *An Interactive Energy System with Grid , Heating and Transportation Systems An Interactive Energy System with Grid , Heating and Transportation Systems*, 2014.
- [10] P. González-Altozano, M. Gasque, F. Ibáñez, and R. P. Gutiérrez-Colomer, "New methodology for the characterisation of thermal performance in a hot water storage tank during charging," *Applied Thermal Engineering*, vol. 84, pp. 196 – 205, 2015.
- [11] Y. Zurigat, A. Ghajar, and P. Moretti, "Stratified thermal storage tank inlet mixing characterization," *Applied Energy*, vol. 30, no. 2, pp. 99 – 111, jan 1988.
- [12] F. Oppel, A. Ghajar, and P. Moretti, "Computer simulation of stratified heat storage," *Applied Energy*, vol. 23, no. 3, pp. 205 – 224, jan 1986.

Conference C2

Unleashing Flexibility from Electric Boilers and Heat Pumps in Danish Residential Distribution Network

Rakesh Sinha, Birgitte Bak-Jensen, Jayakrishnan Radhakrishna Pillai, Bertil Møller-Jensen

The paper has been published in the
Proceeding of CIGRE Session 2018, Paris, 2018, pp. 1–11.

The layout has been revised.

Unleashing Flexibility from Electric Boilers and Heat Pumps in Danish Residential Distribution Network

**Rakesh Sinha^{*(1)}, Birgitte Bak Jensen⁽¹⁾, Jayakrishnan Radhakrishna Pillai⁽¹⁾,
Bertil Møller-Jensen⁽²⁾**

⁽¹⁾Dept. of Energy Technology, Aalborg University

⁽²⁾Aalborg Energi Holding A/S, Aalborg
Denmark

SUMMARY

This paper presents an overview of the electrical and thermal behaviour in a Danish residential area, followed by an examination of the possibility and need for interaction between the heating elements such as electric boilers (EBs) and heat pumps (HPs) and the electric distribution network. Under voltage and grid congestion are main focus issues for investigation of the electric network condition. In this paper, a model of a two layer stratified hot water tank, heated by an EB or a HP for grid integration, is proposed along with its advantages for demand response control. Responses using this model is compared to responses from an average model of the hot water storage tank to evaluate the benefit of the more detailed model. Finally, analysis on consumption patterns of electrical and thermal loads in residential buildings in Northern Jutland, Denmark, are used for analysis of the system and use of thermal units as flexible consumer loads in the low voltage (LV) distribution network grid. The models of EB and HP with storage tank are briefly discussed in relation to the actual control and flexibility based on grid condition and status of storage tank temperature or position of the stratified layer.

The problem formulation and models in the work are conducted based on the requirements and suggestions evolved from discussions with the local heat distribution utility. The requirements are framed based on their experience and vision to integrate more thermal units in the energy systems and thereby improving its techno-economic efficiency. The data used for the evaluation are also from the real household sites in Denmark provided by the district heating utility. Focus is on the low-voltage grid, and that's very relevant since many doesn't expect any flexibility from that voltage level. Study performed shows that usage of HP and storage unit has less impact on the grid voltage and congestion when compared to EB.

KEYWORDS

Electric Boiler, Heat Pump, Thermal storage, Stratification, Flexibility, LV Distribution Network, Demand Response.

1. BACKGROUND AND STATE OF THE ART

With the concept of 4th Generation District Heating (4GDH) and smart grid electrical networks in Denmark, there is now a transition from centralized fossil fuel based energy systems to decentralized energy systems based on renewables [1] [2]. Energy Roadmap 2050, focuses on the electrification of the heating sector which predominantly includes components like electric boilers (EBs) and heat pumps (HPs). The potential growth of district heating in the EU until 2050 is identified with detailed mapping of demand and supply in [3]. Apart from Denmark, Finland, UK, Germany and many other countries are also looking forward for integration of the thermal and electricity sectors [4]. LIVØ project in Denmark (2015-2018) has been working for the establishment of 100% renewable sources such as wind turbine (20 kW) and solar cells (20kW) to supply power for the island of Livø, which is isolated from the mainland grid. These renewable energy sources are looking forward to be combined with an electric boiler (50 kW) and a heat accumulator (2 MWh) for energy storage [5].

The heating infrastructure, based on district heating or small individual HPs and EBs, has been identified as local sustainable solutions for storage and grid support due to the significant price advantages in investment cost of storage and generation [6]. Electrical and thermal networks in Denmark are intended to be integrated further in future. In order to evaluate the possible degree of interaction between the electrical and thermal networks, examination of local energy system and a bottom-top approach of system analysis is very important. In Denmark, wind power produced more electricity than the total load and sometimes the SPOT-marked had negative prices in a year 2015 [7]. As a result, wind turbine owners are subjected to turn off their generation for hours during these hours. On the other hand, space heating and domestic hot waters were supplied to 63% of the private Danish houses through district heating (DH) until end of 2015 [8]. A huge variety of technologies such as combined heat and power plants (CHP), solar heating, waste to energy, gas boilers, biomass boilers and HPs are used to cover the heating supply. With the incentive to phase out fossil fuel based boilers by 2030, 100% of heating demands must be contributed by renewable energy. Thus, flexibility from EBs and HPs, when integrated in the electrical grid network, can be utilised to support grid ancillaries in a renewable generation dominated power systems. The ability of the DH to balance power demand in the smart grid has been widely discussed and identified in [9]. Variety of EBs and HPs with storage tank are readily available in market in various shape and size. Until 2015, electric boilers (as a part of district heating) are installed in 45 different places in Denmark with total load of 488.2 MW (ranging from 0.1 to 93MW) at different voltage levels of 0.4kV, 0.7kV, 10kV, 10.5kV, 15kV and 150kV. The detailed list is provided in [10]. Similarly, there are 18 heat pumps in district heating with total of 4.7MW generating capacity [11].

Electricity consumption in Danish households are for lighting, cooking, washing etc. Space heating and domestic hot water consumption today are provided through networks of district heating or individual oil boilers and some few heat pumps. Electricity consumption at device level, with different patterns and periodicity for flexible operation, is defined in [12]. In [13] an adaptive control methodology for real-time voltage support to distribution grids has been proposed based on adjustment of active and reactive power injection/consumptions of the electric water heater and photovoltaic. A hierarchical arrangement of the distribution system supervision with heat pumps makes demand response to identify, evaluate and tackle the technical constraints in the LV network when voltage drop is the key factor representing the grid constraint [14].

This paper analyses and compares flexibilities in LV residential grid performance (grid voltage, line loading and transformer capacities) when coupled with EBs and HPs. Section 2, and 3 of this paper presents the modeling approaches for EBs and HPs followed by comparison of system performance between simple stratified and non-stratified hot water storage tank. Section 4 discusses the control schemes of the system based on local information such as grid voltage and status of hot water in the storage tank respectively. The LV residential grid along with electrical and thermal load profiles are presented in section 5 and 6 respectively. Various case studies upon integration of EBs and HPs in the LV residential network are identified in section 7 followed by the results and discussion in section 8. Finally, the paper is concluded in section 9.

2. ELECTRIC BOILER (EB) and HEAT PUMP(HP) MODEL

EBs (as shown in Figure 1) are modelled as a constant impedance electrical load with unity power factor as per equation (1) [15] [16]. Equation (1) also shows the dependency of an EB with the grid terminal voltage at the point of common coupling and this property is used to control the EBs and HPs for grid voltage support in this paper.

$$\dot{Q}_{heat} = \frac{\eta}{100} \left(\frac{V_{poc}}{V_{r,b}} \right)^2 P_{r,b} \quad [W] \quad (1)$$

Where, η = efficiency of the boiler [%], V_{poc} = Voltage at point of coupling of EB [V], $V_{r,b}$ = rated voltage of EB [V] and $P_{r,b}$ = rated power of EB [W].

HP is modelled based on [17]. A simple Heat pump (HP) based water heating system (HPWH) is shown in Figure 2. The thermal power produced by the HP is calculated as per equation (2), where COP is the coefficient of performance and P_{HP} is the electrical power rating of the HP. The power factor of the HP ($\cos \theta$) is considered as 0.85 lagging. Thus, the reactive power drawn by the motor driving the compressor of HP is given by equation (3). Taken from the manufacturers' datasheet COP is considered to be 3 for operating HPs during a cold winter season.

$$\dot{Q}_{heat} = COP \cdot P_{HP} \quad [W] \quad (2)$$

$$Q_{HP} = P_{HP} \tan \theta \quad [VAR] \quad (3)$$

3. MODEL OF HOT WATER STORAGE TANK

Figure 1 and Figure 2 show the variable flow diagram for a stratified storage tank operated with an EB and a HP respectively considered for the modelling. The detailed equations and modelling approach of the simplified stratified storage tank and its flexibility in performance compared with a uniform temperature model of the storage tank has been widely described in [15].

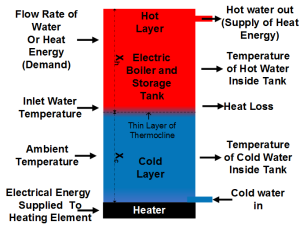


Figure 1: Variable flow diagram in electric boiler and storage tank

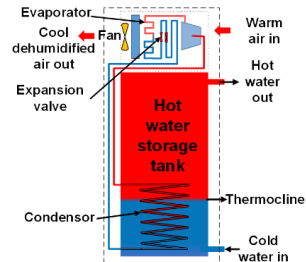


Figure 2: Heat pump and storage

Here the stratified storage tank is a theoretical model with a single thermocline separating the hot and cold layer of water inside the tank. Difference in density of hot and cold water at different temperatures creates the layer of hot and cold region known as thermal stratification [18]. The thermocline is the region with steepest gradient of change in temperature between the layers, which prevents mixing of water between two different temperatures above and beneath it. The effective diffusion factor (ϵ) defines the thickness of thermocline. $\epsilon=1$ represents the laminar flow at the inlet and causes perfect stratification [19]. Following assumptions are considered to model a storage tank with stratified layers [15].

- There exist only two thermal layers, a hot and a cold layer, inside the storage tank.
- The thermocline is horizontal and independent of radial distance.
- Both, the hot and cold, layer are considered to have uniform temperature and the thermocline is dominated by conduction and convection in the fluid rather than conduction through the wall of tank [20].
- The thickness of the thermocline layer (x) can be assumed to be very thin i.e., ($x=0$, for $\epsilon=1$)

- The heating element is attached to the bottom cold layer of tank. When the heater is turned on, due to direct heat transfer from the bottom of the tank, thermal stratification is easily destroyed by water turbulence [21] and there is mixing of hot and cold liquid

With these assumptions, the temperature of hot water from the outlet is calculated as per equation (4) and (5) during presence and absence of thermocline respectively [15].

$$\frac{dT_h}{dt} = \frac{-1}{C_b X_h} [UA_s X_h (T_h - T_a) + UA_t (T_h - T_a)] C_s \quad [\text{K/s}] \quad (4)$$

$$\frac{dT_{avg}}{dt} = \frac{1}{C_b} [\dot{Q}_{heat} \bar{C}_s - \dot{Q}_{demand} - UA(T_{out} - T_a) \bar{C}_s - UA_s X_h (T_{out} - T_a) C_s - UA_t (T_{out} - T_a) C_s - UA_s X_c (T_c - T_a) C_s] \quad [\text{K/s}] \quad (5)$$

Where, A_s, A_t = Surface area of side wall and top roof of the tank respectively [m^2]

C_s = Status of stratification ($C_s = 1$ when heating element is turned OFF and there is some flow of cold water inside the tank, else 0)

C_b = Thermal capacitance of boiler [J/K]

T_{avg} = Average temperature inside the boiler [K]

T_h, T_c, T_{out}, T_a = Temperature of hot water, cold water, outlet and ambient respectively [K]

X_h, X_c = Normalised height of hot and cold water inside the tank respectively

\dot{Q}_{heat} = Heat flow rate of heating element [J/s]

\dot{Q}_{demand} = Heat demand transfer rate due to flow of water (thermal demand) [J/K]

U = Overall heat transfer coefficient [$\text{W/m}^2\text{K}$]

When then heating element (EB or HP) is turned OFF (i.e, $C_a = 0$) and there is presence of stratified layer (i.e, $C_s = 1$) then $T_{out} = T_h$ and equation (4) is used to calculate the temperature of the hot layer in the tank. At the same time, equation (5) calculates the average temperature (T_{avg}) in the storage tank. When the heating element is turned on (i.e, $C_a = 1$ and $C_s = 0$), $T_{out} = T_{avg}$ since the thermocline layer gets disturbed due to turbulence and mixing of water takes place resulting in a temperature calculated by equation (5). Equation (6) represents the uniform temperature model.

$$\frac{dT}{dt} = \frac{1}{C_b} [\dot{Q}_{heat} C_a - \dot{Q}_{demand} - UA(T - T_a)] \quad [\text{K/s}] \quad (6)$$

The advantage of stratified temperature model is that the behaviour of the hot water discharge from the outlet and the measurements of temperature in the different layers of the tank during charging and discharging closely reflects the actual scenario of practical use. Unlike an average model of the hot water storage unit, where the uniform temperature (T) inside the storage unit and energy flow through the system is considered, stratified model considers the practical issues of measurement of different parameters such as temperature, demand and flow. This property enhance the correctness of the demand response capability of the heating system and introduce the heating infrastructure as a flexible active load in the low voltage grid network. Comparison of the storage tank performance between the uniform temperature model and the two layer stratified model is shown in Figure 3. Parameters used are, volume of the tank (V) = 1m^3 , ratio of height to diameter of tank is 2.5, $U = 2.5$ [$\text{W/m}^2\text{K}$], density of water = 1000kg/m^3 , and specific heat capacity of water = 4180 [J/kgK], ambient temperature = 15°C , Temperature of incoming cold water = 30°C .

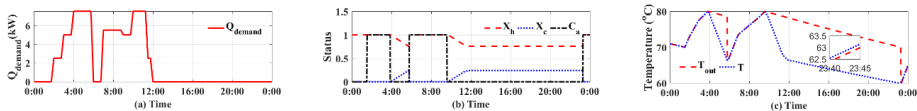


Figure 3: Simulation results for stratified layer and non-stratified layer model of hot water storage tank
 (a) Thermal Demand; (b) ON/OFF status of heater (C_a), level of hot (X_h) and cold (X_c) water in the tank
 (c) Comparison of temperature of outlet water for stratified layer (T_{out}) and uniform temperature models (T)

Figure 3(a) shows the hot water thermal demand with a peak of 7.5kW. The pattern is generated to verify the model with different aspects. Figure 3(b) shows the status of the heater (C_a), to see if the heater is turned ON or OFF. A simple hysteresis control is used for the boiler control based on minimum (70°C) and maximum temperature (80°C) of hot water inside the tank or level of cold water greater than 25% of tank height in the stratified storage model. A graph of X_h and X_c are also plotted to visualize the level of hot and cold water level in the tank respectively. In Figure 3(b), at 01:30Hrs and 23:00Hrs, the boiler is turned ON as the temperature of hot water inside the tank falls below 70°C (Figure 3(c)). It is clearly noticed at 23:00, where the temperature of hot water in the stratified model is around 70°C, whereas it in the average model is around 60°C, which is 10°C lower. Thus, using the stratified storage model, reflects the more flexibility in demand response which can be obtained ensuring more user level comfort. This makes the stratified model superior to the average model of the thermal storage tank for making the right decisions for demand response and flexibility. At 5:45hrs, the heater is ON due to accumulation of cold water in the tank, which is greater than 25%. Figure 3(c) shows the temperature of hot water for the stratified (T_{out}) and non-stratified layer (T). It is seen that (T) is slightly more than (T_{out}) as the loss in the stratified storage model is calculated to be 1% greater than in the uniform model. Decrease in temperature of hot water after 12:00hrs, when there is no demand, is due to losses from the surface of the storage tank.

4. CONTROL OF HEATING ELEMENT (EB or HP)

Two different approaches are taken into consideration to unleash the flexibility from the EB or HP to support grid voltage when integrated in the LV residential network.

- Hysteresis control of the heating unit based on temperature of hot water and accumulation of cold water in the storage tank.
- Hysteresis control of the heating unit primarily based on grid voltage and secondarily based on hysteresis control of temperature of hot water and accumulation of cold water in the storage

The control variables of the heating unit for the EB and HP are presented in Table I. The difference in maximum allowable temperature (T_{max}) for the EB and HP is due to manufacturer's limit of allowable maximum temperature for its operation. The lower bound of minimum temperature (T_{min}) and the allowable limit for collection of cold water inside the tank (X_{cold}) during presence of stratified layers is to maintain minimum temperature of hot water inside the tank to be above 65°C for the EB and 55°C for the HP. The allowable voltage limit (V_{min}) is set to 0.92pu in order to assure the LV network voltages to remain within the limit of $\pm 10\%$. To avoid hunting effect due to voltage control, the recovery voltage of hysteresis band ($V_{recovery}$) is set to 0.98pu. The heating element is turned off ($C_a=0$) when the grid voltage is less than V_{min} or the temperature of hot water in the storage tank is greater than T_{max} . $C_a=1$ when the storage temperature is less than T_{min} or accumulation of cold water in the tank is more than X_{cold} .

Table I: control variables of heating unit

	T_{max} (°C)	T_{min} (°C)	V_{min} (pu)	$V_{recovery}$ (pu)	X_{cold} (%)
EB	80	70	0.92	0.98	25%
HP	70	55	0.92	0.98	25%

5. LOW VOLTAGE RESIDENTIAL ELECTRICAL GRID NETWORK

In order to access the feeder capabilities in the electric network grid integrated with heating units (EB or HP), a 10/0.4kV LV transformer substation with 6 feeders and 164 individual households located at Northern Jutland in Denmark is considered and shown in Figure 4. The grid network has been discussed in [22]. Each house is provided with a heating unit. Steady state power system analysis are performed using the DigSILENT Power System simulation tool to investigate the technical challenges when integrating heating elements in the LV electrical grid. Voltage drop is considered as the major constraint for stable operation of the electrical grid along with other technical challenges such as, transformer capacity and line loading limits. Transformers are designed to withstand approximately 30 years of lifetime with 3-4% annual growth of consumption [22]. This analysis gives a good opportunity to utilize the grid capacity and provide advanced information regarding any upgradation

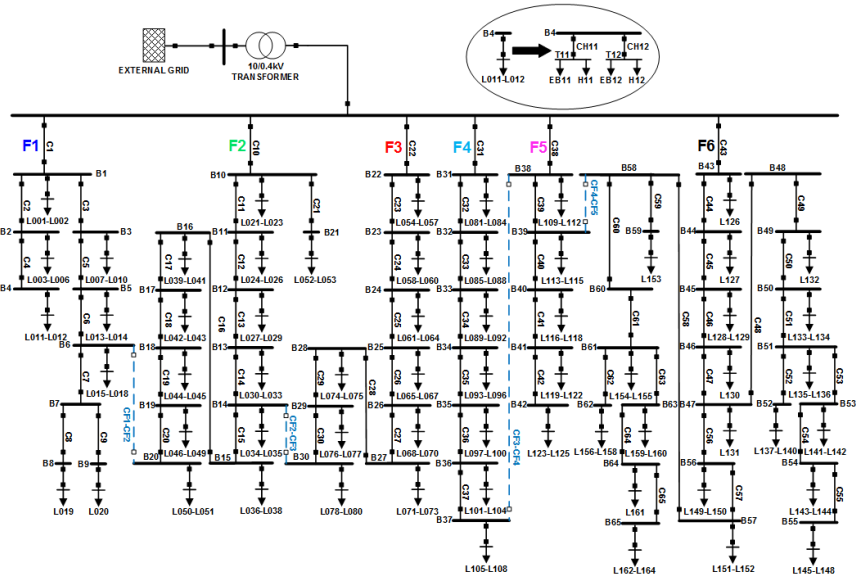


Figure 4: LV distribution network of residential area in Denmark

6. RESIDENTIAL AND THERMAL LOAD PROFILE

A. Residential Load profile

Figure 5 (a) shows the daily load consumption of 164 houses which ranges from 1.15kWh/day to 42.78kWh/day with an average of 10.97kWh/day. Parameters in different feeders (F1-F6 as shown in Figure 4) are coloured uniquely throughout the paper for better perception from analysis of the results. Load consumption data were measured at the transformer side with a resolution of 15 minutes. The load profiles for individual houses are determined using this data and annual electricity consumption. The total electricity consumption of individual houses for 24 hours during a typical winter day is distributed as its percentage in 15 minutes interval to generate load profile of houses as shown in Figure 5 (b). This profile when multiplied with daily load consumption of 164 individual houses generates the load profile of 164 houses for 24 hours, which has same profile but different magnitudes. Random noise is further introduced to the individual houses profile in order to introduce unique load patterns with several peaks and to emulate daily activities resulting in transients of significant magnitudes.

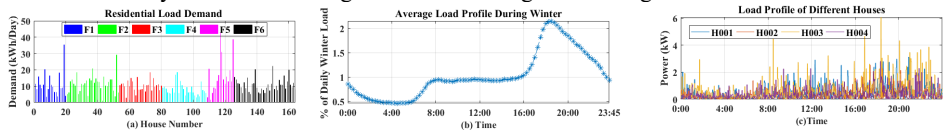


Figure 5: (a) Residential load profile as percentage of daily consumption for 15 minute interval (b) Simulated residential load profile with noise (c) Simulated daily residential load with noise

The noise is generated using a sample and hold function in DigSILENT power factory. Exponential distribution of noise with a rate of 1 and an interval of 3 minutes are chosen to represent average peaks of 2-3kW. These peaks merely represents an electric kettle, an oven or some base load operated 3-15 times per day for 2-5 minutes [23]. Figure 5 (c) shows the load profile of four houses (H001, H002, H003 and H004) with peaks of different magnitudes at various time interval. The magnitude of the peaks ranges between 0.5-16kW for 164 houses. Houses with higher demand has higher peaks which can be due to operation of several loads such as microwave, electric cooking stoves, induction heater, and other electric appliances that are turned ON simultaneously for a short period of time. The daily load factor ranges between 6.7-19.5% with an average and standard deviation of 11.4% and 2.4% respectively.

B. Thermal Load profile

The hourly data on consumption of heat energy through hot water for space heating and domestic hot water usage are analysed for six different buildings situated at Northern Jutland, Denmark. The hourly load profile of thermal demand during peak winter is presented in Figure 6(a) as percentage of its 24 hours total consumption. Figure 6(b) shows the maximum thermal consumption of the different houses during a peak winter day. This profile is used in the simulation model to evaluate the grid condition. The houses with higher electricity demand has been linked with higher thermal demand.

The size of the heating unit and storage tank for the EB and HP as presented in Table II is determined based on the thermal consumption requirement of individual houses to ensure continuous supply of hot water for 16hrs of daily activity, when fully charged. Figure 7(a) shows the EB and HP size associated with the individual houses.



Figure 6: (a) Thermal load profile; (b) thermal consumption of 164 houses

Table II: EB and HP Size allocation

Thermal Demand (kWh)	Storage Size (m ³)	EB Rated Power (kW)	HP Heat Capacity (kW)	No of Units
<40	0.5	3	3	122
40-60	0.75	6	6	38
60-90	1	9	9	4

7. SIMULATION STUDIES

In order to analyse and compare the dynamic behaviour of the proposed system in time domain, three case studies are carried out in DigSILENT power factory simulation tool.

- Case I : With only residential load
- Case II: Residential load with only EBs or HPs in each individual houses respectively based on temperature control.
- Case III: Residential load with only EBs or HPs in each individual houses respectively based on voltage and temperature control
- Case IV: Case II with non-stratified storage tank in EB.

Case I is the base case, where study on the grid conditions such as utilisation of transformer based on its percentage loading, maximum line loading and minimum voltages attained during a period of 24hours. In case II, all the houses are first connected with only EBs and then with only HPs to compare the grid dynamics as discussed in case I. During this study the control of the EBs or HPs are based on temperature control and level of cold water in storage tank. Case III is the repetition of case II with both voltage and temperature control of the EBs or HP to overcome problems associated with the grid voltage limit which is observed in case II. Case IV gives better understanding of using the stratified layer storage tank model compared to average model.

It is unrealistic to start simulations with same initial condition, such as level of cold water in the tank (X_c), temperature of hot water in the tank (T_h) and status of heating unit (C_a) ON or OFF for all the houses. To determine the initial condition of the EBs and HPs with storage, Case II was first simulated with $X_c = 0$, $C_a = 0$, and $T_h = T_{max}$ with only temperature control for a simulation period of 72hours and its final values were used as initial condition for case II and III for further studies of grid dynamics. Figure 7(b) and Figure 7(c) shows the initial condition for operation of the EB and HP respectively. It was noted that $C_a = 1$ if initial condition for $X_c = 0$. This information from the stratified layer tank

model gives better understanding of the status of the storage tank in terms of its capacity to provide thermal demand.

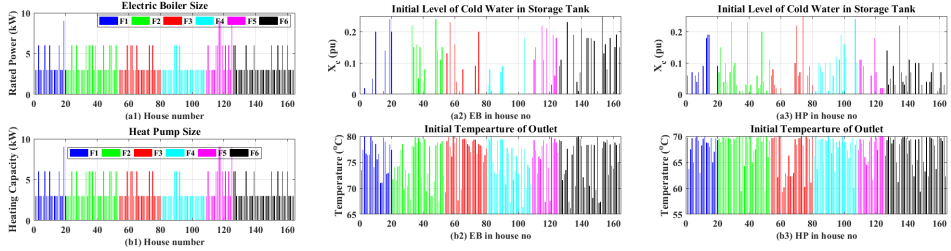


Figure 7 : (a1),(b1): EB and HP size associated with different houses; (a2),(b2): Initial condition of cold water level in storage tank for EB and HP, (a3),(b3): Initial condition of temperature of outlet for EB and HP

8. RESULT AND DISCUSSION

Figure 8 shows the results from case I and case II. Figure 9 shows the results of case III. The case studies results are summarised in Table III with minimum and maximum value of various parameters of grid.

Table III: summary of case studies results

	Case I	Case II (temp. control)	Case III (voltage control)	Case IV		
	Res. load	EBs	HPs	EBs		
Transformer Loading (%)	4.5-28	27-75	9.6-45	26-72		
Minimum Bus Voltages (pu)	0.95-0.99	0.88-0.98	0.91-0.98	0.92-0.98		
Maximum Line loading (%)	1.6-38	3.6-96	2-61	2.7-69		
Daily load factor (%) of 164 houses						
Range (min-max)(%)	6.8-19.5	18.2-44.5	17.6-45.3	10.5-42.6	7.6-45.3	15.3-43.6
Mean	11.43%	30.49%	33.42%	28.77%	30.16%	30%
Std.	2.42%	5.38%	5.53%	6.55%	8.71%	5.57%

Figure 8 and Table III shows that integration of EBs, with temperature control, in every house increases the transformer loading heavily from 28% to 75% with maximum line loading up to 96% which is quite critical for any fluctuation in load as well as growth of sizeable loads.

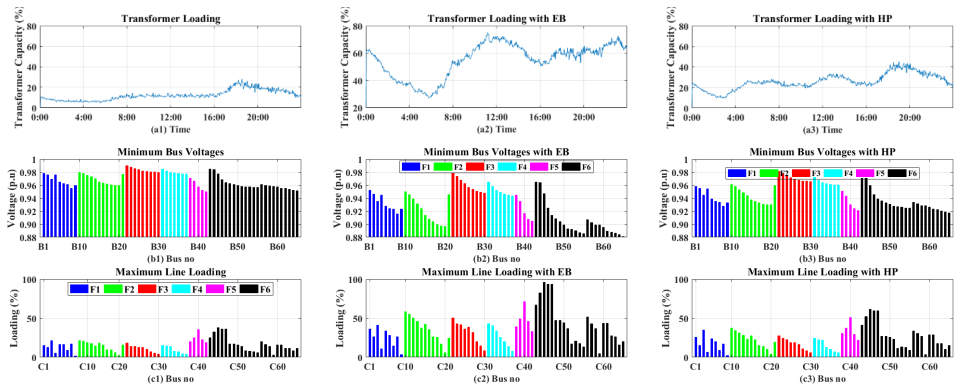


Figure 8: Results of case I and II; (a1), (a2), (a3): transformer loading for residential load, with EBs connected and with HPs connected respectively; (b1), (b2), (b3): Minimum bus voltages at different busbars with residential load, with EBs connected and with HPs connected respectively; (c1), (c2), (c3): Maximum line loadings in cable with residential load, with EBs connected and with HPs connected respectively

Bus voltages in end of feeder F2 and F3 drops below 0.90pu violating the grid regulation of $\pm 10\%$. There is improvement in daily load factor with maximum of 44.5%. When the EBs are replaced with HPs which are able to provide same thermal demand, the grid condition improves drastically. Transformer loading and maximum line loading decreases to 45% and 61% respectively compared to the case with EBs and bus voltages remains within the limit of $\pm 10\%$. This is because of the COP factor of the HP as seen from equation (2). Hence, compared with the EB, the HP uses lesser electricity to generate same amount of thermal energy. The daily load factor is further improved with a maximum value of 45.3% indicating effective utilisation of the HP for peak shaping.

EBs with voltage control improves the grid dynamics to be within the allowable limit (Figure 9 and Table III). However, some of the EBs are not able to operate and fulfil their thermal demand as seen from Figure 9(a1). Some of the EBs at the far end of feeder F2 and F6 are completely filled with cold water due to poor voltage Figure 9(b2). Under the similar condition, when the EBs are replaced with HPs, grid voltages are within the set limit (Figure 9(b3)), and the line loading (Figure 9(c3)) is also significantly reduced. Unlike with the EBs, the HPs are able to supply thermal demand without problems with user comfort as seen from Figure 9(b2) where the storage tank is only filled up to 50% of its capacity with cold water. There is slight decrement in the daily load factor compared to case II for both EBs and HPs as some of the EB and HP units are shut down during the peak hour due to significant voltage drop up to 0.92pu and waits to turn ON until the grid voltage is recovered to 0.98pu. This clearly indicates that, control and flexibility from EB, HP and its storage can be utilised for demand response control to support grid conditions and improving hosting capacity of RE generation. With the use of HP, Figure 9(a3) shows that transformer loading during peak is only up to 45% of its total capacity, there is further possibilities in future for taking account of EV's in the grid

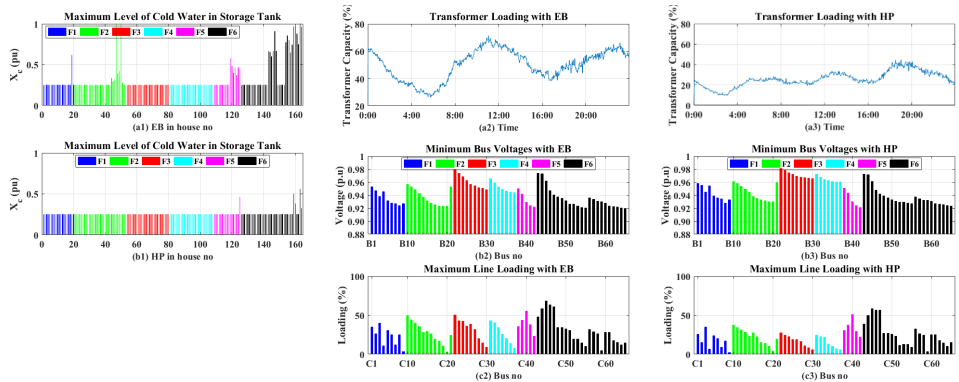


Figure 9: Results case III; (a1),(b1): maximum level of cold water attained in storage tank associated with EBs and HPs respectively; (a2), (a3): , transformer loading, with EBs and with HPs respectively (c2), (c3): Minimum bus voltages at different busbars, with EBs and with HPs respectively; (d2), (d3): Maximum line loadings in cable, with EBs and with HPs respectively

For case IV, where case II is repeated using EBs and non stratified storage tank, it can be seen that there are deeper voltage drops (ranging from 0.87-0.97pu as seen from Figure 10) compared to results presented in Figure 8(b2) where the EB is simulated with the stratified layer storage tank. This is because of the gradual fall in hot water temperature in the average model tank as compared to the stratified model (Figure 3(c)). This shows that use of the better model of EB in the grid analysis, is able to accommodate a higher grid integration of thermal units in reality . Using the stratified model provides more accurate information on the amount of hot water inside the tank and its

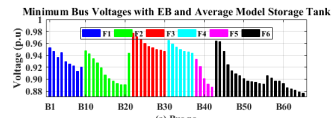


Figure 10: Minimum bus voltages with EB and average model of storage tank

Using the stratified model provides more accurate information on the amount of hot water inside the tank and its

temperature that provides local information for future smart control of EB and HP making it more flexible, which is not possible with the average model.

9. CONCLUSION

The concept of using EBs and HPs as flexible thermal loads in Denmark's low voltage distribution network with its significance on storage of electrical energy is presented in brief. Advantages of using a stratified model of the thermal storage operated by EB or HP in terms of flexibility in operation, measurement and demand response to satisfy end user needs is discussed in short. A brief overview on EB and HP based storage models have been presented. Study on the consumption pattern of electrical and thermal demand are used in a simulation model with different case studies for analysis on grid limitation (based on grid congestion and voltage drop). A strategy based on temperature and voltage control associated with flexible control of the thermal unit are discussed to mitigate the problems with low voltage in week feeders and satisfying the end user need simultaneously. Application of the stratified model compared to the average model improves information about the voltage quality and overcomes the issue of practical measurements of storage tank parameters such as temperature and amount of hot water in the tank for local control of EB.

BIBLIOGRAPHY

- [1] H. Lund, S. Werner, R. Wiltshire, S. Svendsen, J. Eric, F. Hvelplund and B. Vad, "4th Generation District Heating (4GDH) Integrating smart thermal grids into future sustainable energy systems," *Energy*, Vols. 681-11, 2014.
- [2] Danish Ministry of Climate, Energy and Building,, "Smart Grid Strategy-The intelligent energy system of the future," Technical Report, 2013.
- [3] D. Connolly, H. Lund, B. Mathiesen, S. Werner, B. Möller, U. Persson, T. Boermans, D. Trier, P. Østergaard and S. Nielsen, "Heat Roadmap Europe: Combining district heating with heat savings to decarbonise the EU energy system," *Energy Policy*, vol. 65, no. 20, pp. 475-489, 2014.
- [4] "International Energy Agency," [Online]. Available: <https://www.iea.org/statistics/statisticssearch/report/?country=SWEDEN&product=electricityandheat&year=2014>. [Accessed 14 06 2017].
- [5] "COWI," 07 04 2017. [Online]. Available: http://www.cowi.dk/menu/project/industriogenergi/energi/energiforsog_pa_livo_i_gang_med_nyt_fjernvarmenet. [Accessed 14 06 2017].
- [6] P. Maegaard, "Balancing fluctuating power sources," in *2010 World Non-Grid-Connected Wind Power and Energy Conference*, Nanjing, 2010, 2010.
- [7] Energinet.dk, 15 April 2017. [Online]. Available: <http://energinet.dk/EN/EI/Nyheder/Sider/Dansk-vindstroem-slaar-igen-rekord-42-procent.aspx>.
- [8] Danish Energy Agency, "Regulation and planning of district heating in Denmark," Technical Report, 2015.
- [9] Z. Li, W. Wu, J. Wang, B. Zhang and T. Zheng, "Transmission-Constrained Unit Commitment Considering Combined Electricity and District Heating Networks," *IEEE Trans. Sustain. Energy*, vol. 7, no. 2, p. 480-492, 2016.
- [10] M. Blarke, "smartvarme.dk," [Online]. Available: http://www.smartvarme.dk/index.php?option=com_content&view=article&id=1174&Itemid=68. [Accessed 14 06 2017].
- [11] M. Blarke, "smartvarme.dk," [Online]. Available: http://www.smartvarme.dk/index.php?option=com_content&view=article&id=3046&Itemid=80. [Accessed 14 06 2017].

- [12] B. Neupane, T. B. Pedersen and B. Thiesson, "Towards Flexibility Detection in Device-Level Energy Consumption," in *Data Analytics for Renewable Energy Integration Second ECML PKDD Workshop, DARE*, Nancy, France, S, 2014.
- [13] B. P. Bhattarai, I. D. D. C. Mendaza, B. Bak-Jensen and J. R. Pillai, "Local Adaptive Control of Solar Photovoltaics and Electric Water Heaters for Real-time Grid Support,," in *In Proceedings of the Cigré Session 2016, [C6-201] CIGRE..*
- [14] I. D. D. C. Mendaza, I. G. Szczesny, J. R. Pillai and B. Bak-Jensen, "Flexible demand control to enhance the dynamic operation of low voltage networks," *IEEE Trans. Smart Grid.*, vol. 6, no. 2, p. 705–715, 2015.
- [15] R. Sinha, B. Bak-Jensen, J. R. Pillai, C. Bojesen and B. Moller-Jensen, "Modelling of hot water storage tank for electric grid integration and demand response control," in *Accepted, UPEC 2017.*, Greece, 2017.
- [16] I. D. D. Cerio, *An Interactive Energy System with Grid , Heating and Transportation Systems An Interactive Energy System with Grid , Heating and Transportation Systems*, 2014.
- [17] Akmal, B. Fox, D. Morrow and T. Littler, "Impact of high penetration of heat pumps on low voltage distribution networks," in *2011 IEEE Trondheim PowerTech*, 2011.
- [18] P. Gonzalez-Altozano, M. Gasque, F. Ibez and R. P. Gutierrez-Colomer, "New methodology for the characterisation of thermal performance in a hot water storage tank during charging," *Applied Thermal Engineering*, vol. 84, p. 196 – 205, 2015.
- [19] Y. Zurigat, A. Ghajar and P. Moretti, "Stratified thermal storage tank inlet mixing characterization," *Applied Energy*, vol. 30, no. 2, p. 99 –111, 1988.
- [20] F. Opper, A. Ghajar and P. Moretti, "Computer simulation of stratified heat storage," *Applied Energy*6, vol. 23, no. 3, p. 205 – 224, 1986.
- [21] Y. Han, R. Wang and Y. Dai, "Thermal stratification within the water tank," *Renewable and Sustainable Energy Reviews*, vol. 13, no. 5, pp. 1014 – 1026., 2009.
- [22] J. R. Pillai and B. Bak-Jensen, "Electric Vehicle Based Battery Storages for Future Power System Regulation Services.,," in *5th Nordic Wind Power Conference.*, 2009.
- [23] M. Newborough and P. Augood, "Demand-side management oppor-tunities for the uk domestic sector," *IEE Proceedings - Generation, Transmission and Distribution*, vol. 146, no. 3, p. 283–293, May 1999..

Paper B.

Conference C3

Impact Assessment of Electric Boilers in Low Voltage Distribution Network

R. Sinha, B. B. Jensen and J. Radhakrishnan Pillai

The paper has been published in the
2018 IEEE Power & Energy Society General Meeting (PESGM), Portland, OR,
2018, pp. 1–5.

© 2018 IEEE

The layout has been revised.

Impact Assessment of Electric Boilers in Low Voltage Distribution Network

Rakesh Sinha, Birgitte Bak Jensen, Jayakrishnan Radhakrishnan Pillai
Dept. of Energy Technology, Aalborg University, Denmark
Email: ras@et.aau.dk, bbj@et.aau.dk, jrp@et.aau.dk

Abstract—Flexibility from the electricity supply, with high share of intermittent energy sources such as wind and solar, has been offered by combined heat and power (CHP) generation in Denmark for decades. There could be periods where the fuel prices are higher than the electricity prices (even -ve), during high wind production and is idle for electric boilers (EBs) operation. In the future, using EBs, excess electricity from wind turbines can be effectively utilized for heat production, and still meet the thermal demand by decreasing CHP production. Thus, there is need for demand side flexibility that is expected to increase through power-to-heat technologies using electric boilers.

This paper aims to assess the potential of EBs, modelled with simple stratified layers in the storage system, and as smaller units of distributed flexible loads in their individual houses in Denmark. The models of EB in LV-residential grids were simulated to assess the use of EBs to analyze their capacity as well as flexibility as active loads, under various electricity and thermal load profiles of the individual houses during winter. Subjected to high heat and electricity demand in weak grids, flexibility of EBs units with local control incorporated based on grid voltages, restricts the operation of EBs but ensures operation of the distribution system within limits still trying to keep the thermal comfort in the houses.

Index Terms- Electric Boiler, Flexible load, LV distribution network, Hot water storage, Stratification in tank, Voltage Control of EBs.

I. INTRODUCTION

Denmark's desire to attain 100% renewable production in electricity, heating and transportation sector has led the quests for the researchers to investigate a future dynamic flexible smart energy system. A flexible electricity system is required to deal with the variations in renewable generation to balance between supply and demand. One of the possible solutions is use of energy storage systems. In [1], it is estimated that, the reserve requirement increases with 1.5% to 4% for every 10% increment in energy penetration level of wind. However, direct electrical storage of massive scale in an economic way remains a challenge. The other option would be use of a demand-side participation for integration of renewable energy systems and flexible consumer loads. Examples of flexible consumer loads could be heating system [2], plugged in electric vehicles (PEVs) [3], building energy sources such as washing machine, water heaters, refrigeration systems and room heating system [4] [5].

Space heating and domestic hot water are supplied to 63% of the private Danish houses through district heating (DH) until end of 2015 [6]. A wide range of technologies such as combined heat and power (CHP), solar heating, waste to

energy, gas boilers, biomass boilers and heat pumps are used for heating supply in Denmark. With the incentive to phase out fossil fuel based boilers by 2030, 100% of heating demands needs to be contributed by renewable energy. Thus, there is a possibility to integrate the thermal and electric networks together to support grid ancillary services by flexible thermal load. EBs have fast reaction time, lower investment cost and does not depend on the low temperature heat sources compared to electrically driven heat pumps [6].

This paper analyzes the possibilities of coupling EBs in one of the Low Voltage (LV) residential distribution grid in Denmark as test case. Section II briefly discusses about the modelling approach of EB with stratified layer and its significance in demand response management and the appropriate assumptions that are considered. Key features of the Danish distribution grid used are discussed in section III. Generation of residential load and thermal load profile are given in section IV. The case studies considered for the simulations in this article are presented in Section V. Simulations results and discussion of the findings are given in section VI. Finally, the findings of this work is concluded in Section VII.

II. ELECTRIC BOILER(EB) MODEL

A theoretical model of an electric boiler with storage tank is shown in Fig.1. The detailed derivation and validation of the EB model has been presented in [7]. In this model, the hot and cold layer of water in the system is separated by the thermocline of variable height. This height could be measured in practice, allowing system to identify amount of hot water present in the tank. This information together with the knowledge of local voltage at the point of coupling of EB, and temperature of hot water inside the storage tank are processed to control the operation of EBs as flexible consumer load. The flexibility can be obtained in terms of time of operation with respect to energy content inside the

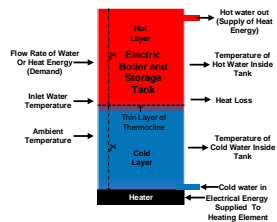


Fig. 1. Electric Boiler Schematic Diagram [7]

storage tank, as well as grid voltage condition based on point of coupling of EBs. Following assumptions are made for the storage tank to simplify the process involved during charging and discharging of hot water inside the tank [7].

- The thermocline inside tank remains only when the boiler is turned OFF, and there are only two thermal layers (upper hot and bottom cold) with uniform temperatures.
- The thermocline is horizontal and independent of radial distance from side wall of the storage tank.
- There are heat losses to the ambient through the surface of the tank wall. No transfer of heat between hot and cold layer.

With these assumptions, the temperature of outlet is calculated as per equation (1) and (2) during presence and absence of thermocline layer respectively.

$$\frac{dT_h}{dt} = \frac{-1}{C_b X_h} [U A_s X_h (T_h - T_a) + U A_t (T_h - T_a)] C_s \quad (1)$$

$$\frac{dT_{avg}}{dt} = \frac{1}{C_b} [\dot{Q}_{heat} \bar{C}_s - \dot{Q}_{demand} - U A (T_{out} - T_a) \bar{C}_s - U A_s X_h (T_{out} - T_a) C_s - U A_t (T_{out} - T_a) C_s - U A_s X_c (T_c - T_a) C_s] \quad (2)$$

Where, A_s and A_t = surface area of side wall and top roof of the tank respectively [m^2] and $A = A_s + A_t$

C_b = thermal capacitance of boiler [J/K]

C_s = status of stratification

\dot{Q}_{demand} = heat demand transfer rate due to flow of water (Thermal Demand) [J/s]

\dot{Q}_{heat} = heat flow rate of heating element [J/s]

T_{avg} = average temperature inside boiler [K]

T_h, T_c, T_{out} , and T_a = temperature of the hot water, cold water, outlet and ambient respectively [K]

U = overall heat transfer coefficient [$W/m^2.K$]

X_h and X_c = normalised height of hot and cold water respectively in the tank

When there is condition for thermocline (i.e. boiler heater is turned OFF) $C_s = 1$, there exist a layer of upper hot and lower cold water in the tank. The temperature of upper hot layer ($T_h = T_{out}$) is calculated as per equation (1). When the boiler heater is turned ON, the thermocline layer gets disturbed by water turbulence, $C_s = 0$, and mixing of water takes place which gives an average temperature of water inside boiler (T_{avg}) as per equation (2). During this period $T_{out} = T_{avg} = T_h$

The electric boiler is assumed to be a constant impedance load [7] [8]. Then,

$$\dot{Q}_{heat} = \frac{\eta}{100} \left(\frac{V_{poc}}{V_{r,b}} \right)^2 P_{r,b} \quad [W] \quad (3)$$

Where, η = efficiency of boiler [%], $P_{r,b}$ = rated power of boiler [W], $V_{r,b}$ = rated voltage of boiler [V] and V_{poc} = voltage at point of coupling of boiler into the grid [V]

Equation(3) shows the dependency of the EB and the grid terminal voltage at the point of coupling. This property has also been discussed in [7] [8]. This relation is useful to investigate interaction between thermal load (based on EB) and

electrical grid, as well as for demand response management and control of EBs.

A. Control of EB

The control signal of the EB is denoted by ' C_a '. Two types of Hysteresis control of the EB are presented. Type I control: It is a hysteresis control of temperature inside tank. Type II control: It is voltage control with override capability. Type I control: It is determined by equation (4). When $C_a = 1$, the heater is turned ON, else turned OFF.

$$C_a = 1 \quad \text{if } T_{out} < T_{min} \quad \text{or} \quad X_c > X_{cold} \\ = 0 \quad \text{if } T_{out} > T_{max} \quad (4)$$

Where, $T_{max} = 80^\circ C$ and $T_{min} = 65^\circ C$ are maximum and minimum allowable temperature of hot water inside tank. These values are based on the analysis of district heating data. $X_{cold} = 0.25 pu$ is the maximum allowable level of cold water inside the storage tank. This value is chosen to maintain temperature of outlet water (T_{out}) above $65^\circ C$.

Type II control: In order to avoid grid voltage to dip below 0.9pu (especially when the grid is weak), a local voltage control scheme is introduced as a primary control and equation (4) as secondary control. With this control, when terminal voltage of EB (V_{poc}) is less than 0.92pu, EB gets shut down until the voltage is recovered to 0.98pu. These values are chosen to keep terminal voltages within range of $1p.u \pm 10\%$ and to avoid hunting effect as well, that can be introduced with smaller range of voltage control. In order to avoid that the storage tank is being completely filled with cold water due to idling caused by voltage control in the Type II control, it is further facilitated with an overriding control. The EB is activated when 60% of the storage tank is filled with cold water and remains on until the temperature of hot water has reached the maximum allowable temperature of $80^\circ C$. This makes sure that the user comfort is not compromised due to control limits of the EB.

III. GRID MODEL

A LV-substation with transformer 10/0.4kV, situated in Northern Jutland Denmark, is considered for the case study. The single line diagram of the LV distribution grid is shown in Fig. 2. This LV grid network supplies today residential customer loads without electrical heating. Grid specifications has been summarized in Table I along with different color coding to represent elements of respective feeders in the graphs. The detailed parameters of cable and lines in the network can be found in [3]. The electric boilers (EBs) are integrated in individual houses in this network to identify the grid hosting capacity.

IV. LOAD PROFILE

A. Generation of Residential Load Profile

Measured data of annual residential load consumptions are divided by 365 to calculate average daily load consumptions. Load profile of houses are needed to be generated in order to simulate the grid conditions (Transformer loading, bus

voltages and line loading) for 24-hours. The total electricity consumption in a typical winter day is distributed as percentage of total daily consumption in 15 minutes interval as shown in Fig. 3. The load profile as shown in Fig. 3 is generated from analysis of data measured at the transformer with time resolution of 15 minutes from month of Nov, Dec, Jan and Feb, as the electricity consumptions are higher with almost same peaks.

Fig. 4a shows the demand per day for 164 houses. It is assumed that the load profile of 164 houses is similar as shown in Fig. 3 with different magnitudes based on their daily consumptions (Fig. 4a). The power factor is considered to be 0.97(inductive) [3]. Consumption per day of an individual house (Fig. 4a) is multiplied by the load profile (Fig. 3) to generate the load profile of the individual house in 15 minutes of time interval throughout the day. Noise is further multiplied to make unique patterns of each residential load with peaks, in order to emulate day to day activities of individual resulting transient peaks of significant magnitude.

The noise is generated using a sample and hold noise generator function in DigSILENT Power factory. There are four distributions available in this function: Uniform, Gaussian, Exponential and Weibull. Uniform and Gaussian distribution function generates negative values as well, which is not applicable to this research as flow of energy from load to grid is not considered. The Weibull distribution has probability to generate unexpected very high peaks. Thus, the exponential distribution is taken into consideration with rate of 1, and frequency of 0.00556Hz (3min interval). The frequency of 3 minutes interval is chosen to represent average peaks of 2-3kW due to electric kettles which are used most frequently (3-15

TABLE I
GRID SPECIFICATIONS

Transformer specification	630kVA, 10/0.4 kV Dyn5, Uk = 4.66% Copper loss = 6.5kW, Iron loss = 1.5kW
Number of feeders	6
number of households	164
Feeder representation color	F1 F2 F3 F4 F5 F6

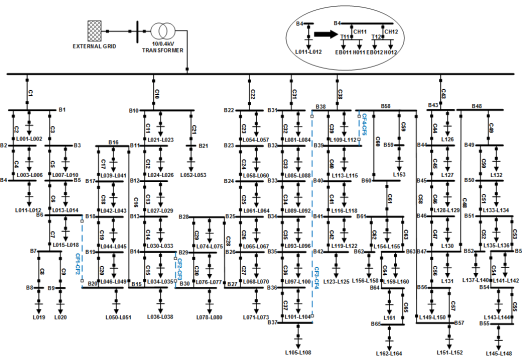


Fig. 2. LV grid network

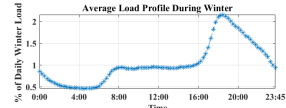


Fig. 3. Load profile as percentage of total daily consumption during typical winter day

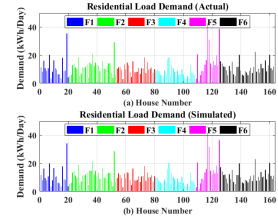


Fig. 4. (a) Actual demand of residence (b) Simulated demand of residence with noise

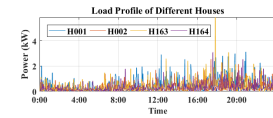


Fig. 5. Simulated load profile of residences

times per day) with duration of 2-5 minutes [9]. Fig. 5 shows the unique load profile of residence H001, H003, H163 and H164. Following observations were made for the simulated load profiles of 164 residential loads.

- The difference between the simulated demand with noise (Fig. 4b) and actual demand (Fig. 4a) for 164 houses, ranges between $\pm 15\%$ with an average value of 0.69% and standard deviation of 0.05%. This difference in values are due to noises whose mean value is not zero because of the exponential distribution.
- Peaks usually lies between 4-7kW in households without electrical space heating [9]. Simulated result shows that the peaks ranges between 0.5-16kW with average of 4.18kW and standard deviation of 2.47kW. Thus, average peak demand suitably represents electric kettle (2-3kW) with some base load. Other higher peaks can be due to microwave and other appliances turned ON simultaneously for short period of time. The higher peaks up to 16kW are only for the houses with a high annual consumption.
- The daily load factor lies in the range of 6.7-19.5% with average of 11.4% and standard deviation of 2.4%.

B. Thermal Load Demand Profile

Fig. 6a shows the load profile of thermal demand during a winter day as percentage of daily consumption. This profile curve has been generated by analysing the hourly data from the meter readings of residential area in Aalborg, Denmark. Thermal demand of a day for different EBs as shown in Fig. 6b and the profile shown in Fig. 6a are multiplied to generate the daily heating load profiles for all boilers. Thus, all EB has similar demand profile with different magnitudes. Due to

TABLE II
EB SIZE ALLOCATION

Thermal Demand (kWh)	Storage Size (m^3)	Heater Power (kW)	No of EBs
< 40	0.5	3	122
40-60	0.75	6	38
60-90	1	9	4

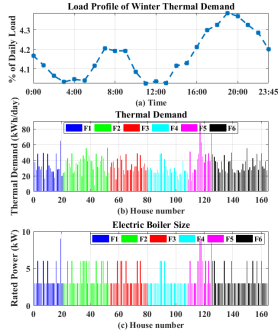


Fig. 6. (a) Load profile of thermal heat demand, (b) Heat demand of different houses, (c) Electric boiler power rating for different houses boilers

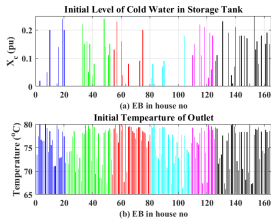


Fig. 7. (a) Initial level of cold water in tank (b) Initial temperature of hot water in tank

storage possibilities in the thermal system, transient behaviour of demand is not taken into consideration. Thermal demands are distributed based on electricity consumption associated with the house they are linked with. Houses with higher electricity demand has higher thermal demand and vice versa. In order to have capacity to provide hot water for at least 16 hours, when the storage tank is full of hot water ($80^{\circ}C$), the tank and the boiler size are determined as shown in Table II. The size of the storage and its associated heater as shown in Table II are commercially available. Fig. 6(c) shows the distribution of EBs size in different houses.

V. SIMULATION

Simulation is carried in DigSILENT Powerfactory in order to analyse the dynamic behaviour of the proposed system in the time domain. Three case studies are carried out.

- Case I: residential load only.
- Case II: residential load with EB and Type I Control.
- Case III: residential load with EB and Type II control.

For case I, the transformer loading, line loading and bus voltages are analysed. For case study II and III, an EB is

introduced in every houses to meet the thermal demand. In case II, the EB is controlled based on Type I control and case III, with Type II control. EBs in individual houses, with parameter $T_h = 80^{\circ}C$, $X_c = 0$ and $C_a = 0$, were first simulated for simulation period of 72Hrs and its final values were recorded. These values, as shown in Fig. 7(a) and (b), were then used as initial condition for simulation of case II and case III. $C_a = 1$ if $X_c = 0$. This was done to avoid same initial conditions for EBs in every individual houses.

VI. RESULT AND DISCUSSION

Simulation results for all three cases are shown in Fig. 8. For case study I, only the residential load without electrical heating is simulated for 24hours, Fig. 8 (a1),(b1) shows the active power through transformer and transformer loading respectively. It is clearly seen that, the transformer is loaded between 5-30% of its capacity. Fig. 8(c1),(d1) shows the minimum bus voltages and maximum line loading of cables respectively in the system for case I. It is clearly seen that feeder 5 (F5) and feeder 6 (F6) are weak feeders where terminal voltages of load farther in the feeder has voltage between 0.95pu to 0.94pu. Maximum loading of all the cables shows that feeder 6 is below 50% and the rest of the feeders are below 30%..

When EBs are introduced in the individual houses with a type I control, the transformer is loaded between 25-75% of its capacity as seen from Fig. 8(b2). Fig. 8(a2) shows the % of EB in operation at different feeders for the period considered in the study. It shows that most of the EBs are operated between mid-night and mid-day. Fig. 8(c2),(d2) shows the minimum bus voltages and maximum line loading of cables respectively in the system for case II. It shows that in all the feeders, except F3 and F4, the terminal voltages goes below 0.96pu and in F2 and F6, its even below 0.9pu at certain time of day because of the high electrical and thermal demands. Cables in F6 are loaded heavily but is below 100% as it is the longest feeder in the grid with the highest number of houses.

In case III, to maintain voltage of the entire system above 0.9pu, EBs are introduced with Type II control. The results are shown in Fig. 8(a3)(b3) where % of EB in respective feeders and transformer loading are shown respectively. The transformer is loaded between 25-70%, which is lower than in case II. The minimum bus voltage attained is 0.91pu shown in Fig. 8(c3). Fig. 8(a3) shows that, the % of EB in operation for case III is lower than that in case II (Fig. 8(a2)) during the period of 8:00-24:00hrs. As a result, some of the storage tanks in feeders F3 and F6 are turned OFF even if the accumulation of cold water(X_c) is more than 25% as shown in Fig. 9(a). With the provision of the overriding control as discussed in section IIA, the EBs are turned ON when $X_c > 0.6$. Due to mixing of stratified layers, the minimum temperature of hot water in storage tank is then $42^{\circ}C$ as shown in Fig. 9(b). Once the EB is turned ON, temperature gradually rises. Thus with this control, grid voltage is above 0.91pu without compromising user level comfort. Table III shows the daily load factor of residential loads. For residential

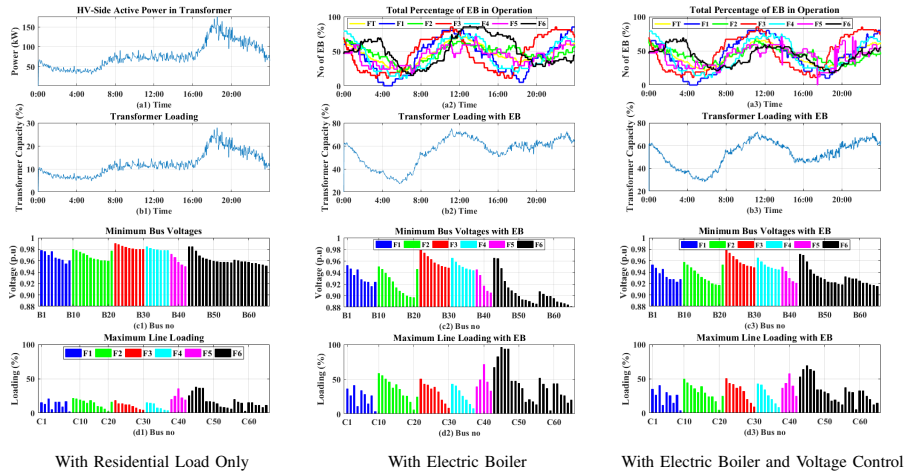


Fig. 8. (a1): HV-side active power in transformer for residential load without electrical heating. (a2),(a3): Percentage of electric boilers in operation for different feeders with Type I and Type II control respectively (b1),(b2),(b3): Transformer loading (b1) with residence load only, (b2) with EB Type I control and (b3) EB with Type II control. (c1),(c2),(c3): Minimum bus voltages (c1) with residence load only, (c2) EB with Type I control and (c3) EB with Type II control. (d1),(d2),(d3): Maximum line loading (d1) with residence load only, (d2) EB with Type I control and (d3) EB with Type II control.

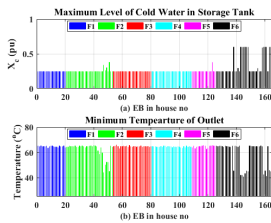


Fig. 9. (a) maximum level of cold water in storage tank throughout the day (b) minimum temperature of hot water in storage tank throughout the day

TABLE III
DAILY LOAD FACTOR

	case I	case II	case III
Range (Min-Max)	6.79-19.53%	18.21-44.50%	17.29-42.64%
Mean	11.43%	30.49%	29.68%
Standard Deviation	2.42%	5.38%	5.56%

loads with electrical heating, the daily load factor increases significantly ranging from 18.21-44.50%. When the EBs are controlled based on grid voltage level as in case III, the daily load factor decreases slightly to 17.29-42.64% due to the fact that some houses are not able to operate their EB. Referring to grid status presented in the result and discussion section, there is a necessity to reinforce the grid in order to handle further growth in electrical load. Other options could be use of heat pumps, because of its high coefficient of performance.

VII. CONCLUSION

Integration of EB in LV residential grid as flexible consumer load has been presented. Use of simple stratified storage tank for EB with two different types of controller based on

temperature of hot water and grid voltage at point of common coupling are discussed. Use of appropriate local control for EBs as distributed consumer load enhances flexibility in LV residential grid under various thermal and electrical load profile.

ACKNOWLEDGMENT

The authors would like to thank DiCyPS project funded by the Danish Innovation fund for funding this research project.

REFERENCES

- [1] H. Holtinen, "Impact of hourly wind power variations on the system operation in the nordic countries," *Wind Energy*, vol. 8, no. 2, pp. 197–218, 2005.
- [2] K. Skytte and O. J. Olsen, "Regulatory barriers for flexible coupling of the nordic power and district heating markets," in *2016 13th International Conference on the European Energy Market (EEM)*, June 2016, pp. 1–5.
- [3] J. R. Pillai, P. Thgersen, J. Mller, and B. Bak-Jensen, "Integration of electric vehicles in low voltage danish distribution grids," in *2012 IEEE Power and Energy Society General Meeting*, July 2012, pp. 1–8.
- [4] M. Tasdighi, H. Ghasemi, and A. Rahimi-Kian, "Residential microgrid scheduling based on smart meters data and temperature dependent thermal load modeling," *IEEE Transactions on Smart Grids*, vol. 5, no. 1, pp. 349–357, Jan 2014.
- [5] M. Tasdighi, P. J. Salamaty, A. Rahimikian, and H. Ghasemi, "Energy management in a smart residential building," in *2012 11th International Conference on Environment and Electrical Engineering*, May 2012, pp. 128–133.
- [6] D. E. Agency, "Regulation and planning of district heating in denmark," techreport, 2015.
- [7] R. Sinha, B. Bak-Jensen, J. R. Pillai, C. Bojesen, and B. Mller-Jensen, "Modelling of hot water storage tank for electric grid integration and demand response control," in *Accepted, UPEC 2017, Greece*, 2017.
- [8] I. D. D. Cerio, *An Interactive Energy System with Grid, Heating and Transportation Systems An Interactive Energy System with Grid, Heating and Transportation Systems*, 2014.
- [9] M. Newborough and P. Augood, "Demand-side management opportunities for the uk domestic sector," *IEE Proceedings - Generation, Transmission and Distribution*, vol. 146, no. 3, pp. 283–293, May 1999.

Paper C.

Journal J1

Autonomous Controller For Flexible Operation Of Heat Pumps In Low Voltage Distribution Network


Rakesh Sinha, Birgitte Bak-Jensen, Jayakrishnan Radhakrishna
Pillai

The paper has been published in the
Energies, 12(8), pp. 1–11, 2018.

The layout has been revised.

Article

Autonomous Controller for Flexible Operation of Heat Pumps in Low-Voltage Distribution Network

Rakesh Sinha , Birgitte Bak-Jensen and Jayakrishnan Radhakrishna Pillai

Department of Energy Technology, Aalborg University, 9220 Aalborg, Denmark; bbj@et.aau.dk (B.B.-J.); jrp@et.aau.dk (J.R.P.)

* Correspondence: ras@et.aau.dk; Tel.: +45-9356-2203

Received: 20 March 2019; Accepted: 15 April 2019; Published: date



Abstract: This paper aims to unleash the potential of a heat pump (HP) and its storage system, as a flexible consumer load, in the low-voltage (LV) distribution network by introducing an autonomous controller. Steady-state analysis using DigSILENT Power Factory, a power system analysis tool, is performed to verify the proposed hypothesis. The proposed controller manages to operate the individual HP and storage within the recommended operating limits of grid voltage, by sharing flexibility within the specific network. It has the capability of sensing local key control parameters for scheduling, re-scheduling, and decision-making on the operation of individual HPs. It also takes the thermal energy comfort of individual consumers into consideration. Measurement of local parameters such as grid voltage, supply temperature and level of cold water in the storage tank defines the priority for operation of HPs based on operating delays for turning it on and off. This enhances the sharing of flexibility for proper coordination, control, and management of HP systems in LV distribution networks with mutual technical benefits. From the results, the application of the proposed controller is found to be effective to manage grid congestions and local voltage regulation, satisfying the thermal energy requirements of the customer.

Keywords: autonomous controller; multi-energy system; flexible load; power-to-heat; heat pumps; LV distribution network

1. Introduction

Hot water is used for space heating and domestic applications. With the concept of power-to-heat (P2H) in smart energy systems to incorporate 100% renewables, heat pumps (HPs) are expected to play an important role for thermal heating and cooling due to their high output-to-input ratio. HPs are also considered to be a key technology supporting the European strategy for thermal systems decarbonization [1]. Furthermore, low-temperature district heating, to reduce transmission loss of thermal energy, requires boosting of hot water for end users [2,3]. The combination of distributed HPs and district heating systems, with high penetration of renewables in power system networks, have a significant potential in low-temperature district heating systems [4]. In [5] the authors investigate the life-cycle cost for use of district heating or distributed HPs and find it depends on the energy system economy. Use of electric boilers (EBs) has been unfavorable due to high electricity prices and taxes in the Swedish system whereas, HPs are providing high flexibility in power-to-heat supply [6] and a high coefficient of performance (COP) when compared to EBs. Individual HPs seem to be the best alternative to district heating to replace individual boilers (based on oil, natural gas or biomass) in rural or suburban areas, where heat densities are lower [7]. This indicates the installation of many HPs in the near future as well as a significant increment in residential electricity demand. Control of HPs plays an immense role in the flexible operation for demand response. HPs can be controlled based on a simple start and stop operation. A wide variety of HPs is available on the market with

on/off regulation supported by a hot water storage tank. Ref. [8] uses on/off control of HP coupled in a single house located in Italy to investigate the dynamics of model based on the seasonal COP. In [9], on/off control method of HP is compared with other common control technique such as Constant hysteresis, Floating hysteresis, and Degree-Minute. Although there are several possibilities to control the HP, the problem here is simplified with just on and off in order to demonstrate the flexibility in the operation of HPs to fulfill thermal demand and support and avoid under-voltage situations in the electrical grid.

This paper is focused on the concept of on/off control, to achieve flexibility from many HPs associated with individual residences (164 houses) in a low-voltage (LV) (0.4 kV) electrical distribution network supplied from a 630 kVA transformer. Individual controllers, linked with the respective HP, functions independently to avoid under-voltage situations in the electrical grid as well as to fulfill the thermal demands simultaneously. The decision-making capability for the controllers is enhanced with delay functions to turn on/off the HPs based on their terminal voltage at the point of coupling as well as temperature and level of hot water in the storage tanks.

Heat storage is essential for the flexible operation of a heating system. The concept of using thermal inertia of a heating grid as energy storage is presented in [10], without addressing the issues related to leakage of thermal fluid and significant heat loss to the surrounding from the transmission pipes. The effective size of the storage tank plays an important role in controlling the grid load by creating enough buffer to supply thermal demand without operation of HPs, during the period of the high electrical load. On the other hand, low-cost electricity during periods of high renewable electricity production from wind and solar can be used for heat generation and storage, increasing the economic efficiency and sustainability of multi-energy systems. Several works of literature have investigated that without proper management of heat generating units in power-to-heat (P2H), problems associated with transformer loadings, line loadings, and voltage drops can be prominent in some of the existing LV distribution networks [11–13]. In [11] hysteresis control of the heating unit based on grid voltage, the temperature of hot water and accumulation of cold water in the storage tank is investigated for flexible operation of thermal units. This technique of control has possibilities of storage tank being fully discharged after the event of low terminal voltage for the long duration operating restriction. In [12], the proposed controller can operate the thermal unit despite low voltage during an event when energy stored in the storage tank is critically low which can stress the grid. Ref. [13] examines the starting current, voltage variation and, active and reactive power impact of single-phase loading of the network suggesting necessity of demand response.

Mixed integer programming based on the daily scheduling of individual heating systems, based on power fluctuation, are derived from their set of optimal schedules using the coordinated algorithm in [14]. This requires frequent and proper communication channel between heating systems. Price-based decentralized load coordination with proper communication is presented in [15]. Ref. [16] studied on flexibility by shifting operation of HPs to optimise operational costs. Ref. [17] examined flexibility in the operating times of HPs against the resulting impact on the end user's comfort. Ref. [18] investigated on the flexibility of distributed HPs for trading on the intra-day market. None of them considered the performance and violation of electric grid parameters. The centralized control algorithm is designed in [19] to exploit flexibility considering end-user thermal comfort which requires proper communication channel. A combination of both centralized and decentralized framework is proposed based on forecasting and power-voltage droop concept respectively in [20], considering fair use of flexibilities from customers. Agent-based control system with complex computation is presented in [21], where it is difficult to predict overall system behavior.

The anticipation of a real-time autonomous controller for coordination in the management of HPs, to overcome these issues, is proposed in this paper by distributing the use of HPs consumption over time. The proposed controller senses local information relatively delay free, enhancing a quick decision-making process compared to a centralized control system [22]. It has the capability of sensing, scheduling, re-scheduling, and decision-making that can act flexibly and autonomously in the specific

environment to meet its design objectives. The main advantage of this proposed control system is that there is no need for extra investment in communication infrastructure for the management of flexible loads. This article focuses on an on/off control strategy (to simplify the problem) to effectively introduce high shares of individual HPs, in low-voltage (LV) residential networks, as a sustainable solution towards P2H systems. The effect on the control strategy based on the selection of different initial conditions and operating power factor of HPs are well illustrated through various case studies.

This paper is organized as follows. A short overview of the working principle of HP and its modeling with respect to power-to-heat (P2H) is presented in Section 2 along with the concept of a model of a simple stratified hot water storage tank. Section 3 presents an overview of the LV residential network and the grid voltage situation with only residential load (without HP connected). The details of the logical concept of the proposed local controller and its significance for the flexible operation of HPs is discussed in Section 4. Simulation environment with various case studies, based on initial conditions, are discussed in Section 5, followed by result and discussion in Section 6. Finally, the outcome of the research is concluded in Section 7.

2. Heat Pump and Storage

A HP basically consists of three major components: evaporator, compressor, and condenser. Liquid refrigerant is exposed to the source, through the HP's evaporator coil, at a low temperature and pressure. As this refrigerant picks up energy from the source, it changes its state from liquid to gas within the evaporator coil. Then the gaseous fluid is passed through the compressor pump where it is pressurized. As a consequence, the temperature of this pressurized refrigerant increases. This heated refrigerant is passed through the condenser (a coil wrapped around the tank, or a pumped heat exchanger to feed a separate water storage tank) to discharge its heat energy. After passing through the condenser, the heated refrigerant cools and condenses back into liquid form. It is then passed through an expansion valve, where its pressure is reduced, and the cycle starts over. Thus, HP does not produce hot water instantaneously when turned on. It takes around 10–15 min to achieve a steady state condition [23]. Figure 1 shows the step response of the HP during turn-on and turn-off. The HP is turned on at time T_1 , but it only starts delivering hot water after time T_2 .

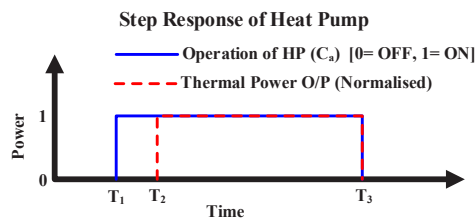


Figure 1. Step response of heat pump during turn-on and turn-off.

HPs can operate down to the voltage level of 0.7 pu or below. Different types of HPs are available in the market. They can be generally divided into two categories: inverter-based and non-inverter-based units. Non-inverter-based directly connected HPs exhibit low harmonic content and high inrush current compared to inverter-based [24]. The power factor of most inverter-based HPs, operating within the voltage range of 0.9–1 pu, is between 1 to 0.95 leading, whereas few HPs operate within 1 to 0.95 lagging [25]. Non-inverter-based HPs draw inrush current nearly 5 times its nominal value, whereas, inverter-driven HP units draw inrush current of the same order of magnitude as per their nominal rating. However, in some inverter drive models of HP, there exist spikes due to the charging of inverter's Direct Current (DC) bus capacitors [25].

The thermal power delivered by the HP is given by Equation (1). Here, P_{HP} is the electrical power rating of the HP (W), \dot{Q}_{Heat} is the heat delivered by HP (W). The step response of HP is modeled as shown in Figure 1 with a time delay of 10 min. The reactive power delivered or consumed by the HP

based on leading or lagging pf respectively is given by Equation (2). The relevant parameters of HP such as flow temperature of hot water $T_{hot} = 70^{\circ}\text{C}$ and $\text{COP} = 3$ during cold winter season (constant value of COP is selected for simplicity) are selected based on the manufacturer's data-sheet.

$$\dot{Q}_{Heat} = \text{COP} \times P_{HP} \quad [W] \quad (1)$$

$$Q_{HP} = \mp P_{HP} \times \tan\theta \quad [VAR] \quad (2)$$

The simplified hot water storage tank, based on a single thermocline layer of varying height as shown in Figure 2, separating the storage tank into two layers (upper hot and bottom cold) is modeled as presented in [11,26] with appropriate assumptions and theoretical validation considering charging and discharging of storage tank. It is assumed that

- The heating element (condenser coil of HP) is attached to the bottom cold layer of the tank.
- There is an exchange of heat between the condenser, at the bottom of the storage tank, and the water inside the storage during operation of the HP.
- The thermocline inside the tank is horizontal and independent of radial distance from the side wall of the storage tank.
- The thermocline remains only when the HP is turned off and there is no exchange of heat between the condenser and the storage tank
- When HP is turned on and there is heat transfer to the storage tank, the thermal stratification is destroyed by water turbulence and there is mixing of hot and cold liquid creating uniform temperature inside the storage tank [27].

The stratified layer provides crucial information on the energy status of the storage tank based on the level of cold water filled inside the tank and temperature of the hot water inside the tank. These parameters are vital for the control logic to flexibly operate HPs as distributed local units and this is discussed in Section 4.

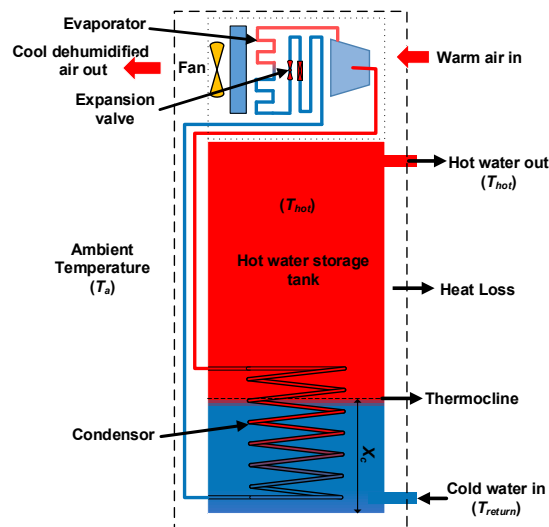


Figure 2. Heat Pump and Storage.

The temperature of hot water (T_{hot}) is calculated as per Equation (3) during the presence of the thermocline layer.

$$\frac{dT_{hot}}{dt} = \frac{-1}{C_b(1 - X_c)} [UA_s(1 - X_c)(T_{hot} - T_a) + UA_t(T_{hot} - T_a)] \quad (3)$$

Here,

A_s and A_t = surface area of side wall and top roof of the storage tank respectively [m^2] and $A = A_s + A_t$

U = overall heat transfer coefficient [$2.5 \text{ W/m}^2 \text{ K}$] [28]

X_c = level of cold water in the storage tank [Normalized with the height of storage tank]

$C_b = C_w m_b$ Thermal capacitance of boiler [J/K]

C_w = specific heat capacity of water [4180 J/kgK]

m_b = mass of water in storage tank [kg]

T_{hot} = temperature of the hot water in the storage tank [K]

T_a = ambient temperature [K]

$T_a = 15 \text{ }^\circ\text{C}$ is considered, and the surface area of storage tank is calculated considering ratio of height to diameter as 2.5.

When the HP is turned on and there is an exchange of heat between the condenser and the storage tank, the thermocline layer gets disturbed by water turbulence and mixing of water inside the storage tank takes place, which gives an average temperature (T_{avg}) of water inside the storage tank as per Equation (4) [11]. During this period $T_{hot} = T_{avg}$.

$$\frac{dT_{hot}}{dt} = \frac{1}{C_b} [\dot{Q}_{heat} - \dot{Q}_{demand} - UA(T_{hot} - T_a)] \quad (4)$$

Here,

\dot{Q}_{demand} = heat demand transfer rate due to flow of water (Thermal Demand) [J/s]

\dot{Q}_{heat} = heat flow rate of heating element [J/s]

3. LV Residential Grid Network

To maintain grid voltage within its operating limit ($\pm 10\%$) in the LV distribution network, when integrated with HPs, good knowledge of voltage profile is necessary. It not only helps to define the control parameters for HP and storage but also provide the environment to evaluate the performance of the proposed controller. A 10/0.4kV LV transformer substation with 6 feeders and 164 individual households located at Northern Jutland in Denmark is considered and is shown in Figure 3. The detailed grid network has been discussed in [29]. It is a real LV residential grid in North Jutland in Denmark, all the relevant electric grid data were supplied by the distribution grid company that owns the network. Thermal and electrical load profile parameters are discussed in detail in [12] and their daily demand are illustrated in Figure 4a,b, respectively. HPs are connected to each individual house. Steady-state power system analysis is performed using the DigSILENT Power Factory simulation tool to investigate the performance of the proposed controller. Table 1 summarizes the LV grid network.

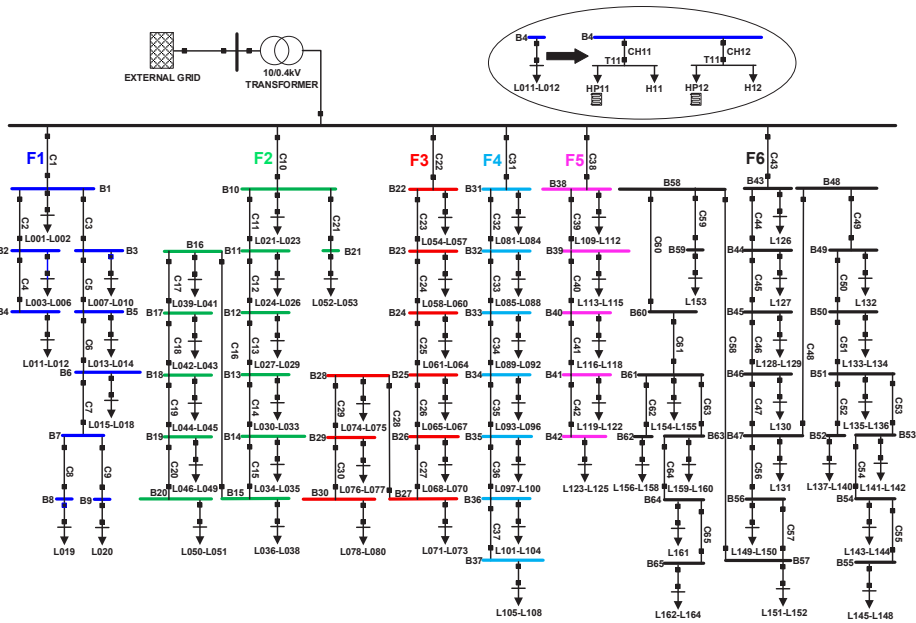


Figure 3. LV Residential Grid Network.

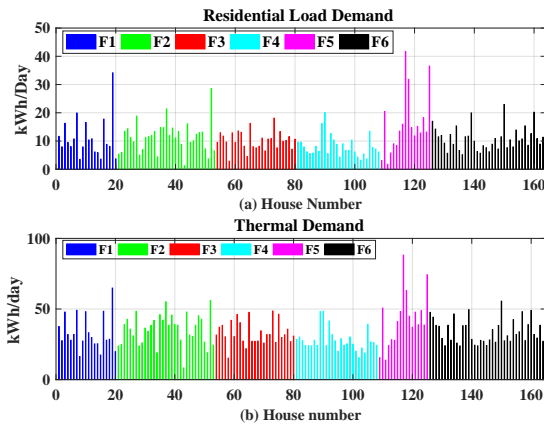


Figure 4. (a) Residential electricity demand (Without HP); (b) Thermal demand for individual houses in their respective feeder.

Table 1. Grid Specifications.

Transformer Specification	630 kVA, 10/0.4 kV Dyn5, Uk = 4.66% Copper Loss = 6.5 kW, Iron Loss =1.5 kW					
Number of feeders	6					
number of households	164					
Feeder representation and color	F1	F2	F3	F4	F5	F6
Total HH Load in respective feeder (kWh/day)	226	376	277	223	278	421
Number of houses in respective feeder	20	33	27	28	17	39

Figure 5a,b shows the minimum terminal voltages of all feeders with only residential loads (i.e., without any HPs connected). It is clearly seen that feeder F3 and F4 is the strongest feeder of all where minimum voltage attained by terminal T19 and T99 is 0.98pu, followed by F2-T47 (Feeder 2, terminal 47). Terminals T19, T125, and T162 attain the minimum voltage of 0.95 pu during peak hour in feeders F1, F5, and F6, respectively. F6 is heavily loaded with 421 kWh/day and 39 houses.

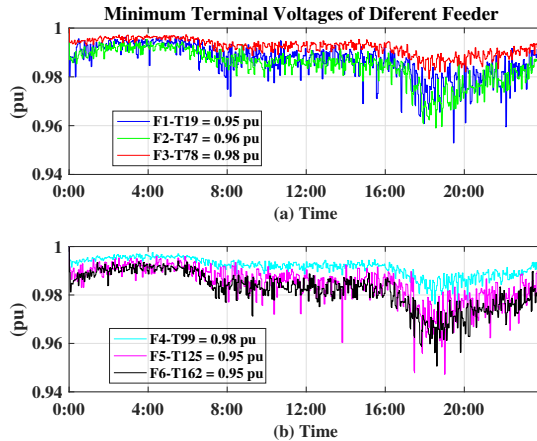


Figure 5. Terminal voltage with the maximum voltage drop of different feeder (a) Terminals in feeder F1, F2, and F3 (b) Terminals in feeder F4, F5, and F6.

4. Control of HP

The complete system structure is illustrated in Figure 6. The proposed strategy of individual control unit (as discussed later in this section with Figure 7) integrated with HP allows proper coordination of HPs in the respective feeder to operate within the grid voltage limit, satisfying thermal demand, without the need for centralized communication for the operational schedule of HPs. This is possible with the local information such as status information from the HP-storage (T_{hot} -Temperature of hot water, X_c -the level of cold water in the storage tank), and information from the grid (V_i -terminal voltage at the point of coupling of HP). This information, along with on/off delay parameters for operation of HP based on the terminal voltage and thermal storage status, is the key control strategy. Hereby, HPs with storages have the potential to contribute as a flexible controllable load to support grid performance (grid voltage, line loading, and transformer capacities), by shifting its operating time. The proposed controller technique is also able to shift the flexibility request among the consumers in the same feeder based on their storage and grid status.

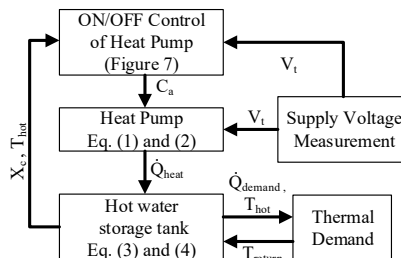


Figure 6. Block diagram of complete system structure.

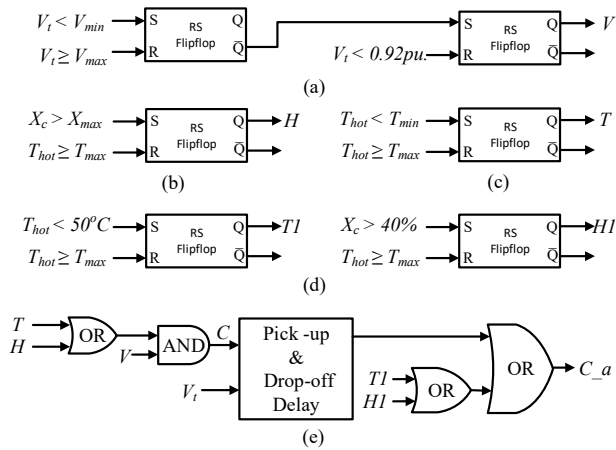


Figure 7. Schematic Control of HP (a) voltage controller (b) Level Controller (c) temperature Controller (d) Critical Controller (e) Delay Controller along with signal for operation of HP (C_a).

To determine the control limit to maintain minimum and maximum working temperature of hot water inside the thermal storage tank, it is necessary to know the purpose of thermal demand as well as working limits of commercially available products for the heat exchanger to fulfill user demand. Domestic use of hot water generally includes hot water for the kitchen and bathroom sinks, tubs, and other appliances. It requires an instantaneous water heater with a heat exchanger to ensure that hot water is produced immediately when tapping starts. There are products commercially available that operates with low district heating supply temperature in the range 50–70 °C with return temperature between 13–18 °C. On the other hand, space heating uses hot water with various techniques such as a radiator or floor heating with a thermostat to control room temperature between 8–28 °C. Thus, in this work the return temperature (T_{return}) of hot water to the system is selected to be 30 °C considering that the thermal demand used for both space heating and domestic uses and is supplied by the same source.

The overall control structure of the HP consists of five different control strategies to ensure proper flexibility in the operation of the HP maintaining grid voltage above its lower operating limit of –10% as well as fulfilling consumer demand. The five control strategies are performed using a level controller, temperature controller, voltage controller, critical controller, and a delay controller.

The voltage controller supports to maintains the terminal voltage (V_t), at the point of coupling of the HP to the electrical network, within the lower operating voltage of –10%. HPs in off state at the terminals where $V_t < 0.94$ pu are not allowed to operate until $V_t \geq 0.97$ pu to avoid hunting effect and is realized using RS-flipflop logic (without considering its inherent time delays) as shown in Figure 7a. However, HPs which are in on state continues to operate until $V_t \geq 0.92$ pu. This set-up allows the smooth operation of the HPs which are in on state and prevents the operation of HPs that are in off state, during the period when $0.92 \leq V_t < 0.94$.

The level controller operates to maintains the level of cold water inside the thermal storage tank (X_c) below a minimum level ($X_{min} = 25\%$) so that the temperature of hot water (T_{hot}) in the storage tank is maintained between 60–70 °C in the storage tank. The level controller sends operating signal (H), to operate the HP, when $X_c \geq X_{min}$ until $T_{hot} \geq T_{max}$ (T_{max} -maximum allowable temperature in storage tank). This hysteresis in level control is realized using the RS-flipflop logic as shown in Figure 7b.

The temperature controller operates to maintains the temperature of hot water (T_{hot}) between 60–70 °C in the storage tank by sending an operating signal (T), to operate the HP, when the minimum temperature (T_{min}) inside the storage tank is below 60 °C. This situation arrives when there is no thermal demand for a long time and due to heat loss from the storage tank, the temperature of hot

water drops over time. The temperature control is realized using RS-flipflop logic, as seen in Figure 7c, to maintain hysteresis in temperature control i.e., temperature control operates when $T_{hot} < T_{min}$ until $T_{hot} \geq T_{max}$.

The operation of the HP is mainly dominated by the voltage controller until a critical situation arrives, which is defined by the condition $T_{hot} < 50\text{ }^{\circ}\text{C}$ or $X_c > 40\%$. The critical controller operates during these critical conditions of the thermal storage tank to maintain T_{hot} between $50\text{--}70\text{ }^{\circ}\text{C}$ despite terminal voltage situation until $T_{hot} \geq 70\text{ }^{\circ}\text{C}$. This ensures a continuous supply of thermal demand for end-user applications such as space heating or domestic use. Figure 7d shows the schematic of a critical controller realized using RS-flipflop logic.

The delay controller determines the delay for the operation of HPs based on V_t . The delay logic based on V_t plays a vital role to allow operation of HPs in the weak feeder to meet the thermal demand. Delays with Lower pick-up and higher drop-off time corresponding to lower terminal voltage (V_t) prioritize the operation of HPs at the lower end of the distribution feeder, where the V_t is lower than the ones closer to the feeder terminal. The controller selects its delay value corresponding to V_t based on information provided in Table 2. If $V_t < 0.94$ pu, HPs are not allowed to connect to the grid until storage is in critical conditions as discussed above. Thus, the critical controller has the highest priority followed by the voltage controller. The temperature and level controller has the least priority in control of HP operation as seen from Figure 7d.

Table 2. Pick-Up and Drop-off Time Delays.

Condition	Pick-up Time (s)	Drop-off Time (s)
$V_t < 0.94$ pu	No HP Connected	$(0.97 - V_t) \times m + 30$
$V_t \geq 0.94$ pu	$(V_t - 0.94) \times m + 60$ $m = 3000$ for minimum delay of 30 s	$(0.97 - V_t) \times m + 30$
$V_t < 0.92$ pu for $t > 60$ s	1800	0
Critical Condition $T1 = 1$ OR $H1 = 1$	0	N/A

For the delay controller the minimum pick-up time delay of 60 s, when $V_t \geq 0.94$, is selected to avoid the controllers to respond at short duration variations in terminal voltages. The addition 60 s for every 0.01 pu rise in voltage is selected to have at least two samples based on the step size used in the simulations (30 s). The pick-up and drop-off time delay for $V_t \geq 0.94$ pu is illustrated in Figure 8.

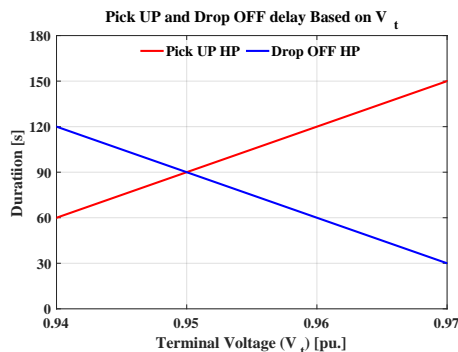


Figure 8. Pick-Up and Drop-Off delay based on V_t .

In case the V_t is lower than 0.92 pu for 60 s (two samples to avoid transients), the drop-off time is 0 s and system reconnects only after 30min (1800 s) of time delay. This is to ensure that the grid does not get stressed frequently due to connection and disconnection of HPs.

During the event of critical condition, as defined in Figure 7d, HP connects instantaneously without any delay, irrespective of V_t , until the temperature of hot water in the storage tank reaches its maximum value T_{max} .

Table 3 shows the value of control parameters associated with the control variables shown in Figure 7 for decision-making to operate HPs. Figure 9 shows the validation of the proposed logic for operation of HPs. Around 07:00hrs, $X_c > X_{min}$ and the logic signal H is set to 1 (Figure 9d). HP delivers heat output 15 min after the HP is turned on (Figure 9f). Around 13:00hrs, HP again tries to connect as $X_c > X_{min}$ (Figure 9d). During this time when HP connect to the grid, the grid voltage goes below 0.92 pu for more than 60 s (Figure 9a). As a consequence, voltage control turns off the HP. Once the HP is disconnected $V_t > 0.97$ pu but HP gain turns on only after 30 minutes (Figure 9f). Again the $V_t < 0.92$ pu and HP turns off. This time V_t does not recover its recovery limit of 0.97 pu (Figure 9c) as a result status of the voltage controller is low, meaning unfavorable condition to connect HP at this terminal. Around 19:00hrs X_c is greater than the critical level of cold water in the storage tank (X_{crit}), i.e., $X_c > X_{crit}$ (Figure 9d) and HP connects instantaneously without any delay and delivers thermal power until storage is fully charged (Figure 9f).

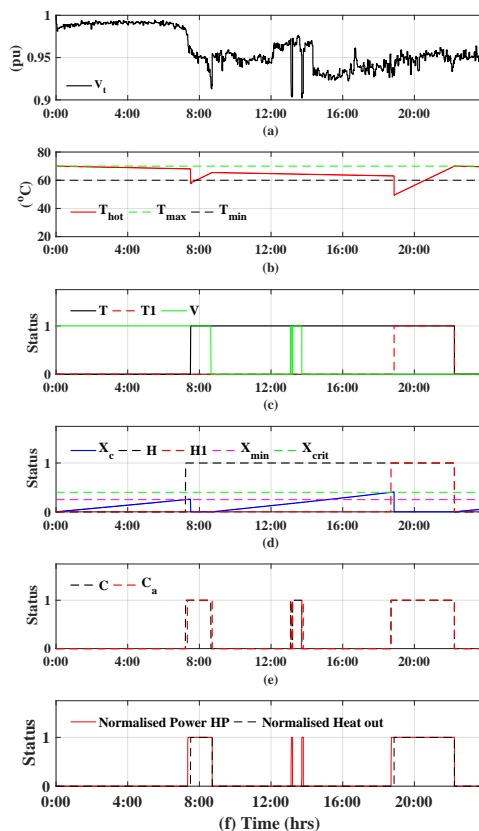


Figure 9. Control Logic (a). terminal voltage (V_t), (b) temperature of hot water inside storage tank, (c,d,e) control logic status, (f) operation of HP.

Table 3. Control Parameters.

T_{max} (°C)	T_{min} (°C)	V_{max} (pu)	V_{min} (pu)	X_{min} (%)
70	60	0.97	0.94	25%

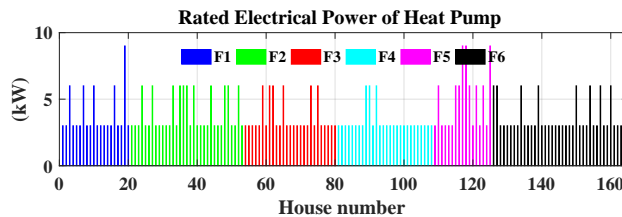
The decentralized control system based on the control logic with local information presented in this section supports the management of HPs in LV-weak grids and is further discussed in the result and discussion section.

5. Simulation Environment

Details on the residential electrical and thermal load demand profile for peak winter is well analyzed in [12]. The houses with higher electricity demand are allocated with higher thermal demand. Table 4 shows the allocation of HP and storage size based on thermal demand to ensure the continuous supply of hot water for at least 8 h during normal operation when fully charged until $X_c > 25\%$. Figure 10 shows the rating of HPs allocated to the individual houses in the proposed LV network.

Table 4. HP and storage tank size allocation.

Thermal Demand (kWh)	Storage Size (m ³)	Rated Electrical Power (kW)	No of HP
< 40	1	3	122
40-60	1.5	6	38
60-90	2	9	4

**Figure 10.** Rated electrical power of HP in individual houses.

Performance of the proposed decentralized controller discussed in Section 4 for integrating HPs in the LV electrical grid is investigated with various case studies. In this work, steady-state power system analysis in the time domain is performed using DigSILENT Power Factory simulation tool. It has the flexibility for developing models and control algorithms of flexible loads and energy storages such as HPs, and further test distribution grid integration and impact studies [30,31]. The model of the heat pump and storage is discussed in Section 2 and the LV residential network is discussed in Section 3.

Various case studies are performed based on different initial conditions for the level of cold water in the storage tank (X_c), the temperature of hot water from the storage (T_{Ctrl}), status of the heating element (C_n), and the operating power factor of the HP as shown in Table 5. In case I, all the storage tanks are fully charged. In case II, all the storage tanks are fully discharged. This situation closely corresponds to the scenario of a power failure due to various causes, such as natural calamities or fault in the power system, for a longer time period. The random situation is selected for case III. The random numbers are generated from MATLAB. Inverter base HPs with inrush current equal to nominal rating, and coefficient of performance (COP) of 3 for winter condition are considered. Since inverter-based HPs operates either at leading or lagging power factor as discussed in Section 2, it is interesting to observe their synergy with the electricity network for both conditions. Therefore, case IV is set up with lagging power factor with initial conditions as in the case I.

Table 5. Case studies with different initial conditions.

Case Study	Initial Conditions			Power Factor (pf)
	X_c	T_{hot}	C_a	
Case I	0	70 °C	0	0.95 leading
Case II	1	30 °C	0	0.95 leading
Case III	random between (0–1)	random between (30 °C–70 °C)	random 0 or 1	0.95 leading
Case IV	0	70 °C	0	0.95 lagging

6. Results and Analysis

Figures 11 and 12 shows the detailed evaluation and comparison of controller performance with respect to transformer loading, line loading, maximum voltage drop, and performance of the hot water storage tank for the case with leading power factor of HP (case I, II, and III) as mentioned in Table 5. Sub-figures in column 1, 2, and 3 are for case I, II, and III, respectively. The summary of results for day 1, 2, and 3 are tabulated in Tables 6 and 7, whereas figures for day 2 are not presented here. Minimum terminal voltages at the different feeders for all case studies are summarized in Table 7.

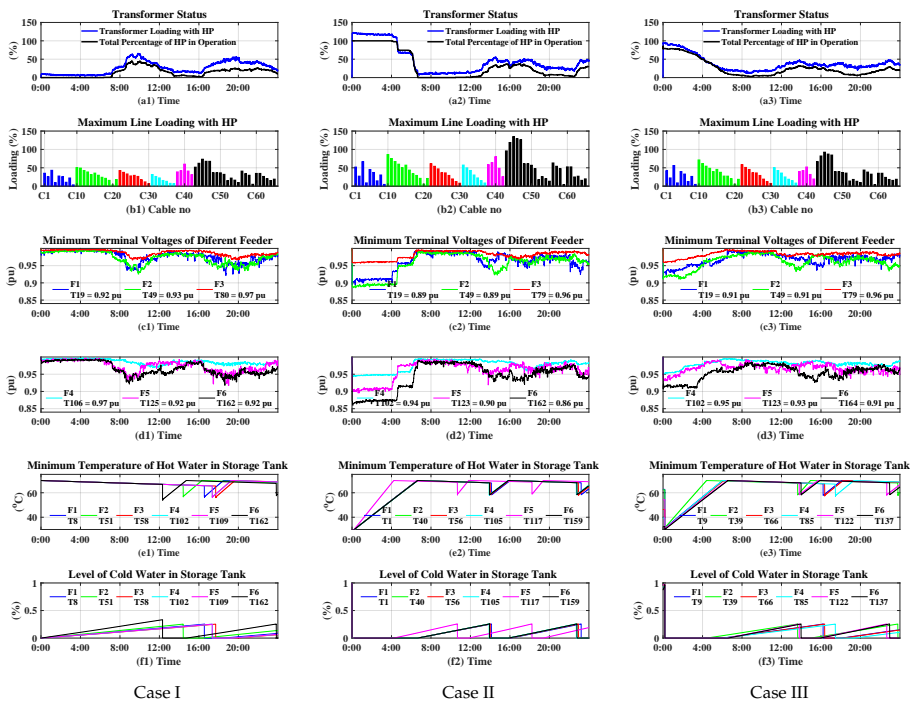


Figure 11. For day 1: sub-figures in column I, II, and III are for the case I, II, and III, respectively. (a) transformer loading and total percentage of HP in operation; (b) maximum line loading; (c) minimum voltage attained in terminals of feeder F1, F2 and F3; (d) minimum voltage attained in terminals of feeder F4, F5 and F6; (e,f) minimum attained supply temperature and associated level of cold water in storage tank respectively, in different feeders

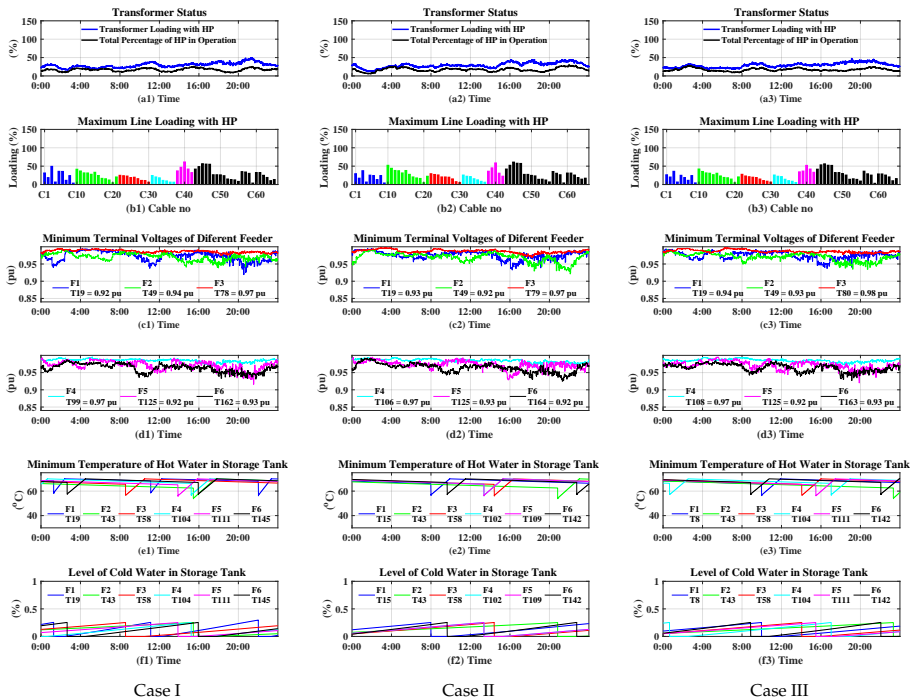


Figure 12. For day 3: sub-figures in column I, II, and III are for the case I, II, and III, respectively. (a) transformer loading and total percentage of HP in operation; (b) maximum line loading; (c) minimum voltage attained in terminals of feeder F1, F2 and F3; (d) minimum voltage attained in terminals of feeder F4, F5 and F6; (e,f): minimum attained supply temperature and associated level of cold water in storage tank respectively, in different feeders

6.1. Day 1 Analysis

Figure 11a shows the transformer loading, and total percentage of HPs operated during the 24 h period starting from midnight. Figure 11b shows the maximum cable loading attained. Figure 11c illustrates minimum terminal voltages attained in feeder F1, F2, F3 and Figure 11d for F4, F5, F6. The corresponding terminal number with minimum voltage in respective feeders are presented in legend. In order to verify that all the thermal demand are fulfilled without any interruption, the temperature profile of hot water and the corresponding level of cold water in a storage tank, which attains maximum temperature drop in each feeder is shown in Figure 11e and Figure 11f respectively. The associated terminal with the maximum temperature drop in each feeder is illustrated as a legend. The feeder with a maximum voltage drop is farther from the feeder terminal (Figure 11c,d) whereas, the maximum temperature drop is closer to the feeder terminal (Figure 11e). This suggests that the thermal unit at the far end of the feeder has higher priority to operate, based on the delay setting to turn on and off (as detailed in Table 2) compared to ones closer to the feeder terminal. Similar observations and graphs are presented for Day 3 in Figure 12.

Day 1 analysis as seen in Table 6 clearly shows that for case II (where the storage tank is fully discharged), all HPs operates together, and the transformer is overloaded 22% more than its rated capacity. Also, the maximum line loading is 135% for cable C45 Feeder F6 and a few others are heavily loaded (Figure 11b2). However, the line loading for all other feeders except F6 can sustain 100% penetration of HPs in operating condition. On the other hand, cable C45 in feeder F6 along with

a few other cables are also overloaded for case III (Figure11b3), where the transformer is loaded up to 95% of its rated capacity (Figure11a3). The maximum level of cold water in a storage tank and the minimum temperature of hot water for case II and III represents the initial condition. However, for case I, the temperature can drop down to 54°C for thermal unit connected at terminal T162 of feeder F6 (Figure11e1). The minimum temperature is attained due to the mixing of hot and cold water in the storage tank due to heat exchange during operation of HP as discussed in Section 2. Table 7 indicates that the controller limits the terminal voltages to go below 0.92 pu for case I. However, for case II, there are many HPs storage unit with the level of cold water or temperature of hot water below the critical level as an initial condition. During such a condition the controllers are not effective because of their LV ride through property during the critical stage of the storage tank. However, in the long run, this problem is solved by the controllers which manage to flexibly operate the HPs and storage as seen in day 2 and day 3 analysis.

Table 6. Summary of case studies.

	X_{mer} Loading max (%)	HP Operation max (%)	Line Loading max (%)	X_c max (%)	T_{hot} min (°C)
Simulation I (Day 1)					
Case I	65	45	73	33	54
Case II	122	100	135	100	30
Case III	95	86	92	100	30
Case IV	58	41	66	41	48
Simulation II (Day 2)					
Case I	49	29	61	26	54
Case II	58	31	70	26	54
Case III	53	26	62	26	54
Case IV	49	28	66	35	53
Simulation III (Day 3)					
Case I	49	26	61	30	54
Case II	44	29	61	26	54
Case III	47	28	56	26	54
Case IV	44	28	55	26	53

6.2. Day 2 and Day 3 Analysis

Similar observations as in Figure 11 are shown in Figure 12 for day 3. Day 2 and Day 3 analysis shows that the maximum transformer loading (60%) and line loading (69%) are well within the limit. In the long run, there are no more than 31% of HPs being operated at any time. Furthermore, the minimum temperature inside the tank is 54°C at the time of operation of HP and the maximum level of cold water in the storage tank is 32% suggesting that the HP and storage are able to operate flexibly fulfilling the thermal demand simultaneously.

In the long run, despite any initial condition, the HPs coordinates to support peak shaping and line loading (Figure 12a,b), while maintaining the grid voltage (Figure12c,d) as well as thermal demand (Table 6- T_{hot}) together. Feeder F3 is the strongest feeder among all with voltage drop down to 0.96 pu, and the weakest one is F6. It is observed from Tables 6 and 7, and Figure 12 that the simulation results for all case studies have the similar outcome with respect to line loading, grid voltages, percentage operation of HP, and transformer loading. The grid parameters are well within their operational limit and satisfy the thermal demand simultaneously.

Table 7. Minimum terminal voltages at different feeder.

	F1 (pu)	F2 (pu)	F3 (pu)	F4 (pu)	F5 (pu)	F6 (pu)
Base Case	0.95	0.96	0.98	0.98	0.95	0.95
Simulation I (Day 1)						
Case I	0.92	0.93	0.97	0.97	0.92	0.92
Case II	0.89	0.89	0.96	0.94	0.90	0.86
Case III	0.91	0.91	0.96	0.95	0.93	0.91
Case IV	0.92	0.92	0.95	0.95	0.92	0.91
Simulation II (Day 2)						
Case I	0.94	0.93	0.97	0.96	0.92	0.93
Case II	0.92	0.94	0.97	0.96	0.92	0.92
Case III	0.93	0.93	0.97	0.97	0.92	0.93
Case IV	0.92	0.93	0.96	0.96	0.91	0.92
Simulation III (Day 3)						
Case I	0.92	0.94	0.97	0.97	0.92	0.93
Case II	0.93	0.92	0.97	0.97	0.93	0.92
Case III	0.94	0.92	0.98	0.97	0.92	0.93
Case IV	0.92	0.92	0.97	0.96	0.92	0.92

6.3. HPs with Lagging Power Factor

Some inverter-based HPs also operates at lagging 0.95 power factor. Thus, it is interesting to observe how the LV grid behaves for HPs with lagging pf. When the pf of all HPs is set to 0.95 lagging, with the initial condition as in the case I, the result is presented in Figure 13. Column I, II, and III of Figure 13 are for the day I, II, and III. Transformer loading and the total percentage of HP in operation is illustrated in Figure 13a. Compared to the case I (where pf is leading), maximum transformer loading and maximum percentage of HPs in operation are reduced (see Table 6), signifying that with lagging pf, the hosting capacity of LV distribution grid decreases. Figure 13b shows that line loading decreases due to reduction in hosting capacity as compared to case I. Terminal voltages of the terminal attaining minimum voltage in each feeder are shown in Figure 13c,d along with the temperature of hot water and level of cold water in storage tank associated with these terminals are shown in Figure 13e and, Figure 13f respectively. It is interesting to see that the terminal voltage of feeder F6, terminal T162 (Figure 13d), goes below 0.92 pu when the HPs associated with this terminal tries to operate. Thus, the HP in T162 is disconnected to support grid voltage. It again tries to connect after the time delay of 30 min and disconnects due to poor voltage, until the level of cold water in the storage tank attains critical limit (greater than 40%) as seen from Figure 13f. Figure 13e shows that the temperature of hot water in the storage tanks in different feeders at the terminal attaining minimum voltage. It shows that the supply temperature of hot water is well above 50 °C. In the long run, as seen from Figure 13 for day II and day III, HP coordinates to support peak shaping and maintain grid voltage simultaneously.

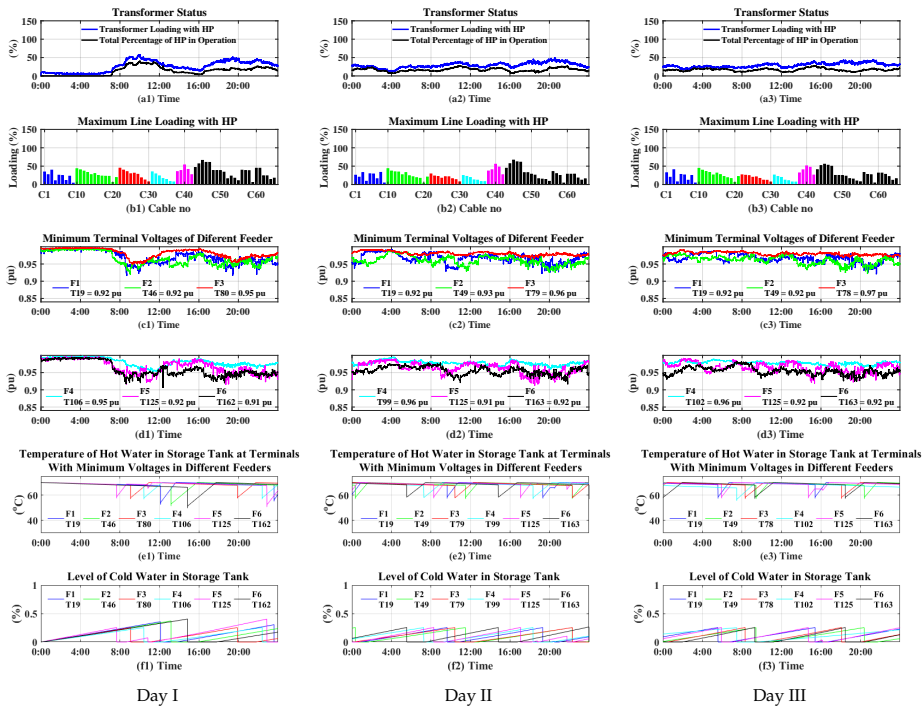


Figure 13. For Case 4 Lagging pf: sub-figures in column I, II, and III are for the Day I, II, and III, respectively. (a). transformer loading and total percentage of HP in operation; (b) maximum line loading; (c) minimum voltage attained in terminals of feeder F1, F2 and F3; (d) minimum voltage attained in terminals of feeder F4, F5 and F6; (e,f) Temperature of supply hot water from storage and level of cold water respectively

6.4. Discussion

The effectiveness of the proposed controller is well explored in this section for strong as well as in weak feeders. The effect of leading and lagging power factor of HPs in grid voltage fluctuation is well observed with the effectiveness of controller performance to set them within the operating limit of terminal voltage between 1–0.9 pu, together with the fulfillment of thermal demand. This enhances application for integrating renewables and synergy with P2H, supporting operation and planning of active grids. More voltage drop is observed with lagging power factor, compared to leading. By controlling its power factor, inverter-based HPs have potential to support grid voltage with many PV or wind turbines. The set points for the controller (control variables) can be specified for a particular network based on its capacity. If required, the set point of controllers can be changed individually (when there are some changes in the grid infrastructure) and is not needed frequently.

Flexibility is shared among the different HPs in the same feeder based on measurement and controlled variables. The controller fails to operate only when many storage tanks are below the critical level as seen in case II and case III initial conditions. In the long run, it manages to stabilize the system flexibility and satisfying demand simultaneously without any need for communication infrastructure, as a cost-effective solution for flexible load management of heating systems, minimizing grid reinforcements.

Along with the necessity to maintain thermal comfort of users at households, the reliable and stable operation of LV distribution grid are equally important when integrating sizeable loads such as

HPs. With an increase in renewable energy generation, these HPs and storages are considered to be one of the major technologies that can provide flexibility to the power system providing efficient heating as well as storage of energy. Therefore, for the successful integration and use of HPs in distribution grids, it is important to understand the overall scenario of how the system is affected. Analysis of the distribution grid from the perspective of HP control and its effect on the grid voltage, line loading and transformer loading along with user comfort (as seen from level and temperature of hot water in the storage tank) presents the effectiveness of the proposed controller. The effect of selecting initial condition regarding the status of HP (on/off) and storage (level and temperature of hot water) in the LV grid are thoroughly analyzed based on its effect on grid voltage, and transformer and cable loadings. Same initial condition as in study case I and II introduces operating bottle necks in the LV grid on day one, whereas in long run despite any initial condition, the total percentage of HP in operation at a time is between 25-30% as seen for the analysis of day 3 analysis in Table 6. This reflects the distributed operation of HP over time that enables flexible peak shaping of the electricity demand as well as preventing under-voltage (day 3—Table 7) in the far end of the radial feeder. The peak loading of the transformer is just below 50% (day 3—Table 6) indicating that with proper demand control, more sizeable electrical loads, such as electric vehicles, can also be integrated in the future by adopting such simple and effective local controls. However, considering grid voltage of feeder F6 (Figures 11, 12 and 13c,d) there is a necessity of grid reinforcement in feeder F6 to ensure terminal voltage at the end nodes are within operating thresholds.

The results show that the proposed control architecture of HPs can reduce the need for costly grid reinforcement as well as a separate communication infrastructure for handling of big data, and complex control architecture. Hence, it is beneficial to both the networks/systems and the involved stakeholders. It not only reduces the network impact but also provides flexibility in production, conversion, storage, and end-use through the efficient coordination of the HP operation, helping to lower the electricity consumption at peak times. Synergies among the thermal and electrical systems with the interaction between local and distributed generation units such as wind solar have potential in the future. Thus, the results and findings from the work are in line with the contemporary integrated sustainable energy system concept. This work can be further carried out with economical aspects, scheduling and aggregation services based on forecasting and energy price.

7. Conclusions

HPs with storage is a good source of P2H in smart energy systems. Higher COP compared to EBs, and storage tank as energy buffer increases its potential as a flexible load and storage solution in future smart grid systems. This paper has analyzed the flexibility of individual HPs in every household, particular to the input voltage in the LV distribution network. The use of a simple local controller can satisfy the consumer demand while coordinating among the various HPs in the same electrical feeder, minimizing transformer loading, line loading, and voltage drop in the long run. Different scenarios based on leading and lagging power factor of HPs, and initial operating condition of HP and storages are demonstrated in a LV network with 164 households. The potential cost-effective solution towards P2H synergy in smart energy system has been presented with the use of the local controller for the individual HP.

Author Contributions: R.S. developed the methodology, corresponding models, and wrote the paper. B.B.-J., and J.R. P. supervised the work and reviewed the paper.

Funding: This work is supported by the Innovation fund Denmark through the DiCYPs project.

Acknowledgments: The data for the analysis has been provided by Aalborg Energi Holding A/S and Aalborg University, Denmark, as per the agreement between project partners for research.

Conflicts of Interest: The authors declare no conflict of interest.

References

1. Connolly, D.; Lund, H.; Mathiesen, B.; Werner, S.; Möller, B.; Persson, U.; Boermans, T.; Trier, D.; Østergaard, P.; Nielsen, S. Heat Roadmap Europe: Combining district heating with heat savings to decarbonise the EU energy system. *Energy Policy* **2014**, *65*, 475–489. doi:10.1016/j.enpol.2013.10.035.
2. Ommen, T.; Markussen, W.B.; Elmegaard, B. Lowering district heating temperatures—Impact to system performance in current and future Danish energy scenarios. *Energy* **2016**, *94*, 273–291. doi:10.1016/j.energy.2015.10.063.
3. Lund, R.; Østergaard, D.; Yang, X.; Mathiesen, B. Comparison of Low-temperature District Heating Concepts in a Long-Term Energy System Perspective. *Int. J. Sustain. Energy Plan. Manag.* **2017**, *12*, 5–18.
4. Neirotti, F.; Noussan, M.; Rivero, S.; Manganini, G. Analysis of Different Strategies for Lowering the Operation Temperature in Existing District Heating Networks. *Energies* **2019**, *12*. doi:10.3390/en12020321.
5. Swing Gustafsson, M.; Myhren, J.A.; Dotzauer, E. Life Cycle Cost of Heat Supply to Areas with Detached Houses—A Comparison of District Heating and Heat Pumps from an Energy System Perspective. *Energies* **2018**, *11*. doi:10.3390/en11123266.
6. Averfalk, H.; Ingvarsson, P.; Persson, U.; Gong, M.; Werner, S. Large heat pumps in Swedish district heating systems. *Renew. Sustain. Energy Rev.* **2017**, *79*, 1275–1284. doi:10.1016/j.rser.2017.05.135.
7. Lund, H.; Möller, B.; Mathiesen, B.; Dyrrelund, A. The role of district heating in future renewable energy systems. *Energy* **2010**, *35*, 1381–1390. doi:/10.1016/j.energy.2009.11.023.
8. Dongellini, M.; Abbenante, M.; Morini, G. A strategy for the optimal control logic of heat pump systems: impact on the energy consumptions of a residential building. In Proceedings of the 12th IEA Heat Pump Conference 2017, Rotterdam, The Netherlands, 15–18 May 2017.
9. Madani, H.; Claesson, J.; Lundqvist, P. A descriptive and comparative analysis of three common control techniques for an on/off controlled Ground Source Heat Pump (GSHP) system. *Energy Build.* **2013**, *65*, 1–9. doi:10.1016/j.enbuild.2013.05.006.
10. Merkert, L.; Haime, A.A.; Hohmann, S. Optimal Scheduling of Combined Heat and Power Generation Units Using the Thermal Inertia of the Connected District Heating Grid as Energy Storage. *Energies* **2019**, *12*. doi:10.3390/en12020266.
11. Sinha, R.; Jensen, B.B.; Pillai, J.R.; Moller-Jensen, B. Unleashing Flexibility from Electric Boilers and Heat Pumps in Danish Residential Distribution Network. In Proceedings of the CIGRE 2018, Paris, France, 26–31 August 2018.
12. Sinha, R.; Jensen, B.B.; Radhakrishnan Pillai, J. Impact Assessment of Electric Boilers in Low Voltage Distribution Network. In Proceedings of the 2018 IEEE Power Energy Society General Meeting (PESGM), Portland, OR, USA, 5–9 August 2018; pp. 1–5. doi:10.1109/PESGM.2018.8586236.
13. Akmal, M.; Fox, B.; Morrow, D.J.; Littler, T. Impact of high penetration of heat pumps on low voltage distribution networks. In Proceedings of the 2011 IEEE Trondheim PowerTech, Trondheim, Norway, 19–23 June 2011; pp. 1–7. doi:10.1109/PTC.2011.6019401.
14. Molitor, C.; Marin, M.; Hernández, L.; Monti, A. Decentralized coordination of the operation of residential heating units. In Proceedings of the IEEE PES ISGT Europe 2013, Copenhagen, Denmark, 6–9 October 2013; pp. 1–5. doi:10.1109/ISGTEurope.2013.6695340.
15. Pudjianto, D.; Djapic, P.; Aunedi, M.; Gan, C.K.; Strbac, G.; Huang, S.; Infield, D. Smart control for minimizing distribution network reinforcement cost due to electrification. *Energy Policy* **2013**, *52*, 76–84. doi:10.1016/j.enpol.2012.05.021.
16. Esterl, T.; Leimgruber, L.; Ferhatbegovic, T.; Zottl, A.; Krottenthaler, M.; Weiss, B. Aggregating the flexibility of heat pumps and thermal storage systems in Austria. In Proceedings of the 2016 5th International Conference on Smart Cities and Green ICT Systems (SMARTGREENS), Rome, Italy, 23–25 April, 2016.
17. Hong, J.; Kelly, N.J.; Richardson, I.; Thomson, M. Assessing heat pumps as flexible load. *Proc. Inst. Mech. Eng. Part J. Power Energy* **2013**, *227*, 30–42. doi:10.1177/0957650912454830.
18. Pedersen, T.S.; Nielsen, K.M.; Andersen, P. Maximizing storage flexibility in an aggregated heat pump portfolio. In Proceedings of the 2014 IEEE Conference on Control Applications (CCA), Nice, France, 8–10 October 2014; pp. 286–291. doi:10.1109/CCA.2014.6981360.

19. Zhang, L.; Chapman, N.; Good, N.; Mancarella, P. Exploiting electric heat pump flexibility for renewable generation matching. In Proceedings of the 2017 IEEE Manchester PowerTech, Manchester, UK, 18–22 June 2017; pp. 1–6. doi:10.1109/PTC.2017.7981266.
20. Bhattarai, B.P.; Kouzelis, K.; Mendaza, I.D.D.C.; Bak-Jensen, B.; Pillai, J.R.; Myers, K.S. Smart Grid Constraint Violation Management for Balancing and Regulating Purposes. *IEEE Trans. Ind. Inform.* **2017**, *13*, 2864–2875. doi:10.1109/TII.2017.2688464.
21. Jennings, N.R.; Bussmann, S. Agent-based control systems: Why are they suited to engineering complex systems? *IEEE Control Syst. Mag.* **2003**, *23*, 61–73. doi:10.1109/MCS.2003.1200249.
22. Baillieul, J.; Antsaklis, P.J. Control and Communication Challenges in Networked Real-Time Systems. *Proc. IEEE* **2007**, *95*, 9–28. doi:10.1109/JPROC.2006.887290.
23. Masuta, T.; Yokoyama, A.; Tada, Y. Modeling of a number of Heat Pump Water Heaters as control equipment for load frequency control in power systems. In Proceedings of the 2011 IEEE Trondheim PowerTech, Trondheim, Norway, 19–23 June 2011; pp. 1–7. doi:10.1109/PTC.2011.6019457.
24. Heffernan, W.J.B.; Watson, N.R.; Buehler, R.; Watson, J.D. Harmonic Performance of Heat-Pumps. *IET J. Eng.* **2013**, *9*, 31–44.
25. Heffernan, W.J.B.; Watson, N.R.; Watson, J.D. Heat-pump Performance: Voltage dip/sag, Under-Voltage and Over-Voltage; in *The Journal of Engineering*, vol. 2014, no. 12, pp. 640–657, Dec 2014. doi: 10.1049/joe.2014.0180
26. Sinha, R.; Jensen, B.B.; Pillai, J.R.; Bojesen, C.; Møller-Jensen, B. Modelling of hot water storage tank for electric grid integration and demand response control. In Proceedings of the 2017 52nd International Universities Power Engineering Conference (UPEC), Crete, Greece, 28–31 August 2017; pp. 1–6. doi:10.1109/UPEC.2017.8231964.
27. Han, Y.; Wang, R.; Dai, Y. Thermal stratification within the water tank. *Renew. Sustain. Energy Rev.* **2009**, *13*, 1014–1026. doi:10.1016/j.rser.2008.03.001.
28. Mawire, A.; Taole, S.H. Heat loss estimation in a small vertical cylindrical stratified oil storage tank. In 2013 Proceedings of the 21st Domestic Use of Energy Conference, Cape Town, 3–4 April 2013, pp. 1–7. 2013; pp. 1–7.
29. Pillai, J.R.; Thøgersen, P.; Møller, J.; Bak-Jensen, B. Integration of Electric Vehicles in low voltage Danish distribution grids. In Proceedings of the 2012 IEEE Power and Energy Society General Meeting, San Diego, CA, USA, 22–26 July 2012; pp. 1–8. doi:10.1109/PESGM.2012.6343948.
30. DigSILENT. Available online: <https://www.digsilent.de/en/powerfactory.html> (accessed on 2 February 2019).
31. Bjerregaard, P.T.; Szczesny, I.G.; de Cerio Mendaza, I.D.; Pillai, J.R. Intelligent control of flexible loads for improving low voltage grids utilization. In Proceedings of the IEEE PES ISGT Europe 2013, Copenhagen, Denmark, 6–9 October 2013; pp. 1–5. doi:10.1109/ISGTEurope.2013.6695287.



© 2019 by the authors. Licensee MDPI, Basel, Switzerland. This article is an open access article distributed under the terms and conditions of the Creative Commons Attribution (CC BY) license (<http://creativecommons.org/licenses/by/4.0/>).

Paper D.

Journal J2

Flexibility From Electric Boiler and Thermal Storage For Multi Energy System Interaction

R. Sinha, B. Bak-Jensen, and J. R. Pillai, H. Zareipour

The paper has been submitted for peer review in the
Sustainable Energy, Grids and Networks Vol. XX(X), pp. XXX–XXX, 2019.

© 201X IEEE

The layout has been revised.

Flexibility From Electric Boiler and Thermal Storage For Multi Energy System Interaction

Rakesh Sinha^a, Birgitte Bak-Jensen^b, Jayakrishnan Radhakrishna Pillai^c, Hamidreza Zareipour^d

^aDepartment of Energy Technology, Aalborg University, Denmark, e-mail: ras@et.aau.dk

^bDepartment of Energy Technology, Aalborg University, Denmark, e-mail: bbj@et.aau.dk

^cDepartment of Energy Technology, Aalborg University, Denmark, e-mail: jrp@et.aau.dk

^dDepartment of Electrical and Computer Engineering, Schulich School of Engineering, University of Calgary, Canada, e-mail: hzareipo@ucalgary.ca

Abstract

Active use of heat accumulators in the thermal system has the potential for achieving flexibility in district heating with the power to heat (P2H) units, such as electric boilers (EB) and heat pumps. Thermal storage tanks can decouple demand and generation, enhancing accommodation of sustainable energy sources such as solar and wind. The overview of flexibility, using EB and storage, supported by investigating the nature of thermal demand in a Danish residential area, is presented in this paper. Based on the analysis, curve-fitting tools, such as neural net and similar day method, are trained to estimate the residential thermal demand. Utilizing the estimated demand and hourly market spot price of electricity, the operation of the EB is scheduled for storing and fulfilling demand and minimizing energy cost simultaneously. This demonstrates flexibility and controlling the EB integrated into a multi-energy system framework. Results show that the curve fitting tool is effectively suitable to acknowledge thermal demands of residential area based on the environmental factor as well as user behaviour. The thermal storage has the capability of operating as a flexible load to support P2H system as well as minimize the effect of estimation error in fulfilling actual thermal demand simultaneously.

Keywords: Energy Flexibility, Power-to-Heat, Multi Energy System, Flexible demand, Thermal storage, Electric boiler, Estimation of thermal demand.

1. Introduction

District heating (DH) supplied hot water to 63% of the private Danish houses in 2015, [1]. The concept of 4th generation district heating/cooling system, supported by renewable, is presented in [2]. With the goal to become carbon neutral in the heating sector by 2030, renewables need to contribute all the heating demands. Thus, there is a possibility to integrate the thermal and electric networks to support grid ancillary services by the flexible electrical loads, such as electric boilers (EBs) and heat pumps (HPs), supporting the thermal system [2][3]. The electricity and heating network are coupled together as power-to-heat (P2H) to utilize renewable electricity for district heating. Integrated heat storage decouples demand and generation, to enhance flexibility for a better adaptation of energy requirements. The concept of P2H in the multi-energy system requires minor expansion of grid and storage [4].

The objective of this paper is to acknowledge flexible operation of the thermal unit consisting of an electric boiler (EB) and a storage tank modelled with stratified layers, as a part of P2H system. This is primarily realized through analysis of thermal consumption data and estimating thermal demand using curve fitting, followed by an optimal schedule of the EB based on the spot price.

Advantages of centralized thermal storage in terms of operational flexibility of CHP for district heating is well-explored in [5]. The flexibility of a district heating network for automatic frequency restoration reserve market is studied in [6]. The bal-

ancing markets provide an opportunity for introducing more EBs into DH and increase its contribution to flexibility [7]. A crucial aspect here is how system deployment can be realized effectively. [8] addresses the flexible operation of heat pumps using predictive control strategy, neglecting consumption of hot water for its highly randomized and hardly predictable nature. The predictive control of the heat pump by estimating only outdoor temperature has been studied in [9]. Thus, there is a necessity to investigate simple and effective methods to determine the influencing parameters for thermal demand prediction to manage the flexible operation of the thermal units in P2H technology.

The perspective of heat electrification in a wind dominated market using resistive heating and storage is the most carbon-intensive method [10] with lower investment cost compared to HP [7] [11]. Further, large HPs takes a long time from a cold start until it reaches its optimal efficiency. Thus, they are not very active at balancing markets between hours, due to short start-stop intervals. Rather, it is mainly used as base load [7]. Hence, the flexibility in easy start-stop in balancing services is the main driver for introducing more EBs into the system. EBs in district heating has the potential for negative secondary control power by increasing consumption and supporting grid balance [12]. [13] realized the benefit of demand-side management and the ability of demand response to improve power system efficiency with integrated wind power and electric heating devices considering constant heat load through the day. Higher potential of HPs in DH systems in future is realized in [14].

Integration of EB with storage in low voltage residential grid as flexible consumer load has been presented in [15]. Hence, there is the potential of good harmony and flexibility between electrical and thermal energy sector supporting each other in multi-energy systems.

The investigation of space heating and domestic hot water needs is presented in [16] based on curve fitting and distribution functions. In [17] peak load ratio index of buildings are used for determining the diversity in thermal loads to generate the thermal profile for residential buildings. [18] calculates the probability of domestic hot water drawn at a time(t) which depends upon probability during the day, weekday, season and holiday as a function of time(t). Higher probability step functions for weekends in comparison to weekdays are used to indicate higher consumption of domestic hot water on weekends. The thermal demand for space heating in a typical winter day is explored in [19]. However, the pattern of usage for the combined effect of space heating (SH) and domestic hot water (DHW) still remains unrealized. Proper knowledge of demand pattern for space heating and domestic use, as presented in this paper, is the key factor for developing a good and applicable estimating tool for thermal demand.

The possibility of estimating heat demand for space heating just a few hours in advance using neural network based on heat consumption in Polish buildings is matched against weather conditions over a 10 year period in [20]. In [20], the forecasting method is based on time series neural network with temperature and thermal consumption at a particular hour, day and previous history are taken into consideration. One month data from a DH network in Riga has been analysed for forecasting in [21] with the comparison between methods using an artificial neural network, polynomial regression model and the combination of both. With these methods, forecasts are performed by updating the statistics of actual load and temperature of the previous measurement. DH from Czech has been analysed in [22] in a forecast model based on time series of outdoor temperature and time-dependent social components, which may vary for different weekdays and seasons. The Box-Jenkins method is used to realize the forecast of the social component. [23] addresses issues on the selection of appropriate input variables from Building Energy Management Systems sensors. Ambient temperature and relative humidity along with solar radiation are the predominant factors for the predictive model [23],[24]. In [25], forecasting based on similar day method is well presented for day-ahead power output for small scale solar PV system. However, none of the literature discussed regarding district heating in both summer and winter, as well as thermal demand prediction based on a combined effect of the time factor and environment variables (such as outdoor temperature, humidity, and wind velocity) together.

In this paper, the proposed methodology to obtain flexibility with EB in P2H is summarised in the block diagram as shown in Fig. 1. The significant contributions in this paper are the identification of thermal demand pattern, estimation of thermal demand using curve fitting tool, and use of stratified storage tank to verify flexible operation of EB. Actual thermal data from DH operator is analysed to unleash the specific consump-

tion pattern of residential areas associated with usage based on different time factors such as hourly, weekdays, weekends and seasonal. These informations are useful while training the curve fitting tool to estimate thermal demand. With reference to [20], [21], [22], thermal demand estimation is based on the past and its current state for winter. A simple, yet effective curve fitting technique for estimating the thermal demand in the residential area, based on dependent parameters such as time factor (based on consumption profile) and environment variables (apparent temperature), has been investigated and compared with actual data as well as results from existing literature. The analysis is performed for thermal demand estimation during winter as well as summer. The curve fitting is simple and overcomes the problem encountered with the update of measured data (due to the failure of measuring equipment) as in time series estimation. The estimated demand is used to determine the optimal schedule of the EB operation in P2H, for the planning of capacities to store and fulfil thermal energy demand simultaneously, based on the spot price of electricity. The use of stratified storage tank in combination with EB emulates the real operating condition where the temperature of hot water being delivered is more realistic compared to ones from an average model of the storage tank, where hot water temperature decreases gradually. The outcome is verified with actual thermal demand to illustrate how the thermal storage copes up with the error in forecasting and contribute as an example of a flexible load in the P2H concept.

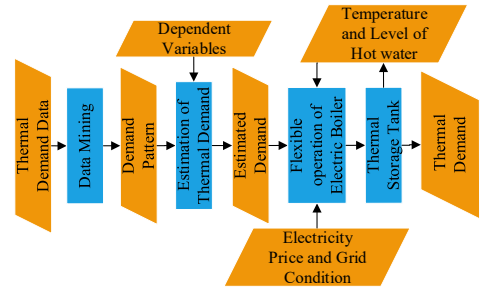


Fig 1. Block Diagram of proposed system for flexible operation of Electric Boiler

The paper is structured as follows. Analysis of thermal load consumption based on actual measurements at one particular residential site in Denmark supplied with five feeders is analysed to unleash the specific usage pattern and is identified in section 2. Selection of parameters for effective estimation of thermal demand using various tools such as neural net fitting, and similar day method are discussed in section 3. Overview of the modelling approach of the stratified hot water storage tank and EB is presented in section 4 along with validation of the model. In section 5, the methodology for optimized operation schedule of EB is presented along with EB ON/OFF control strategy. Results of the estimated demand are discussed in sec-

tion 6, followed with its application in flexible scheduling of the EB for demand response. Finally, the paper is concluded with the outcome of the research work in section 7.

2. Analysis of thermal data

Thermal data measured at the terminal of five thermal distribution feeders ($F_1 - F_5$) supplying a number of residential buildings, in one particular residential area of Aalborg, Denmark are used for analysis. Data of hourly thermal consumption, from the period of 21st Dec 2015 to 4th Dec 2016 are analysed. Fig. 2 shows the total annual consumption of thermal demand (Q_{DHW}) for residences in feeders ($F_1 - F_5$) supplying residential buildings. The annual consumption varies from 723.7MWh as lowest consumption for F_1 to 1278.5MWh as the highest consumption in F_4 . This variation is due to the different number of residents in the area and their level of comfort. The total annual consumption was 5195.7MWh. Fig. 3(a, b) shows the plot of hourly consumption of Q_{DHW} for feeders ($F_1 - F_5$) and their total consumptions respectively, throughout the year. Fig. 3(a, b) clearly shows that there is seasonal variation.

Fig. 3(b) shows that there is a sudden transition in thermal consumption at certain time period such as towards the end of January, mid of March, and beginning of May. However, there is a significant difference in thermal consumption between mid-May to September end which is less than 35% of the peak winter consumption. Thus, to simplify the further analysis, the trend of thermal consumption is roughly divided into two seasons, winter and summer, irrespective of autumn and spring. Hence, October to April is considered as winter season and May to September is considered as summer Season. The transition period at the beginning of May and October is not considered in this analysis. It seems that there is slightly more thermal demand in May than in September, due to transition from winter to summer and is around $30 \pm 5\%$ of the peak winter consumption. It is interesting to see the analysis of data from seasonal perspectives: winter and summer consumption. In the rest of the paper, analysis is done taking the combined effect of all feeders. As a result, the maximum heat demand is likely to be less than the sum of the individual feeder's peak load. This also reduces the intermittent variation in demand for individual feeders.

The average consumption per hour of Q_{DHW} for all the feeders, considering yearly consumption, is 618.5kWh. During winter, it is 881.8kWh, which is 205.8% more than summer consumption of 288.4kWh.

Fig. 4(a,c) shows the graph of hourly average thermal consumption pattern of different days of the week during winter and summer respectively. It is clearly seen that there exist a unique pattern of average thermal consumption with peaks. The pattern is different on weekends (Saturday and Sunday) in comparison to weekdays (Monday-Friday). To simplify the graphs shown in Fig. 4(a,c), graphs with an average consumption of thermal energy during the week, weekdays and weekend has been plotted in Fig. 4(b,d) for winter and summer respectively. It is observed that there are some definite patterns of hourly usage of an average Q_{DHW} . There are two peaks and two valleys. It is clear that the amount of variation in thermal consumption

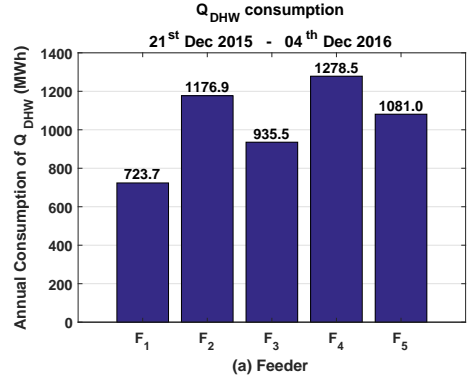


Fig 2. Yearly consumption of Q_{DHW} in different feeders.

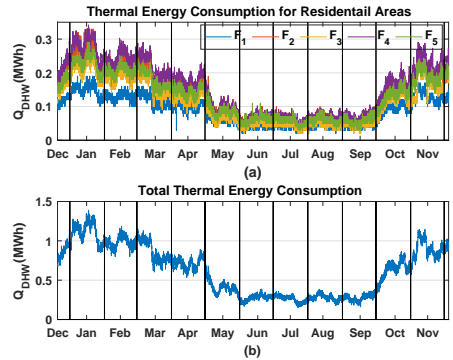


Fig 3. (a) Yearly Q_{DHW} consumption pattern of all feeders. (b) Total yearly Q_{DHW} consumption pattern of all feeders.

with respect to minimum consumption is higher for weekends than for weekdays indicating higher consumption of domestic hot water as mentioned in [18]

Fig. 5 shows the consumption pattern for the week, weekdays and weekends for the period of Dec 2016 to Aug 2017 for winter and summer respectively. Unlike in Fig. 4(b,d) the total consumption at weekends are lower than weekdays. Thus, the amount of thermal consumption based on weekend and weekdays are not much relevant. However, the hourly pattern of consumption for weekdays and weekends are comparable with similar peaks and valley at particular hours seen in Fig. 4(b,d). Hence, knowledge of these patterns of thermal consumption during weekdays and weekend is much helpful to train the estimation tool to compensate for the error due to temperature independent factors such as user behaviour. The lowest consumption is during the period 03:00 to 04:59 Hrs which rises gradually until 07:00 to 07:59 Hrs during normal weekdays when people get ready for their job (Fig. 4(b,d)). On the weekend there is a shift in this peak which is around 10:00-12:59 Hrs. The shift in peak could be because people prefer to wake up late

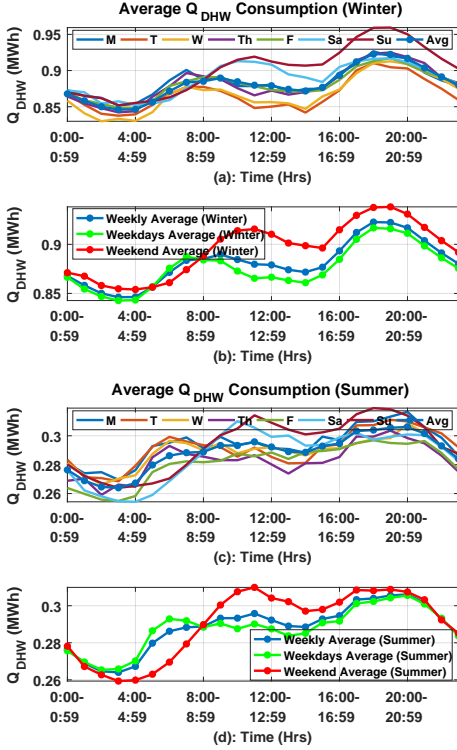


Fig 4. Analysis of Q_{DHW} Dec 2015-Dec 2016
(a,c) Analysis of average thermal consumption in hourly basis for different days of week for summer and winter respectively
(b,d) Analysis of average thermal consumption in hourly basis for a week, weekdays and weekends

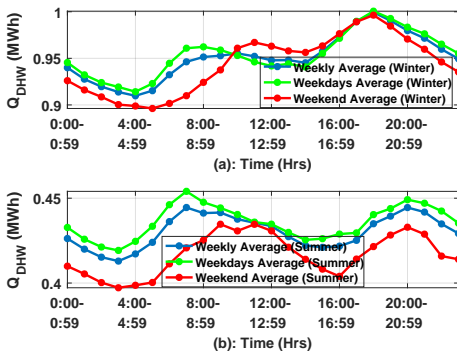


Fig 5. Average hourly thermal consumption of week, weekdays and weekends from period (Dec 2016- Aug 2017) (a) Winter (b) Summer

on the weekend. After the morning peak, there is decrement of thermal consumption until 2:00-3:59 Hrs when people are at work during weekdays. Throughout the week, the evening

peak is around 18:00 to 20:59 which gradually decreases to 4:59 Hrs in the early morning. However, in summer there is a shift in evening peak compared to that in winter. This analysis shows the relevance of time, day and season to determine the usage pattern of thermal consumption and that it is significant for forecasting as seen in [20] for thermal load similar to the forecasting of electrical load [26].

3. Thermal Demand Estimation

It is difficult to estimate thermal demand for the residential area, as it is not only largely depending on the environmental variables (weather), but also on the user behaviour and building geometry. In reality, analysis for occupancy and user level comfort is difficult and leads to challenges incorporated with privacy issues of the individuals. This leads to a significant effort to compromise between errors in estimated variable and dependent parameters. Analysis of thermal data from residential areas gives remarkable information on the pattern of thermal demand, without compromising the privacy issue of individuals. These informations are helpful in selecting effective variables for the estimation of thermal demand from the perspective of user behaviour, which defines the pattern of demand. Time of day and days of the week (weekdays or weekends) are the two major parameters associated with the pattern of thermal consumption based on user level comfort.

The estimated parameters are subjected to identify the flexible operation of the thermal system based on demand, supply, capacity and energy prices. In this paper, for the estimation of thermal consumption in the residential area, thermal data associated with Fig. 5 are used.

3.1. Dependent variables for thermal demand estimation

Thermal demand is highly influenced by the environmental variable such as air temperature. Fig. 6(a) shows the hourly value of thermal demand and corresponding average external temperature of the environment. It shows that decrease in temperature increases thermal demand. Beside air temperature, cold air with high relative humidity increases the conduction of heat from the body in comparison to dry air with the same temperature. In order to incorporate the combined effect of relative humidity, wind and air temperature together, responsible for heat loss from a body, apparent temperature is considered. The apparent temperature is calculated using (1) and (2) [27]. Fig. 6(b) shows the hourly value of thermal demand and corresponding apparent temperature. The correlation coefficient of thermal demand with respect to external ambient temperature and apparent temperature, is -0.88 and -0.89 respectively.

$$AT = T_a + 0.33e - 0.7v - 4.00 \quad (1)$$

$$e = \frac{RH}{100} 6.105 \exp\left(\frac{17.27T_a}{237.7 + T_a}\right) \quad (2)$$

Where, AT = Apparent Temperature [$^{\circ}C$].
 T_a = Dry bulb temperature of external environment [$^{\circ}C$]
 e = water vapour pressure [hpa]
 v = wind speed [m/s]

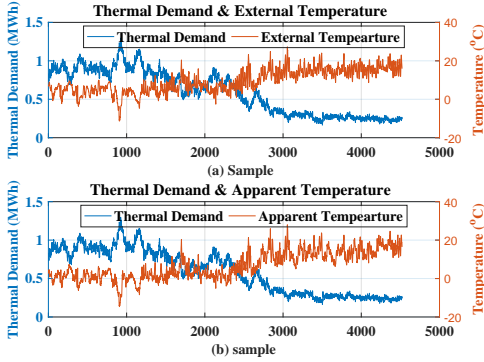


Fig 6. (a) Graph of thermal demand and external temperature; (b) thermal demand and apparent temperature

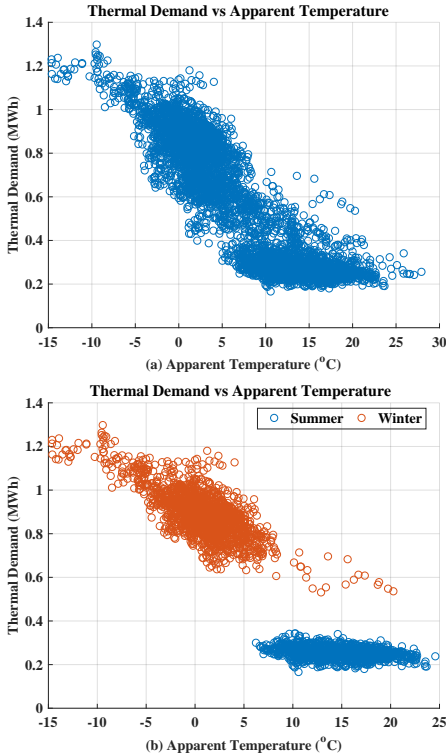


Fig 7. (a) Thermal demand vs apparent temperature throughout the period. (b) Thermal demand vs apparent temperature during winter and summer

RH = Relative humidity [%].

Fig. 7(a) shows the graph of apparent temperature vs thermal demand throughout the period of Dec 2016 to Aug 2017. Fig. 7(b) shows the distribution of thermal demand with re-

spect to apparent temperature during summer and winter only. It is clear from Fig. 7(b) that thermal demand during winter is inversely proportional to the apparent temperature. Whereas, during summer, proportional relationship between each other is very small. This could be due to the reason that apart from external temperature, thermal consumption is mostly for domestic purposes such as bathing, washing, space heating for toilet/bathroom, and transmission losses. Thus, it is logical to conclude that seasonal effect needs to be considered as input variable in the model for estimation.

The parameters for estimation of thermal loads in residential areas are based on factors such as user behaviour (hour, weekdays and weekends), and environmental condition (Apparent temperature and season).

3.2. Estimation technique of thermal demand

Different approaches to estimating thermal demand based on curve fitting technique such as the neural net fitting, and similar day method are considered as they are widely used. MATLAB inbuilt tools and functions are used for developing the estimation model using the neural net tool. Different scenarios based on the seasonal variations (summer and winter) are analysed.

For the neural net fitting tool, 50% of the seasonal data set are used for training, 25% for validating, and 25% for testing to develop the model. The datasets are divided randomly for training, testing, and validation of the model. After developing the model, 50% of the remaining seasonal data set are used in estimation.

For the similar day approach, the hourly data of a day is arranged according to season (summer and winter) and weekdays and weekends as shown in fig 8. 50% of each dataset (week-

Hour	Data Set							
	Summer				Winter			
	Weekdays		Weekend		Weekdays		Weekend	
1	[AT]	[QDHW]	[AT]	[QDHW]	[AT]	[QDHW]	[AT]	[QDHW]
2	[AT]	[QDHW]	[AT]	[QDHW]	[AT]	[QDHW]	[AT]	[QDHW]
3	[AT]	[QDHW]	[AT]	[QDHW]	[AT]	[QDHW]	[AT]	[QDHW]
...
...
...
...
...
24	[AT]	[QDHW]	[AT]	[QDHW]	[AT]	[QDHW]	[AT]	[QDHW]

Fig 8. Data set

days and weekends for summer and winter) are used as the historical data to build a euclidean distance (ED) for measure of similarity. In similar day method, it is assumed that the thermal demand is associated with apparent temperature (AT) for similar day (weekdays and weekends for summer or winter), and will result into similar thermal demand. EDs value based on recorded normalised AT (\hat{AT}) values at particular hour(h) of the day (d) are calculated for each and every historical similar days(d^i) using (3) [25]

$$ED(\hat{AT}, d, d^i) = \sum_{h=1}^{24} (\hat{AT}_h^{(d)} - \hat{AT}_h^{(d^i)})^2 \quad (3)$$

where, $ED(\hat{AT}, d, d^i)$ is the ED between day d and historical days d^i with respect to the value of \hat{AT} . Days with similar

pattern of AT will have very small values of ED, hence corresponding value of thermal demand is selected as the estimated value.

4. Electric Boiler and Stratified storage tank

Modelling of the hot water storage tank for the electric boiler (EB) is equally important to be able to analyze the flexibility in power to heat conversion with effective thermal demand and supply. A storage tank with stratified layers as shown in Fig. 9, has been well-defined in [28] based on the principle of conservation of energy in a control volume and surface. The detailed derivation of EB and storage tank presented here is suitably adapted to utilize flexibility in its synergy operation with the electricity network. Also, the single general equation is derived which is suitable for charging and discharging of the storage tank, with and without discharge of hot water from the tank.

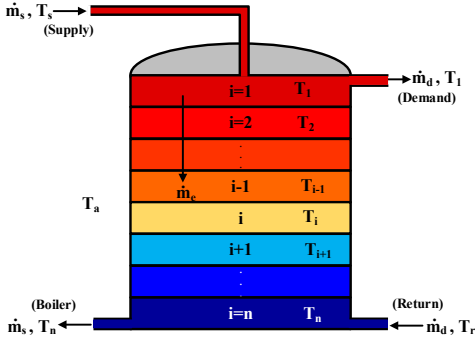


Fig 9. Stratification in hot water storage tank (b) energy flow in stratified layers

In Fig. 9, T_s = temperature of supply hot water in the tank [K]
 T_r = temperature of return water in the tank [K]
 T_a = temperature of ambient environment [K]
 T_i = temperature of i^{th} stratified layers, ($i=1,2,\dots,n$) [K]
 \dot{m}_e = effective mass flow between the stratified layer [kg/s]
 \dot{m}_s and \dot{m}_d are the inlet and demand mass flow [kg/s] of water from the heating source, and out of storage tank respectively.

4.1. modelling of EB and Storage tank

The EB is considered to be a constant impedance load [29] and is operated with constant power ($P_{r,b}$ = rated power of boiler [W]) as shown in (4). Here, $V_{r,b}$ and V_{poc} are rated voltage of boiler [V] and voltage at point of coupling of boiler into the grid [V] respectively. η is the efficiency of boiler [%] and \dot{Q}_{heat} is the heat flow rate of heating element [J/s]. C_w is the specific heat capacity of water [J/kg.K]. As per the manufacturer, the recommended flow of \dot{m}_s is produced at a $\Delta T = 10^\circ C$

($\Delta T = T_s - T_n$) with the EB on full power. However, the allowable maximum flow of \dot{m}_s is produced at $\Delta T = 5^\circ C$.

$$\dot{Q}_{heat} = \frac{\eta}{100} \left(\frac{V_{poc}}{V_{r,b}} \right)^2 P_{r,b} = \dot{m}_s C_w (T_s - T_n) \quad [W] \quad (4)$$

The energy flow in different layers of stratification is shown in Fig. 10. The amount of heat exchanged by the layer i of thickness z with the surrounding layers ($i-1$) and ($i+1$) of same thickness (z) and area (A_q) due to thermal conduction (\dot{Q}_{exc}) in vertical direction of the storage tank is calculated using (5) [28].

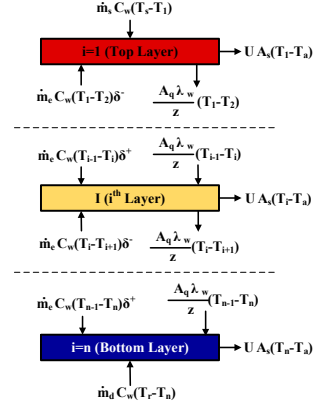


Fig 10. energy flow in stratified layers

$$\begin{aligned} \dot{Q}_{exc,i} &= \dot{Q}_{exc,i-1 \rightarrow i} - \dot{Q}_{exc,i \rightarrow i+1} \\ &= \frac{A_q \lambda_w}{z} (T_{i-1} - T_i) - \frac{A_q \lambda_w}{z} (T_i - T_{i+1}) \\ &= \frac{A_q \lambda_w}{z} (T_{i-1} + T_{i+1} - 2T_i) \end{aligned} \quad (5)$$

Where, λ_w = effective vertical heat conductivity of water (1–1.5 W/mK) [28]. \dot{Q}_{exc} is heat exchange due to natural convection and thermal conduction [W]. The effective mass flow of water between the stratified layer (\dot{m}_e) is given by (6).

$$\dot{m}_e = \dot{m}_s - \dot{m}_d \quad [kg/s] \quad (6)$$

Let, δ^+ (7) and δ^- (8) indicate an effective flow of water inside the storage tank from top to bottom or bottom to top respectively. $\delta^+ = 1$ represents that the heat transfer inside the storage tank due to the water mixing is from top to bottom (downwards). Similarly, $\delta^- = 1$ indicates that the heat transfer inside the storage tank due to the mixing of water is from bottom to top (upward).

$$\begin{aligned} \delta^+ &= 1 & \text{if } \dot{m}_e > 0 \\ &= 0 & \text{if } \dot{m}_e \leq 0 \end{aligned} \quad (7)$$

$$\begin{aligned} \delta^- &= 1 & \text{if } \dot{m}_e < 0 \\ &= 0 & \text{if } \dot{m}_e \geq 0 \end{aligned} \quad (8)$$

Let, $\delta_{(X)}$ be the conditional operator as defined in (9). $\delta_{(X)} = 1$ when conditions defined by X is true, else, $\delta_{(X)} = 0$

$$\delta_{(X)} = \begin{cases} 1 & \text{if } X = \text{True} \\ 0 & \text{if } X = \text{False} \end{cases} \quad (9)$$

A general equation for n stratified layers, considering $i = 1$ as the top layer and $i = n$ as the bottom layer, is derived and given by (10).

$$\begin{aligned} mC_w \frac{dT_i}{dt} = & \dot{m}_s C_w (T_s - T_i) \delta_{(i=1)} + \dot{m}_d C_w (T_r - T_n) \delta_{(i=n)} \\ & + \dot{m}_e C_w (T_{i-1} - T_i) \delta_{(i \neq 1)}^+ + \dot{m}_e C_w (T_i - T_{i+1}) \delta_{(i \neq n)}^- \\ & - U A_s (T_i - T_a) + \frac{A_d \lambda_w}{z} [(T_{i-1} - T_i) \delta_{(i \neq 1)} - (T_i - T_{i+1}) \delta_{(i \neq n)}] \end{aligned} \quad (10)$$

Here, U = overall heat transfer coefficient [$W/m^2.K$]

4.2. Model verification

The dynamic EB storage is verified based on three different scenarios as classified in table 1. These values are taken just to verify the model.

Table 1
EB storage model verification scenarios

Scenario	situation	\dot{m}_d	T_s	T_r
Scenario 1	Discharging	$10 - l/s$	-	$40^\circ C$
Scenario 2	Charging	$0 - l/s$	$80^\circ C$	-
Scenario 2	Charging and Discharging	$10 - l/s$	$80^\circ C$	$40^\circ C$

The technical parameters of EB and storage is presented in table 2. The temperature distribution for a 200-m^3 hot water storage tank with 10 stratified layers are shown in Fig. 11(a) for all three scenarios mentioned in table 1. Fig. 11(b) represents the EB status (ON/OFF) and discharge of hot water from the storage tank (l/s) corresponding to Fig. 11(a).

Scenario 1 represents the temperature dynamic in the storage tank subjected to discharge of hot water at a constant rate of $10 - l/s$ and the constant return temperature of cold water ($T_r = 40^\circ C$). Initially, the storage tank is fully charged and is filled with hot water with an initial temperature of all layers ($T_i(\text{ini})$) equal to $80^\circ C$. The temperature gradient of each layer is different and falls gradually until it reaches $40^\circ C$ and this situation is considered as a fully discharged storage tank. The temperature of the bottom layer drops rapidly compared to the adjacent top layer.

Scenario 2 represents the temperature dynamic in the storage tank subjected to charging with hot water from EB of power rating 2.4MW based on equation (4). The temperature of supply hot water is maintained constant at $T_s = 80^\circ C$. The discharge from the storage tank during this period is $0\text{-}l/s$. The temperature of each layer in the storage tank gradually increases until $T_{10} = 75^\circ C$, so that the allowable maximum flow from EB is not exceeded as discussed in section 4.1. The temperature of

Table 2
Technical Parameters of EB and Storage

Parameters	Definition	Value	Units
V	storage volume	200	$[m^3]$
n	number of stratified layers in storage tank	10	-
λ_w	effective heat conductivity of water	0.644	$[W/mK]$
U	heat transfer coeff. of the storage walls	0.12	$[W/m^2K]$
x	diameter to height ratio of storage	2.24	-
T_a	ambient Temperature	10	$[^\circ C]$
T_s	supply Temperature	80	$[^\circ C]$
T_r	return Temperature	40	$[^\circ C]$
P_b	Rated Power of EB	2.4	$[MW]$
C_w	specific heat capacity of water	4190	$[J/kg.K]$

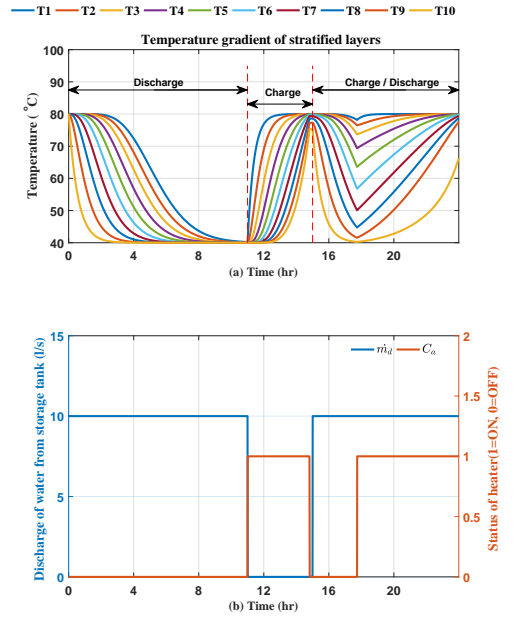


Fig 11. Temperature gradient of stratified layers (a) during discharge, charge, and charge-discharge of storage tank (b) discharge of water from the storage tank and status of the heater (ON/OFF)

the top layer increases quickly compared to the adjacent bottom layer.

Scenario 3 represents the temperature dynamic in the storage tank subjected to both charging and discharging process to re-

semble an actual scenario. Initially, the storage is fully charged. It is then discharged at the rate of 10-l/s with the heater turned off until the temperature of 7th layer is below 50 °C. Now, the heater is turned ON with discharge remaining 10-l/s from the storage tank. During this period, the temperature of water in different layers rises at a slower rate compared to charging without any discharge. The temperature of the bottom layer increases at a much slower rate compared to its adjacent top layer. Hence, the mode of EB storage tank defined by (10) is verified using these different scenarios.

5. Operation Schedule of EB for flexibility

In order to schedule the time of operation of the EB to charge the hot water storage tank, the optimization procedure given by (11) and (12) are followed. The objective function is to minimize the cost of electricity for production of hot water to meet the demand and storage needs. The constraints calculate the energy stored in storage tank and does not allow the storage tank to charge more than its allowable maximum and minimum limit. The energy extracted from the grid is either 0 (when EB is turned OFF) or is equal to the rated power of EB heater (P_b , when EB is turned ON). The energy extracted from the grid must be able to charge the storage as well as fulfil the demand. Although there are possibilities to control the EB power in several stages, the problem here is simplified with just ON and OFF in order to demonstrate the flexibility in operation of EBs under dynamic tariff conditions, with the help of estimated demand. Also, the operation of EB during peak hours in evening are restricted to minimise problems related to grid congestion and under voltage in Danish low voltage residential grid, due to integration and operation of electric boilers (EBs) [30]. The thermal energy stored in the tank at the end of the day is maximized to illustrate that storage tank is not only providing flexibility by supplying the thermal demand at the time of high electricity price and peak electricity demand, but also stores energy during the period of low electricity price during the 24 hour period of spot price in the electricity market.

$$\text{Minimize} \quad \sum_{t=1}^{24} C_t P_{g,t} \quad (11)$$

Constraints

$$\begin{aligned} S_{t+1} &= S_t - Q_{DHW,t} + P_{g,t} \\ S_{min} &\leq S_t \leq S_{max} \\ P_{g,t} &\in [0, P_b \Delta t] \\ P_{g,t} &= 0 \text{ for } 17 \leq t \leq 20 \\ (S_{max} - P_b \Delta t) &\leq S_t \leq S_{max} \text{ for } t = 24 \end{aligned} \quad (12)$$

Here,

C = energy price [EUR/MWh]

P_g = energy extracted from the grid [MWh]

S = energy that can be extracted from storage [MWh]

Q_{DHW} = thermal demand [MWh]

P_b = rated power of EB [2.4 MW]

subscripts: t = time [hr], min = minimum, max = maximum,

ini = initial value.

The maximum energy that can be stored in hot water storage tank is given by (13)

$$S_{max} = M_b C_w (T_s - T_r) / (3600 \times 10^6) \quad [MWh] \quad (13)$$

$$S_{min} = 0.4 \times S_{max} \quad [MWh] \quad (14)$$

Here,

M_b = Mass of water in storage [2×10^5 kg]

T_s = temperature of supply hot water in the tank [80°C]

T_r = temperature of return water in the tank [40°C]

C_w = specific heat capacity of water [4190 J/kg.K]

The optimization problem was solved by minimizing the cost function using brute force optimization in Matlab. All possible candidates for the solutions are generated and then checked against the satisfaction of problem statement as given in (11) and (12). The solutions were verified using "PuLP", linear programming modeller written in python.

5.1. Control of EB

The optimized schedule for operation of the EB is determined based on the estimated thermal demand. On the other hand, the actual thermal demand would vary to some extent compared to the estimated value. This leads to an estimation error. In case the error is large, it can lead storage tank temperature to be away from the specified limit ($T_{10} \leq 75^\circ\text{C}$ when storage is charged and $T_7 \geq 46^\circ\text{C}$ to limit storage discharge up to 70% of its capacity). Thus, in order to compensate for the large error in estimated demand with respect to the actual value, the optimized schedule for operation of EB is reinforced with limit controllers based on hysteresis control, realized with RS flipflop, to turn ON/OFF EB as shown in Fig. 12. This ensures that the temperature of hot water in the storage tank is within the specified limit.

Fig. 12(a) shows that, when the temperature of bottom layer $T_{10} \geq 75^\circ\text{C}$ the EB needs to be turned OFF as discussed in section 4.1. It is turned OFF only for a short period until the temperature of the seventh layer (T_7) is less than 78°C , so that it can further follow the schedule. Fig. 12(b) ensures that if $T_7 < 46^\circ\text{C}$ (storage is discharged more than 70% of its capacity), EB is turned ON until it is fully charged (i.e., $T_{10} \geq 75^\circ\text{C}$). Apart from these two conditions, the EB is operated as per the determined schedule. The overall control strategy is shown in table 3, where C_a is the Control signal for turning ON and OFF of EB and C_{a1} is the signal from scheduled ON/OFF of EB.

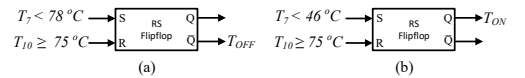


Fig 12. limit controller schematic for ON/OFF operation of EB

Table 3
Control of EB

T_{OFF}	T_{ON}	C_a
1	x	0
x	1	1
0	0	C_{a1}

6. Result and discussion

6.1. Thermal demand estimation

Fig. 13(a) and (b) shows the estimated vs actual demand and associated %error in estimation using the neural net fitting tool are presented respectively. The range of %error associated with the neural net tool is lower than for the similar day method.

13(c) presents the histogram of %error normalized with the frequency of occurrence as well as the probability density function. The normal distribution of %error is well-defined with the mean and standard deviation of error as well as its deviation from the mean. Finally, the average value of estimated data and actual data are compared with respect to time of day, weekdays and weekend in Fig. 13(d). The estimated data closely follow the trend and pattern associated with thermal demand.

Similar analysis has been conducted for a similar day method and is presented in Fig. 14. The range of percentage error between estimated and actual value(Fig. 14(b1,b2)) is higher than with the neural net fitting tool. However, with less number of the dataset, similar day approach is equally reliable as a neural net fitting tool.

Table 4 summarises the results of different methods of esti-

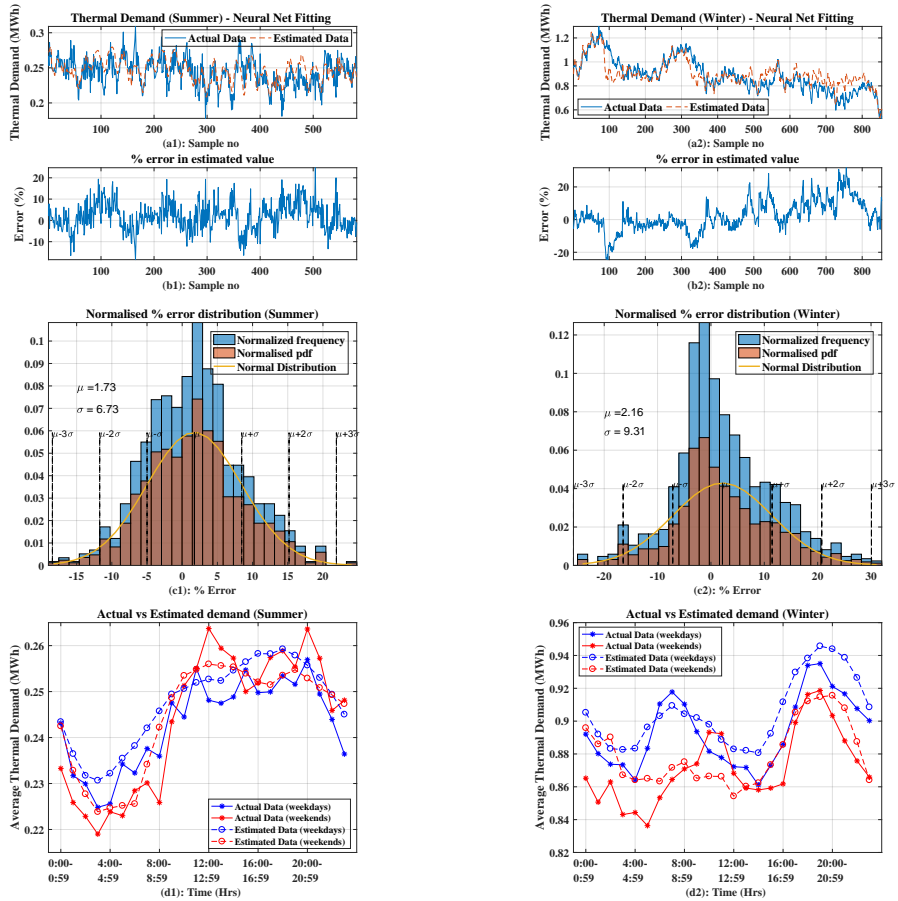


Fig 13. Forecasting of thermal demand using neural net fitting tool for summer and winter.

Row a: actual data and estimated data

Row b: % error associated with estimation of thermal demand

Row c: histogram of %error and its normal distribution

Row d: Analysis of average thermal demand (actual and estimated) in hourly basis for different weekdays and weekends

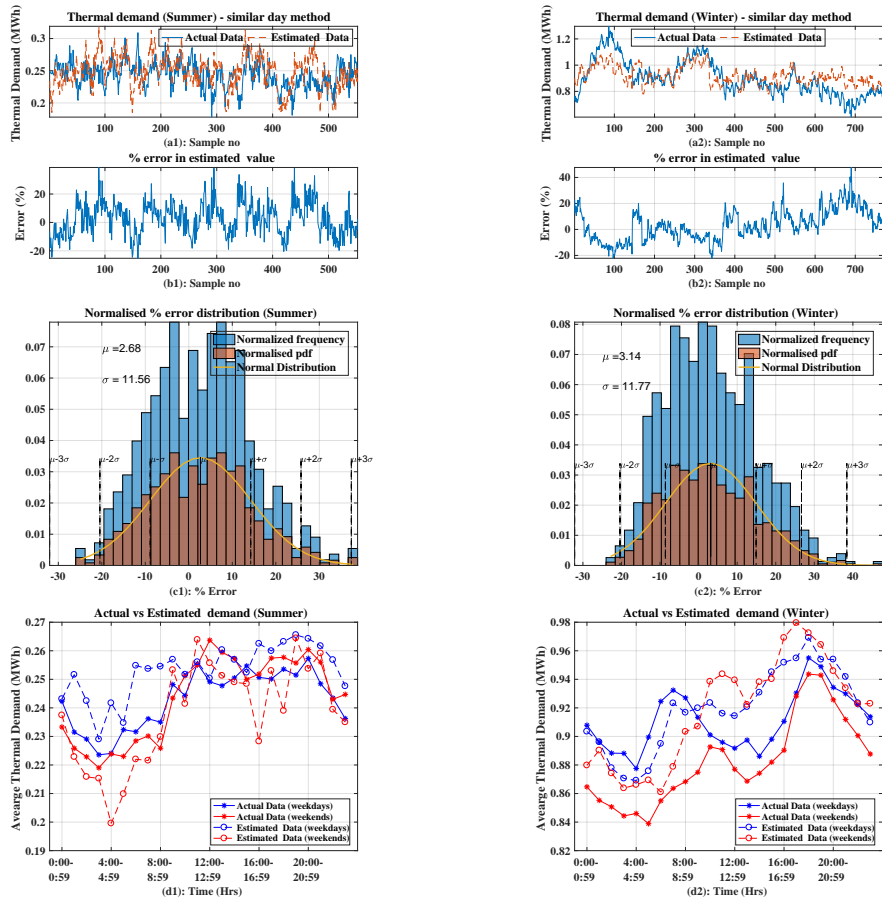


Fig 14. Estimation of thermal demand using similar day method for summer and winter .

Row a: actual data and estimated data

Row b: % error associated with prediction of thermal demand

Row c: histogram of %error and its normal distribution

Row d: Analysis of average thermal demand (actual and estimated) in hourly basis for different weekdays and weekends

Table 4

Errors from thermal demand estimations

	Neural Network		Similar Day	
	Summer	Winter	Summer	Winter
MAPE	5.459	7.30	9.57	9.72
RMSE	0.016	0.08	0.028	0.103
Mean (μ) %error	1.73	2.16	2.68	3.14
Std.Dev (σ)	6.73	9.31	11.56	11.77

mation. Root mean square error (RMSE) is used to measure the difference between the estimated value by a model and the actual values observed. Mean absolute percentage error (MAPE) estimates how close estimated values are to actual values in percentage.

Results in Fig. 13 and Fig. 14 shows that the knowledge of apparent temperature, (which includes the effect of wind, relative humidity, water vapour pressure, and ambient temperature) along with the user pattern behaviour is good enough for the estimation of thermal demand, for both summer and winter season, without considering user behaviour and geometry of the building. The consumption pattern of thermal demand with peaks and valley are well preserved with estimated demand as seen in Fig. 13(d1-d2) and Fig. 14(d1-d2). This pattern is due to training of estimation tool based on parameters such as time, day and season as well. However, the error in the magnitude of estimated demand is expected from the thermal components that are not much dependent on the external temperature, eg., domestic hot water usage. Using a thermal storage tank, error in estimated demand is well compensated.

Results of thermal demand estimation using a curve fitting technique based on neural net fitting are compared with the results from time series estimation, in existing literature, based on estimation errors. Errors in the estimated value using the neural net fitting tool for winter season ranges between -23 to 31 whereas, in [21] it ranges from -33 to 15 (with 10% less range) with use of time series ANN. Further, the MAPE for 24hrs ahead forecast according to [22] is 7.28% for winter which is similar to 7.3% during winter using neural net fitting as discussed here. Also, in [24] the MAPE errors for different machine learning technique and for different area varies between 5-27%. Hence, the curve fitting techniques discussed here is a well effective and simple estimation tool for thermal demand estimation using AT and hourly pattern with respect to weekdays and seasons.

6.2. Flexible operation of electric boiler

One of the important applications of deploying thermal demand estimation is to prepare an algorithm for energy management, to support the future smart grid system. An example of scheduling thermal storage under dynamic tariff condition is introduced in [31] with an average model of the storage tank. Here, a time series based concept for thermal demand forecast and the schedule is proposed for heat pumps without considering ON/OFF delay for thermal production. It usually takes around 10-15 minutes to achieve a steady state condition [32]. In [30] the models of EB and HP with a storage tank having only two stratified layers, are briefly discussed in relation to the actual control and flexibility based on grid condition and status of storage tank temperature or position of the stratified layer.

The EB with a n-stratified layered storage tank as modelled in section 4 is used to acknowledge its operational flexibility. The optimal schedule of the EB is based on estimated thermal demand using the curve fitting technique. The temperature of hot water inside the storage tank at different layers (1,7 and 10 as in Fig. 9) gives the indication of flexibility performance of the storage tank to be able to supply the demand. The operational flexibility in terms of ON and OFF of the EB under dynamic tariff conditions based on estimated thermal demand is presented in this section. The storage is never scheduled to discharged more than up to 40% of its maximum capacity in order to accommodate substantial error in the estimation of thermal demand. Fig. 15 shows the complete system methodology implemented for flexible operation of the EB. Thermal demand estimation and optimized schedule for operation of EB are determined using Matlab. Then the flexibility in the operation of the EB is verified using DigSILENT power factory simulation tool.

Fig. 16(a) shows the day-ahead hourly spot price of Denmark's northern region for case 1: 6th Jan 2017 [33]. On this particular day, the price seems to be decreasing gradually according to the time of the day. Sometimes the prices even go to negative as on case 2: 24th Dec 2016 [33]. This is because of the high electricity generation from renewable sources such as wind or solar. With an optimization problem to reduce energy cost, it is obviously beneficial to turn ON the boiler during low electricity price to store thermal energy.

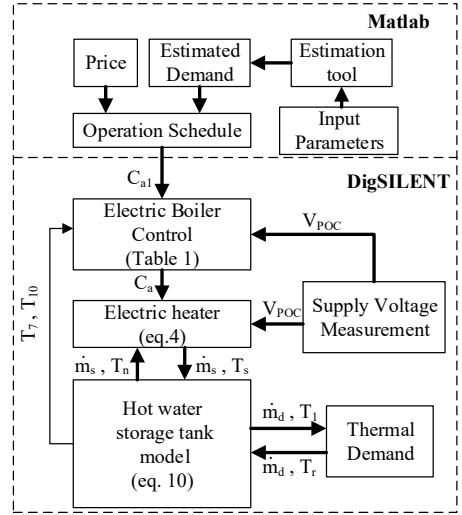


Fig 15. System implementation for flexible operation of EB

Fig. 16(b) shows the estimated thermal demand based on the neural network on 6th Jan 2017 and is compared with actual demand on the same day. Here, the MAPE error is significantly less compared to other days estimation. Based on the estimated thermal demand, the optimal schedule of EB, as well as thermal energy storage status, is determined (0= fully discharged, 1= fully charged) to avoid higher price and time of peak electrical demand as shown in Fig. 16(c) for case 1. Using this schedule for operation of the EB with actual demand, the storage temperature is monitored in Fig. 16(d). It is observed from Fig. 16(c) that the controller (C_a) follows the estimated schedule (C_{a1}). The actual EB status (AS_{status}) is also closer to estimated value (PS_{status}). A similar observation is made for case 2 as well. The storage temperature of the top layer confirms that demand has been fulfilled taking care of grid flexibility and end-user satisfaction. The storage tanks are charged when the electricity price is lower as seen from case 1 and case 2, where spot pricing is different whereas demand remains the same for both cases.

Similarly, Fig. 17(a) shows the electricity price of 23rd Mar 2017. Here, the estimated value of thermal demand has the maximum forecasting error as seen in Fig. 17(b). Estimated EB schedule (C_{a1}) along with the controller action (C_a) is shown in Fig. 17(c). The controller turns OFF the EB twice during, 6th and 24th hour as the storage tank is fully charged as seen in Fig. 17(d). This is due to the over estimation of thermal demand. The temperature of the hot water as seen from Fig. 17(d) indicates that storage has been fully charged and heating element needs to be shut down.

The knowledge of apparent temperature, and hourly pattern of thermal consumption during weekdays or weekends has helped the estimation tool to estimate the thermal demand ef-

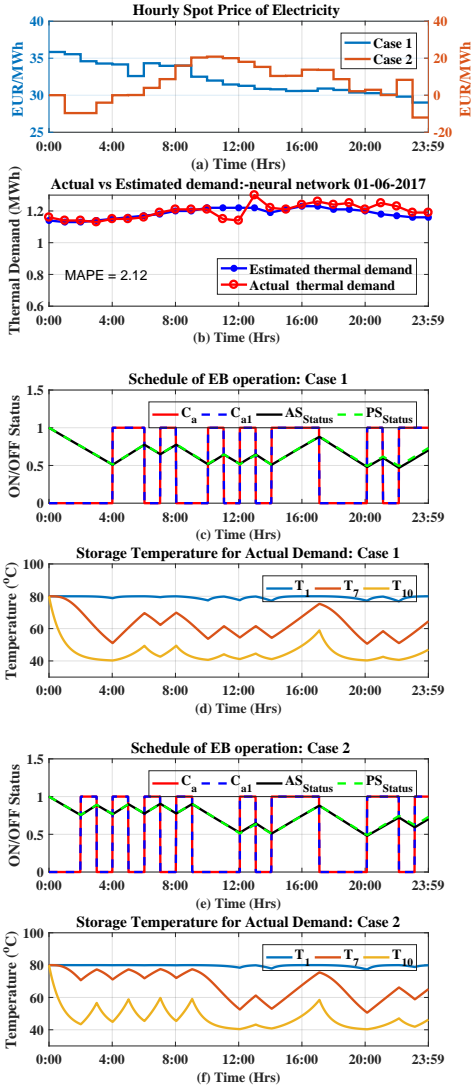


Fig 16. (a) Hourly spot prices of electricity in Denmark region DK1 case 1: 6th Jan 2017 and case 2: 24th Dec. 2016 (b) Actual and estimated thermal demand on 6th Jan 2017 (c) estimated EB schedule based on estimated demand (C_{a1}), estimated EB status (PS_{status}), and actual schedule of EB based on actual demand (C_a), and actual EB status (AS_{status}) (case 1). (d) Storage temperature of various layers for actual demand and schedule (case 1). (e) estimated EB schedule based on estimated demand (C_{a1}), estimated EB status (PS_{status}), and actual schedule of EB based on actual demand (C_a), and actual EB status (AS_{status}) (case 2). (f) Storage temperature of various layers for actual demand and schedule (case 2).

fectively. The estimation of thermal demand has supported immensely in the decision-making process to schedule flexible operation of the EB in the multi-energy system, where en-

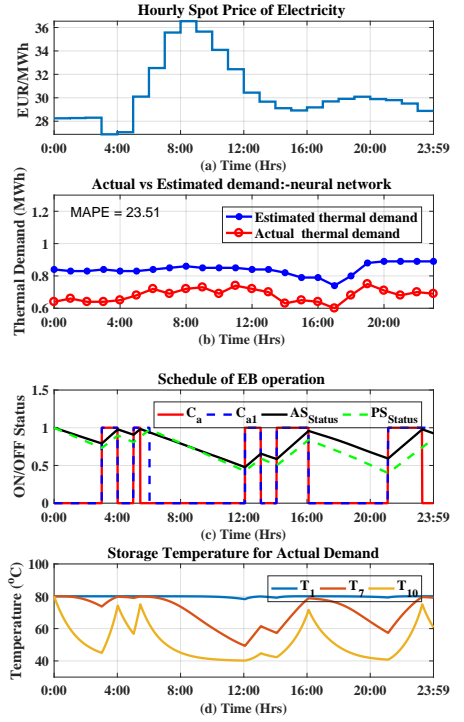


Fig 17. (a) Spot price of electricity in Denmark region DK1 on 23rd Mar. 2017 (b) Actual and estimated thermal demand on 23rd Mar (c) estimated EB schedule based on estimated demand (C_{a1}), estimated EB status (PS_{status}), and actual schedule of EB based on actual demand (C_a), and actual EB status (AS_{status}) (d) Storage temperature of various layers for actual demand and schedule

ergy prices are lower during high generation from renewable sources such as solar and wind. Despite a substantial error in estimation, the thermal storage has the capability of operating as a flexible load by decoupling demand and generation, and enhancing accommodation of renewable energy. The energy in the storage tank tries to attain at its best status to fulfil evening thermal peak demand, as well as avoid EB operation to support peak shaping during high electricity demand in the evening. The temperature of the top bottom and middle layer of stratified hot water storage tank indicates that the thermal demand is fulfilled by maintaining operational flexibility. The use of stratified layered storage tank has the advantage over average temperature model of storage tank, as an average model is not able to illustrate the actual condition of supply temperature which regulates the flow of hot water from the EB to storage tank while charging process and monitor the status of storage tank as realized in practice.

7. Conclusion

This paper shows insight on the daily usage pattern of the thermal energy, during summer and winter, in a residential area along with the factors influencing the estimation of thermal demand such as user behaviour parameters and external environment parameters. Based on these factors, the neural network model and the similar day method for estimation has been implemented. Using this model, estimation of thermal usage for the same area can be achieved, but not for other areas. So, an already available model is unlikely to be used for new subjects. However, the findings of this paper on the use of input parameters for determining the thermal demand of a particular area and its influence on the pattern of usage has been justified.

The findings of the data analysis of thermal consumption (Q_{DHW}) yields some important conclusions on the pattern of energy demand based on time and day of usage reflecting user behaviour without compromising the privacy issue of individuals. This valuable information is useful for determining the generation of thermal demand and need for storage. When large CHP units are replaced by small heat pumps or electric boilers and integrated to the electric grid network, it will increase the electricity demand with the profile discussed in Fig.4. Thus, during off-peak hours, when electricity demand is low, the thermal storage unit can be used to store the surplus electricity generated by wind turbines and other renewable generation. This storage of thermal power can be utilized during its peak hours reducing greenhouse emission on the production of hot water. Further, the estimated value of thermal demand helps in determining the range of requirement of thermal storage to meet the consumer demand as well as demand response to utilizing thermal storage unit as flexible consumer load in the multi-energy system.

Acknowledgement

This work is supported by the Innovation fund Denmark through the Dicyps project. The data for the analysis has been provided by Aalborg Energi Holding A/S and Aalborg University, Denmark, as per the agreement between project partners for research.

References

- [1] Regulation and planning of district heating in denmark, Tech. rep., Danish Energy Agency (DEA) (2015).
- [2] H. Lund, S. Werner, R. Wiltshire, S. Svendsen, J. E. Thorsen, F. Hvelplund, B. V. Mathiesen, 4th generation district heating (4gdh): Integrating smart thermal grids into future sustainable energy systems, *Energy* 68 (2014) 1 – 11.
- [3] Smart grid strategy-the intelligent energy system of the future, Tech. rep., Danish Ministry of Climate, Energy and Building (2013).
- [4] H. Lund, Renewable heating strategies and their consequences for storage and grid infrastructures comparing a smart grid to a smart energy systems approach, *Energy* 151 (2018) 94 – 102.
- [5] T. Nuytten, B. Claessens, K. Paredis, J. V. Bael, D. Six, Flexibility of a combined heat and power system with thermal energy storage for district heating, *Applied Energy* 104 (2013) 583 – 591.
- [6] T. Korpela, J. Kaivosoja, Y. Majanne, L. Laakkonen, M. Nurmoranta, M. Vilko, Utilization of district heating networks to provide flexibility in chp production, *Energy Procedia* 116 (2017) 310 – 319, 15th International Symposium on District Heating and Cooling, DHC15-2016, 4-7 September 2016, Seoul, South Korea.
- [7] K. Skytte, O. J. Olsen, Regulatory barriers for flexible coupling of the nordic power and district heating markets, in: 2016 13th International Conference on the European Energy Market (EEM), 2016, pp. 1–5.
- [8] T. Nuytten, B. Claessens, K. Paredis, J. V. Bael, D. Six, Flexibility of a combined heat and power system with thermal energy storage for district heating, *Applied Energy* 104 (2013) 583 – 591.
- [9] J. Pospíšil, M. Špiláček, L. Kudela, Potential of predictive control for improvement of seasonal coefficient of performance of air source heat pump in central european climate zone, *Energy* 154 (2018) 415 – 423.
- [10] I. Vorushylo, P. Keatley, N. Shah, R. Green, N. Hewitt, How heat pumps and thermal energy storage can be used to manage wind power: A study of ireland, *Energy* 157 (2018) 539 – 549.
- [11] G. Schweiger, J. Rantzer, K. Ericsson, P. Lauenburg, The potential of power-to-heat in swedish district heating systems, *Energy* 137 (2017) 661 – 669.
- [12] D. Böttger, M. Götz, M. Theofilidi, T. Bruckner, Control power provision with power-to-heat plants in systems with high shares of renewable energy sources – an illustrative analysis for germany based on the use of electric boilers in district heating grids, *Energy* 82 (2015) 157 – 167.
- [13] N. Fitzgerald, A. M. Foley, E. McKeogh, Integrating wind power using intelligent electric water heating, *Energy* 48 (1) (2012) 135 – 143, 6th Dubrovnik Conference on Sustainable Development of Energy Water and Environmental Systems, SDEWES 2011.
- [14] K. Kontu, S. Rinne, S. Junnila, Introducing modern heat pumps to existing district heating systems – global lessons from viable decarbonizing of district heating in finland, *Energy* 166 (2018) 862 – 870.
- [15] R. Sinha, B. B. Jensen, J. R. Pillai, Impact assessment of electric boilers in low voltage distribution network, in: accepted for publication in 2018 IEEE PES General Meeting, 2018, pp. 1–6.
- [16] I. D. d. C. Mendaza, A. Pigazo, B. Bak-Jensen, Z. Chen, Generation of domestic hot water, space heating and driving pattern profiles for integration analysis of active loads in low voltage grids, in: IEEE PES ISGT Europe 2013, 2013, pp. 1–5.
- [17] C. Weissmann, T. Hong, C.-A. Graubner, Analysis of heating load diversity in german residential districts and implications for the application in district heating systems, *Energy and Buildings* 139 (2017) 302 – 313.
- [18] U. Jordan, K. Vajen, Dhwcac: program to generate domestic hot water profiles with statistical means for user defined conditions, in: Proceedings ISES Solar World Congress, Orlando, 2005, pp. 8.–12.8.
- [19] S. Clegg, P. Mancarella, Integrated electricity-heat-gas modelling and assessment, with applications to the great britain system. part i: High-resolution spatial and temporal heat demand modelling, *Energy*.
- [20] K. Wojdyga, Predicting heat demand for a district heating systems, *International Journal of Energy and Power Engineering* 3 (5) (2014) 237–244.
- [21] R. Petrichenko, K. Baltputnis, A. Sauhats, D. Sobolevsky, District heating demand short-term forecasting, in: 2017 IEEE International Conference on Environment and Electrical Engineering and 2017 IEEE Industrial and Commercial Power Systems Europe (EEEIC / I CPS Europe), 2017, pp. 1–5.
- [22] B. Chramcov, Heat demand forecasting for concrete district heating system, *International Journal Mathematical Models and Methods in Applied Sciences* 4 (4) (2010) 231–239.
- [23] D.-S. Kapetanakis, E. Mangina, E. H. Ridouane, K. Kouramas, D. Finn, Selection of input variables for a thermal load prediction model, *Energy Procedia* 78 (2015) 3001 – 3006, 6th International Building Physics Conference, IBPC 2015.
- [24] S. Idowu, S. Saguna, C. Åhlund, O. Schelén, Forecasting heat load for smart district heating systems: A machine learning approach, in: 2014 IEEE International Conference on Smart Grid Communications (Smart-GridComm), 2014, pp. 554–559.
- [25] Y. Zhang, M. Beaudin, R. Taheri, H. Zareipour, D. Wood, Day-ahead power output forecasting for small-scale solar photovoltaic electricity generators, *IEEE Transactions on Smart Grid* 6 (5) (2015) 2253–2262.
- [26] H. Chitsaz, H. Shaker, H. Zareipour, D. Wood, N. Amjady, Short-term electricity load forecasting of buildings in microgrids, *Energy and Buildings* 99 (2015) 50 – 60.

- [27] Australian Government Bureau of Meteorology, accessed on 15-Feb-2018.
URL http://www.bom.gov.au/info/thermal_stress/
- [28] U. Eicker, Solar Technologies for Buildings, John Wiley & Sons, 2006.
- [29] R. Sinha, B. B. Jensen, J. R. Pillai, C. Bojesen, B. Moller-Jensen, Modelling of hot water storage tank for electric grid integration and demand response control, in: 2017 52nd International Universities Power Engineering Conference (UPEC), 2017, pp. 1–6.
- [30] R. Sinha, B. B. Jensen, J. R. Pillai, B. Moller-Jensen, Unleashing flexibility from electric boilers and heat pumps in danish residential distribution network, in: Accepted in: Proceedings CIGRE 2018, Paris, 2018.
- [31] H. Harb, T. Schutz, R. Streblow, D. Muller, Adaptive model for thermal demand forecast in residential buildings, Proceedings of WSB.
- [32] T. Masuta, A. Yokoyama, Y. Tada, Modeling of a number of heat pump water heaters as control equipment for load frequency control in power systems, in: 2011 IEEE Trondheim PowerTech, 2011, pp. 1–7.
- [33] NordPool, accessed on 06-Jun-2017.
URL <https://www.nordpoolgroup.com/Market-data1/Dayahead/Area-Prices/DK/Hourly/?view=table>

Journal J3

Operational flexibility of electrified transport and
thermal units in distribution grid

R. Sinha, B. Bak-Jensen, and J. R. Pillai

The paper has been submitted for peer review in the
International Journal of Electrical Power & Energy Systems Vol. XX(X),
pp. XXX–XXX, 2019.

© 201X IEEE

The layout has been revised.

Operational flexibility of electrified transport and thermal units in distribution grid

Rakesh Sinha^a, Birgitte Bak-Jensen^b, Jayakrishnan Radhakrishna Pillai^c

^aDepartment of Energy Technology, Aalborg University, Denmark, e-mail: ras@et.aau.dk

^bDepartment of Energy Technology, Aalborg University, Denmark, e-mail: bbj@et.aau.dk

^cDepartment of Energy Technology, Aalborg University, Denmark, e-mail: jrp@et.aau.dk

Abstract

An autonomous control system is proposed in this paper to assess the potential flexibility from thermal units (eg heat pumps and storages) and electric vehicles (EV) charging systems, in the low voltage distribution network as a multi-energy system. Each thermal system and EV charging has its respective controller. The proposed control technique manages to successfully operate and control the thermal units and EVs charging system within the recommended operating limits of grid voltage, by sharing flexibility within the specific network integrated with multi-carrier energy systems. It has the capability of sensing local key control parameters like node voltage, state of charge of EV, temperature and level of hot water in the storage tank. These control parameters allow scheduling, re-scheduling, and decision making on the operation of individual thermal and EV charging unit with operational priorities. This enhances the sharing of flexibility for proper coordination, control, and management of thermal and EV charging systems in low voltage (LV) distribution networks with mutual technical benefits. From the results, the application of the proposed control architecture is found to be effective to manage grid congestions and local voltage control, satisfying the thermal energy requirements of the customer as well as charging needs of EV.

Keywords: Multi Energy System, Electric Vehicles, Heat Pumps, Thermal Storage, Distribution Grid, Flexibility, Operation and Control

1. Introduction

Flexibility benefits to the power system with the integration to the heating and transport impose a cost-effective solution towards zero-carbon emission [1]. Electric vehicles (EVs) and heat pumps (HPs) offer potential flexibility in a peak shaping in demand and price profiles [2]. The ability of EVs and HPs as a controllable load to suppress the frequency fluctuation in the power system with large integration of renewable is explored in [3] [4]. Flexibility service, concerning power balance and electricity prices, from EVs and HPs for real-time congestion management, is investigated in [5] for congestion management at the distribution level.

To limit the need for grid reinforcement, demand response concept is increasing. The decentralized participation of EVs and HPs as flexible demand in the electricity market is well-explored in [2]. A hierarchical structure for controlling demand response of the LV grid integrated with EV and HP is introduced in [6] to maximize the grid utilization to accommodate high share of EV and HP, without the need of grid reinforcement. Studies in intelligent active demand response from the end consumer units like EV and HP is performed in [7] with the concept of centralized control. All of these concepts ultimately requires a communication infrastructure to operate and handle data. Use of local adaptive controller to adjust active and reactive power of thermal and photovoltaic in LV network is explored in [8], with specific reference parameter based on terminal voltage, for the individual controller at each node in the network. It requires the frequent update of reference pa-

rameters based on increment in new loads. Implementation of voltage regulation at the point of use using individual power electronics devices for all loads in a building is investigated in [9], where power quality suffers as well as the cost of implementation increases.

The significant contribution of this study is to develop and implement adaptive ON/OFF control strategies to EVs and HPs for real-time grid support with the use of an autonomous controller. The impact assessment of the LV grid upon the integration of the HPs and EVs are also evaluated. The ON/OFF control of HPs is studied in [10]. However, there are modifications in the implementation of ON/OFF delay, concerning use and parameters, upon introduction of EVs for proper coordination between EVs and HPs to utilize more flexibility in terms of grid utilisation. All the appropriate assumptions made are based on the analysis of available data. The rule-based decision-making approach is implemented where proper communication infrastructure is not required as in optimisation based technique. The reference parameter settings for the EV and HP controller is uniform throughout the network. The EV controller is also able to determine the charging time of EV based on the state-of-charge (SOC) of the EV battery. The controller is autonomous as there is no proper communication channel between any EV or HP controllers. The controller is adaptive and flexible as it is able to shift the operating time of the individual device (EV or HP) connected to it based on the measurement of local parameters such as the terminal voltage (V_t) at the point of coupling, SOC, level of cold water (X_c) and temperature of hot water

(T_{hot}) in the thermal storage tank. These local parameters determine the operational priority by introduction ON/OFF delays. Thus sharing of flexibility among the devices is possible.

Section 2 presents the state of art. The analysis of EV driving pattern and generation of the depth-of-discharge (DOD) of EV batteries based on driving distance is demonstrated in section 3. A brief overview of the modelling of EV and HP with storage is highlighted in section 4. Integration scenario of EV and HP in LV Network is represented in 5. The charging management of EV is discussed in 6. Section 7 introduces to the concept of ON/OFF control for EV and HP, with verification of the control system. The result of steady-state power simulation with EV and HP in the LV network is explored and presented with the discussion in section 8. Finally, the paper is concluded with discussion in section 9

2. System Framework

Fig. 1 shows the complete architecture of the proposed system. There are three types of loads connected to the LV distribution grid: Residential baseload, EV and HP. EVs and HPs provide flexibility in its operation based on the performance of the respective ON/OFF controller. Based on SOC, EVs are prioritized and their charging slots are determined, as a result, EVs loads are distributed over a period. On the other hand, HPs are prioritized based on T_{hot} and X_c to ensure thermal demand is met. Finally, based on V_t , ON/OFF delays are introduced. Lower turn ON delay for lower V_t and higher turn-OFF delay for lower V_t prioritize devices at the far end of a radial feeder to operate first. On the other hand, higher turn ON delay and lower turn OFF delay of EV over HP provides EV with the highest priority to turn ON and operate.

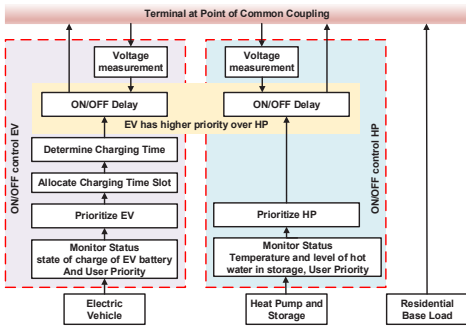


Fig 1. System Architecture

3. Analysis and Generation of Driving pattern

3.1. Analysis of the Driving pattern of Car

Analysis of driving pattern is necessary to determine the energy status of EVs' battery and to establish the proper charging management as proposed in section 7. Upon exceeding the travelling distance, between origin and destination, more than

4 and 8 km for walking and biking respectively, car or public transportation is preferred due to benefit in terms of comfort and travel time. For long distances, the choice of transportation can be public as travellers can be more relaxed. Trip distances of 500-750m hold equal shares of people walking, biking and driving. For approx. 8 km and exceeding, the choice of the car remains relatively stable between 60-70% [11]. The average and standard deviation of the distance between origin and destination for a passenger car is 15.89km and 28.81km respectively [11]. However, the average travel distance per day is 39.5km in 2014 as per [12] with 3 trips per day on average. Also, around 70% of vehicles are connected for charging only once a day [13], and 65% of EVs are fully charged during the first connection. This situation is true when there is not enough infrastructure developed for charging EVs at parking places except than their residences, where start charging time varies. Though people are travelling alone for a shorter distance, sharing is higher for a distance of more than 40 km travel [11]. Thus, the Discharge of the battery would be higher.

Apart from the driving pattern, several other factors affect the SOC of EV batteries such as the number of passenger in the car, driving habits, user comfort level, battery efficiency, weather conditions (hot/cold), and vehicles type or model. This suggests that for the same distance travelled, SOC of different vehicles will be different. This difference in SOC can be taken into an advantage for allocating delay time to charge EV.

3.2. Generation of Driving Distance and SOC

It is assumed in the study that all houses have one EV. Driving distance data from Danish national travel survey were used to generate driving distance. Data from distance travelled in a single trip is taken from [14]. The maximum distance travelled is taken to be 80km as there are a negligible amount of cars travelling a longer distance. Random numbers are generated for each interval of distances, with the average distance travelled in a single trip to be 15km and a standard deviation of 18km. Generated data is comparable with analysis from [11] where average distance travelled by a car driver and car passenger is 12.7km and 15.89km respectively with the standard deviation of 21.85 and 28.81km respectively. The energy consumed by EV for the generated driving distances is calculated by considering 1.4kWh of energy consumption per 10km distance [14].

The DOD of EV is calculated by considering a 24kWh battery size. Driving characteristics determined with experiment in [15] shows that moderate driving consumes 39% of available SOC whereas, aggressive driving consumes 57% (which is 46% more than that during moderate driving). Hence, the random increment of 0-46% in DOD is added to generate the DOD of EV in this study. Since people travel at least twice (origin to destination and destination to origin), the generated DOD is multiplied by 2. If the DOD is more than 80% with 24kWh battery sizes, EVs with 60kWh battery sizes are considered and their DOD is recalculated. EVs are randomly distributed in 164 houses in the test grid and their SOC at the time of connection to charging point are shown in Fig 2. It shows that SOC of EVs

is scattered with the majority between 90-100%. there are only very few vehicles with SOC less than 50%

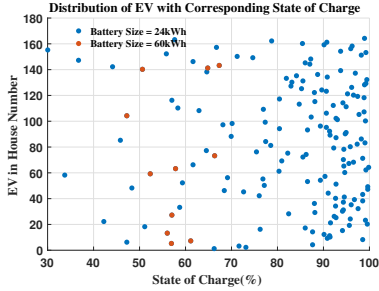


Fig 2. State of Charge in EVs battery when connected for charging

[16] suggests that, 7:00-8:00 hrs is the most common time to start the first trip of the day and 15:00-16:00 hrs the last one. This considers only two trips (home-work-home). [17] suggests that availability of EV at residences is greater than 94% from 16:45hrs. Thus, for simplicity, the time of arrival of EV is randomly distributed between the period of 15:30 to 16:45 with a time resolution of 15min. This suggests that 100% of EV is available for charging after 16:45.

4. Modelling of EV and HP

4.0.1. Modelling of EV

The EV is modelled as a battery with a suitable capacity to represent electrical energy flow during travel and charging process from the electrical grid. According to the analysis of driving pattern as presented in section 3 the total energy dissipated from the EV battery by the time of charging is determined. The state of charge (SOC) of the battery is defined as in (1). The SOC of Battery at any instant of time is calculated using (2).

$$SOC = \frac{\text{Remaining Capacity [Ah]}}{\text{Rated Capacity [Ah]}} \quad [\%] \quad (1)$$

$$SOC_t = SOC_{t_0} + \frac{100}{\text{Rated Capacity[kWh]}} \int_{t_0}^t P_{cb}(\tau) d\tau \quad (2)$$

Here, SOC_{t_0} is the initial SOC(%) at time t_0 when EV is connected for charging, and SOC_t is the SOC(%) at any time t . The integral period t_0 to t is in hours. P_{cb} is the charging power of the battery (kW).

4.0.2. Modelling of HP and storage tank

The details of modelling a stratified hot water storage tank, suitably adapted to utilize flexibility in its synergy operation with the electricity network, is presented in [18]. The detailed model of HP and storage tank is presented in [19] along with its verification. The thermal power produced by the HP is calculated using (3), where COP is the coefficient of performance and P_{HP} is the electrical power rating of the HP. Inverter-based HPs are available in the market with an operating power factor

above 0.95 leading for the voltage range of 0.9-1pu [20]. Thus, the reactive power drawn by the motor driving the compressor of HP is given by (4). COP is considered to be 3 for operating HPs during a cold winter season based on the manufacturers' datasheet. HPs takes around 10-15 minutes to achieve a steady-state condition before it can deliver heat after turned ON [21]. Thus, delay of 15min is considered between turn ON and delivery of heat.

$$\dot{Q}_{Heat} = COP \times P_{HP} \quad [W] \quad (3)$$

$$Q_{HP} = -P_{HP} \times \tan\theta \quad [VAR] \quad (4)$$

A simplified two-layer (upper hot and lower cold) stratified storage tank, with uniform temperature in each layer, as illustrated in Fig 3, is modelled and verified in [18]. Stratification is present in the storage tank when HP is turned OFF. When HP is turned ON, there is an exchange of heat from the heating element at the bottom of the tank, the thermal stratification is destroyed by water turbulence and there is mixing of hot and cold liquid [18].

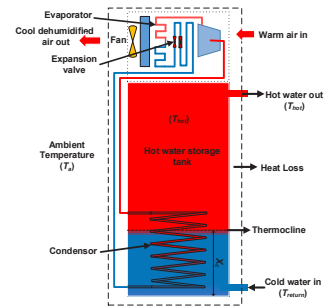


Fig 3. Heat pump and storage system [10]

5. EV and HP Integration Scenario in LV Network

The detailed design parameters of the LV distribution network (630kVA, 10/0.4kV) as shown in Fig. 4 is taken from [22]. The specification of the proposed grid is briefly presented in table 1. Feeder F6 being the longest, the terminals at the far end of feeder F6 attains the lowest voltage up to 0.91pu [10] when operated with HPs. Thus, to integrate EVs, the existing grid is modified by splitting feeder F6 in two radial section as seen in Fig. 4 by adding a new cable (CF6-New) to feeder F6 from the transformer secondary and disconnecting cable C48. The residential electricity demand and thermal demand profiles are detailed in [19]. Fig. 5 shows the distribution of HPs units in the individual house. The HP and storage size associated with each house is based on thermal demand as discussed in [10]. EVs with a battery capacity of 24kWh and 60kWh associated with each house, as shown in Fig. 2, are allocated with a 3-phase charger of 7.4kW and 11kW respectively.

Steady-state power system simulation is carried out to investigate that the operation of HPs and EVs, as flexible consumer

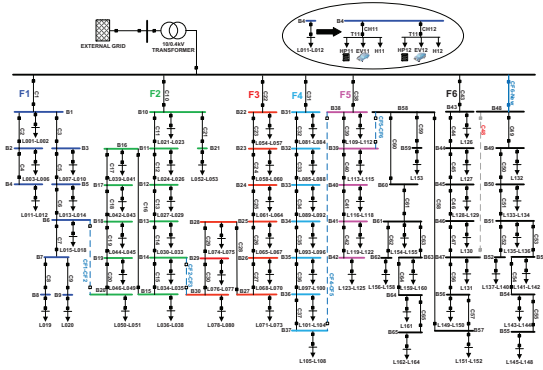


Fig 4. LV Residential Grid Network

Table 1
Grid Specifications

Transformer specification	630kVA, 10/0.4 kV Dyn5, Uk = 4.66% Copper loss = 6.5kW, Iron loss = 1.5kW					
Total Feeders	6					
Households	164					
	F1	F2	F3	F4	F5	F6
Total HH Load (kWh/day)	226	376	277	223	278	421
houses (Nos.)	20	33	27	28	17	39
	Min	Max	avg			
	(kWh/day)					
Residential load	1.2	41	11			
Thermal load	8.3	88.2	34			

load to support LV grid voltage, line and transformer loading remain within its operational limit. As studied in [10], there are around 10-30% of HPs in operation at a time. Thus, the status of HP (ON/OFF) and storage (temperature and level of hot water) at a particular instant when 10% of HPs are in operation is taken as an initial condition. The SOC of EVs is considered as shown in Fig 2.

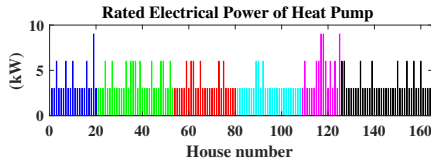


Fig 5. Rated electrical capacity of HP [10]

6. EV Charging Management

To avoid grid congestion, charging time of EVs are distributed over the period, based on its initial SOC (SOC_{i0}). Fig: 6 shows the concept of EV charging management. First of all, based on SOC_{i0} , EVs are categorized into different groups

($P1 - P7$). EVs in group $P1$ are defined by the user for immediate charging.

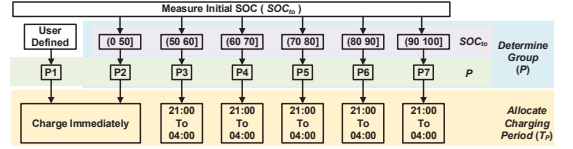


Fig 6. EV charging management

Charging time of EVs are distributed over the period of time (T_p) based on its different group. EVs under the group $P1$ and $P2$ are subjected to charge any time without delay as $P1$ is user-defined and $P2$ has $SOC_{i0} < 50\%$. However EVs in group $P3 - P7$ are allowed to charge only after 21:00 hrs to 04:00 hrs next day, in order to avoid evening peak due to residential demand and to allow buffer time for EVs that are now fully charged until 04:00hrs due to events such as under voltage, later discussed in section 7.

EVs in group $P3 - P7$ are scheduled for charging during the allocated period T_p based on their SOC_{i0} . Charging time (T_{ev}) is allocated to distribute charging of EVs within period T_p , and EV starts charging only after this allocated time. This distribution of charging supports in peak shaping of electricity consumption.

Following procedure is followed to allocate the charging time (T_{ev}) for individual EV in the group $P3 - P7$. Table 2 summarizes the sequential process to determine T_{ev} of EVs with a battery size of 24kWh and 60kWh. EVs under each group (P) with lower SOC (SOC_l) are subjected to charge before EVs with higher SOC (SOC_u)

Let, $t_s = 21:00$ hrs be the start time and $t_e = 04:00$ hrs be the end time. Let B_s and P_{cb} be the battery size (kWh) and charging power (kW) respectively. Then the duration to charge 1% of battery level ($d_{1\%}$), is given by (5). It takes approximately 2min to charge 1% of 24kWh battery with 7.4kW charger, and 3.3 min for 60kWh battery with 11kW charger.

$$d_{1\%} = B_s \times 60 / (P_{cb} \times 100) \quad [min] \quad (5)$$

The total duration necessary for charging a battery with lower (SOC_l) and upper (SOC_u) limit of SOC_{i0} under group (P) is given by (6) and (7) respectively

$$d_u = \frac{B_s \times (100 - SOC_l)}{P_{cb} \times 100} \times 60 \quad [min] \quad (6)$$

$$d_l = \frac{B_s \times (100 - SOC_u)}{P_{cb} \times 100} \times 60 \quad [min] \quad (7)$$

Here, d_u, d_l are charging duration for EVs with SOC_l and SOC_u respectively.

In order to get EV with group (P) and SOC_l , fully charged at 04:00hrs, it needs to start charging at time t_1 (8).

$$t_1 = t_e - d_l \quad [hh : mm] \quad (8)$$

Thus, the total duration (d_t) required for starting charging of EVs and get them fully charged by end time ($t_e = 04:00$ hrs) is determined using (9).

$$d_t = t_1 - t_s \quad [min] \quad (9)$$

In order to charge EVs with SOC_l prior to SOC_u , the delay to start charging ($D(P)_{SOC}$) is given by (10). d_t is evenly distributed into 10 equal parts for every 1% increment in SOC. The determined delay ($D(P)_{SOC}$) is added to t_s to determine charging time of EV as per (11)

$$D(P)_{SOC} = (SOC_{to} - SOC_l) \times \frac{d_t}{10} \quad [min] \quad (10)$$

$$T_{ev} = 21 : 00 + D(P)_{SOC} \quad [hh : mm] \quad (11)$$

For eg, EV with $SOC_{to} = 60$ and battery size 24kWh, $P = P3$ and $SOC_l = 50$ (Fig. 6). Then $D(P3)_{60} = (60 - 50) \times 340/10 = 340min$. i.e., EV starts charging at 21:00hrs + 340min = 02:40hrs. EV is then fully charged by 04:00hrs as it takes around 80min. Similarly, for EV with $SOC_{to} = 51$ and battery size 24kWh, $SOC_l = 50$ and $P = P3$. Then $D(P3)_{51} = 34min$, i.e., EV with $SOC_{to} = 51$ starts charging at 21:34hrs and gets fully charged by 96min (22:36hrs).

Table 2
Scheduling of EV charging

with 7.4kW charger for 24kWh battery size				
Group	SOC_{to} (SOC_l SOC_u) (%)	Charging duration (d_u d_l) (min)	t_l ($t_e - d_t$) (hh:mm)	Total Duration (d_t) ($t_1 - t_s$) (min)
Fig.6-b	Fig.6-b	eq.(6) eq.(7)	eq.(8)	eq.(9)
P3	(50 60]	(100 80]	02:40	340
P4	(60 70]	(80 60]	03:00	360
P5	(70 80]	(60 40]	03:20	380
P6	(80 90]	(40 20]	03:40	400
P7	(90 100]	(20 0]	04:00	420
with 11kW charger for 60kWh battery size				
P3	(50 60]	(165 132]	01:48	288
P4	(60 70]	(132 99]	02:21	321
P5	(70 80]	(99 66]	02:54	354
P6	(80 90]	(66 33]	03:27	387
P7	(90 100]	(33 0]	04:00	420

An illustration of charging management of 50 EVs, battery size of 24kWh, with different SOC level between 51-100% with an increment of 1% is shown in Fig. 7. Charging of EVs in group (P3-P7) are categorised and illustrated separately with SOC and charging power in Fig. 7a-e respectively. EVs under each group is distributed for charging between 21:00hrs to 04:00hrs next day. EVs with lower SOC under each priority level (P) starts charging first and higher SOC starts charging later. Fig. 7f shows the total charging power from the grid with flat peak illustrating an effective charging management strategy.

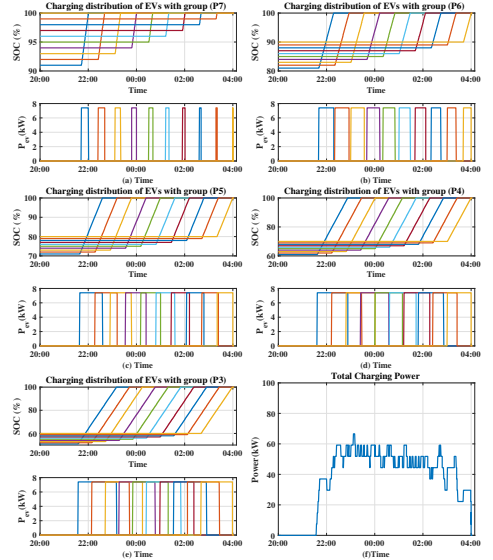


Fig 7. Illustration of charging management of EVs with (a) group P7 (b) group P6 (c) group P5 (d) group P4 (e) group P3 (e) Total Charging power

7. Control of EV and HP

The ON/OFF delay for EV and HP operation based on the terminal voltage (V_t) plays an important role to allow operation of EVs and HPs in the weak feeder. The controller determines its delay value corresponding to V_t based on information provided in table 3 and is illustrated in Fig. 8. Delays with Lower ON delay and higher OFF delay time for lower V_t prioritize the operation of EVs and HPs at the lower end of the distribution feeder, where V_t is lower than the ones closer to the feeder terminal. Charging of EVs has higher priority over operation HPs based on V_t as EVs have lower ON delay and higher OFF delay time compared to HPs (Fig. 8).

Table 3
ON delay and OFF delay Duration Based On V_t

$V_t \geq 0.94$	
ON delay EV	$(V_t - 0.94) \times m + 30$
ON delay HP	$(V_t - 0.94) \times m + 60$
$V_t < 0.92$	
OFF delay EV	$(0.92 - V_t) \times m + 60$
OFF delay HP	$(0.92 - V_t) \times m + 30$
$m = 3000$ for minimum delay of 30s	
if $V_t \leq 0.9$ for $t > 60s$	
ON delay EV	1200s
ON delay HP	1800s

The minimum time delay of 30s for $V_t \geq 0.94pu$, is selected to avoid the controllers to respond at short duration variations in V_t and is increased by two simulation step size (30s) for every

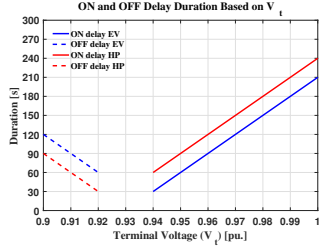


Fig 8. ON delay and OFF delay duration based On V_t

0.01pu increment in V_t . In order to maintain V_t within the range of -10%, no new connection of HP or EV is allowed for $V_t < 0.94pu$, and for $V_t < 0.92pu$ EV and HP starts to disconnect based on the OFF delay duration as illustrated in Fig. 8. In case V_t drops below 0.9pu for more than 60s (to have four samplings to avoid transients), EVs and HPs at these terminals disconnect immediately and connects only after 20min for EVs and 30min for HP, to avoid stressing grid frequently as well as to give EVs priority over HPs.

7.1. EV control

Fig. 9 illustrates the flow diagram of EV and HP control and its validation is illustrated in Fig 10. The availability of EV (A) is defined as a situation when EV is parked and is plugged in for charging and is equal to 1 else 0 logic state. Upon the availability of EV ($A = 1$), it is eligible to be charged if $SOC_t < 100\%$ and the charging signal (S) remains high until fully charged. Fig 10a shows V_t which is determined manually to verify the

proposed control logic. Fig 10b,c shows status of SOC_t , and logic status of A, S respectively.

The EV start charging based on their designated group and allocated time for charging as calculated based on (11). The logic signal C is high at time T_{ev} , indicating EV is ready to charge and remains high until EV is fully charged as shown in Fig 10d.

EVs are not connected for charging instantly based on its allocated charging time T_{ev} , to maintain V_t at the point of coupling of EV to electrical network within the lower operating voltage of -10%. EVs in OFF state at terminals with $V_t < 0.94$ are now allowed to connect until $V_t \geq 0.96pu$ to avoid hunting effect and is realized with logic signal $V1$. The EVs in ON states are allowed to charge until $V_t \geq 0.92pu$ (realized with logic signal $V2$), to allow the smooth operation of EVs which are in ON state. Fig 10e illustrates the status of logic signal $V1$ and $V2$.

With favourable voltage condition ($V1=1$) and EV ready to charge ($C=1$), EVs connects to the grid with connection delay based on V_t as presented in table 3 to avoid a large number of EVs with same SOC_t connect at the same time. logic C_{ev} is set high to represent EVs are connected to the grid for charging. Fig 10f illustrates the logic state C and $V1$ to represent ON delay for charging. It shows that when EV is scheduled to charge at 21:17hrs (as per logic signal C in Fig 10b), C_{ev} turns ON after ON-delay and turns OFF after OFF-delay when $V_t < 0.92pu$ (Fig 10g). When $V_t \geq 0.96pu$ at around 22:00, Hrs, $V1=1$ and $C_{ev} = 1$ after ON delay. When $V_t < 0.9pu$ for more than 60s at around 22:30hrs, charging stops (C_{ev}) and the EV is again connected to start charging after the delay of 20min after $V_t > 0.9pu$ again. Fig 10h shows the charging

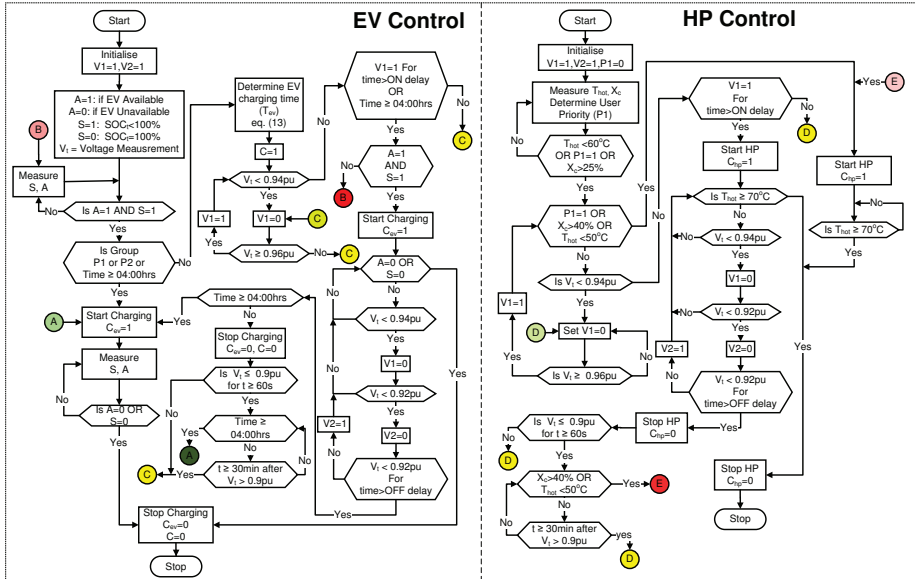


Fig 9. EV and HP Control System

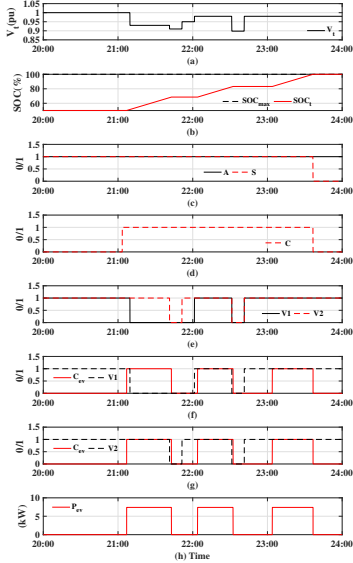


Fig 10. EV Control System (a): terminal voltage (V_t), (b): SOC_t , (c): availability of EV A and status of control logic S, (d): logic status C, (e): logic status V1 and V2 (f): C_{ev} and V1 to illustrate turn ON delay (g): C_{ev} and V2 to illustrate turn OFF delay (h): Power consumed by EV charger

power drawn from the grid to charge the EV. The availability of EV is continuously monitored throughout the charging period. In case the EV is suddenly unplugged, the charging process is interrupted as seen from charging algorithm in Fig. 9, and the charging routine is started from the beginning.

In case EVs are not fully charged until 04:00Hrs, EVs in ON state continues charging and EVs in OFF state are subjected to charge immediately despite any voltage condition until they are fully charged.

7.2. HP control

The concept of HP control for its flexible operation in low voltage distribution network is taken from [10] with modification in position and parameters of ON/OFF delay for better coordination and utilisation of electric grid. The OFF delay is introduced only when $V_t < 0.92pu$ and ON delay is introduced when $V_t \geq 0.94pu$. Also, the parameters of ON-OFF delay has been selected to obtain a fast coordinated response between EVs and HPs based on simulated step size. These modifications allow continuous operation of HPs at lower terminal voltage by shutting down HPs in a neighbourhood with higher V_t and without waiting for V_t to fully recover. Fig. 9 illustrates the flowchart of the complete system structure for flexible operation of HP with the coordinated operation. The decision regarding ON/OFF control for operation of HP is based on local informations such as terminal voltage (V_t) at the point of coupling of HP with the electrical grid, the temperature of hot water (T_{hot}) and level of cold water in the stratified hot water storage tank X_c . The HP is subjected to turn ON when $T_{hot} < 60^\circ C$

or $X_c < 25\%$ and turns OFF when $T_{hot} = 70^\circ C$ [10]. The delay parameter based on V_t , as shown in Fig. 8 (and discussed earlier for EV charging), enhances the flexible operation of HP controller by shifting its operating time and regulating ON/OFF of HP to support grid performance (grid voltage, line loading, and transformer capacities). Based on the control signal (C_{hp}) to turn ON/OFF the HP, heat is delivered from the HP and is stored in the thermal storage tank. Hot water with temperature T_{hot} is delivered from the storage tank and the heat exchanger to fulfil thermal demand.

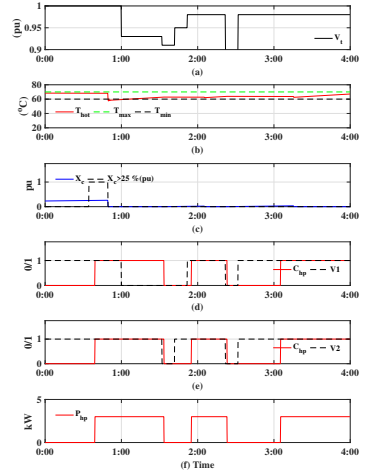


Fig 11. HP Control System (a): terminal voltage (V_t), (b): T_{hot} , (c): X_c , (d): C_{hp} and V1 to illustrate turn ON delay (e): control logic C_o (f): C_{hp} and V2 to illustrate turn OFF delay, (g): Power consumed by HP

Fig. 11 shows the validation of proposed HP control. The terminal voltage is selected manually to highlight controller performance during various terminal voltage condition and is presented in Fig. 11a. The temperature of hot water and the level of cold water in the storage tank is shown in Fig. 7.2b,c respectively. Fig. 11d,e shows the turn ON and OFF delay for logic signal to start HP (C_{hp}) respectively. Fig. 7.2f shows the power consumption by HP during its operation.

In case, HPs are not allowed to operate due to poor voltage condition and $T_{hot} < 50^\circ C$ or $X_c > 40\%$ HPs are turned ON immediately despite any voltage condition until they are fully charged ($T_{hot} = 70^\circ C$).

7.3. Coordination between EV and HP Operation

Fig. 12 illustrate that the operation of EVs has higher priority than HPs connected at the same terminal. On the other hand, EVs and HPs at lower terminal voltage have higher priority than ones from higher terminal voltage for operation as per the proposed control technique. The terminal voltage is selected manually to verify the priority in the operation of EVs and HPs. EV1, EV2, and EV3 are connected at terminal T1, T2, and T3 respectively. HP1, HP2, and HP3 are connected at terminal T1, T2, and T3 respectively. When $V_t < 0.92pu$, C_{hp}

turns OFF consecutively for HP3, HP2, HP1 with OFF delay, calculated according to table 3. Similar is the case with EVs with higher OFF delay. This indicates that EV has priority over HP while turning OFF due to low voltage. Also, EVs and HPs at higher voltage region turn OFF first. When $V_t \geq 0.96pu$, EV and HP connects with their ON delay, calculated according to table 3. When $V_t < 0.92pu$ for short duration around 800s, only the HPs with the low OFF delay at terminal T1 is turned OFF. since V_t recovers before OFF delay of other HPs and EVs, they retain their normal operation.

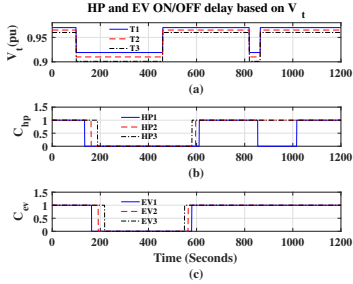


Fig 12. HP and EV ON/OFF delay based on V_t (a): terminal voltage (V_t), (b): C_{hp} , (c): C_{ev}

8. Results and Discussion

Results of the steady-state power system simulation with LV distribution network integrated with EVs and, HPs with storage is presented in Fig. 13 and summary of transformer loading, line loading, percentage of EV-charging and HP operating, minimum temperature of hot water in storage tank along with level of cold water is summarised in table 4. The transformer loading and percentage of EV and HP being operated are shown in Fig. 13a. The transformer is loaded up to 64% of its rated capacity. The maximum percentage of EV-charging and HP being operated is 14% and 35% respectively. 0% of EV being charged after 04:30hrs indicates that all EVs are fully charged.

Fig. 13b,c shows the minimum V_t terminal voltage attained in each feeder. Feeder number, terminal number, and V_t attained is shown in the figure legend. V_t is well within its lower operating limit of -10%. The transients in voltage seen are due to operation of residential load [10], HPs or EVs. table 4 shows that the maximum line loading is 60% of its rated capacity. The maximum level of cold water in storage tank attained is 32% with a minimum temperature of hot water at $52^\circ C$ indicates that thermal demand is fulfilled at all time.

Table 4
Summary of Result

Transformer loading (%)	EV charging (%)	HP operated (%)	Max.line loading (%)	Min. T_{hot} ($^\circ C$)	Max. X_c (%)
64	14	35	60	52	32

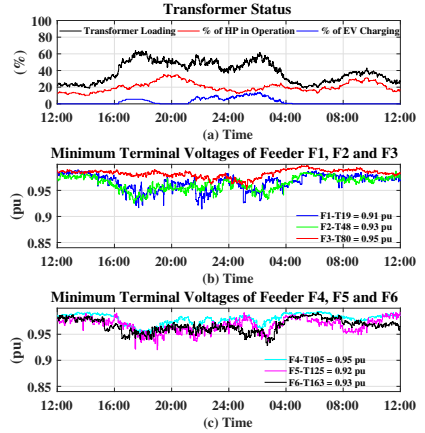


Fig 13. (a): transformer loading, percentage of HP in Operation, and percentage of EV being charged; (b): minimum voltage attained in terminals of feeder F1, F2 and F3; (c): minimum voltage attained in terminals of feeder F4, F5 and F6

The hosting capability of the LV network can become poor with the integration of thermal and EV loads in LV network and has been evaluated stochastically in [23]. The capabilities and limits of LV distribution grid (Fig. 4) integrated with EVs are highlighted in [22] suggesting that the total penetration of EVs corresponding to the minimum and maximum demand hours in this LV grid network is 17% and 6% respectively. This is merely due to a violation of the voltage limit of some feeders more than -6%, though 44% of transformer capacity was left unexploited. Higher voltage drop is due to cable impedances being purely ohmic. With 100% operation of HP, the terminal voltage drops down to 0.86pu in Feeder F6, while the transformer and cable C45 in feeder F6 is loaded 22% and 35% more than its rated capacity respectively [10]. Thus, with minor reinforcement in the LV grid along with proper demand response for operating HPs and EVs flexibly, the autonomous ON/OFF control logic proposed here is effective in managing grid voltage of week feeder within its lower operating limit of -10%.

9. Conclusion

This paper provides insights into the concept of the potential use of EVs and HPs as distributed flexible load and its impact on Denmark's low voltage distribution network. The control strategy based on ON/OFF delay prioritizes the operation of EVs over HPs. On the other hand, this concept also prioritizes the operation of EVs and HPs at lower voltage region over higher voltage region in the LV distribution network. The proposed control strategy plays an effective role in demand response to enhance flexibility in the operation of EVs and HPs while supporting grid voltage and satisfying end-user need simultaneously. The proposed control architecture is local and reduces the need for costly communication infrastructure to handle big data and control architecture.

Acknowledgment

The authors would like to thank DiCyPS project funded by the Innovation Fund Denmark for funding this research project. The data for the analysis of thermal demand has been provided by Aalborg Energi Holding A/S and Aalborg University, Denmark, as per the agreement between project partners for research.

References

- [1] J. Kiviluoma, P. Meibom, Influence of wind power, plug-in electric vehicles, and heat storages on power system investments, *Energy* 35 (3) (2010) 1244–1255.
- [2] D. Papadaskalopoulos, G. Strbac, P. Mancarella, M. Aunedi, V. Stanovic, Decentralized participation of flexible demand in electricity markets—part ii: Application with electric vehicles and heat pump systems, *IEEE Transactions on Power Systems* 28 (4) (2013) 3667–3674.
- [3] T. Masuta, A. Yokoyama, Supplementary load frequency control by use of a number of both electric vehicles and heat pump water heaters, *IEEE Transactions on Smart Grid* 3 (3) (2012) 1253–1262.
- [4] S. Vachirasricirikul, I. Ngamroo, Robust controller design of heat pump and plug-in hybrid electric vehicle for frequency control in a smart micro-grid based on specified-structure mixed H_2/H_∞ control technique, *Applied Energy* 88 (11) (2011) 3860–3868.
- [5] S. Huang, Q. Wu, Real-time congestion management in distribution networks by flexible demand swap, *IEEE Transactions on Smart Grid* 9 (5) (2018) 4346–4355.
- [6] I. D. de Cerio Mendaza, I. G. Szczesny, J. R. Pillai, B. Bak-Jensen, Flexible demand control to enhance the dynamic operation of low voltage networks, *IEEE Transactions on Smart Grid* 6 (2) (2015) 705–715.
- [7] P. T. Bjerregaard, I. G. Szczesny, I. D. de Cerio Mendaza, J. R. Pillai, Intelligent control of flexible loads for improving low voltage grids utilization, in: *IEEE PES ISGT Europe 2013*, 2013, pp. 1–5.
- [8] B. Bhattarai, I. Mendaza, B. Bak-Jensen, J. Pillai, Local adaptive control of solar photovoltaics and electric water heaters for real-time grid support, in: *Proceedings of the Cigré Session 2016*, CIGRE (International Council on Large Electric Systems), 2016.
- [9] G. Connor, C. E. Jones, S. J. Finney, End user voltage regulation to ease urban low-voltage distribution congestion, *IET Generation, Transmission Distribution* 8 (8) (2014) 1453–1465.
- [10] R. Sinha, B. Bak-Jensen, J. Radhakrishna Pillai, Autonomous controller for flexible operation of heat pumps in low-voltage distribution network, *Energies* 12 (8).
URL <http://www.mdpi.com/1996-1073/12/8/1482>
- [11] M. K. Larsen, Analysis of the danish travel survey data on private and public transportation, in: *Annual Transport Conference at Aalborg University 2010*, 2010.
- [12] B. Z. S. Hjalmar Christiansen, Documentation of the danish national travel survey, Tech. rep., DTU Transport Department of Transport (2015).
- [13] J. Quirós-Tortós, L. F. Ochoa, B. Lees, A statistical analysis of ev charging behavior in the uk, in: *2015 IEEE PES Innovative Smart Grid Technologies Latin America (ISGT LATAM)*, 2015, pp. 445–449.
- [14] R. Sinha, E. R. Moldes, A. Zaidi, P. Mahat, J. R. Pillai, P. Hansen, An electric vehicle charging management and its impact on losses, in: *IEEE PES ISGT Europe 2013*, 2013, pp. 1–5.
- [15] C. Bingham, C. Walsh, S. Carroll, Impact of driving characteristics on electric vehicle energy consumption and range, *IET Intelligent Transport Systems* 6 (1) (2012) 29–35.
- [16] I. D. de C. Mendaza, A. Pigazo, B. Bak-Jensen, Z. Chen, Generation of domestic hot water, space heating and driving pattern profiles for integration analysis of active loads in low voltage grids, in: *IEEE PES ISGT Europe 2013*, 2013, pp. 1–5.
- [17] Q. Wu, A. H. Nielsen, J. Ostergaard, S. T. Cha, F. Marra, Y. Chen, C. Træholt, Driving pattern analysis for electric vehicle (ev) grid integration study, in: *2010 IEEE PES Innovative Smart Grid Technologies Conference Europe (ISGT Europe)*, 2010, pp. 1–6.
- [18] R. Sinha, B. B. Jensen, J. R. Pillai, C. Bojesen, B. Moller-Jensen, Modelling of hot water storage tank for electric grid integration and demand response control, in: *2017 52nd International Universities Power Engineering Conference (UPEC)*, 2017, pp. 1–6.
- [19] R. Sinha, B. B. Jensen, J. R. Pillai, B. Moller-Jensen, Unleashing flexibility from electric boilers and heat pumps in danish residential distribution network, in: *Proceedings CIGRE 2018*, Paris, 2018.
- [20] W. J. B. Heffernan, N. R. Watson, J. D. Watson, Heat-pump performance: Voltage dip/sag, under-voltage and over-voltage, Tech. rep., University of Cantebury.
- [21] T. Masuta, A. Yokoyama, Y. Tada, Modeling of a number of heat pump water heaters as control equipment for load frequency control in power systems, in: *2011 IEEE Trondheim PowerTech*, 2011, pp. 1–7.
- [22] J. R. Pillai, P. Thøgersen, J. Møller, B. Bak-Jensen, Integration of electric vehicles in low voltage danish distribution grids, in: *2012 IEEE Power and Energy Society General Meeting*, 2012, pp. 1–8.
- [23] I. D. de Cerio Mendaza, B. Bak-Jensen, Z. Chen, A. Jensen, Stochastic impact assessment of the heating and transportation systems electrification on lv grids, in: *IEEE PES Innovative Smart Grid Technologies, Europe*, 2014, pp. 1–6.

ISSN (online): 2446-1636
ISBN (online): 978-87-7210-498-0

AALBORG UNIVERSITY PRESS